Thesis Title

Astrocyte-induced DNA damage as a mechanism of motor neuron death in amyotrophic lateral sclerosis

Name of student

Jannigje Rachel Kok

Registration number

180154629

A thesis submitted in partial fulfilment of the requirements for the degree of Doctor of Philosophy

The University of Sheffield
Faculty of Medicine, Dentistry and Health
Department of Neuroscience

Submission Date:
September 2022

Preface

This work was conducted in collaboration with AstraZeneca, although the originally planned drug screening that was due to take place unfortunately did not occur due to delays as a result of the COVID-19 pandemic. All experimental work described in Chapters 3-5 were carried out by myself, Jannigje Kok, unless otherwise stated.

Dr Cleide Souza contributed the results and images for γH2AX foci in motor neurons treated with control or ALS astrocyte conditioned medium, and the results and images for p62 foci in motor neurons treated with control or ALS astrocyte conditioned medium. Dr Cleide Souza also contributed the raw datasets of mRNA counts following RNA extraction and Nanostring analysis on motor neurons treated with control or ALS astrocyte conditioned medium, and I analysed the data for the thesis. MSD ELISAs were carried out by Dr Adrian Higginbottom and Dr Ergita Balli, sample preparation and data analysis was carried out by myself.

Chapter 1 introduces the disease the project focuses on, amyotrophic lateral sclerosis, and the two key disease mechanisms the project interrogates: contribution of astrocyte toxicity and DNA damage. Chapter 2 describes the materials and methods used in Chapters 3-5. The first results chapter, Chapter 3, focuses on characterisation of DNA damage and repair in induced neuronal progenitor (iNPC)-derived astrocytes from control and ALS patients. Chapter 4 describes the evidence showing ALS patient astrocytes induce DNA damage and DNA repair impairment in healthy motor neurons. Chapter 5 interrogates two possible mechanisms by which ALS astrocytes might induce DNA damage and/or repair impairment: dipeptide repeat protein secretion and p62 accumulation. Finally, Chapter 6 discusses the main implications of the three results chapters, contextualises the findings and speculates on future directions.

Acknowledgements

I would like to begin by expressing my gratitude to the healthy volunteers and the people with ALS that kindly donated skin biopsies, without whom this research could not have happened.

I would like to thank my supervisors, Professor Laura Ferraiuolo and Professor Sherif El-Khamisy, for their supervision and support, for their feedback on various drafts of the thesis and for their commitment to motor neuron disease research.

Thank you to the organisations who funded this research. This work was supported by an iCase Studentship from the MRC Discovery Medicine North (DiMeN) Doctoral Training Partnership (MR/R015902/1) in collaboration with AstraZeneca. I wish to take this opportunity to thank our collaborators at AstraZeneca, particular Dr Elske Franssen and Dr Michael Perkinton, who supported this research and who provided valuable feedback on the project.

I would especially like to thank Dr Cleide Souza, who worked on this project with me, gave me feedback on my thesis, and who acted as a mentor to me throughout my PhD. She has always been immensely supportive, and her advice has been invaluable, both with regards to experimental work, career progression and maintaining a healthy work-life balance. I would also like to thank and acknowledge the help of Dr Monika Myszczynska, who kindly gave me feedback on multiple chapter drafts, and trained me on cell culture, Western blotting and general good lab practice when I first arrived at SITraN.

It would be remiss of me not to acknowledge my colleagues and friends, Allan Shaw, Marco Destro and Andre Varcianna, with whom I have shared the struggles and successes of working towards the completion of a PhD, and I wish them all the best with the completion of their own thesis. I would also like to thank all members, past and present, of the Ferraiuolo and El-Khamisy lab groups for their help with experiment protocols, optimisations, provision of cells and feedback over the course of the last four years.

Finally, I would like to thank my mother, Angela Kok, for her unwavering support and for keeping me sane and fed while I was writing my thesis from home.

Declaration

*I, the author, confirm that the Thesis is my own work. I am aware of the University's Guidance on the Use of Unfair Means (*www.sheffield.ac.uk/ssid/unfair-means*). This work has not previously been presented for an award at this, or any other, university.*

Publications

Kok, J.R., Palminha, N.M., Dos Santos Souza, C., El-Khamisy, S.F. and Ferraiuolo, L., 2021. DNA damage as a mechanism of neurodegeneration in ALS and a contributor to astrocyte toxicity. Cellular and Molecular Life Sciences, 78(15), 5707-5729. (Review Article)

Abstract

Amyotrophic lateral sclerosis (ALS) is a neurodegenerative disease that affects motor neurons in the brain and spinal cord, leading to paralysis and death. 95% of ALS cases are classed as sporadic and 5% occur due to an inherited mutation in an ALS-linked gene, the most common of which are the C9ORF72 and SOD1 genes. The cause of motor neuron degeneration remains unclear, however, several studies have shown increased DNA damage and astrocyte toxicity as consistent features of sporadic and familial ALS. ALS astrocyte toxicity is transmitted through secreted factors, but the mechanisms and molecules involved remain elusive. It was hypothesised that astrocyte-induced DNA damage could contribute to motor neuron death in ALS.

To test this, induced astrocytes (iAstrocytes), which retain hallmarks of ageing, were obtained from healthy controls, and patients with sporadic ALS, SOD1-ALS or C9ORF72-ALS. Increased DNA damage and impaired DNA repair was observed in specific ALS astrocyte lines but was not consistently altered in any genetic subgroup, indicating some ALS astrocytes may be affected by the same cell-autonomous DNA damage observed in motor neurons. Conditioned medium derived from C9ORF72-ALS and sporadic ALS astrocytes, but not SOD1-ALS astrocytes, was found to induce an increase in DNA damage and an impairment in DNA damage signalling in healthy iPSC-derived motor neurons. The mechanism for astrocyte-induced DNA damage remains unclear. C9-ALS astrocytes were found to express and secrete dipeptide repeat proteins, which have previously been shown to induce DNA damage. ALS astrocyte conditioned medium was also found to induce p62 aggregation, which may lead to DNA damage and repair impairment, however further work is needed to verify this. In summary, our work identifies a new mechanism by which ALS astrocytes may induce cell death in motor neurons and suggests that DNA damage signalling or p62 may be a potential therapeutic target.

Table of Contents

List of Abbreviations

Abbreviation	Full Name
53BP1	p53 binding protein 1
8-OHdG	8-hydroxy-2-deoxyguanosine
8-oxodG	8-oxo-2-deoxyguanosine
ADA	Adenosine deaminase
ADP	Adenosine di-phosphate
ALS	Amyotrophic lateral sclerosis
alt-NHEJ	Alternative NHEJ
AMPAR	Alpha-amino-3-hydroxy-5-methyl-4-isoxazole propionic acid receptor
AP	Abasic
APE1	Apurinic/apyrimidinic endonuclease 1
ATM	Ataxia telangiectasia mutated
ATR	ATM and Rad3 related
BCA	Bicinchoninic acid assay
BER	Base excision repair
BSA	Bovine serum albumin
C9-ALS	ALS patients with a repeat expansion in the C9ORF72 gene
C9ORF72	Chromosome 9 open reading frame 72
c-NHEJ	Canonical NHEJ
CNS	Central nervous system
CPT	Camptothecin
CSF	Cerebrospinal fluid
Cx43	Connexin 43
DDR	DNA damage response
DNA	Deoxyribonucleic acid
DNA-PK	DNA-dependent protein kinase
DNA-PKcs	DNA protein kinase catalytic subunit
DPR	Dipeptide repeat protein
EAAT2	Excitatory amino acid transporter 2
fALS	Familial ALS
FTD	Frontotemporal dementia
FUS	Fused in sarcoma
FUS-ALS	ALS patients with a mutation in the FUS gene
GA	Glycine alanine
GABA	Gamma-aminobutyric acid
GAT	Gamma-aminobutyric acid transporter
Glu	Glutamate
GluR2	Glutamate ionotropic receptor AMPA type subunit 2
GN	GABAergic neuron
GP	Glycine proline
GR	Glycine arginine
GSH	Glutathione
GSS	Glutathione synthetase
HEK	Human embryonic kidney

HR	Homologous recombination
iAstrocytes	Induced astrocytes
ICC	Immunocytochemistry
iNeuron	Induced neuron
iNPC	Induced neuronal progenitor cell
IP	Immunoprecipitation
iPSC	Induced pluripotent stem cell
KEAP1	Kelch-like ECH-associated protein 1
KIR	Keap1 interacting region
LC3	Microtubule-associated protein 1A/1B-light chain 3
MCT	Monocarboxylate transporter
MHCI	Major histocompatibility complex class I
MMEJ	Microhomology-mediated end-joining
MN	Motor neuron
MND	Motor neuron disease
MRN	MRE11–RAD50–NBS1
MRP4	Multidrug resistance protein 4
MSD ELISA	Meso scale discovery enzyme-linked immunosorbent assay
MTOR	Mammalian target of rapamycin
NER	Nucleotide excision repair
NF-κB	Nuclear factor kappa B
NGF	Nerve growth factor
NHEJ	Non-homologous end-joining
NPC	Neuronal progenitor cell
NRF2	Nuclear factor erythroid 2–related factor 2
NSC	Neural stem cells
OdG	Oxidised deoxyguanosine
OG	Oxidised guanosine
p75NTR	p75 neurotrophin receptor
PA	Proline alanine
PAR	Poly(ADP-ribose)
PARP1	Poly(ADP-ribose) polymerase 1
PE	Phosphatidylethanolamine
pNF-H	Phosphorylated neurofilament heavy
PolyP	Inorganic polyphosphate
PR	Proline arginine
RAN	Repeat-associated non-AUG
RNA	Ribonucleic acid
ROS	Reactive oxygen species
RRE	RNA repeat expansion
sALS	Sporadic ALS
SDS	Sodium dodecyl sulphate
Slc16a4	Solute Carrier Family 16 Member 4
SNARE	Soluble N-ethylmaleimide-sensitive factor attachment proteins receptors
SOD1	Superoxide dismutase 1
SOD1-ALS	ALS patients with a mutation in the SOD1 gene

SQSTM1/p62	Sequestosome 1
SSA	Single-strand annealing
TARDBP	Transactive response DNA binding protein 43 kDa
TDP-43	Transactive response DNA binding protein 43 kDa
TE	Tris-EDTA
TGFβ1	Transforming growth factor beta 1
TNFα	Tumour necrosis factor alpha
TOP1cc	TOPO1:DNA cleavage complex
TOPO1	Topoisomerase 1
Ub	Ubiquitin
UBA	Ubiquitin-associated domain
VCP	Valosin-containing protein
XRCC1	X-ray repair cross complementing 1
γH2AX	Phosphorylation of histone H2AX

List of Tables

List of Figures

Chapter 1: Introduction

1.1 Amyotrophic Lateral Sclerosis

In the nineteenth century, Jean-Martin Charcot was the first to describe amyotrophic lateral sclerosis (ALS) after observing that patients with progressive muscle wastage and paralysis exhibited specific patterns of grey and white matter damage in the anterior horn of the spinal cord (Charcot's original findings reviewed by Goetz, 2000). Muscle weakness in the upper or lower limbs (limb-onset), or difficulties with speech or swallowing (bulbar-onset) are early symptoms of ALS. Over time, generalised weakness and muscle atrophy progresses, leaving patients paralysed. ALS is ultimately fatal, with most patients dying within two to three years of symptom onset, and death is normally the result of respiratory failure following weakening of the respiratory muscles (Zarei et al., 2015). There are currently only two treatments approved worldwide, riluzole and edaravone, which lead to a modest improvement and lifespan increase (Miller et al., 2012; Yoshino and Kimura, 2006).

Motor neurons are the primary affected cell type in ALS, and post-mortem analyses have shown both upper and lower motor neuron death in the brain and spinal cord, respectively (Lawyer and Netsky, 1953). Motor neurons are not the only affected neuron type however, as there is evidence of loss of parvalbumin-positive GABAergic inhibitory interneurons (Nihei et al., 1993) and cortical inhibitory neuron signalling deficits (Enterzari-Taher et al., 1997) in ALS. Additionally, sites of motor neuron degeneration, including the motor cortex and spinal cord, contain large numbers of reactive astrocytes and reactive microglia (Murayama et al., 1991; Schiffer et al., 1996; Turner et al., 2004), suggesting glial cells are also affected in ALS. Indeed, the presence of wild-type non-neuronal cells in chimeric $SOD1^{G93A}$ or $SOD1^{G37R}$ mouse models has been shown to extend mouse survival (Clement et al., 2003; Yamanaka et al., 2008a). Furthermore, selective depletion of mutant SOD1 in microglia or astrocytes in a $SOD1^{G37R}$ mouse model had little effect on disease onset but delayed disease progression and extended survival (Boillée et al., 2006; Yamanaka et al., 2008b), suggesting glial cells contribute to disease progression in ALS.

ALS patients are divided into two major classes: sporadic patients (sALS) and familial patients (fALS) (Tandan and Bradley, 1985). Most ALS patients have no family history of the disease and are, therefore, classed as sporadic, whereas systematic review and meta-analysis suggests 5% of ALS patients have an inherited mutation in one of a number of ALS-associated genes (Byrne et al.,

2011). However, sALS and fALS are clinically indistinguishable. Diagnosis of ALS requires three criteria to be met (Shefner et al., 2020):

1. Evidence of progressive motor impairment that was preceded by normal motor function
2. Evidence of upper and lower motor neuron dysfunction in at least 1 body region, or evidence of lower motor neuron dysfunction in at least 2 body regions
3. Evidence excluding other diseases or conditions that could be causing dysfunction (e.g. Parkinson's disease)

The two most common genetic mutations found in fALS patients are a repeat expansion in the chromosome 9 open reading frame 72 (C9ORF72) gene (DeJesus-Hernandez et al., 2011; Renton et al., 2011), and mutations in the copper−zinc superoxide dismutase (SOD1) gene (Rosen et al., 1993). Most of the suggested mechanisms of motor neuron degeneration in ALS have been identified from studies looking at genes identified from sequencing of fALS patients (Table 1) and include protein aggregation, excitotoxicity, oxidative stress and defects in important cellular pathways such as RNA metabolism, autophagy and the DNA damage response (Ferraiuolo et al., 2011a).

Table 1. Key Mendelian genes associated with ALS (from Kok et al., 2021).

Gene	Full Name	WT Protein Role	fALS Prevalence
C9ORF72	Chromosome 9 open reading frame 72	Autophagy	3-34%
SOD1	Superoxide dismutase type-1	Oxidative stress response	15-30%
TARDBP	Transactive response DNA binding protein 43 kDa	RNA metabolism, DDR	1-4%
FUS	Fused in sarcoma	RNA metabolism, DDR	3-6%
NEK1	Never-in-mitosis A related protein kinase 1	Cell cycle, DDR	3%
OPTN	Optineurin	Autophagy	3%
VCP	Valosin-containing protein	Proteasome, vesicle trafficking, autophagy, DDR	1-2%
TBK1	TANK-binding kinase 1	Autophagy	1%
SETX	Senataxin	R loop resolution	<1%
SQSTM1 or p62	Sequestosome 1 or p62	Ubiquitination, autophagy, DDR	<1%
ALS2	Alsin	Vesicle trafficking	<1%
CHCHD10	Coiled-coil-helix-coiled-coil-helix domain-containing protein 10	Mitochondrial function	<1%
CHMP2B	Charged multivesicular body protein 2B	Vesicle trafficking, autophagy, lysosomal pathway	<1%
MATR3	Matrin 3	Transcription, RNA metabolism	<1%
PFN1	Profilin 1	Cytoskeleton, axon growth	<1%
UBQLN2	Ubiquilin 2	Proteasome, autophagy	<1%
VAPB	Vesicle-associated membrane protein-associated protein B/C	Autophagy	<1%

Genes associated with DNA damage signalling or repair are highlighted. ALS genetics reviewed comprehensively in Ghasemi and Brown, 2017. Prevalence of <1% indicates gene mutations have

only been identified in a few families or cohorts, preventing accurate prevalence measurement. From Kok et al., 2021, title: Key Mendelian genes associated with ALS, creator: Jannigje Kok, copyright information: CC BY 4.0 (https://creativecommons.org/licenses/by/4.0/).

1.2 Genetic Causes and Mechanisms of ALS

1.2.1 Sporadic ALS

As previously described, sALS patients are defined as patients with no family history of ALS, however several sALS cases have been identified as carrying de novo mutations in genes also identified in fALS patients (Table 1). As with fALS, C9ORF72 repeat expansion is the most common genetic determinant of sALS, but only accounts for approximately 6-7% of sALS cases (Dekker et al., 2016; Majounie et al., 2012) compared to 34% of fALS cases (Zou et al., 2017). Mutations in other ALS genes including SOD1, FUS and TARDBP, have also been identified as being present in low numbers of sALS patients (Dekker et al., 2016).

In total, known ALS gene mutations have been shown to account for approximately 11% of sALS cases (Renton et al., 2014), meaning in the vast majority of cases the cause of disease remains unknown. Lifestyle or environmental factors have been suggested as contributing factors to developing sALS, however these risk factors are highly debated and remain controversial (Ingre et al., 2015). Tobacco smoking is considered to be one of the more well-established lifestyle risk factors for ALS, with one study reporting that smoking doubled the risk of developing ALS and that there was a dose-response relationship between number of years smoking and risk for ALS (Gallo et al., 2009). Interestingly, it has been reported that risk of ALS amongst smokers is significantly higher in women than men, indicating a compounding involvement of sex differences (Weisskopf et al., 2004). Other proposed factors linked with increased risk of ALS include athleticism, head trauma, metabolic disease, viral infection, pesticides, metal exposure (lead, manganese, etc), and even electrical occupations (reviewed in Ingre et al., 2015). A clear link between these disparate factors remains to be identified.

Despite the different possible explanations for how disease may arise, sALS patients show similar pathological hallmarks indicating possible common disease mechanisms if not disease initiators. These features are often also observed in fALS cases, although this can vary based on gene mutation. Misfolding and aggregation of SOD1 protein has been observed in sALS (Paré et al., 2018) and fALS, irrespective of gene mutation (Forsberg et al., 2019). TDP-43 is a primarily nuclear RNA/DNA binding protein, which undergoes a number of changes in sALS and fALS (excluding SOD1-ALS and FUS-ALS) (Mackenzie et al., 2007; Scotter et al., 2015; Vance et al., 2009). There is

loss of nuclear TDP-43 as TDP-43 becomes mislocalised to the cytoplasm where it can be fragmented and phosphorylated (Scotter et al., 2015). Additionally, cytoplasmic TDP-43 can also aggregate into ubiquitin-positive inclusions (Arai et al., 2006; Neumann et al., 2006). FUS is another RNA/DNA binding protein which can also be found aggregated in cytoplasmic inclusions in sALS and fALS (including TARDBP-ALS), but not in SOD1-ALS (Deng et al., 2010). Cytoplasmic inclusions positive for p62, a protein primarily known for its role in autophagy, are also a consistent feature in sALS and fALS (Mizuno et al., 2006), including FUS-ALS (King et al., 2015) and has been observed in a mouse model of SOD1-ALS (Gal et al., 2007). The consistency of proteinopathy across sALS and fALS and across ALS genetic subtypes could indicate that there are common mechanisms linking different forms of ALS.

1.2.2 C9ORF72-ALS

The most common cause of fALS is a hexanucleotide (GGGGCC) repeat expansion in the first exon of the chromosome 9 open reading frame 72 (C9ORF72) gene. Over 30 repeats are thought to be required to render the C9ORF72 gene pathogenic (DeJesus-Hernandez et al., 2011; Renton et al., 2011), however hundreds or thousands of repeats are observed in some C9-ALS patients (Dols-Icardo et al., 2014). Normal physiological function of C9ORF72 has been linked with the autophagy pathway, as C9ORF72 depletion leads to defective autophagosome formation, impaired lysosome biogenesis, and reduced clearance of protein aggregates (Sellier et al., 2016; Shi et al., 2018). The C9ORF72 repeat expansion has been shown to lead to reduced levels of C9ORF72 mRNA and protein, and depletion of C9ORF72 in wild type motor neurons leads to reduced motor neuron survival (Shi et al., 2018), suggesting C9ORF72 haploinsufficiency may play a role in motor neuron degeneration in C9-ALS.

In addition to haploinsufficiency, toxic gain of function is likely to play a role in C9-ALS. There are two key unique pathological features of C9-ALS: the RNA repeat expansion (RRE) aggregated into nuclear RNA foci, and dipeptide repeat proteins (DPRs) generated from repeat associated non-ATG translation of RREs (Figure 1) (Mackenzie et al., 2014). A study using a mouse model expressing the C9ORF72 repeat expansion found that toxicity was associated with the production of DPRs but not with the number of RNA foci, suggesting DPRs are a greater source of toxicity (Tran et al., 2015). Five different DPR species have been identified in C9-ALS patient CNS tissues: poly(GA), poly(GP), poly(GR), poly(PA) and poly(PR) (Ash et al., 2013; Mori et al., 2013a; Zu et al., 2013). DPRs generated by translation of the sense RNA transcript (GA and GR) are more abundant than DPRs

produced from the anti-sense transcript (PA and PR), suggesting preferable translation of the sense transcript (Mackenzie et al., 2015), although the reason for this remains unclear. GR, PR and GA DPRs have been shown to induce cell death (Table 2) in motor neurons, pointing to DPRs as possibly contributing to neurodegeneration in C9-ALS (May et al., 2014; Wen et al., 2014).

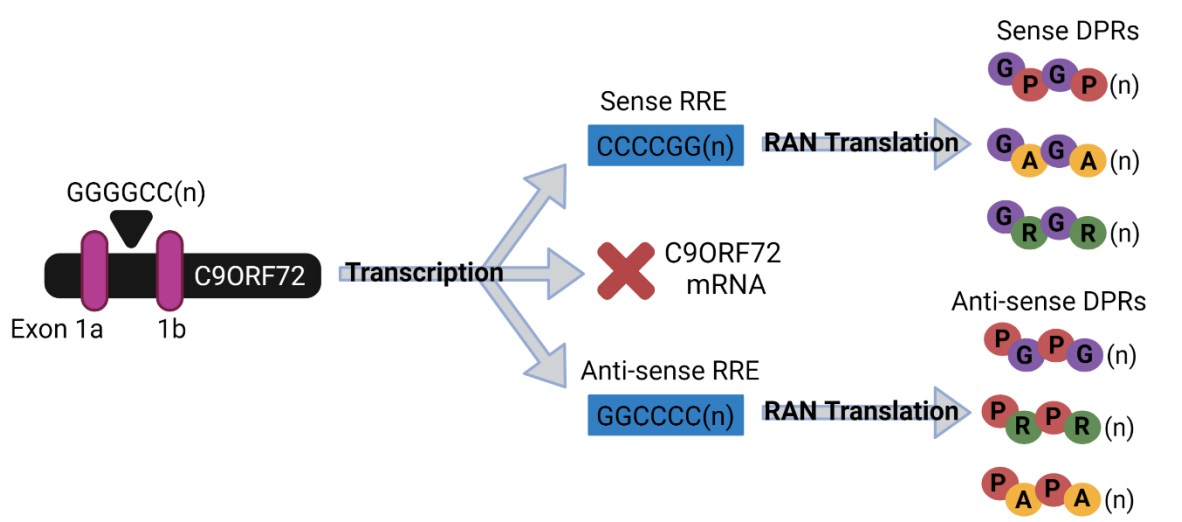

Figure 1. Transcription and translation of the C9ORF72 repeat expansion (created with Biorender.com). The C9ORF72 repeat expansion leads to reduced production of C9ORF72 mRNA. The repeat expansion itself is transcribed in the sense and anti-sense directions to produce a sense and anti-sense RNA repeat expansion (RRE). Both RREs can undergo repeat-associated non-ATG (RAN) translation to produce a total of five species of dipeptide repeat protein (GP, GA, GR, PA, PR). Poly(GP) is produced by translation of both the sense and anti-sense transcripts. RRE = RNA repeat expansion, DPR = dipeptide repeat protein.

Table 2. Summary of DPR properties (from Kok et al., 2021)

DPR Species	Transcript	Toxic to Motor Neurons?	Induces DNA damage?	References
Poly(GA)	Sense	Yes	Yes[1]/No[2]	(May et al., 2014) (Walker et al., 2017)[1] (Lopez-Gonzalez et al., 2016)[2]
Poly(GR)	Sense	Yes	Yes	(Yang et al., 2015) (Lopez-Gonzalez et al., 2016) (Wen et al., 2014) (Farg et al., 2017)
Poly(GP)	Sense and anti-sense	No	Not reported	(May et al., 2014)
Poly(PA)	Anti-sense	No	Not reported	(May et al., 2014)
Poly(PR)	Anti-sense	Yes	Yes	(Yang et al., 2015) (Wen et al., 2014) (Farg et al., 2017)

[1] Walker *et al.*, 2017 showed transfecting cells with poly(GA) led to increased DNA damage, but [2] Lopez-Gonzalez *et al.*, 2016 did not find the same effect. From Kok et al., 2021, title: Summary of DPR properties, creator: Jannigje Kok, copyright information: CC BY 4.0 (https://creativecommons.org/licenses/by/4.0/).

It is unclear why GA, GR and PR are toxic and PA and GP are non-toxic (May et al., 2014; Mizielinska et al., 2014; Wen et al., 2014). GR, PR and GA are the only DPRs that have been shown to have significant protein interactions, while PA and GP are relatively inert (Freibaum and Taylor, 2017). Additionally, the arginine-rich DPRs (GR, PR) are considered highly charged and polar, while GA, GP and PA are uncharged (Freibaum and Taylor, 2017). The exact mechanisms of DPR toxicity in ALS remain to be elucidated, although several mechanisms have been suggested, including: nucleolar dysfunction (Lee et al., 2016; Mizielinska et al., 2017; White et al., 2019), altered splicing (Kwon et al., 2014), impaired nucleocytoplasmic transport (Jovičič et al., 2015), and impaired proteasome function (May et al., 2014). A common mechanism that links GR, PR and GA toxicity, is that all three of these DPRs have been shown to induce DNA damage (Table 2) when transfected into cells (Lopez-Gonzalez et al., 2016; Nihei et al., 2020; Walker et al., 2017).

DPRs are not confined to the cell they have been produced in. Indeed, it has been shown that neurons expressing DPRs can transmit all five DPR species to other neurons and glial cells through exosome-dependent and independent pathways (Chang et al., 2016; Westergard et al., 2016; Zhou et al., 2017). Motor neurons are likely not the only source of DPR transmission as astrocytes can uptake polyGA DPRs by endocytosis and then transmit polyGA to motor neurons (Marchi et al., 2022). Importantly, DPR transmission may lead to some of the commonly observed ALS proteinopathies as cell-to-cell transmission of polyGA has been shown to induce TDP-43 mislocalisation and proteasome dysfunction in receiving cells (Khosravi et al., 2020). Consequently, it has been suggested that blocking DPR transmission may have therapeutic benefit and in fact, anti-polyGA immunisation was found to reduce neuron death, reduce TDP-43 mislocalisation and ultimately prevent motor deficits in a polyGA-expressing mouse model (Zhou et al., 2020).

1.2.3 SOD1-ALS

Mutations in the copper-zinc superoxide dismutase (SOD1) gene were the first identified cause of fALS (Rosen et al., 1993), and remain a common fALS cause worldwide (Zou et al., 2017). The main function of SOD1 is to convert reactive oxygen species (ROS) to oxygen and hydrogen peroxide, but it is also involved in repression of respiration and immunomodulation (Saccon et al., 2013). SOD1 has also been shown to play a role in suppressing inflammation (Hwang et al., 2020), which can be caused or exacerbated by ROS (Ranneh et al., 2017).

SOD1-ALS has been suggested to occur due to loss of SOD1 function as homozygous knockout of SOD1 in mice leads to increased age-related skeletal muscle denervation (Kostrominova, 2010) and

locomotion deficits (Muller et al., 2006). Supporting a loss of function effect, mutant SOD1^{G93A}-expressing mice exhibit increased expression of pro-inflammatory genes (Yoshihara et al., 2002), although interestingly deletion of a pro-inflammatory protein in mutant SOD1^{G93A}-expressing mice did not improve survival and, in fact, accelerated disease onset (Ribon et al., 2021). Notably, overall SOD1 activity is reduced for most SOD1 mutations studied (Saccon et al., 2013), however there are a few notable exceptions, including the G37R mutation where specific SOD1 enzyme activity is increased, suggesting that gain of function may also play a role (Borchelt et al., 1994).

Mutant SOD1 and wild type SOD1 have been observed to aggregate into inclusions, and can misfold under certain conditions, which could reduce SOD1 activity or confer toxicity (Bosco et al., 2010). Other possible gain of function effects include novel protein interactions generated by SOD1 mutations that are not observed with wild type SOD1 (Kunst et al., 1997), mutant SOD1^{G93A}-induced mitochondrial dysfunction (Igoudjil et al., 2011; Pickles et al., 2016), and increased free radical production in SOD1^{G93A} mutants (Pickles et al., 2016; Yim et al., 1996), all of which could lead to increased toxicity. It is therefore possible that both loss and gain of function contribute to SOD1-ALS, however this is likely to vary by mutation type.

1.3 Astrocyte Toxicity in ALS

1.3.1 Astrocytes in Brain Function

Astrocytes are the most abundant cell type in the central nervous system (CNS), and historically have been considered to act as support cells that assist with the function and development of neurons (Figure 2). However, the role of astrocytes in the CNS is now understood to be far broader than initially thought (Ransom and Ransom, 2012).

Classically, astrocytes are known for their function in the support of neurons. Astrocytes use anaerobic glycolysis to convert glycogen to lactate, which is secreted through monocarboxylate transporters (MCTs) and taken up by neurons to be used as an energy substrate (Bouzier-Sore et al., 2002). It has been suggested that astrocyte lactate production is regulated by neural activity through neural secretion of glutamate (Pellerin and Magistretti, 1994). Persistent extracellular glutamate expression has been shown to be toxic to neurons, and a key function of astrocytes is to remove glutamate from the extracellular space (Amin and Pearce, 1997) through the Na^+-dependent excitatory amino acid transporters 1 and 2 (EAAT1, EAAT2) (Schousboe et al., 2004). Glutamate is then metabolised to glutamine and secreted into the extracellular space to be taken up again by neurons (Bröer and Brookes, 2001). Glutamate uptake by astrocytes was shown to

stimulate aerobic glycolysis and lactate production, suggesting an increase in neural activity could consequently lead to an increase in metabolic support provided by astrocytes (Pellerin and Magistretti, 1994).

Glutamate is not the only neurotransmitter taken up by astrocytes, GABA is also taken up by astrocytes through GABA transporters (GAT) (Schousboe et al., 2004). Additionally, astrocytes are capable of exocytosis-mediated glutamate secretion (Bezzi et al., 2004), though the function of astrocyte-secreted glutamate remains unclear, with suggestions that astrocyte-secreted glutamate may synchronise excitatory neuron firing or increase inhibitory activity (Mahmoud et al., 2019).

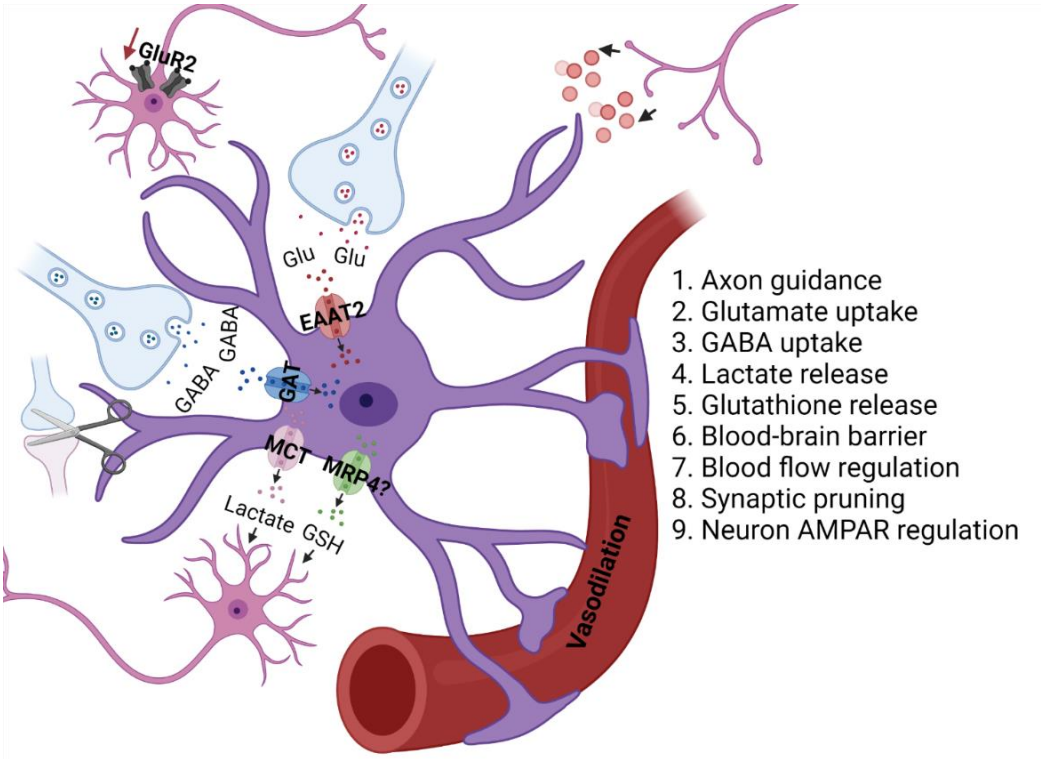

Figure 2. Astrocytes perform numerous functions to support neurons in a healthy central nervous system (created with Biorender.com). Astrocytes contribute to synaptic pruning, can promote axon guidance by secreting molecules that promote or inhibit axon growth, can support neurons through the secretion of lactate and glutathione, and can regulate neuronal AMPA receptor expression. Astrocytes can also prevent toxic accumulation of neurotransmitters by uptake of glutamate and GABA from the extracellular space through the EAAT2 and GAT channels, respectively. Astrocytes also constitute an active part of the blood-brain barrier and can regulate vasoconstriction and dilation in response to changes in neuron activity. EAAT2= excitatory amino acid transporter 2, GABA= gamma-aminobutyric acid, GAT= gamma-aminobutyric acid transporter, Glu= glutamate, GluR2= glutamate ionotropic receptor AMPA type subunit 2, GSH= glutathione, MCT= monocarboxylate transporter, MRP4= multidrug resistance protein 4.

In addition to supporting neuron function, astrocytes have also been shown to influence neurons during development. Similarly to microglia, astrocytes phagocytose excitatory and inhibitory

synapses during development and in adulthood (Chung et al., 2013). Astrocytic synapse pruning can be promoted by increased neural activity and is mediated through the MEGF10 and MERTK pathways, as knockout of either MEGF10 or MERTK leads to reduced astrocyte phagocytic index (Chung et al., 2013). In addition to pruning synapses, astrocytes can also promote excitatory synapse maturation through the secretion of chordin-like 1, which induces an increase in synaptic GluA2 AMPA receptors and represses synaptic plasticity (Blanco-Suarez et al., 2018). Astrocytes can also control neuron axon growth through the secretion of chemoattractive and chemorepulsive molecules (Liesi and Silver, 1988; Wang et al., 2008).

Astrocytes also play important roles in blood-brain barrier maintenance and regulation of blood flow. Astrocytic endfeet contact and surround cerebral vasculature and can promote endothelial cell tight-junction formation (Janzer and Raff, 1987), suggesting an involvement in blood-brain barrier formation and maintenance. Indeed, ablation of astrocytes in adult mice disrupted the integrity of the blood-brain barrier, leading to increased leakage (Heithoff et al., 2021). Through endfeet contact with endothelial cells, astrocytes are also capable of regulating blood flow. Computer modelling suggested astrocytic endfeet could act as a K^+ syphon, transferring K^+ released by active neurons directly to arteriole walls and inducing vasodilation (Paulson and Newman, 1987). However, this has since been disputed as glial depolarisation failed to induce changes in arteriole diameter in the rat retina (Metea et al., 2007). Astrocytes may also regulate blood flow independent of neural activity. Blocking astrocytic calcium signalling or prostaglandin release leads to vasocontriction, suggesting astrocytes induce tonic vasodilation (Rosenegger et al., 2015). Additionally, in response to decreases in cerebral perfusion pressure, astrocyte calcium signalling-dependent mechanisms lead to increases in sympathetic nerve activity and increased heart rate (Marina et al., 2020), thus astrocytes play a number of roles in regulating blood flow.

Notably, astrocytes are not a homogenous group of cells, but display different properties based on regional identity and function. There is heterogeneity between brain regions, with evidence that astrocytes isolated from the mouse cortex or hippocampus show a clear separation in gene expression (Batiuk et al., 2020) and differences in activity-related sodium transients and calcium signalling (Ziemens et al., 2019). There is also diversity within CNS regions. It has been shown that there are differences in astrocyte morphology, gene expression (Lanjakornsiripan et al., 2018) and calcium dynamics (Takata and Hirase, 2008) between layers of the mouse cortex. Similarly, three

subtypes of astrocyte were identified in mouse ventral spinal cord white matter, which differed in terms of positional identity and expression of guidance molecules (Hochstim et al., 2008).

Single-cell RNA sequencing has allowed better elucidation of astrocyte subtypes. One study, using astrocytes isolated from mouse cortex and hippocampus, identified five distinct astrocyte subtypes with differing expression of genes involved in astrocyte functions (synaptogenesis and plasticity, phagocytosis and immune function, neurotransmission, ion and water transport, blood brain barrier maintenance) (Batiuk et al., 2020). Astrocyte subtype 4 had enriched expression of genes associated with neurogenesis and was specific to the hippocampus, while astrocyte subtypes 1, 2 and 3 were common in both the cortex and hippocampus and showed increased expression of genes associated with synaptogenesis, synaptic plasticity and neurotransmission (Batiuk et al., 2020). Astrocyte heterogeneity thus might allow for astrocytes to be specialised for certain functions and be localised to regions those functions are required.

Under healthy conditions, microglia and astrocytes are considered to exist in a resting state but can become activated following injury or infection. Activated astrocytes respond to the insult by increasing proliferation, clearing debris and dead cells by phagocytosis, releasing factors that promote neuron survival, promoting scar formation and participating in blood-brain barrier repair (Liddelow and Barres, 2017). It has been suggested that brain injury induces two distinct astrocyte activation states, termed A1 and A2. A1 astrocytes assume a pro-inflammatory phenotype and are harmful to neurons, whereas A2 astrocytes upregulate neurotrophic factors that promote neuronal survival, however this is likely to be an overly simplistic classification (Liddelow and Barres, 2017).

It is clear that astrocytes play many active and important roles within the CNS, and thus it is perhaps unsurprising that their dysfunction has been linked with several neurodegenerative diseases, including multiple sclerosis, Alzheimer's disease, Parkinson's disease and ALS. Reactive astrogliosis, where astrocytes become activated, rapidly proliferate, and alter their morphology in response to injury or disease (Pekny and Pekna, 2014), is a pathological feature of ALS (Murayama et al., 1991; Schiffer et al., 1996), indicating a key role for astrocytes in ALS pathogenesis.

1.3.2 Astrocyte Toxicity in ALS

The majority of ALS-associated genes encode ubiquitously expressed proteins (key genes summarised in Table 1), suggesting all cells are affected but motor neurons are particularly vulnerable (Taylor et al., 2016). Accordingly, glia from ALS patients, including astrocytes,

oligodendrocytes and microglia, exhibit toxicity to neurons that is not observed in healthy cells suggesting a contribution of non-cell autonomous mechanisms to motor neuron death (Valori et al., 2014).

Astrocyte toxicity in ALS is the best studied of the toxic glia and toxicity appears consistent across sALS and fALS. The first evidence of astrocyte toxicity in ALS came from a SOD1 mouse model which showed delayed disease progression and extended survival when the SOD1 transgene was knocked down selectively in the astrocytes (Yamanaka et al., 2008b). Since then, co-culture studies have shown that astrocytes from sALS, C9ORF72-ALS and SOD1-ALS patients, as well as from SOD1-ALS and FUS-ALS mouse models, induce cell death in healthy motor neurons (Di Giorgio et al., 2008; Haidet-Phillips et al., 2011; Kia et al., 2018; Madill et al., 2017; Marchetto et al., 2008; Nagai et al., 2007; Re et al., 2014). Toxicity to motor neurons has also been observed with ALS induced astrocytes (iAstrocytes), which are generated by direct reprogramming and retain hallmarks of ageing (Gatto et al., 2020; Meyer et al., 2014). ALS astrocyte toxicity is thought to be selective for motor neurons as ALS astrocytes do not induce cell death when co-cultured with GABAergic or dorsal root ganglion neurons (Di Giorgio et al., 2008; Haidet-Phillips et al., 2011; Nagai et al., 2007; Re et al., 2014), suggesting motor neurons are more vulnerable to the insult the astrocytes provide.

1.3.3 Mechanisms of Astrocyte Toxicity

Mechanisms by which ALS astrocyte induce motor neuron death remain unclear (Figure 3). There is evidence that in ALS, astrocytes become less supportive to neurons. ALS astrocytes exhibit downregulation of solute carriers, including solute carrier family 16 member 4 (Slc16a4), which is involved in lactate transport (Ferraiuolo et al., 2011b). Consequently ALS astrocytes secrete less lactate (Ferraiuolo et al., 2011b), resulting in less substrate available for motor neurons to use as a source of energy. Similarly, ALS astrocytes show a reduction in the purine metabolism enzyme, adenosine deaminase (ADA), leading to decreased bioenergetic output (Allen et al., 2019).

In addition to being less supportive to neurons, there is evidence that ALS astrocytes may secrete factors that are actively toxic to neurons. Numerous studies have shown that application of ALS astrocyte conditioned medium alone is sufficient to induce neuron death (Di Giorgio et al., 2008; Haidet-Phillips et al., 2011; Kia et al., 2018; Madill et al., 2017; Nagai et al., 2007; Re et al., 2014), thus secreted factors are likely to play a role. Extracellular vesicles, such as exosomes, may be a vehicle by which toxic factors are taken up by motor neurons, and indeed exosomes isolated from C9-ALS astrocyte conditioned medium were shown to be toxic to healthy motor neurons (Varcianna

et al., 2019). Furthermore, inhibition of soluble N-ethylmaleimide-sensitive factor attachment proteins receptor (SNARE)-dependent exocytosis in astrocytes delayed disease progression in a mouse model of SOD1-ALS (Kawamata et al., 2014).

Exosome toxicity has been attributed to microRNA cargo (Varcianna et al., 2019), however this may be specific to C9-ALS as another study showed no difference in exosome microRNA cargo in SOD1-ALS (Jovičić and Gitler, 2017). Exosomes may also allow transmission of ALS proteinopathy. C9-ALS astrocytes may promote propagation of DPRs as astrocytes have been shown to take up extracellular polyGA DPRs and transmit them to neurons (Marchi et al., 2022). Additionally, SOD1 and TDP-43 protein have been detected in wild type cell conditioned medium exosome fractions (Grad et al., 2014; Iguchi et al., 2016). Indeed, primary astrocytes isolated from mice expressing human $SOD1^{G93A}$ have been found to secrete higher levels of SOD1 and valosin-containing protein (VCP), another ALS-linked protein, than controls, a proportion of which is packaged in exosomes (Basso et al., 2013). On the other hand, recently C9-ALS patient-derived astrocytes were shown to secrete reduced levels of SOD1, as well as other antioxidant proteins, SOD2 and glutathione synthetase (GSS) (Birger et al., 2019). This implicates oxidative stress as a possible cause of astrocyte-induced toxicity. Consequently, C9-ALS astrocytes both exhibited higher levels of ROS and induced an increase in ROS in conditioned medium-treated motor neurons (Birger et al., 2019). Further supporting the suggestion of oxidative stress as a mechanism of toxicity, upregulation of antioxidant pathways by Nrf2 overexpression in SOD1-ALS astrocytes has been shown to rescue toxicity (Vargas et al., 2008).

Oxidative stress can trigger inflammation, and vice versa (Ranneh et al., 2017). Accordingly, ALS astrocytes have also been shown to exhibit altered cytokine release. Tumour necrosis factor-alpha (TNFα) is secreted by FUS-ALS astrocytes and FUS-ALS astrocyte toxicity was partly rescued with the use of TNFα neutralising antibodies (Kia et al., 2018). Interestingly, TNFα stimulates NF-κB signalling and consequently leads to increased expression of major histocompatibility complex class I (MHCI) (Cornel et al., 2020), however SOD1-ALS astrocytes induce a reduction in MHCI in healthy motor neurons when co-cultured (Song et al., 2016). SOD1-ALS astrocytes express major histocompatibility complex class I inhibitory receptors at higher levels than control astrocytes, and overexpressing MHCI $H2\text{-}K^{b}$ molecules in motor neurons protected them from the astrocyte-induced cell death (Song et al., 2016).

Inorganic polyphosphate (polyP), which is known to activate the pro-inflammatory NF-κB pathway (Hassanian et al., 2017), was found to be present in and secreted by ALS astrocyte expressing SOD1, TARDBP or C9ORF72 mutations (Arredondo et al., 2022). Further evidence supporting a role for inflammation in ALS astrocyte toxicity is that blockade or knockdown of the gap junction protein, connexin-43 (Cx43), which has previously been demonstrated to reduce inflammation in models of demyelinating injury and spinal cord injury (Cronin et al., 2008; Li et al., 2020), has been shown to reduce sALS and fALS astrocyte toxicity to motor neurons (Almad et al., 2022). Additionally, Cx43 blockade reduced astrogliosis, reduced motor neuron degeneration and slowed disease progression in a $SOD1^{G93A}$ mouse model (Almad et al., 2022).

Pro-inflammatory cytokines, including TNFα, can trigger astrocyte secretion of nerve growth factor (NGF) (Gadient et al., 1990; Kuno et al., 2006). Notably, astrocytes derived from a $SOD1^{G93A}$ mouse model secrete increased levels of NGF, and NGF depletion from conditioned medium reduced toxicity to motor neurons (Ferraiuolo et al., 2011b). NGF binds the p75 neurotrophic receptor (p75NTR), expression of which is increased in motor neurons co-cultured with $SOD1^{G93A}$ mouse astrocytes, and toxicity could be rescued by with a p75NTR inhibiting antibody (Ferraiuolo et al., 2011b).

Inflammation can trigger activation of astrocytes to a reactive state. Indeed, wild type reactive astrocytes have been shown to exhibit similar toxicity to motor neurons as ALS astrocytes (Tripathi et al., 2017). It was suggested that wild type reactive astrocyte toxicity was mediated through increased secretion of the cytokine transforming growth factor beta 1 (TGFβ1) (Tripathi et al., 2017). On the other hand, another study has suggested reactive astrocyte toxicity to neurons is mediated through secretion of saturated lipids (saturated long chain free fatty acids and very-long-chain fatty acid acyl chains) (Guttenplan et al., 2021). Of course, wild-type reactive astrocytes are not a direct model of ALS, so it remains to be determined whether increased secretion of these factors occurs in ALS astrocytes.

Notably, TGFβ1 secretion by reactive astrocytes was shown to induce protein aggregation similar to that observed in ALS, including aggregation of TDP-43, SOD1, p62, ubiquitin, phosphorylated neurofilament H (pNF-H) and even Tau (Tripathi et al., 2017). It was shown that reactive astrocytes could induce autophagy defects in motor neurons through activation of the mTOR pathway (Tripathi et al., 2017). Similarly, C9-ALS astrocyte conditioned medium has also been shown to induce autophagy defects in motor neurons, including p62 accumulation and LC3-II reduction,

leading to increased expression of SOD1 but not TDP-43 (Madill et al., 2017). Interestingly, activation of autophagy in these cells rescued accumulation of p62 but not SOD1 (Madill et al., 2017). These results suggest autophagy may be another pathway by which ALS astrocyte exert toxicity.

In addition to loss of astrocytic support, oxidative stress, inflammation and autophagy, recent work has started to suggest DNA damage may play a role in ALS astrocyte toxicity. Preliminary unpublished data from the Ferraiuolo lab have shown that treating healthy mouse motor neurons with conditioned medium derived from C9-ALS astrocytes induced an increase in cells positive for γH2AX, a marker of DNA damage response activation, suggesting C9-ALS iAstrocyte conditioned media is capable of inducing DNA damage, implicating another possible mechanism by which ALS astrocytes induce motor neuron death.

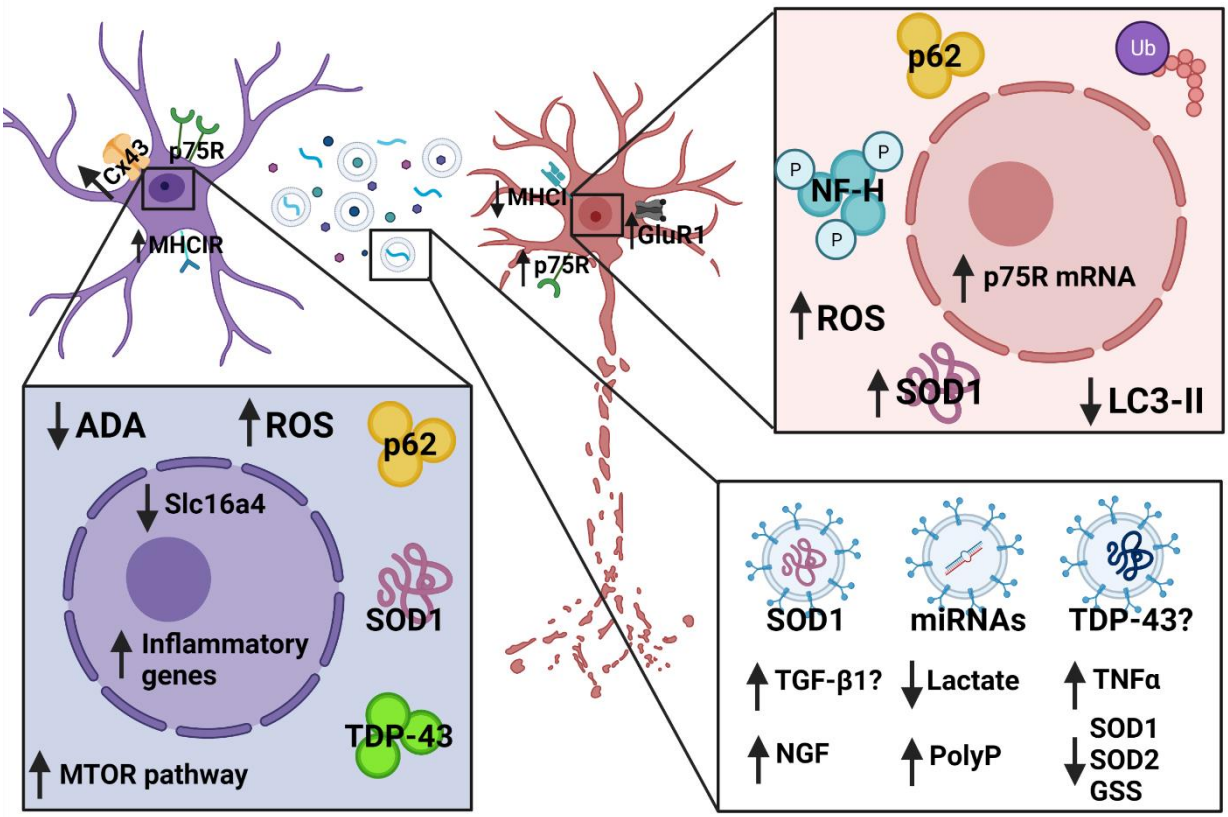

Figure 3. Mechanisms of astrocyte toxicity in ALS (created with Biorender.com). ALS astrocytes exhibit changes in gene and protein expression compared to control astrocytes. ALS astrocytes have been observed to have changes in secreted proteins, some of which are packaged in extracellular vesicles. The exact cause of motor neuron death remains unclear, but ALS astrocytes are known to have effects on various pathways in motor neurons. ADA= adenosine deaminase, Cx43= connexin 43, GluR1= Glutamate ionotropic receptor AMPA type subunit 1, GSS= glutathione synthetase, MHCI= major histocompatibility complex class I, miRNA- microRNA, MTOR= mammalian target of rapamycin, NF-H= neurofilament heavy, NGF= nerve growth factor, p75R= p75 neurotrophin

receptor, PolyP= inorganic phosphate, ROS= reactive oxygen species, SOD= superoxide dismutase, TDP-43= transactive response DNA binding protein 43 kDa, TGFβ1= transforming growth factor β1, TNFα= tumour necrosis factor α, Ub= ubiquitin.

1.4 DNA Damage and Repair

1.4.1 DNA Damage

DNA damage is defined as any modification to DNA that affects transcription or replication, or that leads to alteration in the DNA base code. DNA damage occurs commonly in cells, with each cell estimated to suffer 10^4-10^5 DNA lesions per day. If left unrepaired DNA lesions can lead to cell death, normally through p53-mediated transcription of pro-apoptotic factors (Giglia-Mari et al., 2011). DNA damage can occur naturally as an intermediate step during transcription or DNA repair, or occur aberrantly in these processes, and DNA damage can also be induced by harmful genotoxic agents (Kazak et al., 2012). Examples of DNA damage (Figure 4) include DNA double and single-stranded breaks, oxidation or deamination of DNA bases, and DNA base insertion, deletion or substitutions (Jackson and Bartek, 2009).

Methods of detecting oxidative DNA damage usually involve assays for oxidised versions of deoxyguanosine. Oxidation of deoxyguanosine leads to the generation of two interconverting tautomers: 8-hydroxy-2-deoxyguanosine (8-OHdG) and 8-oxo-2-deoxyguanosine (8-oxodG) (Valavanidis et al., 2009). Studies of oxidative DNA damage in ALS often use the tautomer names interchangeably as though they refer to the same compound (Barbosa et al., 2010; Mitsumoto et al., 2008). Similarly, two companies supply the oxidative DNA damage antibody clone 15A3 (Abcam: ab62623, SantaCruz: sc-66036) however one company states it binds 8-oxodG, whereas the other states it binds 8-OHdG. To avoid confusion 8-OHdG and 8-oxodG will both be referred to as oxidised deoxyguanosine (OdG) in this thesis.

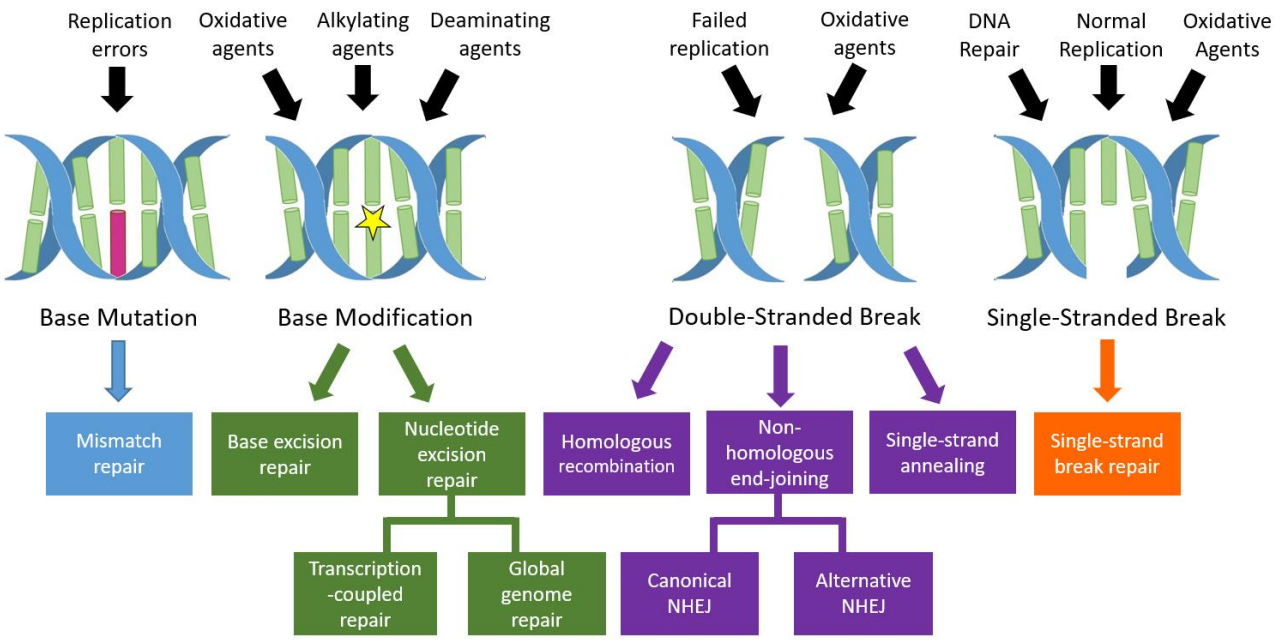

Figure 4. DNA damage repair pathways (from Kok et al., 2021). There are several different types of DNA damage that can occur, which can be induced by endogenous or exogenous genotoxins or can occur aberrantly or as an intermediate step in a cellular pathway. Different types of DNA damage will be repaired by different repair pathways. NHEJ= non-homologous end joining. From Kok et al., 2021, title: DNA damage and related repair pathways, creator: Jannigje Kok, copyright information: CC BY 4.0 (https://creativecommons.org/licenses/by/4.0/).

1.4.2 DNA Damage Response

Following the detection of DNA damage, cells activate the DNA damage response (DDR) which is a signal transduction pathway (Figure 5) that ultimately leads to either DNA repair or apoptosis. Several factors have been identified which directly bind DNA following DNA damage, each of which typically responds to one or more types of DNA damage and leads to activation of a specific DNA repair pathway. The first step in this process is the activation of master DNA repair kinases, which include ataxia telangiectasia mutated (ATM) and ATM and Rad3 related (ATR). These master repair kinases induce a phosphorylation cascade that activates effector proteins involved in cell cycle arrest, chromatin remodelling, DNA repair, and apoptosis (Jackson and Bartek, 2009). Histone H2AX phosphorylation (γH2AX) commonly occurs following DNA damage and is thought to act as a docking site for DDR signalling and DNA repair, as several DDR components co-localise with γH2AX foci. γH2AX is thus commonly used as a marker of DNA strand breaks and DDR activation (Giglia-Mari et al., 2011).

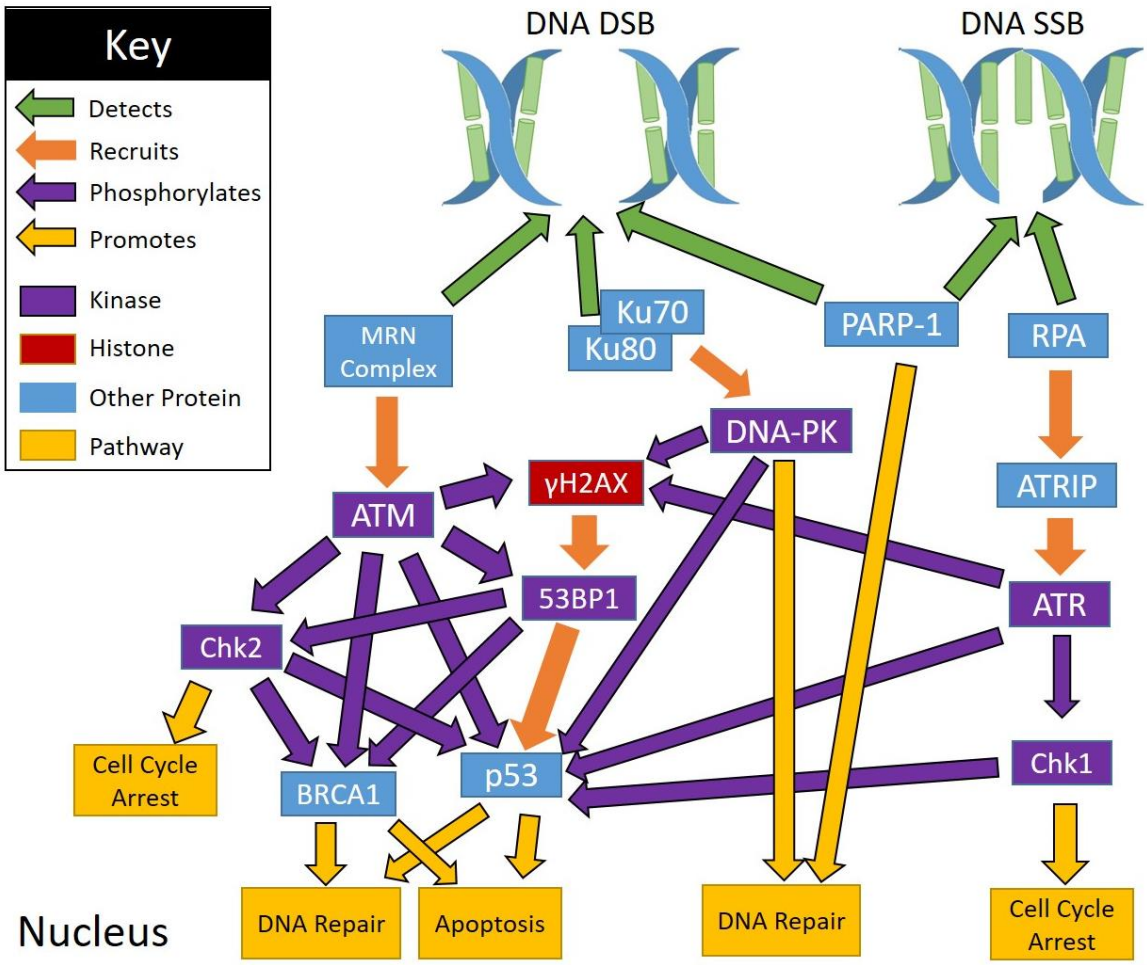

Figure 5. Schematic showing simplified DNA damage response (created with Microsoft PowerPoint). DNA damage is detected by DNA damage sensors (MRN, Ku70/Ku80, PARP1, RPA) which activate master DNA repair kinases (ATM, ATR). The repair kinases phosphorylate several targets to activate cellular pathways involved in cell cycle arrest, apoptosis and DNA repair.

1.4.3 DNA Double-Strand Break Repair

DNA double-strand breaks are serious DNA lesions that if left unrepaired can lead to genetic instability through chromosome fragmentation, deletions and translocations. There are three main pathways through which double-strand breaks are repaired: homologous recombination (HR), non-homologous end-joining (NHEJ) and single-strand annealing (SSA) (SSA is beyond the scope of this study and will not be discussed further). Notably, NHEJ can occur by two different mechanisms, referred to as canonical NHEJ (c-NHEJ) and alternative NHEJ (alt-NHEJ) (Chang et al., 2017). HR is considered to be less error-prone than NHEJ as it utilises the undamaged homologue to retrieve the sequence information for repair whereas NHEJ only involves the damaged homologue. Due to the requirement of a sister chromatid, HR repair is restricted to the S and G2 phases of the cell cycle whereas canonical NHEJ (c-NHEJ) can take place at any time (Jasin and Rothstein, 2013). C-NHEJ involves recognition of DNA double-strand breaks by the Ku70/Ku80 heterodimer, which binds the

DNA ends and recruits the DNA protein kinase catalytic subunit (DNA-PKcs) to form the DNA-PK complex. The DNA-PK complex recruits c-NHEJ factors including Artemis, polymerases and a ligase complex composed of XRCC4, XLF and DNA ligase IV which acts to directly ligate the DNA double-strand break ends (Lieber, 2010).

HR is a more complicated process that begins when DNA double-strand breaks are recognised and bound by the MRE11–RAD50–NBS1 (MRN) complex (Gnügge and Symington, 2021). Poly(ADP-ribose) polymerase 1 (PARP1), which can directly bind DNA at single-strand and double-strand break sites and which plays a number of roles in different DNA repair processes, has been suggested to help recruit the MRN complex to sites of double-strand breaks (Ray Chaudhuri and Nussenzweig, 2017). The MRN complex recruits CtIP and ATM. CtIP is phosphorylated in a cyclin-dependent kinase (CDK)-dependent manner and recruits BRCA1, which is phosphorylated by ATM. CtIP and the MRN complex act together to promote DNA end resection, a process where the DNA 5' strands undergo nucleolytic degradation to leave a 3' single-stranded DNA (ssDNA) overhang on either side of the DNA double strand break (Gnügge and Symington, 2021). The 3' ssDNA ends are rapidly coated with RPA molecules (primarily associated with single-strand break repair), which are displaced by Rad51 with the assistance of mediator proteins (Rad52, BRCA2) (Jasin and Rothstein, 2013). DNA-bound Rad51 facilitates the invasion of the 3' ssDNA into the unaffected sister chromatid DNA duplex where the ssDNA binds through sequence homology, forming a D-loop. Rad51 then dissociates to expose the 3'-end of the damaged ssDNA and DNA synthesis proceeds and is resolved through at least three possible pathways, which will not be discussed here (Krejci et al., 2012). Alt-NHEJ (also referred to as microhomology-mediated end joining or MMEJ) similarly to HR repair, begins with the MRN complex binding DNA ends and requires CtIP-dependent DNA end resection. The pathways then diverge as alt-NHEJ requires PARP1, DNA polymerase θ, DNA ligase 1 and DNA ligase 3 to promote microhomology annealing (Han and Huang, 2019).

DNA end resection is critical for DNA repair pathway choice and is regulated by 53BP1 and BRCA1 which are mutually antagonistic. When activated ATM phosphorylates H2AX at damaged chromatin to form γH2AX. γH2AX formation leads to a series of recruitment and phosphorylation events that result in the recruitment of the E3 ubiquitin ligase proteins RNF8 and RNF168 which ubiquitinate damaged chromatin at several sites (van Attikum and Gasser, 2009). Ubiquitination of lysine 15 of H2A/H2AX by RNF168 is necessary, along with monomethylation or dimethylation of lysine 20 of histone H4 for the recruitment of 53BP1 to DNA double-strand breaks (Panier and Boulton, 2013).

53BP1 recruits effector proteins RIF1 and PTIP and it is thought that the presence of chromatin-bound 53BP1-RIF1 prevents recruitment of BRCA1 to MRN-bound CtIP and thus prevents DNA end resection, pushing DNA repair towards the NHEJ pathway rather than HR (Panier and Boulton, 2013). Conversely, BRCA1 in association with CtIP has been suggested to remove 53BP1-RIF1 from chromatin and thus push repair towards HR (Chapman et al., 2012).

1.4.4 DNA Single-Strand Break Repair

DNA single-strand breaks can occur due to genotoxic insult but are also a necessary intermediate step in several processes including transcription, replication and certain DNA repair pathways (Abbotts and Wilson, 2017). Base excision repair (BER) is a repair pathway used for small deoxynucleotide lesions such as base deamination and oxidisation or alkylation of deoxynucleotides, which involves a single-strand break as an intermediate step. BER begins with recognition of the DNA lesion by a specific glycosylase, for example OGG1 recognises OdG lesions and excises the damaged base leaving an abasic site (AP site). APE1 recognises AP sites and induces a nick in the DNA backbone at the AP site to create a single-strand break (Parsons and Dianov, 2013), and in the absence of APE1 this function can also be performed by APE2 (Lin et al., 2021). Single-strand breaks can be recognised and bound by PARP1, which binds XRCC1 to act as a scaffold for factors that repair the break. The missing nucleotide is replaced by DNA polymerase β and the DNA nick is ligated by DNA ligase 1 or DNA ligase 3 (Abbotts and Wilson, 2017).

Single-strand breaks can also result from topoisomerase 1 (TOPO1) activity. TOPO1 makes ssDNA nicks to relax supercoiled DNA for replication or transcription and normally religates the nick, however this process can be interrupted resulting in a single-strand break and a TOPO1:DNA cleavage complex (TOP1cc) (Chowdhuri and Das, 2021). TOP1ccs are cleaved and removed by TDP1 (Zaksauskaite et al., 2021), which is recruited and activated by PARP1. PARP1 covalently links poly(ADP-ribose) (PAR) polymers onto itself and its target proteins, including TDP1, in a process called PARylation which can facilitate recruitment to DNA damage sites (Ray Chaudhuri and Nussenzweig, 2017). The PARP1:TDP1 complex can then recruit XRCC1 to the break site, and then, as before, lead to recruitment of single-strand break repair factors and repair of the single-strand break (Chowdhuri and Das, 2021).

1.5 DNA Damage and ALS

1.5.1 sALS and DNA Damage

The first studies reporting DNA damage in ALS found increased levels of OdG, indicative of oxidative DNA damage, in sALS patient post-mortem spinal cord and motor cortex, but not in the parietal cortex or cerebellum, suggesting DNA damage in ALS is specific to regions where motor neurons degenerate (Ferrante et al., 1997; Fitzmaurice et al., 1996). DNA damage is not unique to end stage of disease as increased levels of OdG have been observed in the cerebrospinal fluid (CSF), urine, blood plasma and blood serum of living sALS patients (Blasco et al., 2017; Bogdanov et al., 2000; Ihara et al., 2005; Mitsumoto et al., 2008; Murata et al., 2008). Levels of DNA damage have been suggested to relate to clinical measures of disease. In one study, urine OdG levels over time correlated negatively with two measures of ALS disease progression (Bogdanov et al., 2000), however this could not be replicated (Mitsumoto et al., 2008). Similarly, another study showed that CSF OdG levels positively correlated with disease duration at time of sampling but did not correlate with disease score (Murata et al., 2008). It is possible that DNA damage may accumulate over time with ALS, but this does not reflect disease progression.

Both ALS incidence and DNA damage levels have been shown to increase with age (Alonso et al., 2009; Bogdanov et al., 2000), while DNA repair efficiency decreases in ALS and with age (Gorbunova et al., 2007). If DNA damage is a mechanism by which ALS can occur, it may be that unexplained sALS cases arise due to age-related accumulation of DNA damage in motor neurons. Notably, smoking and exposure to chemicals, pesticides and metals, are all potential sources of genotoxic agents and have been suggested as risk factors for developing ALS (Ingre et al., 2015). Motor neurons are post-mitotic and are not capable of self-renewal, thus if DNA damage accumulates in these cells, either by chance accumulation over time or due to exposure to genotoxins, and is not repaired, this could lead to motor neuron degeneration in sALS. Interestingly, samples of mitotic cells like bone marrow mesenchymal stem cells and whole blood (containing peripheral blood mononuclear cells) do not exhibit increases in DNA damage in sALS (De Benedetti et al., 2017; Wald-Altman et al., 2017), possibly because mitotic cells are more capable of repairing DNA. Mitotic status may therefore affect DNA damage in ALS and explain motor neuron vulnerability.

1.5.2 C9ORF72 and DNA Damage

Several studies have shown DNA damage to be a consistent feature of C9ORF72-ALS. γH2AX expression is increased in C9ORF72-ALS patient post-mortem spinal cord tissue and iPSC-derived

motor neurons, from which we can infer increased DNA double-strand breaks (Farg et al., 2017; Higelin et al., 2018; Lopez-Gonzalez et al., 2016; Walker et al., 2017). Additionally, the number of strand breaks has been shown to increase with age in C9ORF72-ALS iPSC-derived motor neurons (Lopez-Gonzalez et al., 2016), however this could not be replicated (Higelin et al., 2018), possibly due to the comparatively low motor neuron purity and fewer cell lines in the latter study. Viral expression of C9ORF72-ALS RREs or certain DPRs (Table 2) in neuronal cells is sufficient to induce DNA strand breaks and increased γH2AX levels (Farg et al., 2017; Lopez-Gonzalez et al., 2016), indicating DNA damage in C9ORF72-ALS could be caused by RREs or DPRs.

1.5.3 SOD1 and DNA Damage

As SOD1 is involved in resolving ROS, a number of studies have investigated oxidative DNA damage in SOD1-ALS with mixed results. Increased OdG levels have been observed in the CSF of SOD1-ALS patients (Bogdanov et al., 2000; Ihara et al., 2005), however motor cortex OdG levels were reduced in SOD1-ALS patients (Ferrante et al., 1997). Contrastingly, in $SOD1^{G93A}$ mouse models increased OdG levels have been observed in the spinal cord, frontal cortex and the striatum, but not the cerebellum which is spared from neurodegeneration (Aguirre et al., 2005; Fang et al., 2010; Warita et al., 2001). On the other hand, another study found no difference in spinal cord tissue DNA double-strand breaks or single-strand breaks in adult $SOD1^{G93A}$ mice, or γH2AX staining in co-cultured embryonic $SOD1^{G93A}$ mouse motor neurons and astrocytes (Penndorf et al., 2017). Penndorf *et al.* (2017) suggested the disparity was due to the other groups' use of lumbar spinal cord which exhibits more cell death, however DNA damage was observed prior to morphological changes (Warita et al., 2001), which could suggest DNA damage is a cause of motor neuron degeneration, rather than a consequence of DNA cleavage in apoptosis (Bortner et al., 1995). DNA damage in $SOD1^{G93A}$ mice was suggested to be primarily mitochondrial in one study (Warita et al., 2001), however nuclear DNA damage has also been identified (Aguirre et al., 2005). Contrasting results could be due to differences in the strain or background of the $SOD1^{G93A}$ models used, which has been shown to affect disease onset and progression (Mancuso et al., 2012).

1.6 In Vitro Models of ALS

1.6.1 Historically

Historically, ALS has been studied using peripheral samples from ALS patients (urine, blood, cerebrospinal fluid), post-mortem tissue and animal models. Post-mortem tissue and animal models were the only methods through which to examine motor neurons and other cells involved

in ALS, although the fixed and end-stage of disease nature of post-mortem tissue limited possible findings (Turner et al., 2013). Thus, mouse models were one of the primary tools through which to study ALS and the interaction between cell types. However, mouse studies are inherently limited by species differences and confined to modelling specific known genetic causes of ALS and cannot be used to model sALS where the cause remains unclear (Van Damme et al., 2017). With the dawn of reprogramming technology, the field of ALS research has benefited from an ability to model a broader spectrum of the disease.

1.6.2 Induced Pluripotent Stem Cells

In 2006, Takahashi and Yamanaka were the first to describe generating induced pluripotent stem cells (iPSCs) from adult mouse fibroblasts (Takahashi and Yamanaka, 2006) and in 2007 this was replicated with adult human fibroblasts (Takahashi et al., 2007). The potential of this technology was an introduction of a non-invasive method of generating specific cell populations from patients, thus posing an alternative to animal models. In 2008, the first iPSCs derived from an ALS patient carrying a SOD1 mutation were generated and successfully differentiated into motor neurons (Dimos et al., 2008). Since then, motor neurons and a number of other cell types including astrocytes (Serio et al., 2013) have been generated from patient-derived iPSCs with different ALS backgrounds (Richard and Maragakis, 2015).

There are several advantages of using iPSCs to model ALS over other methods. iPSCs can be generated from any patient, allowing disease modelling of rare genetic variants of ALS and modelling of sALS, which cannot be modelled in animal models because often the cause of disease is unknown (Van Damme et al., 2017). Once iPSCs have been generated, they can be differentiated into any cell type of interest, which for ALS is of great importance as motor neurons are not the only affected cell type. Glial cells, including astrocyte and microglia, are affected in ALS (Nagai et al., 2007; Valori et al., 2014) and can be generated from iPSCs and then co-cultured with motor neurons to allow study of the interaction between neurons and glia (Madill et al., 2017; Zhao et al., 2020).

There are also, however, several disadvantages of using iPSC-derived cells to study ALS and other diseases. iPSC reprogramming involves an epigenetic ‘reset’, resulting in cells that epigenetically resemble embryonic stem cells (ESCs), with increased histone acetylation and methylation, compared to the original cell population (Mattout et al., 2011). This consequently affects the ageing features of the reprogrammed cells. Cells differentiated from iPSCs have been reported to exhibit

an immature, embryonic-like phenotype compared to non-reprogrammed cells (Koivumäki et al., 2018). Additionally, while iPSCs can be reprogramed from any patient's fibroblasts, iPSCs derived from elderly donors exhibit longer telomere length, less nuclear morphology abnormalities, reduced DNA damage and reduced expression of senescence markers compared to the non-reprogrammed parental cells (Lapasset et al., 2011; Tang et al., 2017), indicating a loss of age-related features. As ALS is an ageing-related disease, where ALS incidence increases with age (Alonso et al., 2009), iPSC-derived cells may not recapture all features of the disease.

1.6.3 Induced Neuronal Progenitor Cells

One method of overcoming the limitations of using iPSCs is using direct reprogramming. Direct reprogramming converts fibroblasts (or any other cell) to the desired cell of interest without going through the iPSC stage and thus avoiding the epigenetic reset (Wang et al., 2021). Indeed, direct reprogramming has been shown to retain age-related nuclear morphology abnormalities, DNA damage levels and telomere shortening, when converting aged fibroblasts to motor neurons (Tang et al., 2017). There are however some disadvantages to using this method. Motor neurons are post-mitotic by nature, and thus directly reprogrammed neurons represent a population of cells that cannot be further expanded. It is possible to overcome this by directly converting to an expandable progenitor cell type, such as neuronal progenitor cells (NPCs). Indeed, a method has been described through which to obtain induced NPCs (iNPCs) from ALS patient fibroblasts (Meyer et al., 2014). These iNPCs retain their ageing features and can be differentiated into three different cell types: induced astrocytes (iAstrocytes), induced oligodendrocytes and induced neurons (iNeurons). iAstrocytes have previously been characterised and found to retain much of their ageing phenotype including reduced telomere length, increased nuclear morphology abnormalities and increased DNA damage (Gatto et al., 2020).

There are, however, limitations to this model of astrocytes. iAstrocytes express Hox9 (unpublished data from the Ferraiuolo lab), indicating lumbar specification (Rux and Wellik, 2017), but beyond this it is unclear whether iAstrocytes represent any particular astrocyte subgroup. It is now well understood that astrocytes are a diverse cell type, with differences in morphology, expression and function both within and between CNS regions (see 1.3.1). Furthermore, it has been shown that in mutant $SOD1^{G93A}$-expressing mice, cortical astrocytes and spinal astrocytes show distinct but differing dysfunctional phenotypes compared to controls (Gomes et al., 2020). Thus, it is a potential concern that iAstrocytes may not capture any or all disease relevant astrocyte populations.

1.7 Summary

ALS is a fatal neurodegenerative disease, which primarily affects motor neurons, however the cause of motor neuron degeneration remains unclear (Ferraiuolo et al., 2011a). Non-cell autonomous mechanisms have been suggested to contribute to motor neuron death in ALS, particularly astrocytes as ALS astrocytes have consistently been shown to be toxic to healthy motor neurons (Haidet-Phillips et al., 2011), with the exception of TARDBP-ALS astrocytes, where the data are controversial (Serio et al., 2013; Tong et al., 2013). Preliminary unpublished data from the Ferraiuolo and El-Khamisy labs has suggested astrocytes from ALS patients with a repeat expansion in the C9ORF72 gene can induce DNA damage in motor neurons, which could explain astrocyte toxicity in ALS. Increased DNA damage has been a well-established feature of sALS, C9ORF72-ALS and SOD1-ALS (Farg et al., 2017; Ferrante et al., 1997; Fitzmaurice et al., 1996; Lopez-Gonzalez et al., 2016; Walker et al., 2017). Current evidence suggests a cell autonomous increase in DNA damage in ALS motor neurons (Lopez-Gonzalez et al., 2016; Walker et al., 2017), however it is possible that these effects are exacerbated by toxic astrocytes, leading to motor neuron degeneration.

1.8 Hypothesis, Aims and Objectives

In this study I hypothesised that astrocyte induced DNA damage contributes to motor neuron death in ALS. To address this hypothesis, I aim to characterise the levels and types of DNA damage induced by ALS astrocytes, determine possible mechanisms through which ALS astrocytes induce DNA damage, and target identified pathways with compounds to see if we can rescue ALS astrocyte toxicity.

To model astrocyte toxicity in ALS, I will be using induced astrocytes (iAstrocytes) generated through a method of direct reprogramming (Meyer et al., 2014). ALS astrocytes produced in this manner have been shown to be toxic to motor neurons (Meyer et al., 2014) and also maintain their aged phenotype (Gatto et al., 2020). I will be using directly reprogrammed astrocytes rather than cells generated more conventionally through iPSC reprogramming because iPSC reprogramming has been shown to reset certain features of cells including DNA damage, which does not occur during direct reprogramming (Tang et al., 2017).

Induced neural progenitor cell (iNPC) lines were previously established in the lab using skin fibroblasts obtained from healthy donors and ALS patients with different causes of disease (sALS, C9ORF72-ALS and SOD1-ALS) according to an established protocol (Meyer et al., 2014). iNPCs will

be differentiated into iAstrocytes as previously described (Meyer et al., 2014), and I will characterise DNA damage in control and ALS iAstrocytes using immunocytochemistry and the comet assay to assess DNA strand breaks and oxidative DNA damage.

To assess the effects of ALS astrocytes on motor neurons, I will differentiate motor neurons from human iPSCs using an established protocol (Du et al., 2015). As I am primarily interrogating the effects of the ALS astrocytes themselves, it is not as important for the motor neurons to retain their ageing phenotype as for the astrocytes. Astrocyte toxicity has been shown to occur through secreted factors (Haidet-Phillips et al., 2011), thus I will model ALS astrocyte toxicity by treating motor neurons derived from healthy donors with control or ALS iAstrocyte conditioned media for a set period of time. I will use motor neurons derived from healthy donors rather than motor neurons derived from ALS patients as this will allow us to isolate and identify the effects of the ALS astrocytes themselves rather than the diseased motor neuron response.

Various assays will be run on the treated motor neurons to characterise levels and types of DNA damage, as well as activation of the DNA damage response. As with characterisation of the ALS iAstrocytes, this will involve immunocytochemistry and Western blotting assays to examine the expression, foci formation and localisation of various markers. I will also run more specific assays, such as the comet assay, to directly assess DNA strand breaks and specific types of DNA damage. Finally, I will attempt to identify the mechanisms through which ALS astrocytes induce DNA damage in motor neurons, whether this occurs through the secretion of genotoxic molecules by the ALS astrocytes or through secretion of molecules that impair motor neuron DNA damage response.

Chapter 2: Materials and Methods

2.1 Materials

2.1.1 Cell Lines

Induced pluripotent stem cell (iPSC) lines were obtained or purchased from various sources (Table 3). Induced neuronal progenitor cell (iNPC) lines (Table 4) were previously reprogrammed from control and patient fibroblasts obtained from skin biopsies according to an established protocol (Meyer et al., 2014). Skin biopsy donors provided informed consent prior to collection of biopsies under study number STH16573, research committee reference 12/YH/0330.

Table 3. Information on iPSC cell lines.

Cell Line	Diagnosis	ALS Genotype	Sex	Age at Collection (years)	Source
CS01	Healthy	-	Male	6	Cedars-Sinai
CS14[1]	Healthy	-	Female	30-35	Cedars-Sinai
GM23338	Healthy	-	Male	55	Coriell Institute
MIFF1[2]	Healthy	-	Male	Fetal	University of Sheffield
ALS 28	ALS	C9ORF72	Male	47	Cedars-Sinai
ALS 29	ALS	C9ORF72	Male	47	Cedars-Sinai
ALS 52[1]	ALS	C9ORF72	Male	49	Cedars-Sinai
Isogenic 29	N/A	C9ORF72 Corrected	Male	47	Cedars-Sinai
Isogenic 52	N/A	C9ORF72 Corrected	Male	49	Cedars-Sinai

[1] CS14 and ALS 52 lines are also available as iNPCs. [2] MIFF1 (Desmarais et al., 2016) was kindly provided by Professor Peter Andrews and Dr Ivana Barbaric (Centre for Stem Cell Biology, University of Sheffield).

Table 4. Information on iNPC cell lines.

Cell Line	Diagnosis	ALS Genotype	Sex	Age at Collection (years)	Source	Onset to Death (months)
AG8620[1]	Healthy	-	Female	64	Coriell Institute	-
CS14[2]	Healthy	-	Female	30-35	University of Sheffield	-
155	Healthy	-	Male	40	University of Sheffield	-
161	Healthy	-	Male	31	University of Sheffield	-
3050	Healthy	-	Male	55	University of Sheffield	-

52[2]	ALS	C9ORF72	Male	49	University of Sheffield	NA
78	ALS	C9ORF72	Male	66	University of Sheffield	31.7
183	ALS	C9ORF72	Male	50	University of Sheffield	27
201	ALS	C9ORF72	Female	66	University of Sheffield	19.4
009	ALS	sALS	Female	61	Ohio State University	21
12	ALS	sALS	Male	29	Ohio State University	72
17	ALS	sALS	Male	47	Ohio State University	90
ND29509	ALS	SOD1 (D90A)[3]	Male	56	Coriell Institute	Collected at death
100	ALS	SOD1 (A4V)	Female	63	Ohio State University	NA
102	ALS	SOD1 (A4V)	Female	40	Ohio State University	NA

[1] Control AG08620 fibroblast line was purchased from the Coriell Institute biobank under material transfer agreement. [2] Control CS14 and C9-ALS 52 were purchased as fibroblasts from Cedars-Sinai and converted to iNPCs at the University of Sheffield. [3] The D90A mutation is heterozygous. NA: Information not available.

2.1.2 Cell Culture Reagents

Table 5. Cell culture reagents.

Reagent	Purpose	Supplier	Catalogue Number
DMSO	Freezing cells	Sigma	D2650-100mL
Penicillin/Streptomycin	Medium	Lonza	DE17-603E
DMEM	Medium	Gibco	11520416
Foetal bovine serum (FBS)	Medium	Life Science Production	5-001A-H1-BR
KnockOut™ serum replacement	Medium	Gibco	11520366
Phenol red free neurobasal media	Medium	Gibco	12348017
Dickkopf related protein 1 (DKK1)	Medium	Peprotech	120-30
Sonic hedgehog (SHH)	Medium	Peprotech	100-45
DMEM/F12 GlutaMAX™	Medium	Gibco	11524436
FGF-2	Medium	Peprotech	100-18B
KnockOut DMEM/F12	Medium	Gibco	12660012
N-2 supplement	Medium	Gibco	15410294
B-27 supplement	Medium	Gibco	11530536
mTeSR™-Plus™ Medium	Medium	StemCell Technologies	05825
Ciliary neurotrophic factor (CNTF)	Medium	Peprotech	450-13
Compound-E	Medium	Tocris	6476
Insulin-like growth factor 1 (IGF1)	Medium	Peprotech	100-11

Brain derived neurotrophic factor (BDNF)	Medium	Peprotech	AF-450-02
Neurobasal media	Medium	Gibco	11570556
CHIR 99021	Medium	Merck Millipore	SML1046-25MG
DMH-1	Medium	Merck Millipore	D8946-25MG
SB 431542	Medium	Peprotech	3014193
Valproic acid (VPA)	Medium	Merck Millipore	PHR1061-1G
All-trans retinoic acid	Medium	STEMCELL Technologies	72264
Purmorphamine (PUR)	Medium	Merck Millipore	SML0868-25MG
GlutaMAX™	Medium	Gibco	35050061
Accutase	Passage	Sigma-Aldrich	A6964-100ML
ReLeSR	Passage	StemCell Technologies	05872
HBSS	Passage	Thermo Fisher Scientific	14170112
Y27632 ROCK inhibitor	Passage	Peprotech	1293823
Polyornithine	Plate coating	Sigma	P3655-100MG
Fibronectin	Plate coating	Merck Millipore	FC010-10MG
Knockout DMEM	Plate coating	Gibco	10829018
Matrigel	Plate coating	Corning	356230

Table 6. Cell cultureware.

Item	**Purpose**	**Supplier**	**Catalogue Number**
10 cm plates	iAstrocyte plating	Thermo Fisher Scientific	172931
Corning 6-well plates	iPSC/MN/GN plating	Corning	3506
Greiner 6-well plates	iAstrocyte plating	Greiner	657 160
24-well plate	iAstrocyte plating	Greiner	662 160
Clear 96-well plates	BCA assay	Greiner	655 180
Optic 96-well plates	Plating for ICC	Greiner	G655090
13 mm coverslips	iAstrocyte plating	Scientific Laboratory Supplies	MIC3336

2.1.3 General Reagents and Viruses

Table 7. General reagents.

Item	**Purpose**	**Supplier**	**Catalogue Number**
Bromophenol blue	Buffer	Thermofisher Scientific	B/P620/44
Dithiothreitol (DTT)	Buffer	Roche	10708984001
Ethylenediaminetetraacetic acid (EDTA)	Buffer	Thermofisher Scientific	17892
Glacial acetic acid	Buffer	Thermofisher Scientific	A/0360/PB17
Glycerol	Buffer	Thermofisher Scientific	G/0650/17

Glycine	Buffer	Melford	G36050-5000.0
HEPES	Buffer	Sigma	90909C
Hydrochloric acid (HCl)	Buffer	VWR Chemicals	20252.335
Ponceau S powder	Buffer	Sigma	P3504-10G
Potassium chloride (KCl)	Buffer	Thermofisher Scientific	P/4280/53
Sodium chloride	Buffer	Thermofisher Scientific	S/3161/65
Sodium deoxycholate	Buffer	Sigma	D6750-25G
Sodium dodecyl sulfate	Buffer	Thermofisher Scientific	S/5200/53
Sodium hydroxide	Buffer	Sigma	505-8
Tris	Buffer	Melford	T60040-5000.0
Trizma	Buffer	Sigma	T-5003
Tween 20	Buffer	Sigma	P1379-1L
β-mercaptoethanol	Buffer	Sigma	M3148
Agarose	Comet assay	Sigma	A9539
Low melting point agarose	Comet assay	Sigma	A4018-25G
Recombinant human OGG1	Comet assay	Abcam	ab98249
SYBR green	Comet assay	Sigma	S9430-5ML
2 ml phase lock gel tube light	DNA extraction and digest	Quantabio	733-2477
BsrG1	DNA extraction and digest	New England Biolabs	R0575S
EcoR1	DNA extraction and digest	New England Biolabs	R0101S
Ethanol	DNA extraction and digest	Thermofisher Scientific	463700250
Ethidium bromide	DNA extraction and digest	Sigma	46067-50ML-F
Glycogen	DNA extraction and digest	Thermofisher Scientific	R0561
Hind3	DNA extraction and digest	New England Biolabs	R0104S
MaXtract high density tube	DNA extraction and digest	Qiagen	129065
Phenol/chloroform isoamyl alcohol	DNA extraction and digest	Thermofisher Scientific	15593031
Sodium acetate	DNA extraction and digest	Sigma	S2889-250G
Spermidine	DNA extraction and digest	Merck Millipore	85580
Ssp1	DNA extraction and digest	New England Biolabs	R0132S
Xba1	DNA extraction and digest	New England Biolabs	R0145S
BCA assay kit	Immunoblotting	Thermofisher Scientific	23227
Bovine serum albumin (BSA) powder for block	Immunoblotting	Merck Millipore	A9418-50G

Bovine serum albumin (BSA) solution for BCA	Immunoblotting	Thermofisher Scientific	23210
Bradford assay reagent	Immunoblotting	Biorad	5000006
EZ-ECL Enhanced Chemiluminescence Detection Kit	Immunoblotting	Biological Industries	20-500-120
Nitrocellulose membrane	Immunoblotting	Merck Millipore	GE10600015
PageRuler™ Prestained Protein Ladder, 10 to 180 kDa	Immunoblotting	Thermofisher Scientific	26616
Phenylmethanesulfonyl fluoride (PMSF)	Immunoblotting	Roche	PMSF-RO
PhosSTOP	Immunoblotting	Roche	4906837001
Protease inhibitor cocktail	Immunoblotting	Sigma	S8830-20TAB
Skim milk powder	Immunoblotting	Merck Millipore	70166-500G
Sodium azide	Immunoblotting	Sigma	S2002-100G
Acetone	Immunocytochemistry	VWR Chemicals	20066-330
CellROX orange	Immunocytochemistry	Thermofisher Scientific	C10443
Donkey serum	Immunocytochemistry	Merck-Millipore	S30-100ML
Hoescht 33342	Immunocytochemistry	Invitrogen	H3570
Methanol	Immunocytochemistry	Sigma	32213-2.5L-M
Paraformaldehyde	Immunocytochemistry	Thermofisher Scientific	28908
ProLong Glass Antifade Mountant	Immunocytochemistry	Invitrogen	P36982
Triton X-100	Immunocytochemistry	Alfa Aesar	A16046
Protein G beads	Immunoprecipitation	Invitrogen	10004D
Camptothecin	Treatment	Cell Signalling Technologies	#13637
Hydrogen peroxide	Treatment	Sigma	H1009-100ml
RNAse A	Treatment	Invitrogen	12091021
RNAse H	Treatment	New England Biolabs	M0297S
Acrylamide (30%)	Western blotting	Geneflow	A2-0072
Ammonium persulphate (APS)	Western blotting	Sigma	A3678-25G
Isopropanol	Western blotting	Thermofisher Scientific	P/7500/17
TEMED	Western blotting	Melford	T18000-0.1

Table 8. Viral constructs used for transduction.

Short Name	Construct	Titer	Supplier
Control shRNA	AAV2-GFP-U6-scrmbl-shRNA	$1.4x10^{13}$ GC/mL	Vector Biolabs
P62 shRNA	AAV2-GFP-U6-SQSTM1-shRNA	$5.5x10^{12}$ GC/mL	Vector Biolabs

2.1.4 Primary and Secondary Antibodies

Table 9. Primary antibody information.

Marker	Species	Company	Catalogue Number	Concentration
53BP1	Rabbit	Novus Biologicals	NB100-304	1:1000 (ICC)
APE1	Rabbit	Cell Signalling Technologies	#10519	1:1000 (WB)
Beta actin	Mouse	Abcam	Ab6276	1:10,000 (WB)
Beta tubulin (TUJ1)	Chicken	Merck Millipore	AB9354	1:1000 (ICC)
CD44	Rabbit	Abcam	ab157107	1:300 (ICC)
CD63	Rabbit	Invitrogen	PA5-78995	1:1000 (DB)
DNA/RNA damage *	Mouse	Abcam	ab62623	1:3000 (ICC)
GFP	Chicken	Invitrogen	PA1-9533	1:1000 (WB)
KEAP1	Mouse	Invitrogen	MA5-17106	1:1000 (WB)
Ki67	Rabbit	Abcam	ab15580	1:1000 (ICC)
Ku80	Rabbit	Cell Signalling Technologies	#2753	1:1000 (WB)
LC3B	Rabbit	Novus Biologicals	NB100-2220	1:1000 (WB)
MAP2	Guinea pig	Synaptic Systems	188 004	1:1000 (ICC)
Nucleolin	Rabbit	Abcam	ab22758	1:1000 (ICC) 1:1000 (WB)
P62	Mouse	BD Biosciences	610833	1:200 (ICC) 1:500 (WB)
P62	Rabbit	Proteintech	18420-1-AP	1:100 (IP)
P75NTR	Rabbit	Cell Signalling Technologies	#8238	1:1000 (WB)
PARP1	Rabbit	Cell Signalling Technologies	#9532	1:1000 (WB)
Poly(GA) DPR	Rabbit	Proteintech	24492-1-AP	1:500 (DB) 1:100 (ICC)
Poly(GP) DPR	Rabbit	Proteintech	24494-1-AP	1:1000 (DB) 1:100 (ICC)
Poly(GR) DPR	Rabbit	Proteintech	23978-1-AP	1:1000 (DB) 1:100 (ICC)
Poly(PA) DPR	Rabbit	Proteintech	24493-1-AP	1:100 (ICC)
Poly(PA) DPR	Rat	Merck Millipore	MABN1790	1:1000 (DB)
Poly(PR) DPR	Rabbit	Proteintech	23979-1-AP	1:2000 (DB) 1:100 (ICC)
RNA:DNA Hybrids (S9.6)	Mouse	Kerafast	ENH001	1:500 (ICC)
TDP-43	Mouse	Abnova	H00023435-M01	1:1000 (WB)
TDP-43 (C-terminal)	Rabbit	Proteintech	12892-1-AP	1:100 (IP)
TOPO1	Mouse	Santa Cruz	sc-32736	1:1000 (WB)
Vimentin	Chicken	Merck Millipore	AB5733	1:1000 (ICC)

XRCC1	Rabbit	Cell Signalling Technologies	#2735	1:1000 (WB)
γH2AX	Mouse	Merck Millipore	05-636	1:500 (ICC)
γH2AX	Rabbit	R&D Systems	AF2288	1:1000 (WB)

* DNA/RNA damage is the antibody name for oxidised DNA/RNA (OG/OdG). DB = Dot blotting, ICC = immunocytochemistry, IP = immunoprecipitation, WB: Western blotting,

Table 10. Secondary antibody information.

Antibody Target	Species	Conjugate	Company	Catalogue Number
Anti-chicken	Goat	HRP*	ThermoFisher Scientific	A16054
Anti-mouse	Goat	HRP*	Promega	W4021
Anti-rabbit	Goat	HRP*	Promega	W4011
Anti-rat	Goat	HRP*	Invitrogen	62-9520
Anti-chicken	Goat	AlexaFluor 488 nm	Invitrogen	A11039
Anti-rabbit	Donkey	AlexaFluor 488 nm	Invitrogen	A21206
Anti-rabbit	Goat	AlexaFluor 568 nm	Invitrogen	A11036
Anti-mouse	Donkey	AlexaFluor 568 nm	Invitrogen	A10037
Anti-guinea pig	Goat	AlexaFluor 647 nm	Invitrogen	A21450

2.2 Cell Culture Protocols

2.2.1 iPSC maintenance

For iPSCs and derivatives (NPCs, motor neurons), Matrigel was diluted to 0.1 µg/ml in knockout DMEM and left to coat the plate for one hour at room temperature. Human induced pluripotent stem cells (iPSCs) were maintained in 6-well plates in complete mTeSR™-Plus™ medium. Media was replaced every 48 hours, and every 4-6 days cells were passaged as clumps using ReLeSR™, according to manufacturer's instructions. For all the experiments in this thesis, iPSCs were used between passage 20 and 35, and all iPSCs and other cells were cultured in 5% CO_2 at 37°C.

2.2.2 iPSC to NPC differentiation

Differentiation of iPSCs to NPCs (Figure 6-Figure 7) was performed as previously described (Du et al., 2015) with modifications. iPSCs at 100% confluence were washed once with PBS and neuralisation was initiated by switching to iPSC-NPC day 1-6 differentiation media (Table 11), which was replaced every 24 hours. On day 7 of differentiation, cells were switched to day 7-12 iPSC-NPC differentiation media (Table 11), which was also replaced every 24 hours. Between day 7 and 9, cells should begin to show signs of lifting and are passaged. For the passage, cells were washed with HBSS and incubated for 7 mins with Accutase at 37°C. Accutase was neutralised with equal quantity of medium and the cell suspension was centrifuged at 200 g for 4 mins. The supernatant was

discarded and the cell pellet was resuspended in medium supplemented with 10 µM Y27632 ROCK inhibitor. Cells were re-plated onto new Matrigel-coated 6-well plates at a ratio of 1:1 and differentiation was continued. By day 12 of differentiation, cells should no longer exhibit the rounded iPSC morphology and neural rosettes should have formed. On day 12 of differentiation, cells were passaged with Accutase and re-plated onto new Matrigel-coated 6-well plates at a ratio of 1:6 in the presence of 10 µM Y27632 ROCK inhibitor. Cells were previously characterised at day 12 of differentiation by Dr Cleide Souza and were found to express classical NPC markers (Pax6, Nestin, Olig2) and did not express iPSC markers (Oct4, Sox2, Noggin, SSEA-4). NPCs were maintained in NPC expansion media (Table 11), which was changed every 48 hours, and cells were expanded to 100% confluence. Media was always changed 24 hours after incubation with ROCK inhibitor. At this point, NPCs could be frozen with 10% DMSO and stored at -80^{o}C or in liquid nitrogen until needed, or differentiation to motor neurons or GABAergic neurons could be initiated.

2.2.3 NPC to motor neuron differentiation

Differentiation of NPCs to motor neurons (Figure 6) was performed as previously described (Du et al., 2015) with modifications. Once NPCs reached 100% confluence, cells were switched from NPC expansion media to motor neuron day 13-18 media (Table 11) which was changed every 48 hours. On day 19 of differentiation, cells were switched to motor neuron day 19-28 differentiation media (Table 11) which was also changed every 48 hours. On day 20-21, cells were passaged with Accutase, counted using a haemocytometer (0.100 mm depth, Marienfeld) and re-plated onto Matrigel-coated plates in the presence of 10 µM Y27632 ROCK inhibitor. 1-2 million cells were replated per well on a 6-well plate for pelleting or the comet assay, and 20,000-30,000 cells were replated per well on an optic 96-well plate for staining experiments. Cells were switched to fresh medium 24 hours later and differentiation continued. On day 29 of differentiation, cells were switched to day 29-40 media (Table 11) which was changed every 48 hours until or after day 40 of differentiation. Cells were previously characterised at day 40 of differentiation by Dr Cleide Souza and were found to express classical mature motor neuron markers (ChAT, SMI32, Islet 1/2, MAP2, NeuN).

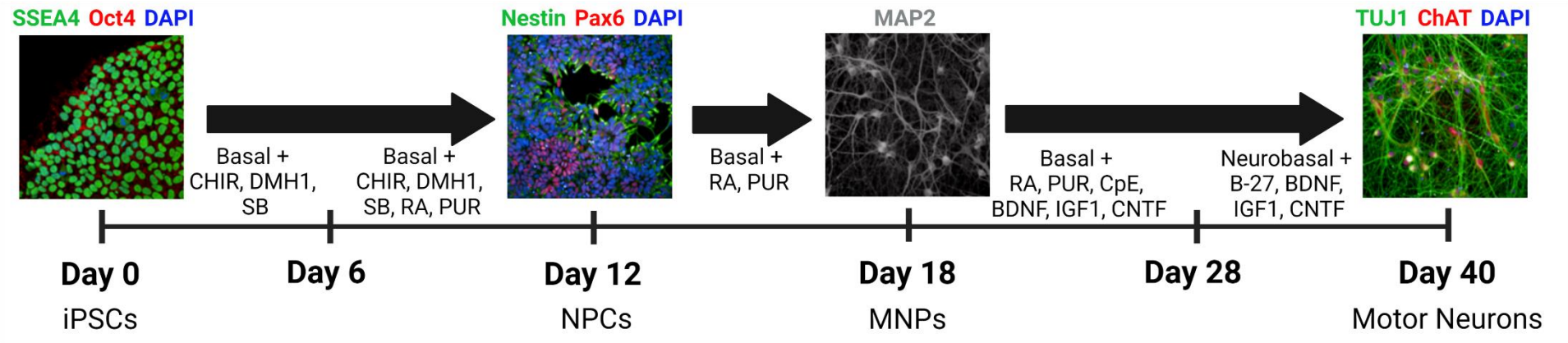

Figure 6. Schematic showing iPSC to spinal motor neuron differentiation protocol (created with Biorender.com). Images showing cells stained for classical markers obtained from Dr Cleide Souza. iPSCs = induced pluripotent stem cells, NPCs = neural progenitor cell

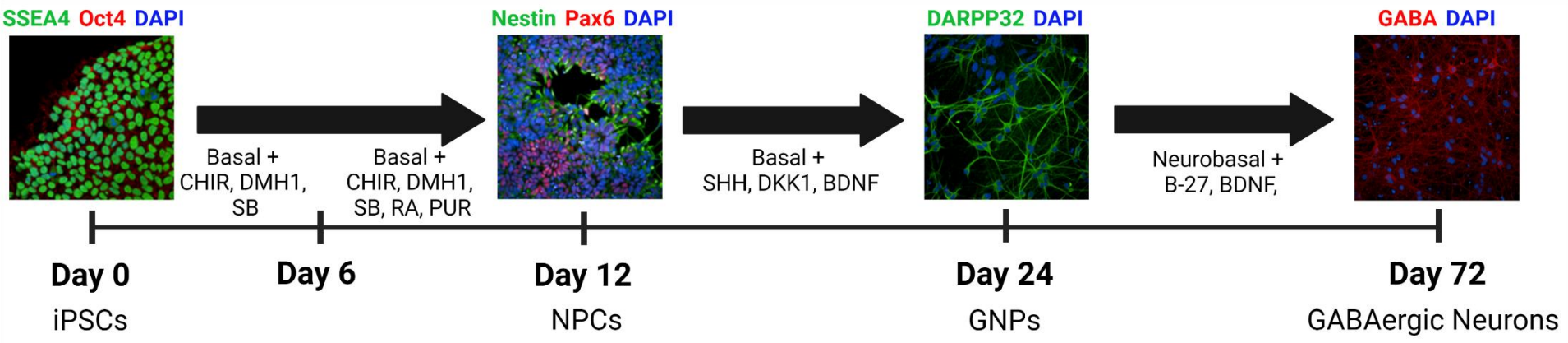

Figure 7. Schematic showing iPSC to striatal GABAergic neuron differentiation protocol (created with Biorender.com). Images showing cells stained for classical markers obtained from Dr Cleide Souza. iPSCs = induced pluripotent stem cells, NPCs = neural progenitor cells, GNPs = GABAergic neuron progenitor cells

Table 11. Protocol for differentiation of iPSCs to spinal motor neurons.

Day of Differentiation	Media Base	Factors	Concentration	Supplier	Catalogue Number
1-6 (iPSC-NPC)	Basal media (Table 12)	CHIR 99021	3 µM	Merck Millipore	SML1046-25MG
		DMH-1	2 µM	Merck Millipore	D8946-25MG
		SB 431542	2 µM	Peprotech	3014193
7-12 (iPSC-NPC)	Basal media (Table 12)	CHIR 99021	1 µM	Merck Millipore	SML1046-25MG
		DMH-1	2 µM	Merck Millipore	D8946-25MG
		SB 431542	2 µM	Peprotech	3014193
		All-trans retinoic acid	0.1 µM	STEMCELL Technologies	72264
		Purmorphamine (PUR)	0.5 µM	Merck Millipore	SML0868-25MG
NPC expansion	Basal media (Table 12)	CHIR 99021	3 µM	Merck Millipore	SML1046-25MG
		DMH-1	2 µM	Merck Millipore	D8946-25MG
		SB 431542	2 µM	Peprotech	3014193
		All-trans retinoic acid	0.1 µM	STEMCELL Technologies	72264
		Purmorphamine (PUR)	0.5 µM	Merck Millipore	SML0868-25MG
		Valproic acid (VPA)	0.5 mM	Merck Millipore	PHR1061-1G
13-18 (NPC-MN)	Basal media (Table 12)	All-trans retinoic acid	0.5 µM	STEMCELL Technologies	72264
		Purmorphamine (PUR)	0.1 µM	Merck Millipore	SML0868-25MG
19-28 (NPC-MN)	Basal media (Table 12)	All-trans retinoic acid	0.5 µM	STEMCELL Technologies	72264
		Purmorphamine (PUR)	0.1 µM	Merck Millipore	SML0868-25MG
		Compound-E	0.1 µM	Tocris	6476
		Brain derived neurotrophic factor (BDNF)	10 ng/ml	Peprotech	AF-450-02
		Ciliary neurotrophic factor (CNTF)	10 ng/ml	Peprotech	450-13
		Insulin-like growth factor 1 (IGF1)	10 ng/ml	Peprotech	100-11
29-40 (MN maturation)	Neurobasal media	B-27 supplement	2% (v/v)	Gibco	11530536
		Brain derived neurotrophic factor (BDNF)	10 ng/ml	Peprotech	AF-450-02
		Ciliary neurotrophic factor (CNTF)	10 ng/ml	Peprotech	450-13
		Insulin-like growth factor 1 (IGF1)	10 ng/ml	Peprotech	100-11

Table 12. Basal media composition

Component	Concentration	Company	Catalogue Number
KnockOut DMEM/F12	48% (v/v)	Gibco	12660012
Neurobasal media	48% (v/v)	Gibco	11570556
B-27 supplement	1% (v/v)	Gibco	11530536
N-2 supplement	0.5% (v/v)	Gibco	15410294
GlutaMAX™	1% (v/v)	Gibco	35050061
Penicillin/Streptomycin	1% (v/v)	Lonza	DE17-603E

2.2.4 NPC to striatal GABAergic neuron differentiation

Differentiation of NPCs to striatal GABAergic neurons (Figure 7) was performed as previously described (Lin et al., 2015). Once NPCs reached 100% confluence, cells were switched from NPC expansion media to GABAergic neuron day 13-24 media (Table 13) which was changed every 48 hours. On day 20-21, cells were passaged with Accutase, counted using a haemocytometer (0.100 mm depth, Marienfeld) and re-plated onto Matrigel-coated plates in the presence of 10 µM Y27632 ROCK inhibitor. 1-2 million cells were replated per well on a 6-well plate for pelleting or the comet assay, and 20,000-30,000 cells were replated per well on an optic 96-well plate for staining experiments. Cells were switched to fresh medium 24 hours later and differentiation continued. On day 25 of differentiation, medium was switched to GABAergic neuron day 25-72 media (Table 14), which was changed every 48 hours until day 72. Cells were previously characterised at day 72 of differentiation by Dr Cleide Souza and were found to express classical mature GABAergic neuron markers (DARPP32, GABA, MAP2, NeuN).

Table 13. GABAergic neuron day 13-24 media composition.

Component	Concentration	Company	Catalogue Number
Basal media (Table 12)	Media base	NA	NA
BDNF	30 ng/ml	Peprotech	AF-450-02
Sonic hedgehog	200 ng/ml	Peprotech	100-45
DKK-1	100 ng/ml	Peprotech	120-30

Table 14. GABAergic neuron day 25-72 media composition.

Component	Concentration	Company	Catalogue Number
Neurobasal media	Media base	Gibco	11570556
B-27 supplement	2% (v/v)	Gibco	11530536
Penicillin/Streptomycin	1% (v/v)	Lonza	DE17-603E
BDNF	50 ng/ml	Peprotech	AF-450-02

2.2.5 Fibroblast to iNPC conversion

Skin fibroblasts from controls, sALS and C9-ALS and SOD1-ALS patients (Table 4) were reprogrammed as previously described (Meyer et al., 2014). Conversion of fibroblasts to iNPCs was done by Allan Shaw and Professor Laura Ferraiuolo (Figure 8A). Once fully reprogrammed, iNPCs were routinely maintained and plated for differentiation by past and present members of the Ferraiuolo lab.

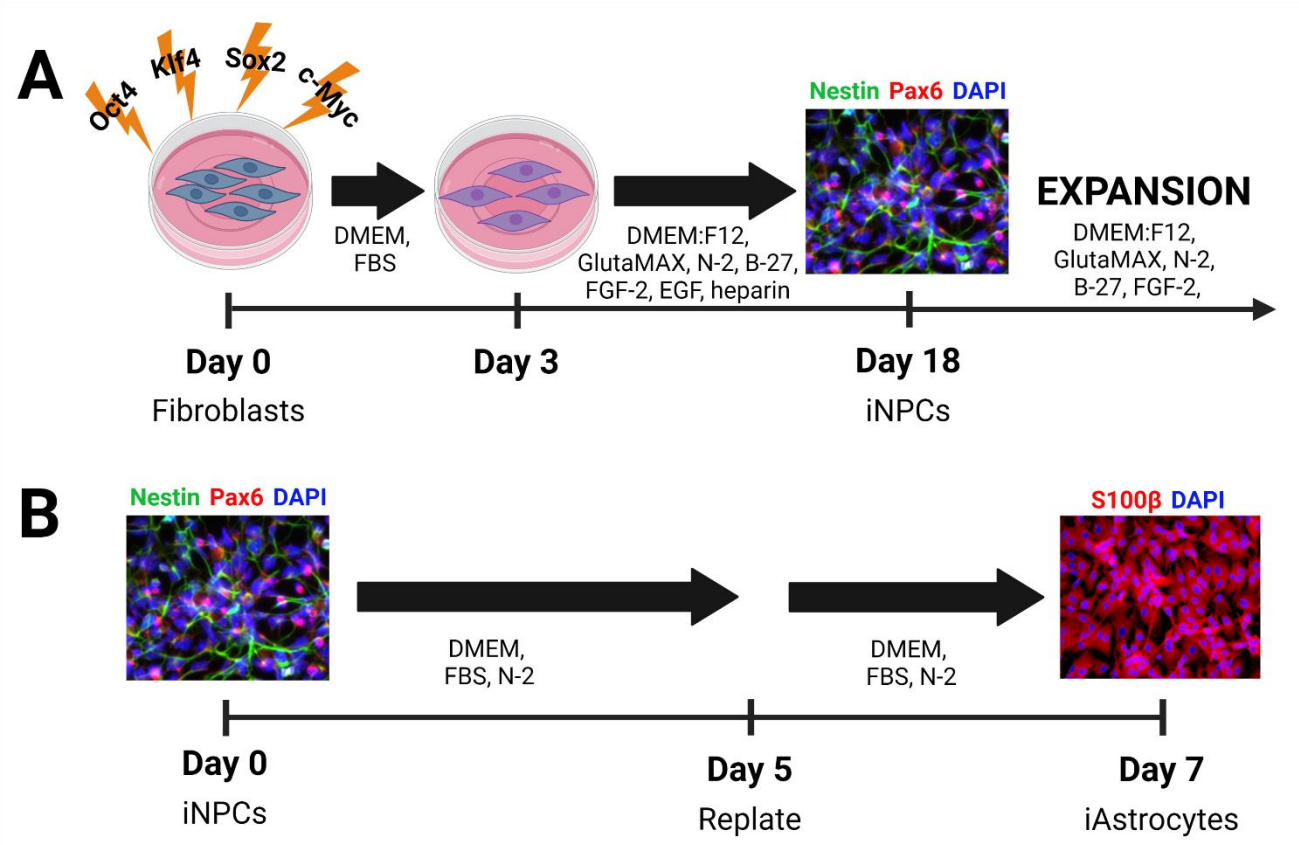

Figure 8. Schematic showing differentiation of fibroblasts to iNPCs and iNPCs to iAstrocytes (created with Biorender.com). A: Differentiation of skin fibroblasts to iNPCs. iNPCs are expanded prior to differentiation to other cell types. B: Differentiation of iNPCs to iAstrocytes. Cells are typically passaged and replated on day 5 of differentiation.

2.2.6 iNPC to astrocyte differentiation

Established iNPC lines were expanded and maintained on 10 cm plates coated for 5 mins at room temperature with 5 µg/ml fibronectin diluted in phosphate-buffered saline (PBS). iNPC lines were maintained in iNPC expansion media (Table 15) until 70-100% confluent or showing signs of stress and then were passaged with Accutase and replated at approximately 40% confluence on 10 cm plates coated for 5 mins at room temperature with 2.5 µg/ml fibronectin diluted in PBS. iNPCs were differentiated into astrocytes (Figure 8B) as previously described (Meyer et al., 2014) by switching the media to astrocyte differentiation media (Table 16) for seven days. Cells were previously

characterised at day 7 of differentiation by members of the Ferraiuolo lab and were found to express classical astrocyte markers (vimentin, GFAP, CD44, S100β) and no longer express NPC markers (Pax6, Nestin). For staining experiments, cells were passaged with Accutase on day 5 of differentiation. For the passage, cells were washed twice with PBS and incubated for 5 mins at 37°C with 1 ml Accutase. Following a resuspension in 3 ml PBS, cells were centrifuged for 4 mins at 200g. The supernatant was discarded and the pellet was resuspended in a volume of astrocyte culture medium appropriate for counting using a haemocytometer (0.100mm depth; Marienfeld). For most staining experiments, 8000 cells per well were plated onto optic 96-well plates coated for 5 mins at room temperature with 2.5 µg/ml fibronectin diluted in PBS. For high-resolution confocal imaging, 13 mm coverslips were sterilised in 70% industrial methylated spirit for 1 hour, and then were transferred to a 24-well plate using sterilised forceps. Coverslips were incubated overnight with 0.05 mg/ml polyornithine diluted in distilled water. Coverslips were washed three times with PBS and then coated with 2.5 µg/ml fibronectin diluted in PBS for 5 mins at room temperature. 30,000 cells were replated per coverslip.

Table 15. iNPC expansion media composition.

Component	Concentration	Company	Catalogue Number
DMEM/F12 GlutaMAX™	Media base	Gibco	11524436
B-27 supplement	1% (v/v)	Gibco	11530536
N-2	1% (v/v)	Gibco	15410294
FGF-2	40 ng/ml	Peprotech	100-18B
Penicillin/Streptomycin	1% (v/v)	Lonza	DE17-603E

Table 16. iAstrocyte differentiation media composition

Component	Concentration	Company	Catalogue Number
DMEM	Media base (1X)	Gibco	11520416
N-2	0.2% (v/v)	Gibco	15410294
Foetal bovine serum (FBS)	10% (v/v)	Life Science Production	5-001A-H1-BR
Penicillin/Streptomycin	1% (v/v)	Lonza	DE17-603E

2.2.7 HEK293T Cell Maintenance and Transfection

HEK293T cells were maintained and transfected with cDNA constructs encoding the sense or antisense RNA repeat expansion as described previously (Walker et al., 2017). HEK293T cells were cultured in HEK293T cell media (DMEM, 10% FBS, 1% penicillin/streptomycin), until at 80% confluence by Nikita Soni of Dr Guillaume Hautbergue's group. 200,000 HEK293T cells per well of a 6-well plate or 50,000 HEK cells per well of a 24-well plate were transfected with 700 ng pcDNA3.1 encoding the sense (RAN-G4C2x38) and/or the anti-sense (RAN-C4G2x39) repeat expansion

transcript, using 3.5 µg/ml PEI and 1:10 OptiMEM in HEK293T cell media. HEK293T cell transfection was performed by Dr Lydia Castelli of Dr Guillaume Hautbergue's group. Conditioned media was collected 48 hours after transfection, proteins were extracted 72 hours after transfection for dot blotting.

2.3 Astrocyte Exosome Isolation

iNPCs were differentiated into astrocytes to day 5 as previously described. On day 5 of differentiation, plates were washed twice with PBS to remove serum and cells were kept in extracellular vesicle-free astrocyte media: DMEM, 10% KnockOut™ serum replacement, 0.2% N-2; or plain DMEM for 48 hours (Figure 9A). Exosomes were isolated from the conditioned medium (Figure 9B) as previously described (Varcianna et al., 2019). Conditioned media was removed and pooled from four 10 cm plates for each cell line and centrifuged at 300 g for 10 mins. Supernatant was filtered through a 0.22 µm filter to remove cell debris and centrifuged at 37,000 rpm (70ti rotor and Beckman Coulter Ultracentrifuge) at 4°C for 90 mins. Supernatant was discarded leaving the exosome pellet which was resuspended in 50 µl of a solution appropriate for the following experiments: for MSD ELISA experiments, exosomes were resuspended in 5% SDS buffer (5% SDS, 50 mM Tris, pH 7.4); for dot blot experiments, exosomes were resuspended in immunoprecipitation (IP) lysis buffer 1 (150 mM NaCl, 50 mM HEPES, 1 mM EDTA, 1 mM DTT, 0.5% Triton-X100, pH 8.0).

2.4 Conditioned Media Treatment

To obtain astrocyte conditioned media, astrocytes were passaged with Accutase on day 5 of astrocyte differentiation and 1 million cells per line were re-plated onto each well of a 6-well plate. Media was left to condition for 48 hours and was collected on day 7 of astrocyte differentiation. For transfected HEK293T cell conditioned media, media was left to condition for 48 hours after transfection. Conditioned media was passed through a 0.22 µm filter to remove detached cells or cell debris. Mature motor neurons derived from an unaffected control were treated with a 1:1 solution of fresh motor neuron media and the conditioned media for 24 or 72 hours. Fresh motor neuron media was included to reduce neuron stress. Due to variability in HEK293T cell transfection, 100% HEK293T cell conditioned media was used for conditioned media treatment with no dilution in normal motor neuron media. For untreated controls, conditioned media was substituted for fresh media (e.g. astrocyte media substitute for astrocyte conditioned media).

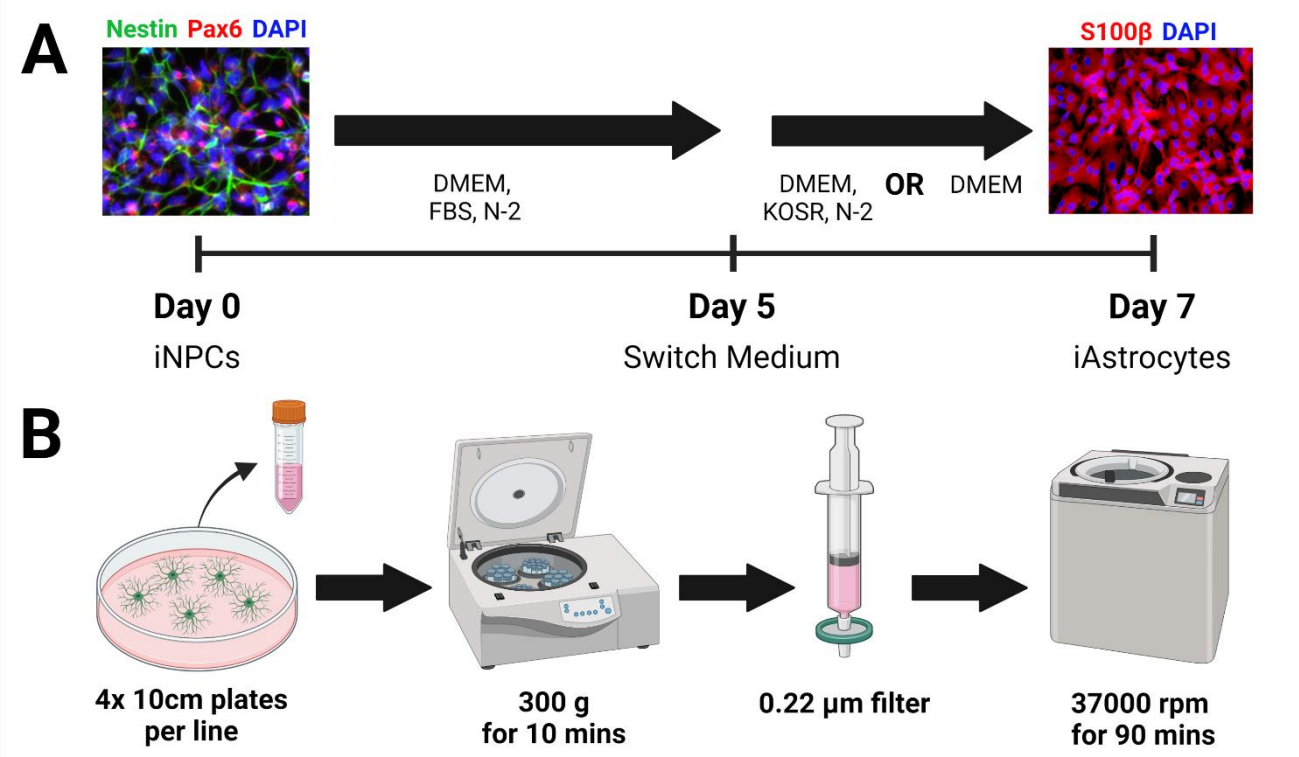

Figure 9. Astrocyte exosome isolation protocol (created with Biorender.com). A: iAstrocytes were differentiated from iNPCs as before, but on day 5 medium was switched to DMEM supplemented with knockout serum replacement (KOSR) and N-2, or plain DMEM. B: On day 7, medium was pooled from four 10 cm dishes per cell line and was centrifuged at 300g for 10 mins. Medium was filtered to remove cell debris and ultracentrifuged at 37000 rpm for 90 mins.

2.5 Astrocyte Viral Transduction

For transduction optimisation, astrocytes were replated onto 96 well plates at different densities on day 3 of differentiation and transduced with control shRNA virus (Table 8) at different MOIs. For transduction, media was discarded and replaced with 50 µl per well fresh astrocyte media supplemented with virus. After six hours, media was topped up with a further 50 µl per well of fresh astrocyte media. Approximately 24 hours after transduction, media was discarded and replace with fresh astrocyte media. To assess number of cells expressing the reporter GFP, plates were scanned every 24 hours on the Opera Phenix™ High Content Screening System (Perkin Elmer) at × 40 magnification, using brightfield and eGFP channels, with live imaging settings activated (5% CO_2 and 37°C). Six days post-transduction, cells were fixed with 4% paraformaldehyde (PFA), stained for Hoescht 33342 (see 2.7.1) and imaged on the Opera Phenix to assess transduction efficiency.

For transduction followed by conditioned media collection, 300,000 astrocytes per cell line were replated onto 6-well plates on day 3 of differentiation. Cells were transduced with 500,000 MOI control shRNA or p62 shRNA virus (Table 8) made up in 1 ml of astrocyte media. After six hours, a

further 2 ml of media was added per well. 24 hours after transduction, media was discarded and replaced with 3 ml fresh astrocyte media. On day 5 of differentiation, astrocytes were lifted and replated as normal for conditioned media production (see 2.4) at a density of 400,000 cells per well onto a 6-well plate. Conditioned medium was collected 72 hours after transduction, media was replaced and conditioned medium was collected again 24 hours later (96 hours after transduction). Astrocyte cell pellets were also collected at 96 hours post-transduction (see 2.8.1).

2.6 Drug Treatments

As a positive control for DNA damage, astrocytes or neurons were treated with warm 100 µM hydrogen peroxide solution made up in the appropriate cell media for 15 mins at room temperature. Alternatively, astrocytes or neurons were treated with 14 µM camptothecin (CPT) made up in the appropriate cell media for 1 hour at 37^{o}C. To validate staining, RNAse A was used to remove RNA from samples. Permeabilised cells were treated with 10 µl/ml RNAse A and incubated at 37°C for 30 mins. RNAse was discarded, cells were washed with PBS and staining continued as normal.

2.7 Fluorescence Assays

2.7.1 Immunocytochemistry (ICC)

Cells were washed with PBS and incubated with fixative solution for 10 mins at room temperature, then washed with PBS and stored at 4°C until staining. 4% paraformaldehyde warmed to approximately 37°C was used as a fixative for most staining, except OdG and S9.6 staining that required fixation and permeabilisation with ice cold 50% (v/v) methanol + 50% acetone (v/v) solution. Fixed motor neurons were permeabilised with 0.3% Triton X-100 in PBS for 5 mins and incubated in 5% donkey serum blocking solution for 1 hour to block non-specific staining. Fixed astrocytes were permeabilised and blocked by incubating with 0.5% Triton X-100 made up in 5% donkey serum for 1 hour. Antibodies were made up in 5% donkey serum. Cells were incubated with primary antibodies (Table 9) overnight at 4°C, then were washed three times with PBS (5 mins per wash). Cells were incubated with AlexaFluor secondary antibodies (1:500 dilution) (Table 10) for 1 hour at room temperature in the dark and were washed once with PBS before being incubated in 1:10,000 Hoescht for 5 mins at room temperature in the dark. Cells were washed three times with PBS (5 mins per wash) and stored in the dark at 4^{o}C until imaging.

2.7.2 CellROX Assay

To detect reactive oxygen species (ROS) in live cells, CellROX™ Orange Reagent for oxidative stress detection was used according to manufacturer's instructions. Briefly, media was removed and cells were incubated in 5 µM CellROX reagent and 1:2000 Hoescht, made up in normal cell media, for 30 mins at 37^{o}C. Cells were washed once with PBS and kept in phenol red free neurobasal media for imaging.

2.7.3 Imaging

Unless otherwise stated, all imaging was performed using the Opera Phenix™ High Content Screening System (Perkin Elmer) at × 40 magnification. Live imaging was used for the CellROX assay, with settings set at 5% CO_2 and 37°C. Z-stacks of at least five or more planes separated by 0.5 µm were obtained from a minimum of 20 fields per well from three technical replicate wells per experiment. 405, 488 and 594 and 647nm lasers were used, along with the appropriate excitation and emission filters. Settings were kept consistent while taking images from all cultures. For immunofluorescence DPR staining, imaging was performed using a Leica or Nikon A-1 confocal microscope.

2.7.4 Analysis

ICC image analysis was performed using Harmony High-Content Imaging and Analysis Software (PerkinElmer) to allow high throughput analysis without experimenter bias. For foci analyses, the total number of foci were counted and divided by the total number of cells or the total area (e.g. nuclear area for nuclear foci). For intensity analyses, the total intensity was determined and divided by the total number of cells or the total area (total nuclear area in the case of nuclear signal, total staining area in the case of CellROX).

2.8 Immunoblotting Assays

2.8.1 Cell and Exosome Lysis

Cells were washed twice with PBS to remove serum, detached with a cell scraper and collected and centrifuged at 17,000 g for 5 mins. Supernatant was discarded and pellets were stored at -80°C until needed. Different lysis buffers were used for different experiments, all lysis buffers were supplemented with protease inhibitor cocktail unless otherwise stated. For experiments looking at phosphorylated proteins, lysis buffers were supplemented with phosphatase inhibitors (PhosSTOP). Both protease inhibitor cocktail and phosSTOP were used at a final concentration of 1X.

For Western blots, pellets were re-suspended in RIPA buffer 1 (150 mM NaCl, 50 mM Tris, 0.5% (w/v) Triton X-100, 0.5% (w/v) SDS). Cell solutions were passed through a 22-gauge needle ten times and left on ice to lyse for 45 mins. For immunoprecipitation (IP), pellets were resuspended in IP lysis buffer 2 (20 mM Tris pH8, 137 mM NaCl, 1% Triton X-100, 2 mM ETDA) and left on ice to lyse for 15 mins. Lysed cell pellets were centrifuged at 17,000 g for 10 mins and the supernatant containing soluble proteins was reserved. For dot blotting of exosomes, exosome pellets were re-suspended in 50 µl IP lysis buffer 1 supplemented with 1X phenylmethylsulfonyl fluoride, passed through a 22-gauge needle ten times and left on ice for 10 mins.

2.8.2 Protein Quantification

For non-RIPA buffer lysates, protein concentration was quantified using the Bradford assay. Bradford assay reagent was diluted 1:5 with distilled water. 1 µl cell lysate was added to 1 ml of diluted Bradford reagent, mixed by inverting and examined for colour change. If no colour change was observed, an additional 1 µl cell lysate would be added until a colour change could be observed. Colour change was then quantified using a spectrophotometer to measure the absorbance at 595 nm. Protein concentration was calculated using the Beer-Lambert Law ($A=\varepsilon LC$), where the length of the cuvette was 1 cm and the slope of the standard curve was estimated to be 15. If more than 1 µl cell lysate was used, the protein concentration would need to be diluted by the number of µl cell lysate.

For RIPA buffer lysates, the Bradford assay was not possible due to the high salt concentration of the RIPA buffer. Instead, protein concentration was quantified using the Pierce™ BCA Protein Assay Kit according to manufacturer's instructions. Protein samples were pipetted into individual wells of a 96-well plate, along with bovine serum albumin (BSA) standards diluted in lysis buffer to the following concentrations: 0, 25, 125, 250, 500, 750, 1000, 1500, 2000 µg/ml. Samples and standards were incubated with BCA assay working reagent (one part BCA reagent B, 50 parts reagent A) for 30 mins at 37^{o}C. Absorbance at 560nm was measured using a PHERAstar plate reader (BMG Labtech). Absorbance readings for BSA standards was used to generate a standard curve, which allowed determination of protein concentration of samples using the linear graph equation $y=mx+c$. If samples were diluted (e.g. 1:10) for the BCA assay, then the estimated protein concentration was divided by the dilution factor.

2.8.3 Immunoprecipitation

Immunoprecipitation (IP) was performed according to the protocol supplied by Abcam (https://www.abcam.com/protocols/immunoprecipitation-protocol-1), using method B (IP with antibody-agarose conjugate). 70 µl protein G beads per sample were pelleted using a magnetic rack (Invitrogen #12321D) and washed three times with twice the volume of IP lysis buffer 2. Beads were then incubated with primary antibody (Table 9) made up in IP lysis buffer 2 and incubated overnight on a rotor at 4°C. No antibody control was also prepared, following the same protocol but excluding any primary antibody. The following day, cell lysates were prepared, and protein concentration calculated as described in 2.8.1 and 2.8.2. Conditioned media samples were incubated 1:5 with lysis buffer and left on ice while the cell lysate samples were prepared. During optimisation, different lysis conditions were tested on conditioned media samples including standard lysis (IP lysis buffer 2), hypotonic lysis (10 mM Tris-HCl, pH 7.5) and sonication (three rounds of 5 seconds sonication). Beads were pelleted, washed three times with IP lysis buffer 2 to remove any unattached antibody. For cell lysates, beads were incubated with 50 µg protein diluted in IP lysis buffer to a final volume of 100 µl. For conditioned medium samples, beads were incubated with 500 µl lysed conditioned medium. Incubation of beads with lysates was done overnight on a rotor at 4°C. The following day, beads were pelleted, and the supernatant was reserved as the immunodepleted fraction. Beads were washed three times with IP lysis buffer 2 to remove any unattached protein. During optimisation, glycine buffer elution was used which involved incubating the beads with 70 µl glycine buffer (0.2M glycine, pH 2.6) with gentle or harsh agitation for 10 mins, pelleting the beads and repeating the elution twice more, pooling the eluate for each sample. Due to the low pH, the total eluate for each sample had to be neutralised with equal volume of Tris pH 8.0. SDS buffer elution was also used, which involved incubating the beads with 70 µl 2X SDS buffer without DTT (100 mM Tris-Cl pH 6.8, 4% (w/v) SDS, 0.2% (w/v) bromophenol blue, 20% (v/v) glycerol) at 50°C for 10 mins. IP eluate and depleted samples were analysed by Western blot (see 2.8.4 and 2.8.6).

2.8.4 Western Blotting

Standard protein samples were diluted to 25 µg in lysis buffer and 4X Laemmli buffer (228 mM Tris-HCl, 38% (v/v) glycerol, 277 mM SDS, 0.038% (w/v) bromophenol blue, 5% (v/v) β-mercaptoethanol, pH 6.8) to a final volume of 24 µl and boiled at 95°C for 5 mins. For IP samples, 18 µl of the depleted fraction and the glycine buffer eluate were supplemented with 6 µl 4X Laemmli buffer and boiled as above. SDS buffer eluates were supplemented with 100 µM DTT and were not boiled.

For each sample, 20 µl was loaded per lane of an SDS-polyacrylamide gel made up from resolving gel (8%-15%) and 5% stacking gel (Table 17) in a Mini-PROTEAN® Tetra Vertical Electrophoresis Cell (Bio-Rad). The percentage of resolving gel used depended on the molecular weight of the proteins being probed. 2 µl pre-stained protein ladder was also loaded into one lane of each gel to allow determination of molecular weight of bands. Electrophoresis apparatus was filled with running buffer (25 mM Tris, 3.5 mM SDS, 20 mM glycine), and gels were run at 50 V for 30 mins to allow protein to travel slowly through stacking buffer, and then gels were run at 150 V for approximately 1.5 hours or until the dye front reached the bottom of the gel. Proteins were transferred to a nitrocellulose membrane soaked in transfer buffer (47.9 mM Tris, 38.6 mM glycine, 1.38 mM SDS, 20% (v/v) methanol) using Biometra Fastblot semi-dry transfer apparatus (Analytik Jena) set to the power of 250 V constant and the current of 0.15 milliampere (mA) per gel for 1 hour. Transfer success was determined by reversible protein staining with Ponceau S staining solution (0.5% (w/v) Ponceau S, 1% (v/v) acetic acid).

Table 17. SDS polyacrylamide gel composition.

Gel Component	5% Stacking Gel	8% Resolving Gel	10% Resolving Gel	12% Resolving Gel	15% Resolving Gel
Acrylamide	5%	8%	10%	12%	15%
Resolving buffer (1.5 M Trizma®, 13.9 mM SDS, pH 8.8)	N/A	25%	25%	25%	25%
Stacking buffer (0.5 M Trizma®, 13.9 mM SDS, pH 6.8)	25%	N/A	N/A	N/A	N/A
APS	0.05%	0.05%	0.05%	0.05%	0.05%
TEMED	0.2%	0.2%	0.2%	0.2%	0.2%

2.8.5 Dot Blotting

Dot blot apparatus was set up with a nitrocellulose membrane soaked in transfer buffer (47.9 mM Tris, 38.6 mM glycine, 1.38 mM SDS, 20% (v/v) methanol). Due to the low protein abundance, it was not possible to accurately estimate the protein concentration of the exosome solution, so 200 µl of undiluted exosome solution was loaded per well. For cell lysates, protein concentration was estimated using the Bradford assay according to manufacturer's instructions and 80-200 µg protein was loaded per well. A vacuum was applied to the dot blot apparatus for 20 mins and the nitrocellulose membrane was left to dry at room temperature for 10 mins to 1 hour.

2.8.6 Membrane Processing and Imaging

Western blotting and dot blotting membranes were processed and imaged in the same way. For phosphorylated proteins, membranes were blocked with 5% BSA in TBST (10 mmol Tris, 150 mmol NaCl, 0.1% Tween 20) for 1 hour at room temperature. For non-phosphorylated proteins, membranes were blocked with 5% milk in TBST for 1 hour at room temperature. Membranes were then incubated with primary antibody (Table 9) made up in the blocking solution overnight at 4°C. Membranes were washed three times with TBST for 5 mins each time and then incubated with a secondary antibody (Table 10) conjugated to horseradish peroxidase made up in block for one hour. Following three further washes with TBST, membranes were incubated with ECL for 1 min and imaged using a G:BOX (Syngene) with GeneSys software.

2.8.7 Analysis

Dot blot and IP results were qualitative and thus were not quantified. Western blotting images were analysed using ImageJ. Images were converted to 8-bit and a rectangle of equal dimensions was drawn around each band. The relative density was plotted, and the background was determined manually and subtracted from each density plot. The plots were labelled, allowing determination of the area and percentage values for each lane. For each protein of interest, the percent value of a particular band was divided by the percent value of the corresponding loading control (β-actin). For conditioned medium experiments, data was normalised to the untreated condition to take into account baseline differences between motor neuron differentiations.

2.9 Comet Assay

The comet assay for DNA strand breaks was performed as previously described (Speit and Hartmann, 2008) with some modifications. Slides were pre-coated with 0.6% normal agarose gel made up with PBS and left to set overnight at 4°C. Motor neurons or astrocytes were harvested with Accutase, 45,000 cells per condition were isolated and kept on ice until plating. Cells were centrifuged at 5,000 rpm for 2 mins, washed with PBS twice and the pellet was re-suspended in PBS. The cell solution was mixed at a ratio of 1:1 with 1.2% low melting point agarose gel made up in PBS and plated on top of the pre-coated slides. Slides were left in the dark at 4°C for 30 mins for gel to set. Lysis buffer (1.5M NaCl, 60mM EDTA, 10mM Tris, pH 10) was supplemented with 1:100 DMSO and 1:100 Triton X-100, applied to the slides and slides were left to incubate in the dark at 4°C for one hour. For the oxidative DNA damage comet assay, following lysis slides were incubated in 0.5 µg/ml hOGG1 made up in enzyme reaction buffer (0.4M HEPES, 1M KCl, 5mM EDTA, 2mg/ml

BSA, 10M NaOH, pH 8.0) and incubated at 37°C for 1 hour. Slides were washed three times with enzyme reaction buffer and the assay resumed as normal. For the standard comet assay, the OGG1 and washing steps were skipped. Slides were then placed in a comet electrophoresis tank and allowed to equilibrate in electrophoresis buffer (50mM NaOH, 1mM EDTA, 1% (v/v) DMSO) in the dark at 4°C for 45 mins. Electrophoresis was then run at 12V for 25 mins in the dark at 4°C. Slides were removed and neutralized in 0.4M Tris pH 7 overnight at 4°C in the dark. DNA was stained with 1:10,000 SYBR green, and comets were visualized with a fluorescence microscope (Nikon, Eclipse TE300).

2.9.1 Analysis

At least 100 cell comets per condition per repeat were scored using Comet IV software (Instem), scoring was done blinded where the experimenter was unaware of the cell line or condition being scored. Tail moment was determined for each scored cell by the Comet IV software, limiting experimenter bias. Comet experiments were run at least in triplicate, meaning a minimum of three independent repeats were run for each cell line or treatment using a new differentiation each time. Mean tail moment of all cells per condition was determined for each repeat and the mean of the three independent repeats per cell line or condition was calculated and used for statistical analysis.

2.10 DNA:RNA Immunoprecipitation

2.10.1 DNA Extraction and Digest

Astrocytes were pelleted as described previously (2.8.1) and each sample was resuspended in 1.6ml TE buffer (1M Tris, 0.5M EDTA, pH 8.0). To each sample, 50 µl 20% w/v SDS and 10 µl 10 mg/ml proteinase K were added, and samples were mixed by inverting 4-6 times. Samples were incubated at 37°C overnight. Cell lysate was then added to a 15 ml MaXtract high density tube, which was previously centrifuged at 1500 g for 10 mins to pellet the gel. 1.6 ml phenol/chloroform isoamyl alcohol was added to each tube, tubes were inverted 4-6 times to mix contents and tubes were centrifuged at 1500 g for 10 mins. Supernatant should appear clear, if not tubes were centrifuged again until the supernatant appeared clear. Supernatant was transferred to a standard 15 ml tube. 4 ml 100% ethanol and 160 µl 3M sodium acetate pH 5.2 were added to each tube and the tubes were left to mix on a roller or rotary mixer at 10 rpm for at least 10 mins until a white DNA precipitate was visible. DNA was spooled with a cut 1000 µl tip and transferred to a clean 2 ml Eppendorf. DNA was washed three times with 80% ethanol. For each wash, 1.5 ml 80% ethanol was added to DNA, tubes were inverted 4-6 times and then tubes were left to stand for 10 mins before

discarding ethanol. DNA was air dried in a class II hood for 30 mins until DNA appeared white. 125 µl TE buffer was added to the DNA pellet without resuspending and left to incubate on ice for 1 hour and then resuspended with a cut 200 µl tip. DNA was then incubated with restriction enzymes (Table 18) overnight at 37°C.

Table 18. Solution used for DNA digest.

Component	Quantity
DNA	70 µl
NEBuffer 2.1 (supplied with restriction enzymes)	15 µl
100X BSA	1.5 µl
Restriction enzymes: • Ssp1 (New England Biolabs #R0132S) • BsrG1 (New England Biolabs #R0575S) • EcoR1 (New England Biolabs #R0101S) • Hind3 (New England Biolabs #R0104S) • Xba1 (New England Biolabs # R0145S)	30 U each
Distilled water	Up to final volume of 150 µl
Spermidine	1.5 µl

Following the overnight incubation, DNA solution should be less viscous and easy to pipette. 5 µl of digested DNA sample was reserved to verify success of the DNA digest (see 2.10.2). A 2 ml phase lock gel tube light per sample was centrifuged for 1 min at 16000g at room temperature to pellet the gel. The remainder of the digested DNA was added to each phase lock gel. To each tube, 105 µl nuclease-free water and 250 µl phenol/chloroform isoamyl alcohol were added and the tubes were inverted 4-6 times to mix. Samples were centrifuged for 10 mins at 16,000g at room temperature. In a standard 1.5ml Eppendorf, 625 µL 100% ethanol, 25 µL 3M sodium acetate and 1.5 µL glycogen were mixed and the DNA supernatant was added. Tubes were inverted 4-6 times to mix and then were incubated at -80°C for 1 hour. Tubes were centrifuged at 16,000g for 35 mins at 4°C. Supernatant was discarded and 200 µL ice-cold 80% ethanol was added to the pellet without resuspending. Tubes were centrifuged at 16000g for 10 mins at 4°C. Supernatant was again discarded, taking care to remove as much of the ethanol as possible. DNA was air-dried in a fume hood for 30-60 mins until the DNA appeared translucent. 50 µL TE buffer was added to each DNA sample and left on ice for at least 1 hour before the DNA was gently resuspended into solution with a cut 200 µL tip. DNA concentration was measured, and 260/280 ratio was measured by Nanodrop 1000 (Thermo Scientific).

2.10.2 DNA Digest Quality Control

To verify the DNA digest, 5 µl of digested DNA sample was mixed with 1 µl purple gel loading dye (New England Biolabs # B7024S) and was run along with 3 µl Quick-Load® Purple 1 kb DNA Ladder (New England Biolabs #N0552S) on a 0.8% agarose gel containing ethidium bromide at 100 V for 1 hour. Gel was transferred to a Bio-Rad ChemiDoc imaging chamber and imaged using ImageLab software. Successful DNA digest was assessed by looking for a 'smear' of signal mostly in the 0.5-6kb range.

2.11 MSD ELISA

Cell pellets and exosomes were collected as previously described (2.8.1 and 2.3). Cell pellets were lysed with 30-100 µL RIPA buffer (150 mM NaCl, 1.0% IGEPAL® CA-630, 0.5% sodium deoxycholate, 0.1% SDS, 50 mM Tris, pH 8.0) supplemented with 2% SDS and 1X cOmplete protease inhibitor (Roche #11836170001) and left on ice for 15 mins. Samples were sonicated on ice with a probe sonicator three times for five seconds and centrifuged at 17000g for 20 mins at room temperature. The supernatant was transferred to a new tube and the pellet was discarded. Protein concentration was estimated using the BCA assay (2.8.2) and samples were diluted to 2 µg/µl and stored at -80°C until needed. Samples were diluted 1:1 with EC buffer and were given to Dr Adrian Higginbottom and Dr Ergita Balli who ran the meso scale discovery enzyme-linked immunosorbent assay (MSD ELISA) for the different DPR proteins. The MSD ELISA was run in technical duplicate (two wells per condition).

2.11.1 Analysis

To quantify the results of the MSD ELISA, the mean absorbance reading for the blank sample (no DPRs) was subtracted from the remainder of the results. The absorbance readings for the DPR peptide standard were plotted on a standard curve and a non-linear regression model was applied. DPR protein concentration for each sample was determined by interpolating the mean absorbance readings of the technical replicates of each sample. For MSD ELISA experiments where the standard curve did not work, the raw absorbance readings were used instead. Quantification was performed for at least three independent repeats (each a different differentiation batch) and the average was taken for each cell line and used for statistical analysis.

2.12 Statistics

Unless stated otherwise, all experiments were run at least in triplicate, meaning a minimum of three independent repeats were run for each cell line/astrocyte conditioned medium treatment using a new differentiation each time. The mean of the three independent repeats was calculated and used for statistical analysis. For assays using 96 well plates, each experimental repeat represents a mean value of three technical replicates (two for the MSD ELISA) within an assay plate.

Statistical analysis was performed, and graphs were generated using GraphPad Prism v7.04 (GraphPad Software, La Jolla California USA, www.graphpad.com). Data was tested for normality using the Shapiro Wilk test. For analysis comparing two groups, if data met assumption for normality then an unpaired t-test was run, if data did not meet assumption for normality then the Kolmogorov-Smirnov test was run to compare cumulative distributions. For data comparing three or more groups, if data met assumptions for normality, then a one-way ANOVA was run with either Dunnett's post-hoc multiple comparisons test (comparing each result to the controls or the untreated condition) or Tukey's post-hoc multiple comparisons test (comparing each result to each other). Where data did not meet assumptions of normality, Kruskal-Wallis test was used instead with Dunn's post-hoc multiple comparisons test. For experiments looking at changes in groups over time, two-way RM ANOVA was used with post-hoc multiple comparisons tests. The significance threshold was set as $\alpha = 0.05$. Means and standard deviations are shown for data analysed with one-way ANOVA or two-way RM ANOVA, medians and 95% confidence intervals are shown for data analysed with Kruskal-Wallis test.

Chapter 3: DNA Damage and Repair in ALS Astrocytes

3.1 Introduction

3.1.1 DNA Damage in ALS Neurons

DNA damage has been well-established to be increased in motor neurons in both sporadic and familial forms of ALS (Kok et al., 2021). ALS motor neurons exhibit an increase in expression of oxidised deoxyguanosine (OdG) (Ferrante et al., 1997; Fitzmaurice et al., 1996), a marker of oxidative DNA damage (Valavanidis et al., 2009), as well as an increase in expression and nuclear foci formation of γH2AX (Farg et al., 2017; Naumann et al., 2018; Walker et al., 2017), a marker of DNA damage response activation (Kuo and Yang, 2008). These neurons often correspondingly show increased DNA strand breaks when measured with the comet assay (Higelin et al., 2018; Lopez-Gonzalez et al., 2016; Qiu et al., 2014).

Two key mechanisms proposed as causing increased DNA damage in C9-ALS are oxidative stress and R-loops. Reactive oxygen species (ROS) are common biproducts of mitochondrial respiration that are usually removed by antioxidants such as SOD1 and catalase (Turrens, 2003). If ROS are produced excessively or if antioxidant defences are not sufficient, then ROS can induce oxidative damage to DNA, RNA and proteins (Turrens, 2003). Indeed, ROS have been shown to be increased in C9-ALS iPSC-derived motor neurons (Lopez-Gonzalez et al., 2016) and C9-ALS astrocytes (Birger et al., 2019), possibly due to mitochondrial dysfunction in these cells (Lopez-Gonzalez et al., 2016).

Similarly R-loops have also been shown to be increased in C9-ALS post-mortem spinal cord motor neurons (Walker et al., 2017). R-loops are three-stranded structures that form when nascent RNA hybridises to a DNA strand, thus displacing the other strand. Once formed, the RNA:DNA hybrid structure is very stable and if left unresolved it can affect gene transcription and lead to DNA double-strand breaks (Aguilera and García-Muse, 2012). The C9ORF72 repeat expansion has been shown to be prone to R-loop formation (Haeusler et al., 2014; Reddy et al., 2014) and R-loops appeared to be increased in cells expressing the C9ORF72 RNA repeat expansion or polyGA DPRs (Walker et al., 2017).

DNA damage in ALS has been less well studied in non-neuronal cells and the results of such studies have been mixed. Bone marrow mesenchymal stem cells and blood cells from sALS patients and iPSCs from FUS-ALS, NEK1-ALS and C9-ALS patients do not exhibit increased levels of baseline DNA damage (De Benedetti et al., 2017; Higelin et al., 2016, 2018; Wald-Altman et al., 2017), whereas

dermal fibroblasts from sALS patients do (Riancho et al., 2020). Notably, these non-neuronal cells are mitotic whereas neurons are post-mitotic, which may account for the differences in DNA damage. Unlike post-mitotic cells, mitotic cells are capable of repairing DNA double-strand breaks by homologous recombination (HR) during the S and G2 phases of the cell cycle (Jasin and Rothstein, 2013). Additionally, mitotic cells experience cell turnover where damaged cells can undergo apoptosis and be replaced by cell division or a proliferative stem cell population (Post and Clevers, 2019), while neurogenesis in the adult brain is restricted to specific populations in the hippocampus and olfactory bulb (Gage, 2002), preventing the replacement of damaged neurons. Notably, dermal fibroblasts, which in ALS exhibited increased DNA damage and reduced DNA repair, also had reduced proliferation rate compared to control fibroblasts (Riancho et al., 2020), which may explain why they exhibit increased DNA damage similar to ALS motor neurons.

While there have been extensive studies characterising DNA damage and repair in ALS motor neurons, very few of them examine these parameters in ALS astrocytes. Moreover, the few that do attempt to characterise astrocytes are usually focussed on only one subtype of ALS and only examine expression of one marker, which limits understanding of which types of DNA damage (if any) may be altered in ALS astrocytes.

3.1.2 DNA Damage and Repair in Astrocytes

Like any other cell type, astrocytes are vulnerable to internal and external DNA damage agents and have mechanisms that can repair DNA damage. Interestingly, it has been suggested that healthy astrocytes have reduced DDR signalling. Expression of ATM, ATR, MRE11, MDC1, CHK2 and p53 are reduced in astrocytes compared to neural stem cells, and following irradiation astrocytes fail to induce pATM and 53BP1 foci formation (Schneider et al., 2012). Astrocytes are still capable of γH2AX foci formation, with H2AX being phosphorylated by DNA-PK (Schneider et al., 2012), and are capable of repairing DNA strand breaks, as measured with the comet assay (El-Khamisy et al., 2009; Katyal et al., 2007).

Despite these findings, healthy astrocytes have been shown to be efficient at DNA repair. Following DNA damage induction, astrocytes upregulate expression of repair factors involved in non-homologous end-joining (NHEJ) and HR (Bylicky et al., 2019). It has even been suggested that astrocytes repair oxidative damage to mitochondrial DNA (Hollensworth et al., 2000) and O^6-methylguanine lesions (LeDoux et al., 1996) more efficiently than other glial cells. On the other hand, nucleotide excision repair (NER) has been suggested to be less efficient in astrocytes and

neurons than non-CNS cell types (Yamamoto et al., 2007). Furthermore like neurons, astrocytes show an age-related decline in DNA repair, specifically base excision repair (BER) has been reported to be less efficient in aged astrocytes, and this consequently leads to an age-related increase in DNA damage (Swain and Subba Rao, 2011).

DNA damage and repair have previously been investigated in ALS astrocytes to a limited extent. Astrocytes derived from C9-ALS patient iPSCs (Lopez-Gonzalez et al., 2016) and primary astrocytes from embryonic SOD1-ALS mice (Penndorf et al., 2017) have been shown to have comparable DNA damage to astrocytes derived from controls. DNA repair studies have been more limited. One study suggested PARP1 expression was increased in sALS astrocytes, possibly indicating DNA repair signalling dysfunction (Kim et al., 2003). Another study showed that in SOD1-ALS mouse astrocytes, overexpression of SIRT6, a DNA double-strand break sensor protein that can activate the DNA damage response (Onn et al., 2020), reduced their toxicity to motor neurons (Harlan et al., 2019).

3.1.3 Aims and Objectives

The aim of this chapter was to characterise DNA damage and repair in astrocytes from sALS, C9-ALS and SOD1-ALS patients to determine if either of these mechanisms is altered in ALS astrocytes and whether differences in DNA damage and/or repair exist between different ALS genotypes. I also aimed to look at possible causes of DNA damage in ALS astrocytes, including levels of ROS and R-loops.

In order to carry out these aims, control and ALS astrocytes were differentiated from established iNPC lines and were subjected to immunocytochemistry and biochemical assays. To interrogate oxidative stress, I stained cells for OdG and measured ROS using CellROX reagent. I also used staining to characterise R-loops in ALS astrocytes. As I had access to a previous lab member's unpublished transcriptomic data from the control and ALS astrocytes, with help from Dr Jon Griffin, a senior PhD student in the El-Khamisy lab group, we were able to run upregulated and downregulated transcripts through an online R-loop database to determine whether these transcripts were more likely to have R-loop forming sequences (RLFS) and could therefore be affected by R-loops.

To characterise levels of DNA damage, I assessed γH2AX and 53BP1 via immunocytochemistry. These markers are well-established and commonly used, but primarily show activation of the DNA damage response rather than allow direct quantification of DNA damage (Kuo and Yang, 2008). The

comet assay on the other hand, allows quantification of levels of DNA strand breaks, and can be modified with the inclusion of the OGG1 enzyme that cleaves DNA at sites of oxidative DNA damage, to allow quantification of oxidative DNA damage (Collins, 2004, 2014). To assess DNA repair, I ran Western blotting for DNA repair factors including APE1, TOPO1, XRCC1, Ku80 and PARP1. To assess DNA repair over time, I treated the cells with camptothecin (CPT), a DNA topoisomerase I inhibitor that induces DNA damage (Liu et al., 2000), allowed the cells to recover and stained the cells for γH2AX and 53BP1.

By accomplishing these aims, I could determine whether there are changes in DNA damage or repair between control and ALS astrocytes that could potentially explain the toxicity of the ALS astrocytes, or help us understand how astrocytes become toxic. Additionally, if there are any genotype specific changes, these could inform us of potential mechanisms by which astrocytes exert toxicity.

3.2 DNA Damage Agents in ALS astrocytes

3.2.1 Reactive Oxygen Species in ALS Astrocytes

Oxidative stress has long been established as a possible mechanism of neurodegeneration in ALS (Ferraiuolo et al., 2011a) and has been put forward as a potential driver of DNA damage (Cadet and Davies, 2017). In fact, reactive oxygen species (ROS) are biproducts of respiration and can cause oxidative damage to DNA, RNA and proteins (Turrens, 2003). To examine levels of ROS, I differentiated astrocytes from induced neuronal progenitor cells (iNPCs) derived from control, sALS, SOD1-ALS and C9-ALS patients as previously described (Meyer et al., 2014). Mature live astrocytes were stained with CellROX reagent (Figure 10), which fluoresces when oxidised by ROS. I normalised CellROX intensity to area rather than number of cells to consider differences in cell size between different astrocyte cell lines. Due to differences in intensity between staining plates, data on each plate was normalised to control cell line 3050, which showed stable CellROX staining across repeats.

Interestingly, the samples carrying the same mutations, i.e. SOD1 and C9ORF72, displayed similar CellROX intensity levels within their genetic subgroup, while sALS patient lines displayed much higher variability (Figure 10A-B). Two out of three sALS lines showed a clear increase in CellROX intensity, while the third sALS line showed intensity levels similar to control, SOD1-ALS and C9-ALS astrocytes. When I grouped the data (Figure 10C), I observed no significant change (one-way ANOVA, $p=0.38$) in CellROX intensity per μm^2 across the ALS genotypes.

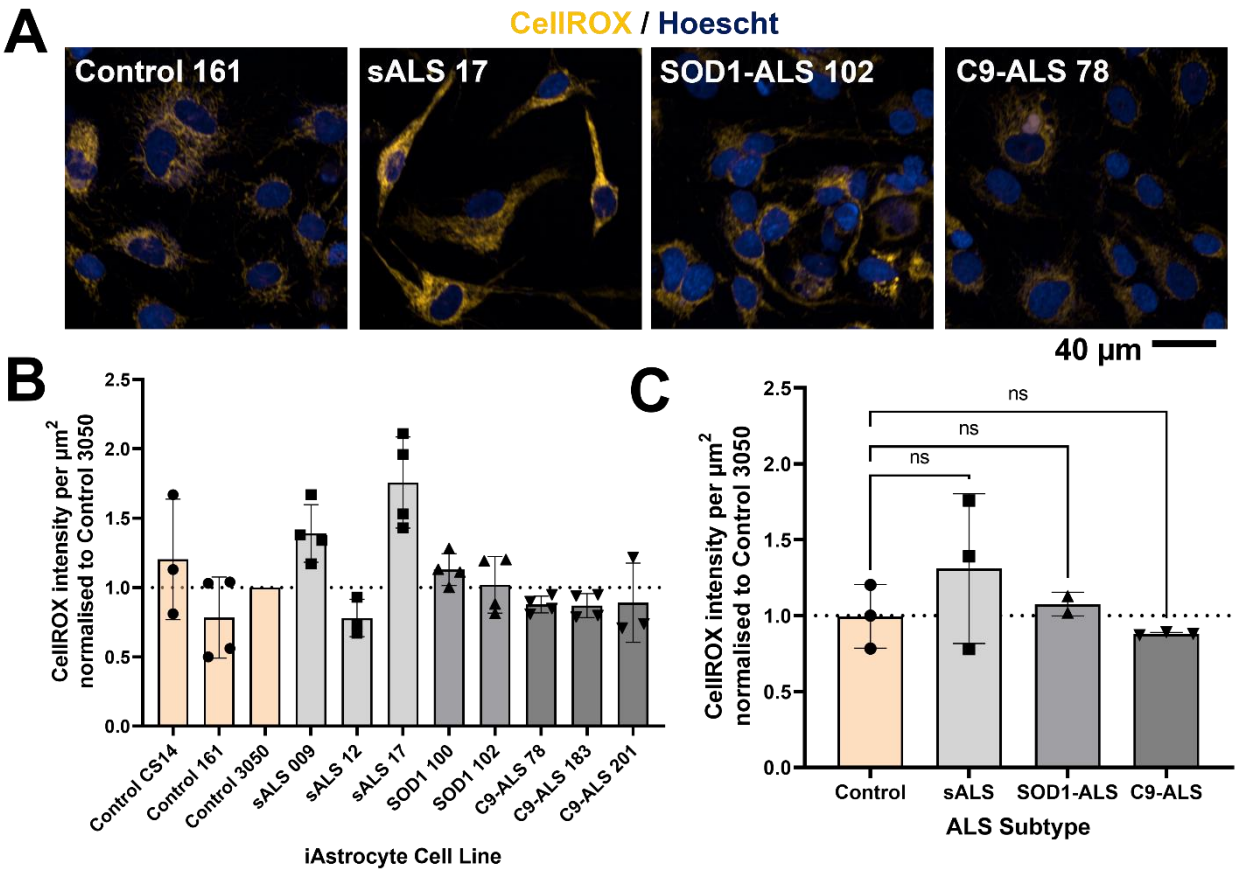

Figure 10. Reactive oxygen species are selectively increased in certain sALS astrocyte lines. A: Example images of CellROX staining in control and ALS astrocytes. B: Quantification of CellROX intensity per µm^2 in control (n=3), sALS (n=3), SOD1-ALS (n=2) and C9-ALS (n=3) astrocytes. Means and standard deviations shown, each datapoint represents one repeat. All datapoints normalised to control 3050 to take into account differences in staining intensity between plates. C: Grouped CellROX quantification results. Data met assumption for normality, one-way ANOVA (p=0.38). Means and standard deviations shown, each datapoint represents mean result of one cell line.

3.2.2 Oxidised Guanosine in ALS Astrocytes

As ROS levels were elevated in two out of three sALS lines, I wanted to assess whether oxidative damage was increased in ALS astrocytes. For this purpose, I decided to use an antibody that reportedly detects oxidative RNA and DNA damage by binding oxidised guanosine (OG) and oxidised deoxyguanosine (OdG) respectively. Staining was optimised by adapting an existing protocol using the same antibody (Debelec-Butuner et al., 2016), with different cell fixation (4% PFA vs 100% methanol) and blocking approaches (donkey serum or bovine serum albumin). I found that the best staining was achieved using methanol fixation, donkey serum blocking and low antibody concentration (1:3000) which led to loss of most of the cytoplasmic signal but retained the nuclear foci (see Appendix 7.1).

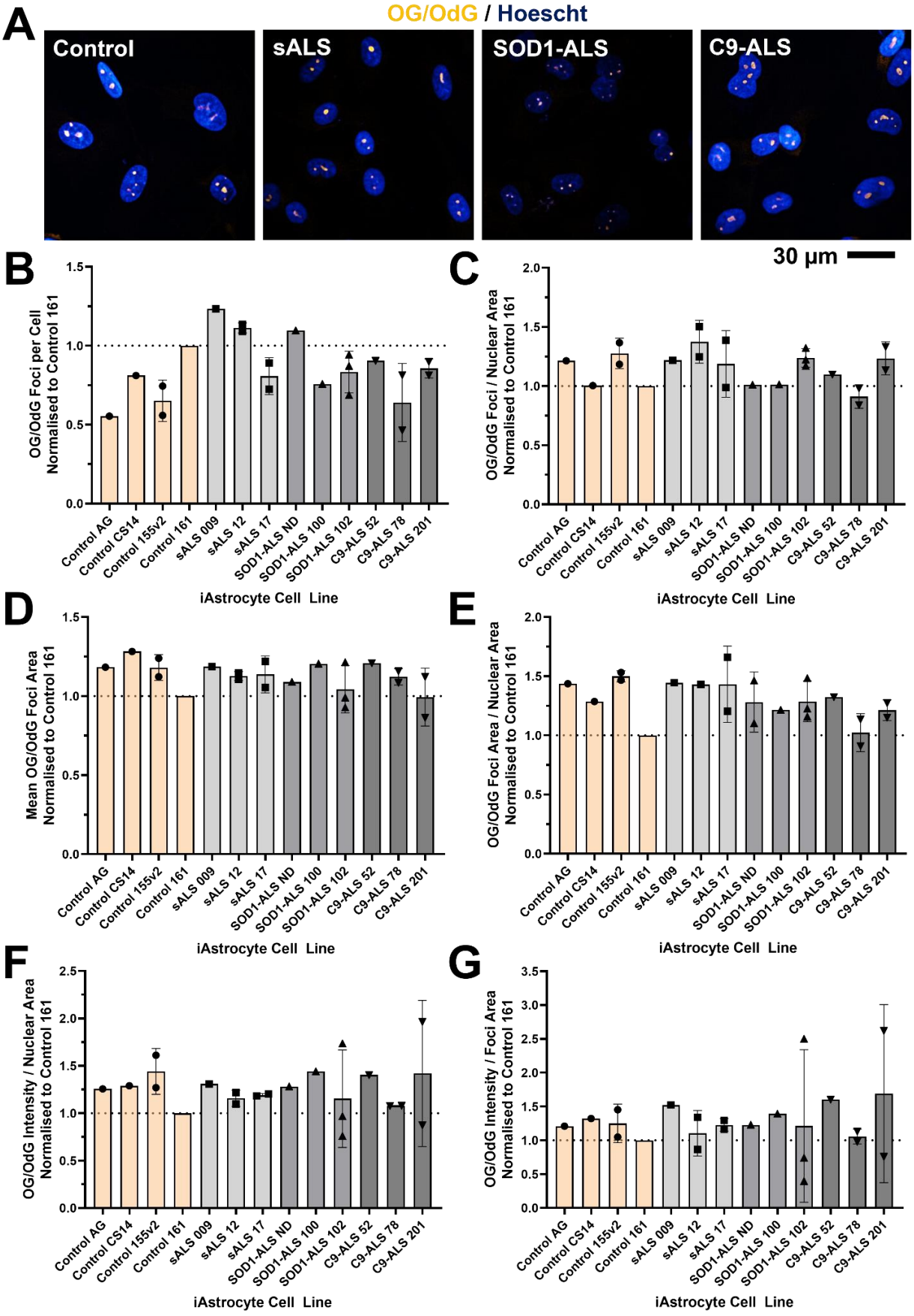

Figure 11. OG/OdG staining is inconclusive in control and ALS astrocytes. A: Example images of OG/OdG staining in control and ALS astrocytes. B-C: Foci number quantification. D-E: Foci size

quantification. F-G: OG/OdG intensity quantification. Mean and standard deviations shown, each datapoints represents one repeat. All datapoints normalised to control 161, which was consistently available for all repeats, to take into account differences in staining intensity. No statistics run due to missing datapoints.

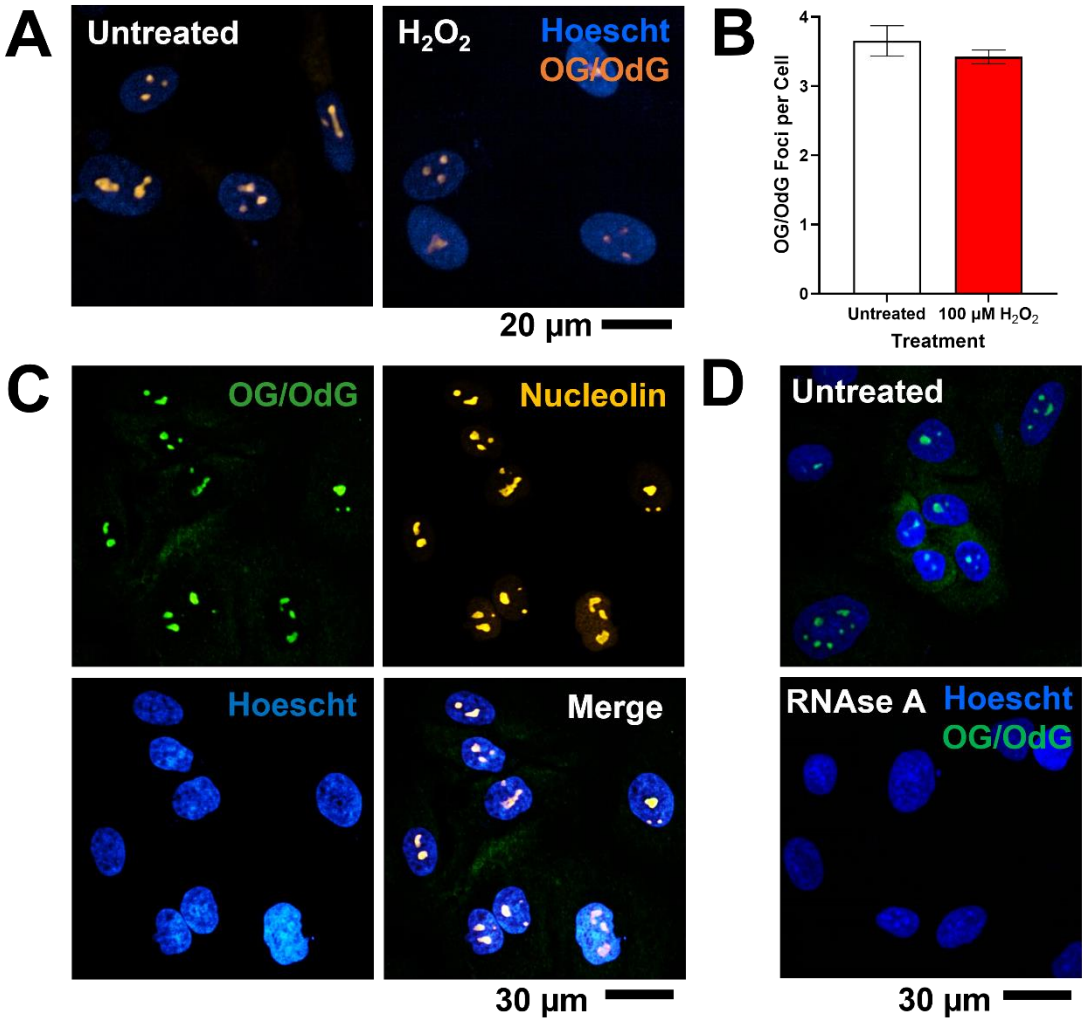

Figure 12. Validation of OG/OdG antibody shows the signal is nucleolar and sensitive to RNAse A. A-B: OG/OdG foci are not increased following hydrogen peroxide treatment. Graphs shows means and standard deviations for three technical replicates of a control cell line left untreated or treated with 100 µM hydrogen peroxide. C: OG/OdG staining co-localises with nucleoli. D: OG/OdG staining is ablated by RNAse A treatment indicating the staining is more likely to be OG rather than OdG.

Following staining optimisation, I stained control and ALS astrocytes using the OG/OdG antibody (Figure 11A). Patterns of nuclear signal looked similar between controls and ALS astrocytes, and I could detect no difference between control and ALS astrocytes after analysing multiple different parameters including foci number (Figure 11B-C), foci size (Figure 11D-E) and signal intensity (Figure 11F-G). Importantly, I also observed no change following treatment with hydrogen peroxide (Figure 12A-B), which induces oxidative damage to DNA and RNA (Ransy et al., 2020) and therefore should function as a positive control, indicating a possibility that this was not oxidised signal. Furthermore,

I observed high levels of signal in the control lines, and I did not observe an increase in signal for the two sALS lines that had elevated ROS levels, which would have been expected. The nuclear foci were suggested to resemble nucleoli, so I ran a co-stain for the RNA/DNA damage antibody and the nucleoli marker, nucleolin. The RNA/DNA damage signal appeared completely colocalised with nucleolin (Figure 12C), indicating the signal was primarily present in nucleoli. To determine whether the signal was specifically related to oxidised RNA or DNA, I treated cells with RNAse A, which completely ablated the nuclear signal (Figure 12D). I thus concluded the signal was likely nucleolar RNA. I did not complete the experiment in triplicate as I could not be certain what I was staining and early results showed no difference between control and ALS astrocytes.

3.2.3 R-loops in ALS Astrocytes

R-loops have been shown to be increased in cells expressing the C9ORF72 repeat expansion (Reddy et al., 2014; Walker et al., 2017), thus I decided to characterise levels of R-loops in the control and ALS astrocytes. As ROS-induced DNA single and double-strand breaks in actively transcribed regions have been suggested to lead to the formation of R-loops (Tan et al., 2020; Teng et al., 2018), I included the sALS and SOD1-ALS astrocytes as well in the characterisation although I hypothesised that R-loops would be elevated in C9-ALS astrocytes only.

I stained control and ALS astrocytes for the S9.6 antibody, which stains RNA:DNA hybrids (Figure 13A-B). While I found no significant change in nuclear S9.6 foci per cell across the ALS subtypes (one-way ANOVA p=0.21), there was an increase in S9.6 foci in two (C9-ALS 183 and 201) out of four C9-ALS astrocyte lines (Figure 13C). S9.6 staining closely resembled nucleoli and co-staining of S9.6 and nucleolin confirmed that the S9.6 signal was co-localised with nucleoli, with little to no non-nucleolar signal observed (Figure 13D). R-loops are reported to be resistant to RNAse A treatment, but sensitive to RNAse H treatment (Phoenix et al., 1997). The initial attempt at validating the S9.6 staining suggested the signal was R-loop specific as it was not affected by RNAse A treatment, however further validation with fresh reagent revealed the S9.6 signal was completely ablated by RNAse A (Figure 13D-E), indicating the signal may not be R-loop specific.

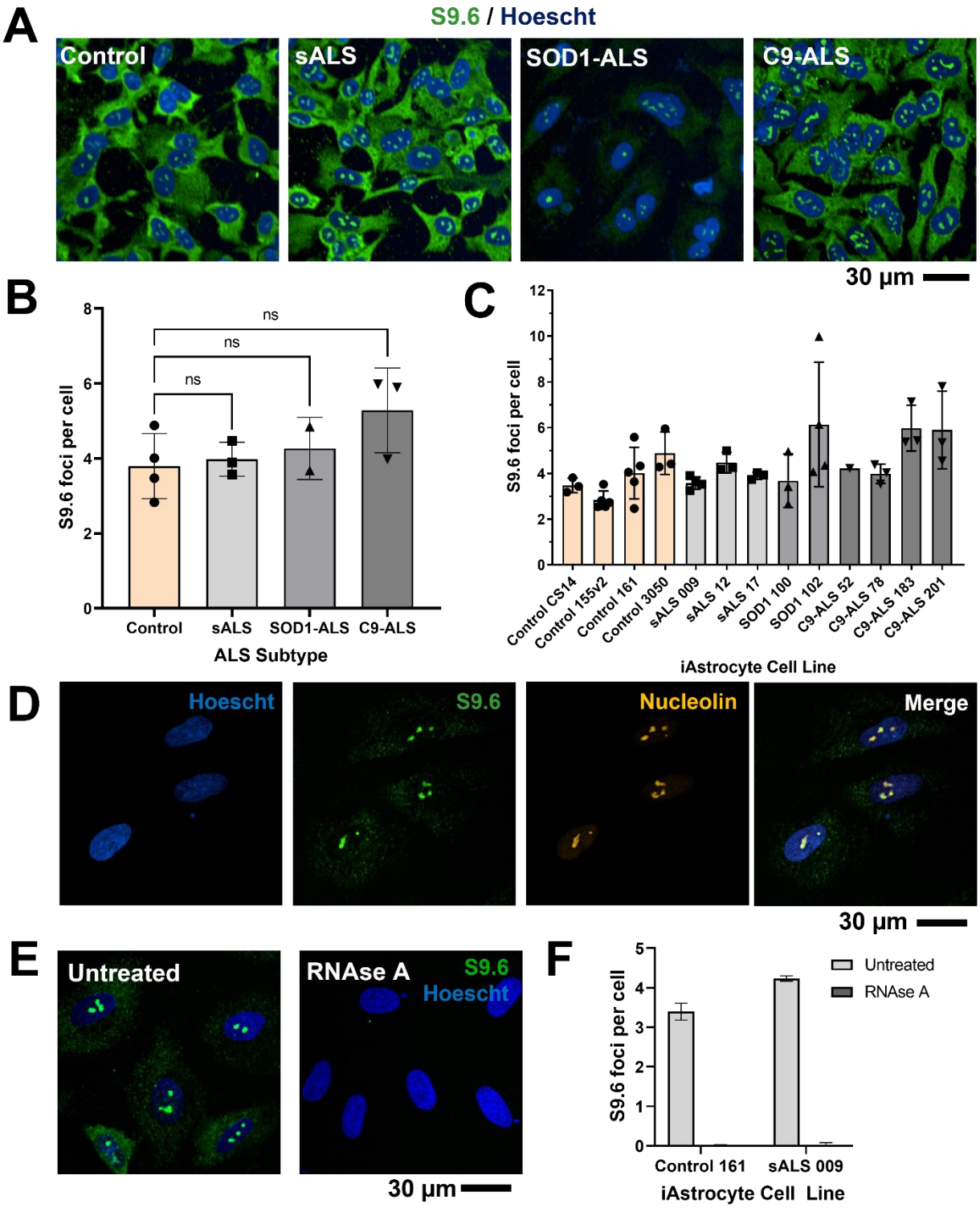

Figure 13. S9.6 foci are increased in certain C9-ALS astrocyte cell lines. A-B: Immunocytochemistry results for S9.6 staining in control (n=3), sALS (n=3), SOD1-ALS (n=2) and C9-ALS (n=3) astrocytes. Data met assumption of normality, one-way ANOVA (p=0.21). Means and standard deviations shown, each datapoint represents one cell line, three biological repeats per cell line. C: S9.6 foci per cell results for each cell line. Means and standard deviations shown, each datapoint represents one repeat, 1-4 repeats per cell line. D: S9.6 nuclear foci colocalise with nucleoli. E-F: S9.6 nuclear foci completely ablated with 10 µg/ml RNAse A treatment. Means and standard deviations of technical triplicate shown for two cell lines.

3.2.4 Nucleoli

Both my OG/OdG and S9.6 staining co-localised with nucleoli, which are known to play a role in DNA damage signalling and repair. The nucleolar proteome has been shown to contain a number of DNA repair proteins including APE1, Ku70, Ku80 and the catalytic subunit of DNA-PK, which translocate out of the nucleolus following DNA damage induction (Lirussi et al., 2012; Moore et al., 2011). Furthermore, nucleolar proteins like TCOF1, nucleophosmin, nucleolin and RPS3 have been found to localise to sites of DNA damage and interact with DNA repair proteins (Ogawa and Baserga, 2017). I therefore decided to characterise nucleoli in control and ALS astrocytes to see if there were any alteration in nucleoli number or morphology. Nucleolin staining led to nuclear foci as expected, which were disrupted by CPT treatment (Figure 14A), which has previously been shown to induce nucleolar disruption (Karyka et al., 2022; Pietrzak et al., 2011). Furthermore, unlike other nucleolar-like staining I have performed (OdG/OG, S9.6), RNAse A treatment only induced a reduction in nucleolin signal intensity but did not completely ablate the nuclear foci (Figure 14B), thus indicating the antibody was not binding non-selectively to RNA and that my staining was specific for nucleoli.

Data was normalised to control cell line 161, to take into account differences in automated analysis between staining plates. Quantification of nucleolin foci number (Figure 14C-E) revealed no significant difference in nucleoli per cell across the ALS subtypes (Kruskal-Wallis p=0.39), however two out of three C9-ALS lines (C9-ALS 183 and C9-ALS 201) showed a considerable increase in nucleoli per cell compared to the controls. Notably, these were the same cell lines that showed an increase in S9.6 foci per cell (Figure 13C). I observed the same pattern when I normalised to nuclear area rather than cell number, however this was again not significant (Kruskal-Wallis p=0.66). It therefore may be that the increase in S9.6 foci per cell observed in certain C9-ALS astrocyte lines could result from an increase in nucleoli number. Nucleolar size has been suggested to be increased in neurons expressing the C9ORF72 repeat expansion (Mizielinska et al., 2017), so I quantified two measures of nucleolar size: mean nucleolar area and ratio of nucleolar area to nuclear area (Figure 14F-G). I observed no significant change in either parameter (mean nucleoli area – one-way ANOVA p=0.57, nucleoli area / nuclear area - Kruskal-Wallis test p=0.73). I again observed that C9-ALS 183 and C9-ALS 201 showed a reduction in mean nucleolar area that was not seen with C9-ALS 78.

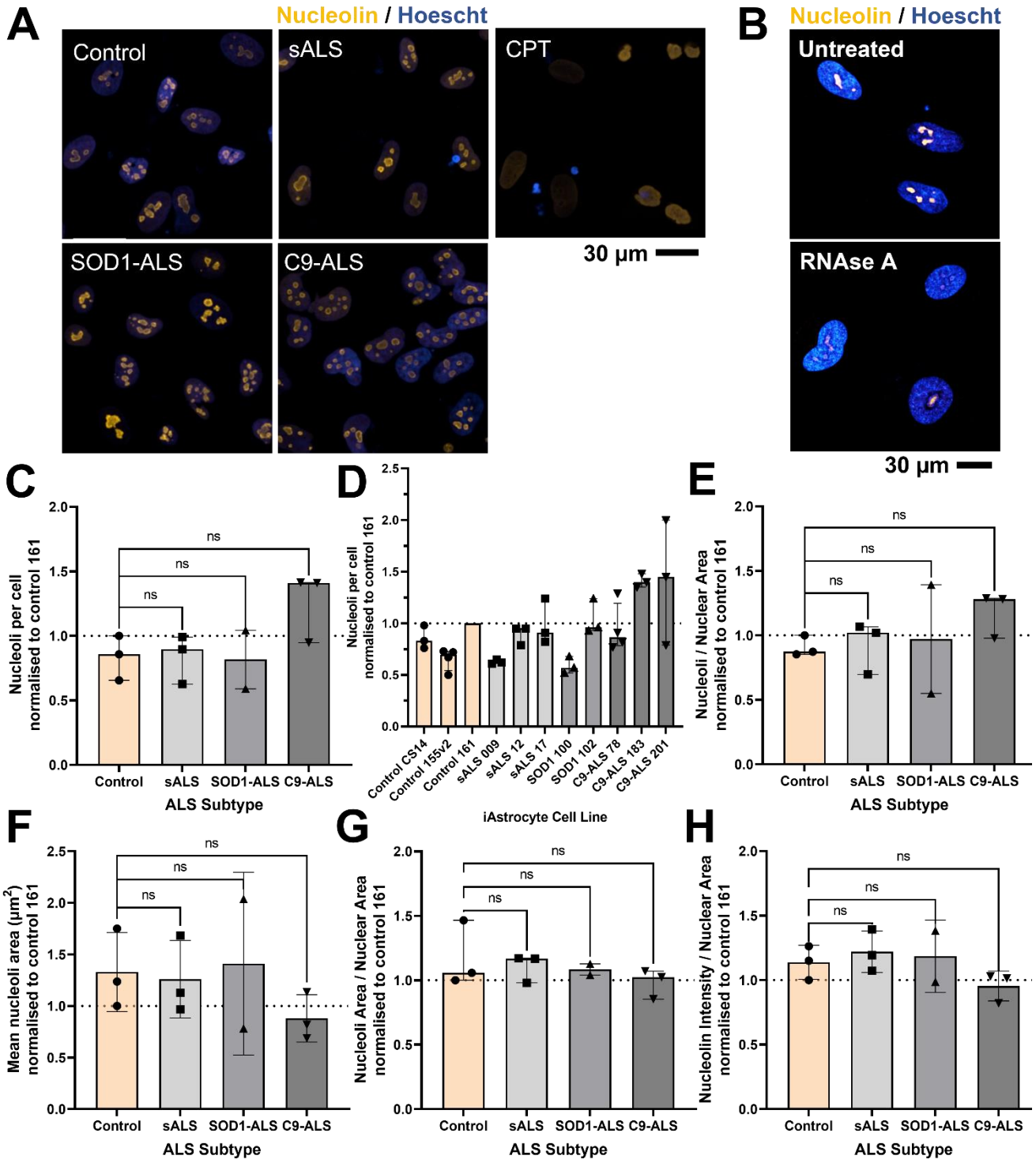

Figure 14. Nucleoli number and morphology are altered in certain C9-ALS astrocyte lines. A: Example images of nucleolin staining in control (n=3), sALS (n=3), SOD1-ALS (n=2) and C9-ALS (n=3) astrocytes and astrocytes treated with 14 µM CPT. B: Nucleolin staining is not ablated by 10 µg/ml RNAse A treatment. C: Quantification of nucleoli foci per cell. Data did not meet assumption for normality, Kruskal-Wallis test (p=0.39). D: Quantification of nucleoli foci per cell for each cell line. E-H: Quantification of nucleoli / nuclear area (data did not meet assumption for normality, Kruskal-Wallis test p=0.66), mean nucleoli area (data met assumption for normality, one-way ANOVA p=0.57), nucleoli area / nuclear area (data did not meet assumption for normality, Kruskal-Wallis test p=0.73) and nucleolin intensity / nuclear area (data met assumption for normality, one-way ANOVA p=0.30)

in control (n=3), sALS (n=3), SOD1-ALS (n=2) and C9-ALS (n=3) astrocytes. Means and standard deviations shown for data analysed by one-way ANOVA, median and interquartile range shown for data analysed by Kruskal-Wallis test. Each datapoint represents one cell line, three biological repeats per cell line. CPT= camptothecin.

Nucleolin has been suggested to have a role in DNA double-strand break repair. Nucleolin knockdown reduces efficiency of both HR and NHEJ (Kobayashi et al., 2012), and it has been suggested that nucleolin recruitment to DNA damage by the MRN complex allows for nucleolin to remove histone proteins, enabling DNA repair factors to access the lesion site (Goldstein et al., 2013). Thus, I decided to quantify nucleolin staining intensity (Figure 14H), however there was no significant change in nucleolin intensity (one-way ANOVA, p=0.30). To assess whether nucleolin expression was changed in ALS astrocytes, I performed a Western blot (Figure 15). Nucleolin expression did appear to be reduced in sALS, SOD1-ALS and C9-ALS astrocytes compared to two out of three controls, but this difference did not reach significance (one-way ANOVA p=0.052).

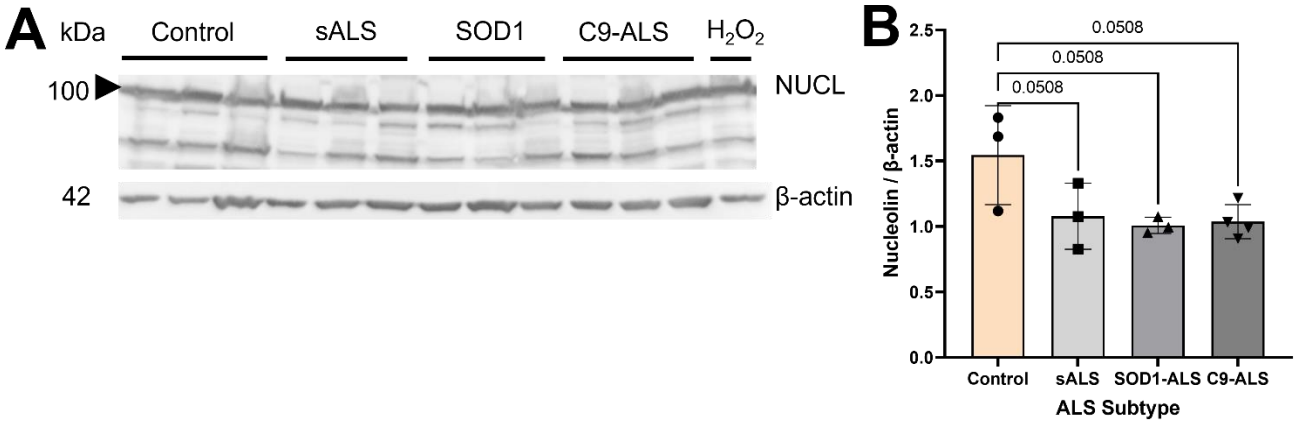

Figure 15. Nucleolin expression appears to be reduced in ALS astrocytes. A-B: Western blotting of nucleolin expression in control (n=3), sALS (n=3), SOD1-ALS (n=3) and C9-ALS (n=4) astrocytes. Data met assumption for normality, one-way ANOVA (p=0.052). Means and standard deviations shown, each datapoint represents one cell line, three biological repeats per cell line.

3.2.5 R-loop Forming Sequences and DRIP qPCR in ALS Astrocytes

Although I observed an increase in S9.6 foci in two out of three C9-ALS astrocyte lines compared to controls, there were some questions raised as to whether this was an actual increase in R-loops or whether it was an increase in nucleoli foci. To determine whether R-loops were increased in C9-ALS astrocytes, I decided to look at R-loop forming sequences (RLFS) in genes that were differentially expressed between control and C9-ALS astrocytes to determine whether R-loops could be affecting gene expression in C9-ALS.

Previous Ferraiuolo lab member, Dr Chloe Allen had generated a transcriptomic dataset for differentially expressed genes in astrocytes from healthy controls and patients with sALS, SOD1-ALS or C9-ALS (thesis under embargo). Genes that met a significance threshold of p=0.05 were run through a currently unpublished automated pipeline designed by Dr Jon Griffin, a senior PhD student in the El-Khamisy lab group, which utilises R-loopDB. R-loopDB is a freely available online database of computationally predicted R-loop forming sequences (RLFS) across the genome (Jenjaroenpun et al., 2017). In this way, I was able to assess across the transcriptomic datasets whether there was a change in the number of predicted RLFS in our patient sample subgroups (Figure 16). For C9-ALS and sALS, but not SOD1-ALS, I found a significant increase in predicted RLFS per 10 kb (C9-ALS $p<0.0001$, sALS $p=0.0003$, SOD1-ALS $p=0.90$) and predicted RLFS gene coverage (C9-ALS $p=0.002$, sALS $p=0.002$, SOD1-ALS $p=0.49$) in downregulated genes compared to upregulated genes. This data indicates that RLFS are more common in genes downregulated in C9-ALS and sALS and could suggest that R-loops may be contributing to transcription downregulation.

As RLFS data is only an indicator of predicted R-loops, I sought to determine whether R-loops were in fact increased in differentially expressed genes using DNA:RNA immunoprecipitation qPCR (DRIP-qPCR). R-loops are considered to be more of a feature of C9-ALS (Reddy et al., 2014; Walker et al., 2017), so I decided to focus on genes that were differentially expressed in C9-ALS astrocytes. I first sought to identify specific gene candidates for DRIP qPCR (Figure 17A). There were 1910 total differentially expressed genes in C9-ALS astrocytes compared to control astrocytes, I filtered the genes based on p adjusted value, RLFS prediction and functional relevance, which resulted in 19 candidate genes. Initially I wanted to look at both up and downregulated genes with high levels of predicted RLFS, as R-loop formation on genes can be a cause of both up and downregulation. However I then considered that, as R-loops are generated during transcription, it would be predicted that higher levels of transcription would be associated with higher levels of R-loops (Aguilera and García-Muse, 2012) and thus it would be difficult to conclude whether R-loop formation on upregulated genes would be a cause or consequence of the upregulation. I therefore decided to focus on the downregulated genes identified by the selection process (Table 19). Of the six downregulated candidate genes I decided to start with GRIN2B and KCNMA1 as they encode ion channels involved in action potential regulation. I performed some initial optimisations to test the DRIP protocol and confirmed the DNA digestion was successful (Figure 17B). Unfortunately due to time constraints as a result of the COVID-19 pandemic, I was unable to proceed with this work.

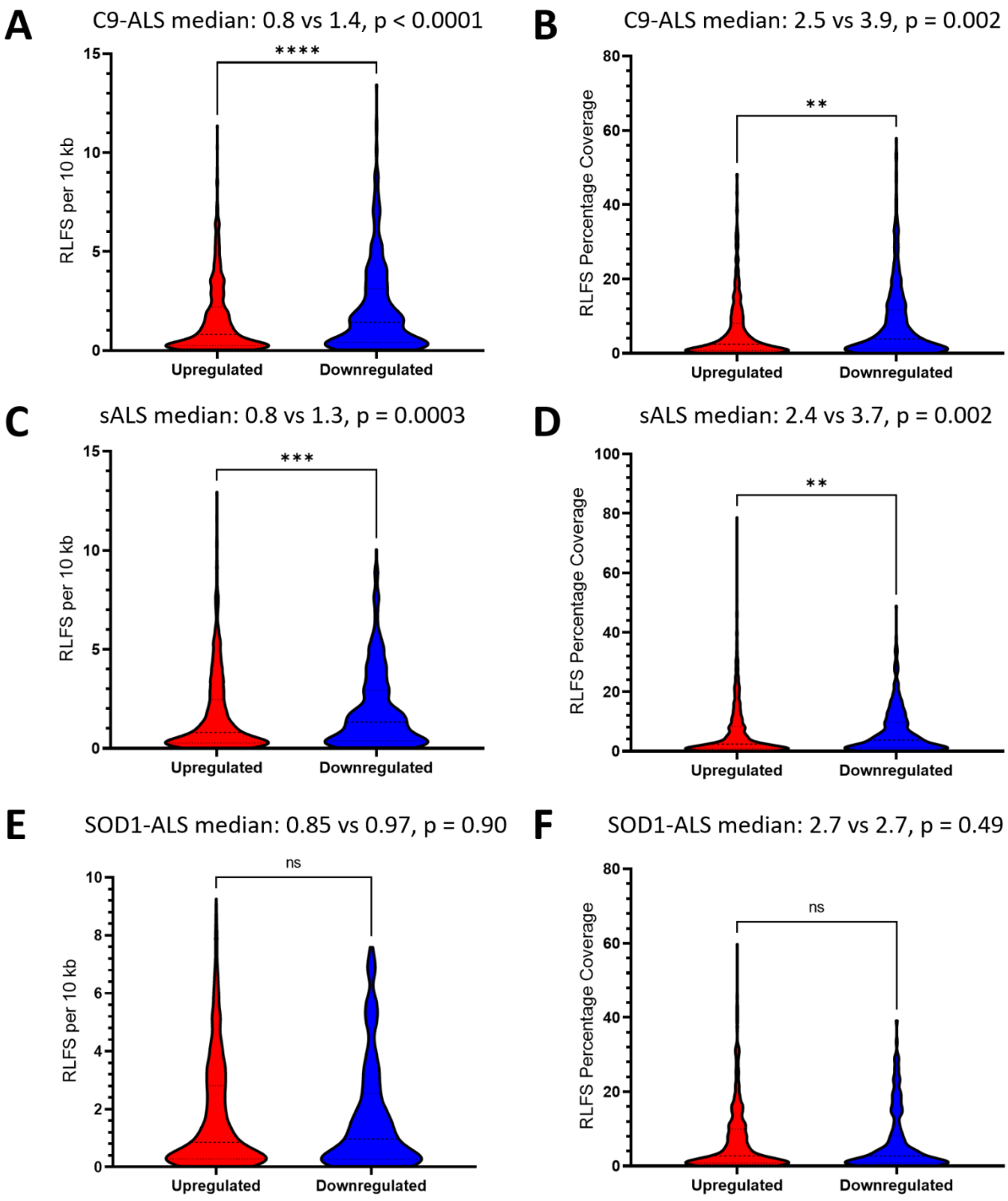

Figure 16. Predicted R-loop forming sequences (RLFS) in differentially expressed genes in C9-ALS, sALS and SOD1-ALS astrocytes (data from Dr Jon Griffin, El-Khamisy lab). A-B: RLFS per 10 kb and RLFS percent coverage in genes that were up or downregulated in C9-ALS astrocytes compared to control astrocytes. C-D: RLFS per 10 kb and RLFS percent coverage in genes that were up or downregulated in sALS astrocytes compared to control astrocytes. E-F: RLFS per 10 kb and RLFS percent coverage in genes that were up or downregulated in SOD1-ALS astrocytes compared to control astrocytes. Kolmogorov-Smirnov test used to compare up and downregulated RLFS measurements for each ALS subtype, results shown above each graph.

Table 19. Candidate genes for DRIP qPCR.

Gene Name	Log2 Fold Change	Expression Change	RLFS Percent Coverage	Number of RLFS	Protein Function
H2AC19	-2.3	Downregulated	16.63	4	Nucleosome structure
KCNMA1	-4.6	Downregulated	0.99	33	Voltage-gated potassium channel activity.
ITGB2-AS1	-4.8	Downregulated	12.95	5	Associated with astrocytoma
PSCA	-6.5	Downregulated	19.88	7	May act as a modulator of nAChR activity
WNT7A	-7.5	Downregulated	9.49	21	Wnt signalling, blood brain barrier regulation
GRIN2B	-8.6	Downregulated	0.55	15	NMDA Receptor

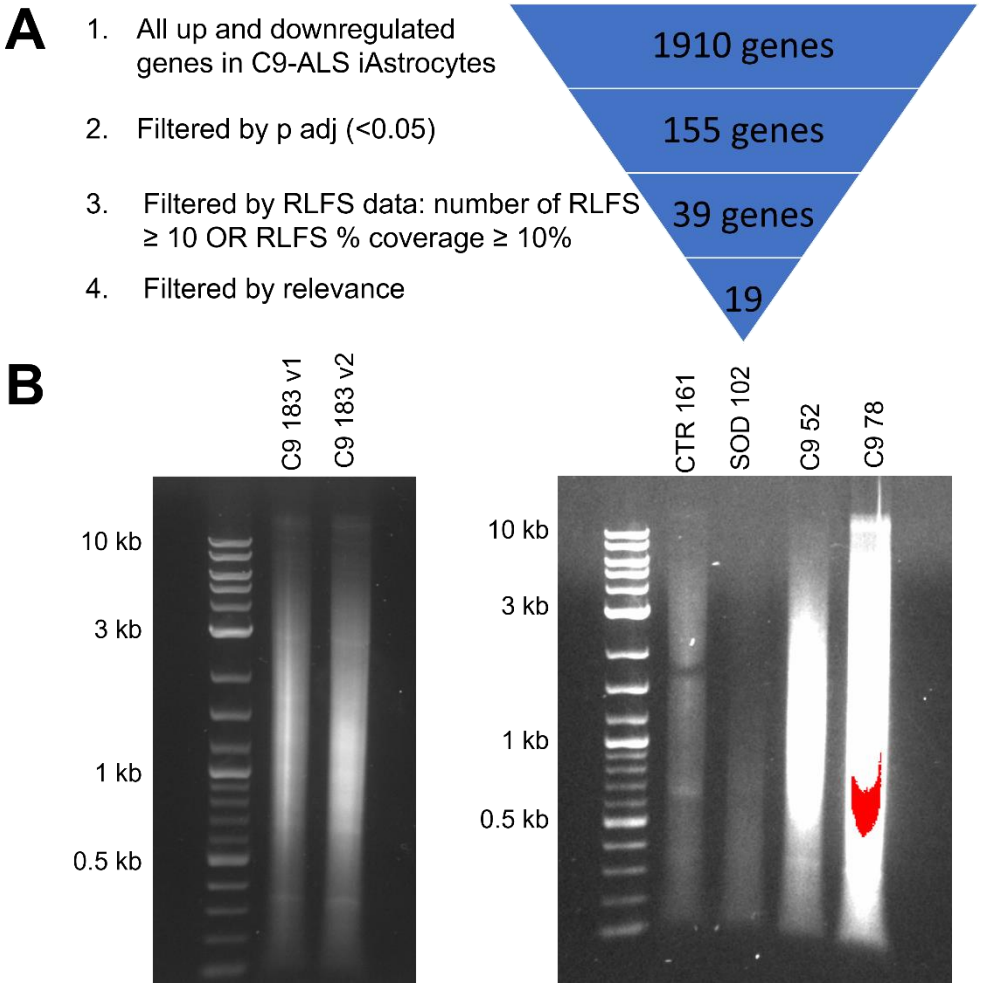

Figure 17. Early DRIP qPCR optimisation in control and C9-ALS astrocytes. A: Gene candidate selection for qPCR based on differentially expressed genes in C9-ALS astrocytes. B: Validation of DNA digest in control and C9-ALS astrocyte samples.

3.3 DNA Damage in ALS Astrocytes

3.3.1 DNA Strand Breaks

To investigate DNA damage directly I ran the alkaline comet assay, which assesses DNA single and double strand breaks, in control and ALS astrocytes (Figure 18). In brief, the comet assay involves electrophoresis being applied to lysed cells which have been embedded in a gel. Within the nucleus, DNA exists as a series of loops. The presence of a DNA strand break within a loop relaxes the supercoiling of that loop, which can move towards the anode when electrophoresis is applied. As the number of DNA strand breaks increases, the more DNA moves toward the anode, leading to the characteristic 'comet' appearance (Figure 18A). The number of DNA strand breaks can be approximately measured by quantifying the tail migration, such as by measuring the tail length or tail intensity (Collins, 2004).

I quantified tail moment, which takes into account both tail length and intensity. Comet tail moment was shown to be increased following hydrogen peroxide treatment, indicating the assay was working correctly (Figure 18B). I observed no significant change in mean comet tail moment across the groups (one-way ANOVA, $p=0.42$), indicating DNA strand breaks were not increased in ALS astrocytes (Figure 18C). When I separated the data out for each cell line (Figure 18D), I observed that sALS 009 did appear to have an increase in DNA strand breaks compared to the controls, but this was not consistent across the sALS group.

In addition to looking at strand breaks, I also sought to adapt the alkaline comet assay to assess oxidative DNA damage. This involves plating each sample on two separate slides, one of which is treated with an enzyme that cleaves DNA at sites of oxidative DNA damage (Collins, 2014). The difference in DNA strand breaks between the treated and untreated slide can then be used as a measure of oxidative DNA damage (Collins, 2014). Formamidopyrimidine glycoslyase (FPG) and endonuclease III are more commonly used for this procedure but have been shown to also cleave DNA at sites of alkylation DNA damage, whereas 8-oxoguanine DNA glycosylase (OGG1) is a human DNA repair enzyme which is considered to be more specific for oxidative DNA damage (Collins, 2014). Unfortunately, I was unable to successfully optimise the assay with OGG1 and observed variability in OGG1 activity between repeats, so I have not presented this data.

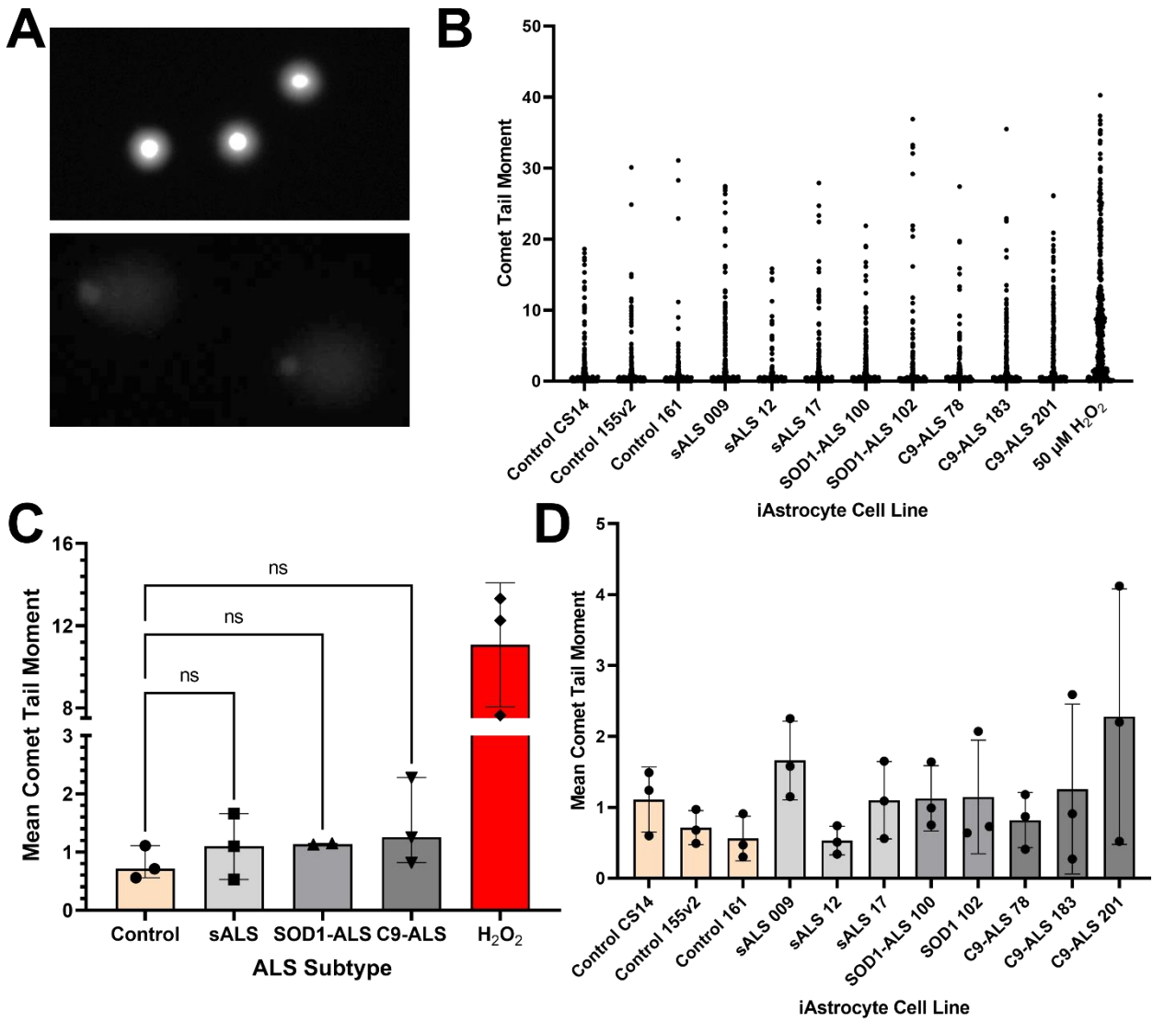

Figure 18. Alkaline comet assay shows no difference in DNA strand breaks between control and ALS astrocytes. A: Example images from comet assay, top image shows cells with no comet tail, bottom image shows cells with clear comet tail. B: Comet tail moment data distributions for each astrocyte cell line, each datapoint represents one cell, minimum 350 cells scored per cell line. C: Mean comet tail moment results for control (n=3), sALS (n=3), SOD1-ALS (n=2) and C9-ALS (n=3) astrocytes. Data met assumption for normality, one-way ANOVA (p=0.42). Means and standard deviations shown, each data point represents one cell line. D: Data from C separated to show results for each cell line. Means and standard deviation shown, each datapoint represents one repeat.

3.3.2 γH2AX and 53BP1 in ALS Astrocytes

Although I observed no significant change in the alkaline comet assay between the control and ALS astrocytes, it has been reported that the comet assay is not as sensitive as more indirect markers of DNA damage, such as γH2AX immunofluorescence (Kuo and Yang, 2008). Therefore, as another method of detecting DNA damage, I stained control and ALS astrocytes for γH2AX (Figure 19A), a well-characterised marker of DNA damage response activation (Turinetto and Giachino, 2015). The

number of γH2AX foci increased following treatment with the DNA topoisomerase I inhibitor, CPT, which acted as a positive control (Figure 19A-C).

The number of γH2AX foci per cell and percentage of γH2AX positive cells varied across the control and different ALS genotypes (Figure 19B-C). No significant difference was detected for γH2AX positive cells across the groups (one or more foci, one-way ANOVA p=0.19), however a significant change was observed for number of γH2AX foci per cell (Kruskal-Wallis, p=0.020). Post-hoc tests indicated there was a significant increase in γH2AX foci in SOD1-ALS (p=0.049) astrocytes compared to controls. There was also a trend towards an increase in γH2AX foci in C9-ALS (p=0.075) astrocytes compared to controls, however this fell short of reaching significance.

As in previous experiments (Figure 13, Figure 14, Figure 18), I observed high variability in the SOD1-ALS and C9-ALS groups (Figure 19B-C). When I separated out the data for the different cell lines (Figure 19D), I identified that DNA damage was elevated in the SOD1-ALS 100, SOD1-ALS 102, C9-ALS 183 and C9-ALS 201 astrocyte lines, with SOD1-ALS 102 and C9-ALS 201 showing the largest increase. Notably, this was not consistent within the genetic subgroups as SOD1-ALS ND, C9-ALS 52 and C9-ALS 78 showed comparable DNA damage levels to controls, indicating that increased DNA damage is a cell line specific feature and is not specific to the given genotype as a whole.

As well as indicating an increase in DNA damage, γH2AX foci are known to form during cell division (Turinetto and Giachino, 2015), thus I hypothesised that differences in cell proliferation rate could have affected the results. To measure the astrocyte proliferation rate, cells were co-stained γH2AX and Ki67 (Figure 19E), a marker of cell proliferation (Ross and Hall, 1995). Nuclear γH2AX foci were selectively counted in Ki67-negative cells, and the pattern of results for γH2AX foci per non-dividing cell was very similar to the pattern for γH2AX foci per cell (Figure 19D,F), indicating cell proliferation was likely not considerably affecting the results. To validate the γH2AX staining data, I also ran Western blotting for γH2AX in control and ALS astrocytes (Figure 19G-H). Indeed, there was no significant change in γH2AX expression across the groups (one-way ANOVA, p=0.36), but the Western blot data confirmed the γH2AX staining data, indicating that C9-ALS astrocytes from donors 183 and 201, and SOD1-ALS astrocytes from donors 100 and 102, displayed higher levels of DNA damage.

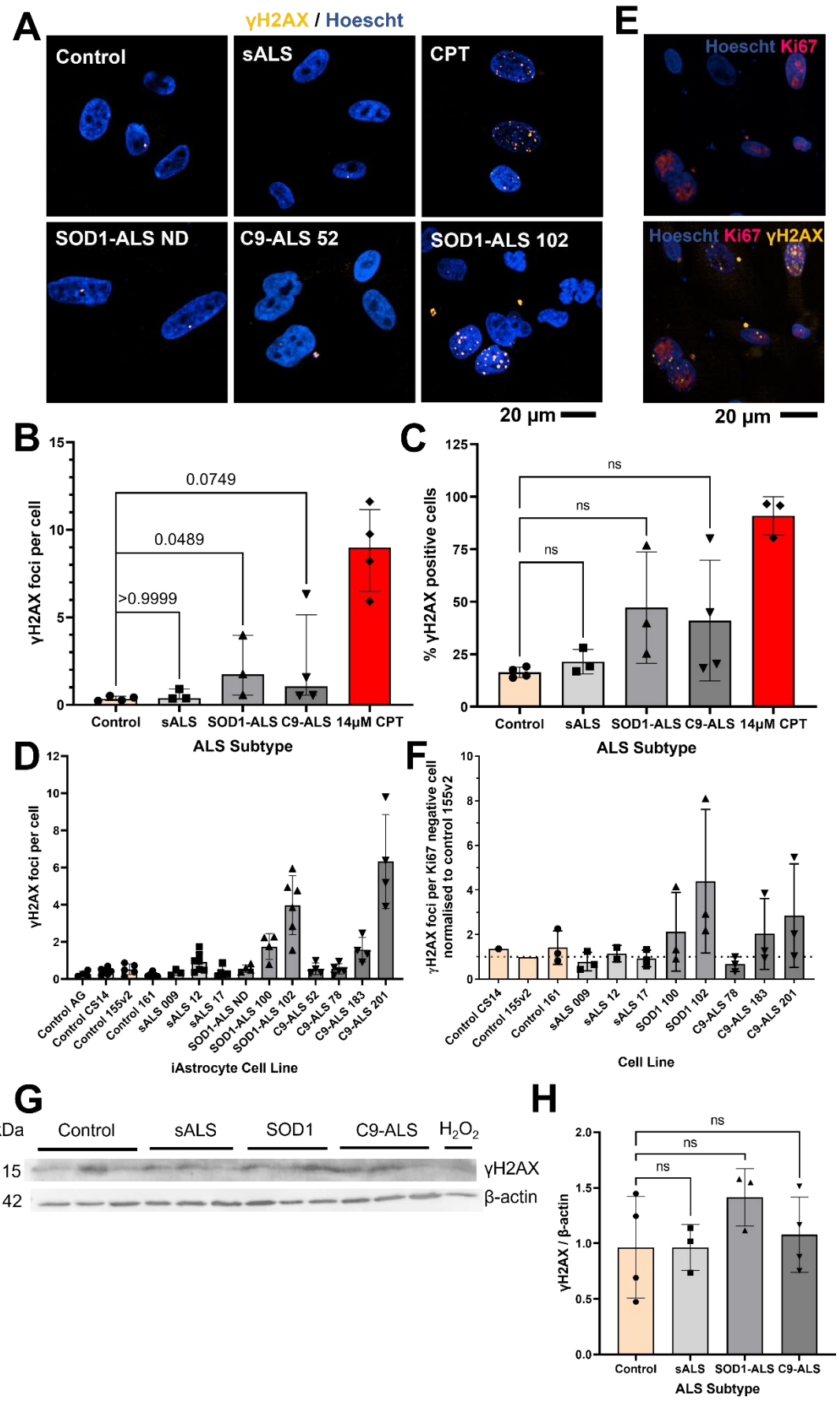

Figure 19. γH2AX foci are increased in specific ALS astrocyte lines. A: Example images of γH2AX staining in control and ALS astrocytes and astrocytes treated with 14 µM CPT. Staining done with help

from Sam Boldan, an undergraduate student under my supervision. B-C: Quantification of γH2AX foci per cell and percentage γH2AX positive cells (1 or more foci) in control (n=4), sALS (n=3), SOD1-ALS (n=3) and C9-ALS (n=4) astrocytes. Each datapoint represents one cell line, minimum of three biological repeats per cell line. B: Data did not meet assumption for normality, Kruskal-Wallis test (p=0.02), Dunn's multiple comparisons test (Control vs sALS p>0.99, control vs SOD1-ALS p=0.049, control vs C9-ALS p=0.075). C: Data met assumption for normality, one-way ANOVA (p=0.19). D: Quantification of γH2AX foci per cell results for each cell line. Means and standard deviations shown, each datapoint represents one repeat. E: Example images of Ki67 staining in astrocytes. F: Quantification of γH2AX foci in Ki67 negative cells, normalised to control 155v2 to take into account differences in automated analysis between staining plates. Means and standard deviations shown, each datapoint represents one repeat. G-H: Western blotting of γH2AX in control (n=3), sALS (n=3), SOD1-ALS (n=2) and C9-ALS (n=3) astrocytes. Data met assumption for normality, one-way ANOVA (p=0.36), each datapoint represents one cell line, three biological repeats per cell line. For data analysed by one-way ANOVA, means and standard deviations are shown. For data analysed by Kruskal-Wallis test, median and interquartile range are shown.

In addition to looking at γH2AX foci, I also decided to look at 53BP1, a DDR protein which is involved in DNA double-strand break repair (Mirza-Aghazadeh-Attari et al., 2019). I stained control and ALS astrocytes for 53BP1 as previously described (Figure 20A). Similarly to γH2AX, the number of 53BP1 foci increased following CPT treatment (Figure 20A-C) and the 53BP1 foci were co-localised with γH2AX as expected (Figure 20B), indicating the staining was specific for 53BP1. Likewise, I observed a significant increase in 53BP1 foci per cell (Kruskal-Wallis test, p=0.012) and 53BP1 positive cells (Kruskal-Wallis test, p=0.008) across the groups (Figure 20C-D), of which the increase in 53BP1 foci per cell and 53BP1 positive cells was statistically significant in both SOD1-ALS astrocytes (p=0.030, p=0.030) and C9-ALS astrocytes (p=0.043, p=0.034) compared to control astrocytes. Notably, there was again high variability in the SOD1-ALS and C9-ALS groups due to two SOD1-ALS lines (100, 102) and one C9-ALS (201) astrocyte line having much higher 53BP1 foci per cell (Figure 20D). Removing these datapoints from the dataset (Figure 20E) does show that the remaining SOD1-ALS and C9-ALS astrocyte lines still display increased 53BP1 foci per cell compared to controls, although with a smaller effect size.

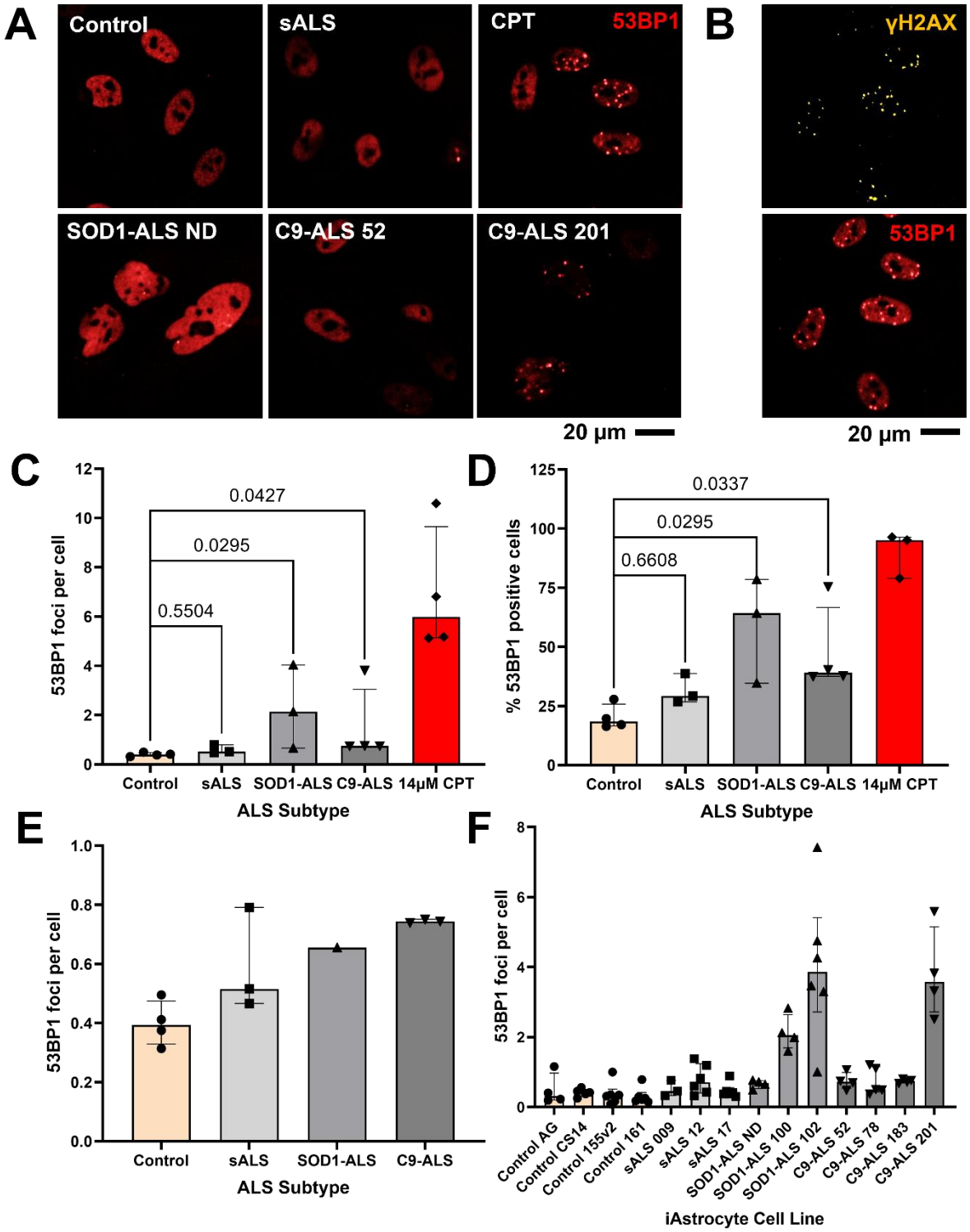

Figure 20. 53BP1 foci are increased in SOD1-ALS and C9-ALS astrocytes. A: Example images of 53BP1 staining in control (n=4), sALS (n=3), SOD1-ALS (n=3) and C9-ALS (n=4) astrocytes and astrocytes treated with 14 µM CPT. Staining done with help from Sam Boldan, an undergraduate student under my supervision. B: Example images showing co-localisation of γH2AX and 53BP1 foci. C-D: Quantification of 53BP1 foci in control and ALS astrocytes. Data did not meet assumption for normality, Kruskal-Wallis test (53BP1 foci per cell p=0.012, 53BP1 positive cells p=0.008) and Dunn's multiple comparisons test. Median and interquartile range shown, each datapoint represents one repeat. E: Results from C but excluding datapoints higher than 1 foci per cell, to illustrate smaller

differences in 53BP1 foci across the groups. Median and interquartile range shown, each datapoint represents one cell line. F: Quantification from C showing biological repeat results for each cell line. Median and interquartile range shown, each datapoint represents one repeat.

3.3.3 DNA Repair Kinetics

After observing increased DNA damage in certain ALS astrocyte lines, I hypothesised that ALS astrocytes may show impaired DNA repair. To test this, I treated control and ALS astrocytes with CPT for 1 hour and then allowed the cells to recover for various timepoints (0hrs, 1h, 3hrs, 6hrs and 24hrs). I stained the treated cells for γH2AX and 53BP1 and measured the change in number of foci over the different repair periods (Figure 21). As expected, controls exhibit low levels of γH2AX and 53BP1 foci at baseline, and the number of foci are considerably increased following 1 hour of CPT treatment (timepoint 0hr). Following withdrawal of CPT treatment, the number γH2AX foci reduce considerably within one hour and then reduce more gradually over the next 24 hours. 53BP1 foci decline more slowly than γH2AX foci, with the number of 53BP1 foci reducing considerably within three hours of CPT withdrawal and then declining more gradually over the next 24 hours. After 24 hours of CPT withdrawal, γH2AX and 53BP1 foci remain higher than at baseline prior to CPT treatment.

Compared to the controls, I observed some differences in DNA repair across the ALS subtypes (Figure 21B and F), however, consistent with the other assays, I observed considerable variability. As there was a difference in endogenous levels of γH2AX and 53BP1 across the ALS subtypes (see 3.3.2), I normalised the data of each ALS genotype to their corresponding untreated condition to better visualise the delta between baseline and DNA repair after insult (Figure 21C and G). The normalised to untreated dataset suggested that the SOD1-ALS and C9-ALS astrocyte showed the smallest increase in γH2AX and 53BP1 immediately following treatment, which was the opposite of what was observed in the original dataset (Figure 21B and F). This might be due to γH2AX and 53BP1 levels being elevated at baseline in SOD1-ALS and C9-ALS astrocytes, making the delta in γH2AX and 53BP1 foci appear less than in control or sALS astrocytes despite the number of foci following CPT treatment at timepoint 0 being relatively similar across the groups. Bearing this in mind, I also normalised the data to timepoint 0 (Figure 21D and H) which helped us better visualise the change in γH2AX and 53BP1 foci over the 24-hour repair period.

Looking at data normalised to timepoint 0, DNA repair in sALS astrocytes appeared similar to controls, with the pattern of foci for both γH2AX and 53BP1 declining at similar rates. On the other hand, DNA repair in SOD1-ALS and C9-ALS astrocytes appeared abnormal. γH2AX and 53BP1 foci

showed very little decline following CPT withdrawal and after 24 hours, foci numbers were considerably higher than control or sALS foci at the same timepoint. Statistical analysis of γH2AX and 53BP1 results is reported in Table 20 and Table 21 respectively. Time was a significant source of variation for all the datasets, as expected. There were considerable differences between individual patient lines. However, only the normalised to untreated datasets identified ALS subtype as a significant source of variation, with post-hoc multiple comparison tests (see full results in Appendix: 7.3, 7.4, 7.5) identifying a significant difference between control and C9-ALS γH2AX foci per cell at timepoint 0hr ($p=0.002$) and significant differences between control and C9-ALS 53BP1 foci per cell at timepoint 0hr ($p=0.024$), 1hr ($p=0.036$) and 3hr ($p=0.022$).

Notably, for all datasets there was considerable variation within the SOD1-ALS and C9-ALS groups. To determine what the source of variation might be, I separated out the γH2AX and 53BP1 data for the different cell lines (Figure 22). It became clear, that while there was some variation between repeats of the same cell line, the main reason for the large differences in results was that some SOD1-ALS and C9-ALS lines had comparable repair kinetics to controls (SOD1-ALS ND, C9-ALS 78) whereas other lines showed very different repair profiles (SOD1-ALS 100 & 102, C9-ALS 52, 78 & 201), indicating a heterogeneity within the ALS subtypes. Notably, this is the same heterogeneity that was observed in the baseline γH2AX and 53BP1 datasets, where the lines with the most γH2AX and 53BP1 foci at baseline have the most abnormal repair kinetics.

To determine whether increased cell death following CPT treatment could be influencing the results, I examined change in cell number over time following CPT treatment (Figure 23). The ALS subtypes showed similar trends to the controls, with the sALS lines having the greatest cell loss following CPT treatment, but this was not significant (Table 22).

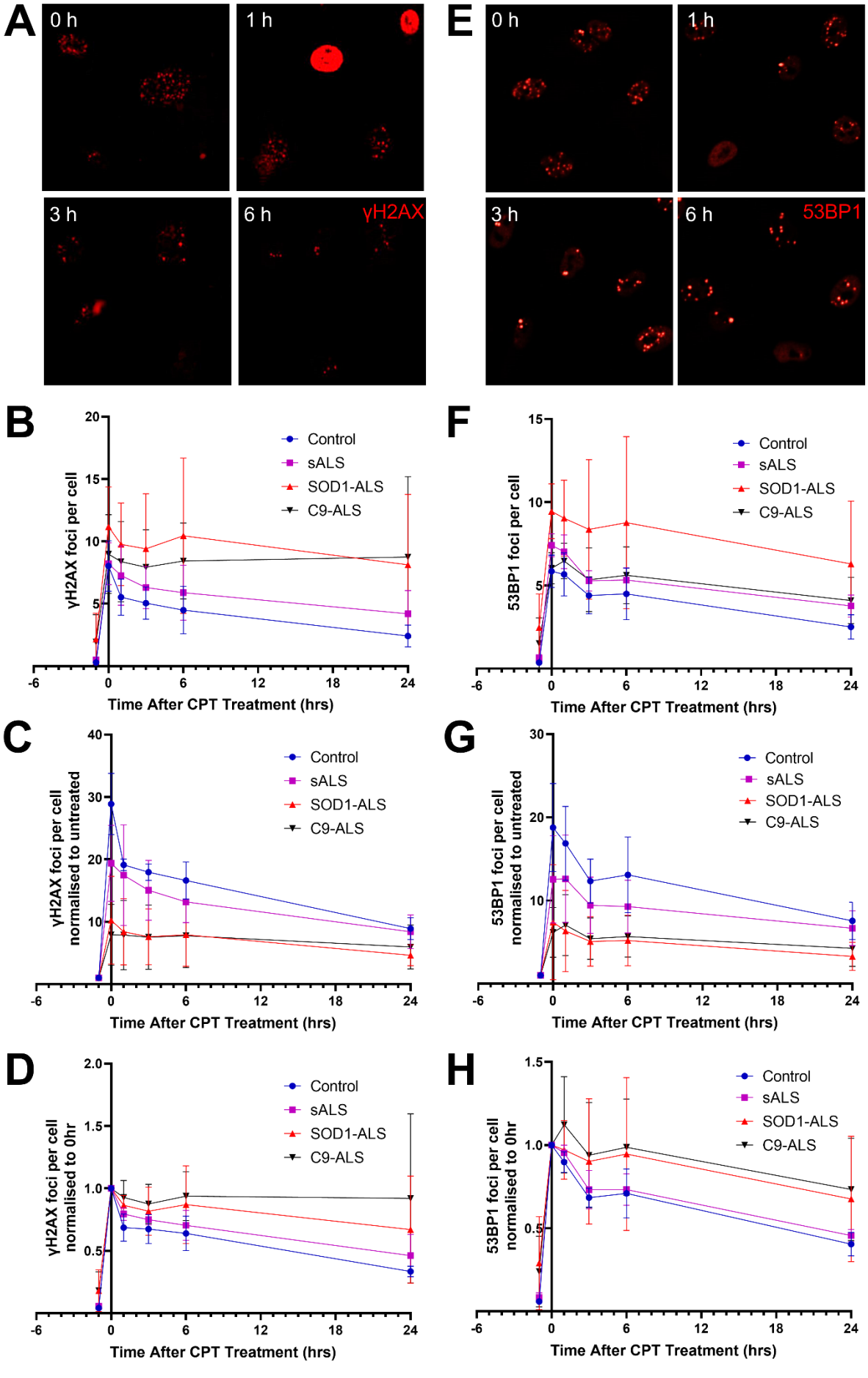
A
0 h
1 h
3 h
6 h
γH2AX
E
0 h
1 h
3 h
6 h
53BP1
B
γH2AX foci per cell
Control
sALS
SOD1-ALS
C9-ALS
Time After CPT Treatment (hrs)
F
53BP1 foci per cell
Control
sALS
SOD1-ALS
C9-ALS
Time After CPT Treatment (hrs)
C
γH2AX foci per cell normalised to untreated
Control
sALS
SOD1-ALS
C9-ALS
Time After CPT Treatment (hrs)
G
53BP1 foci per cell normalised to untreated
Control
sALS
SOD1-ALS
C9-ALS
Time After CPT Treatment (hrs)
D
γH2AX foci per cell normalised to 0hr
Control
sALS
SOD1-ALS
C9-ALS
Time After CPT Treatment (hrs)
H
53BP1 foci per cell normalised to 0hr
Control
sALS
SOD1-ALS
C9-ALS
Time After CPT Treatment (hrs)

Figure 21. γH2AX and 53BP1 repair kinetics are altered in SOD1-ALS and C9-ALS astrocytes (grouped). A: Example images of γH2AX staining in control (n=4), sALS (n=3), SOD1-ALS (n=3) and C9-ALS (n=3) astrocytes treated with CPT and allowed to recover over time. Staining done with help from Sam Boldan. B-D: Quantification of γH2AX foci over time, with no normalisation (B), normalised to untreated (C) and normalised to timepoint 0 (D). Means and standard deviations shown. E: Example images of 53BP1 staining in control (n=4), sALS (n=3), SOD1-ALS (n=3) and C9-ALS (n=3) astrocytes treated with CPT and allowed to recover over time. Staining done with help from Sam Boldan. F-H: Quantification of 53BP1 foci over time, with no normalisation (F), normalised to untreated (G) and normalised to timepoint 0 (H). Means and standard deviations shown.

Table 20. Two-way RM ANOVA results for γH2AX DNA repair kinetics in control and ALS astrocytes

	Source of Variation	% of total variation	P value	Summary
γH2AX Not Normalised	Time x ALS Subtype	3.667	0.3658	ns
	Time	38.06	<0.0001	****
	ALS Subtype	16.88	0.2039	ns
	Subject	30.61	<0.0001	****
	Source of Variation	**% of total variation**	**P value**	**Summary**
γH2AX Normalised to Untreated	Time x ALS Subtype	12.75	<0.0001	****
	Time	39.92	<0.0001	****
	ALS Subtype	25.76	0.0083	**
	Subject	12.37	<0.0001	****
	Source of Variation	**% of total variation**	**P value**	**Summary**
γH2AX Normalised to Timepoint 0hr	Time x ALS Subtype	4.213	0.6206	ns
	Time	61.60	<0.0001	****
	ALS Subtype	7.838	0.0803	ns
	Subject	8.636	0.0123	*

Table 21. Two-way RM ANOVA results for 53BP1 DNA repair kinetics in control and ALS astrocytes

	Source of Variation	% of total variation	P value	Summary
53BP1 Not Normalised	Time x ALS Subtype	1.759	0.8771	ns
	Time	50.05	<0.0001	****
	ALS Subtype	19.28	0.0676	ns
	Subject	19.67	<0.0001	****
	Source of Variation	**% of total variation**	**P value**	**Summary**
53BP1 Normalised to Untreated	Time x ALS Subtype	9.342	0.0002	***
	Time	36.01	<0.0001	****
	ALS Subtype	26.58	0.0230	*
	Subject	17.83	<0.0001	****
	Source of Variation	**% of total variation**	**P value**	**Summary**
53BP1 Normalised to Timepoint 0hr	Time x ALS Subtype	2.093	0.7443	ns
	Time	64.80	<0.0001	****
	ALS Subtype	6.665	0.2755	ns
	Subject	14.88	<0.0001	****

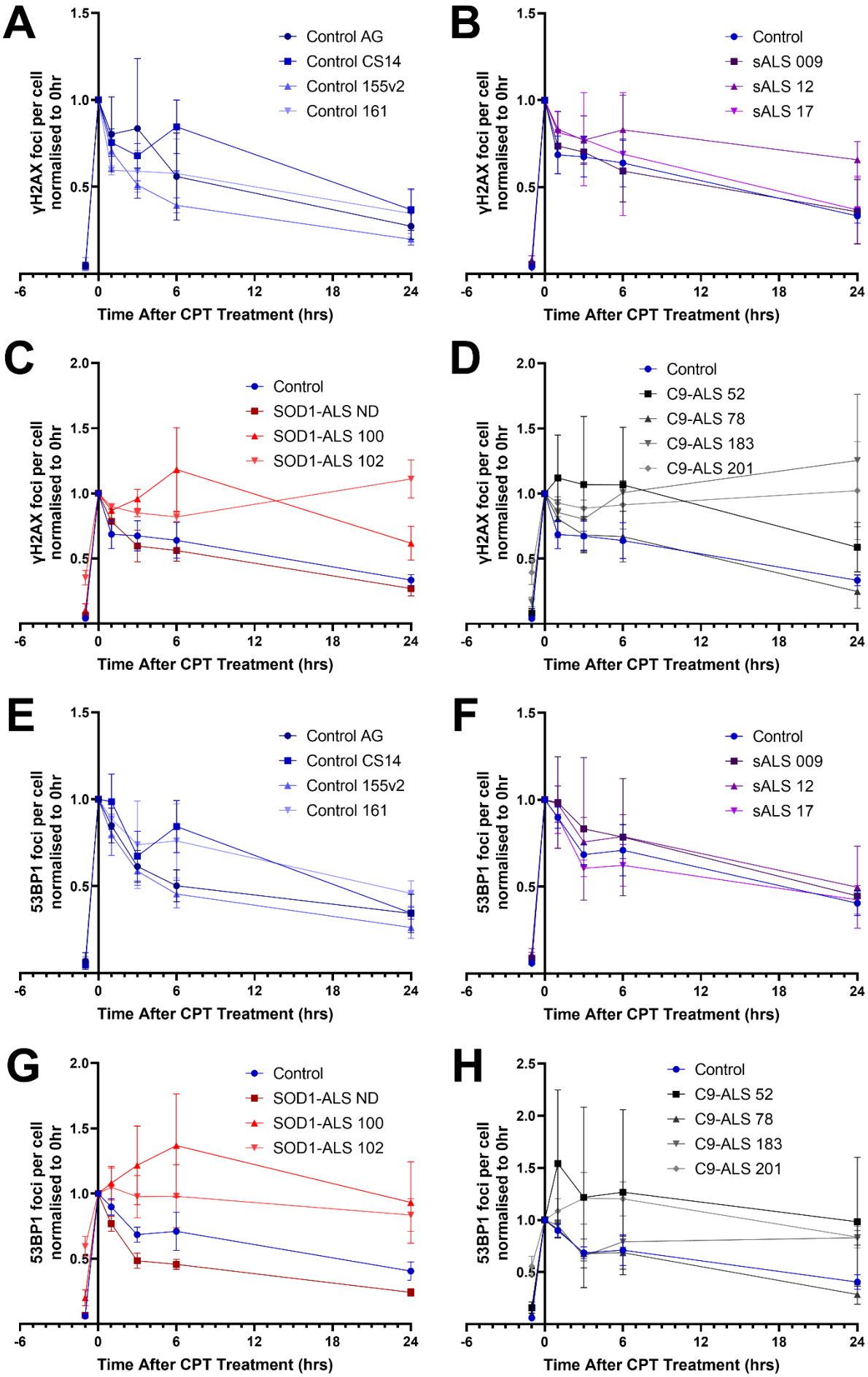
A
γH2AX foci per cell normalised to 0hr
Control AG
Control CS14
Control 155v2
Control 161
Time After CPT Treatment (hrs)
B
γH2AX foci per cell normalised to 0hr
Control
sALS 009
sALS 12
sALS 17
Time After CPT Treatment (hrs)
C
γH2AX foci per cell normalised to 0hr
Control
SOD1-ALS ND
SOD1-ALS 100
SOD1-ALS 102
Time After CPT Treatment (hrs)
D
γH2AX foci per cell normalised to 0hr
Control
C9-ALS 52
C9-ALS 78
C9-ALS 183
C9-ALS 201
Time After CPT Treatment (hrs)
E
53BP1 foci per cell normalised to 0hr
Control AG
Control CS14
Control 155v2
Control 161
Time After CPT Treatment (hrs)
F
53BP1 foci per cell normalised to 0hr
Control
sALS 009
sALS 12
sALS 17
Time After CPT Treatment (hrs)
G
53BP1 foci per cell normalised to 0hr
Control
SOD1-ALS ND
SOD1-ALS 100
SOD1-ALS 102
Time After CPT Treatment (hrs)
H
53BP1 foci per cell normalised to 0hr
Control
C9-ALS 52
C9-ALS 78
C9-ALS 183
C9-ALS 201
Time After CPT Treatment (hrs)

Figure 22. γH2AX and 53BP1 repair kinetics are altered in certain sALS, SOD1-ALS and C9-ALS astrocyte cell lines. A-D: Quantification of γH2AX staining in control (n=4), sALS (n=3), SOD1-ALS (n=3) and C9-ALS (n=3) astrocytes treated with CPT and allowed to recover over time, showing results for each cell line (3-4 repeats per line) normalised to timepoint 0. E-H: Quantification of 53BP1 staining in control (n=4), sALS (n=3), SOD1-ALS (n=3) and C9-ALS (n=3) astrocytes treated with CPT and allowed to recover over time, showing results for each cell line (3-4 repeats per line) normalised to timepoint 0. Means and standard deviations shown.

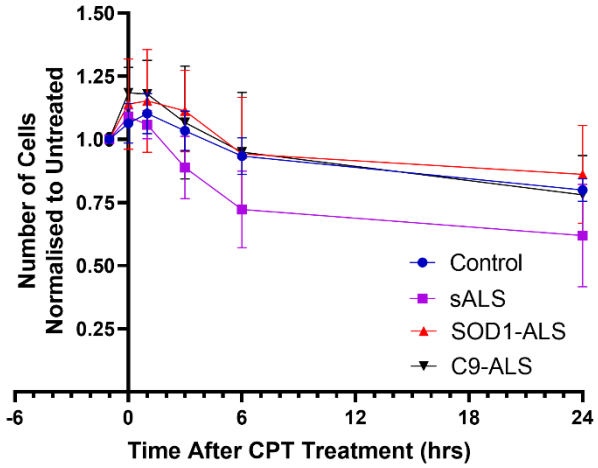

Figure 23. ALS astrocytes do not show increased cell death following CPT treatment. Control (n=4), sALS (n=3), SOD1-ALS (n=3), C9-ALS (n=4), normalised to untreated. Means and standard deviations shown.

Table 22. Two-way RM ANOVA results for γH2AX DNA repair kinetics in control and ALS astrocytes

Source of Variation	% of total variation	P value	Summary
Time x ALS Subtype	4.826	0.3358	ns
Time	47.69	<0.0001	****
ALS Subtype	8.147	0.4056	ns
Subject	25.41	<0.0001	****

3.3.4 DNA Repair Proteins

Due to the observed increase in the repair protein 53BP1 in SOD1-ALS and C9-ALS astrocytes, and the alteration in DNA repair kinetics observed in certain cell lines, I decided to investigate the expression of other DNA repair factors. Several studies have, in fact, shown that DNA repair and expression of DNA repair factors is altered in ALS motor neurons (reviewed in Kok et al., 2021), thus it may be that DNA repair factors are also altered in ALS astrocytes. To investigate this, I ran Western blotting for repair factors involved in different DNA repair processes (Figure 24), including base excision repair (APE1), single-strand break repair (XRCC1, PARP1), and double-strand break repair (Ku80, PARP1). As TOPO1-induced DNA damage has previously been implicated in C9-ALS motor neurons (Walker et al., 2017), I also probed for TOPO1. The results were highly variable and I

observed no significant change in expression of APE1 (Kruskal-Wallis, p=0.89), XRCC1 (one-way ANOVA, p=0.45), TOPO1 (one-way ANOVA, p=0.28), PARP1 (Kruskal-Wallis, p=0.22) or Ku80 (Kruskal-Wallis, p=0.70).

Notably I had considerable heterogeneity within the control group, which affects interpretation of the results. Control 155v2 displayed vastly higher levels of APE1, TOPO1 and Ku80 than the other controls, while control CS14 showed vastly reduced levels of XRCC1. Taking control heterogeneity into account, APE1 levels were elevated in the SOD1-ALS 102 and C9-ALS 183 astrocyte lines compared to three out of four controls. PARP1 was observed to be increased in the sALS 12, sALS 17, SOD1-ALS 100, SOD1-ALS 102 and C9-ALS 201 cell lines compared to controls. XRCC1, on the other hand, was generally reduced in sALS and SOD1-ALS astrocytes compared to three out of four control lines, but levels were elevated in C9-ALS 183. TOPO1 levels were slightly elevated in the SOD1-ALS 100, C9-ALS 183 and C9-ALS 201 astrocyte lines compared to three out of four controls. For graphs showing data for each cell line, see Appendix (7.2). Notably, most of the ALS lines where higher levels of one or more factors was reported were lines that were identified as exhibiting higher levels of DNA damage (3.3.2). Overall, I concluded that astrocytes from different patient groups do not display aberrant activation or repression of DDR factors when unstimulated.

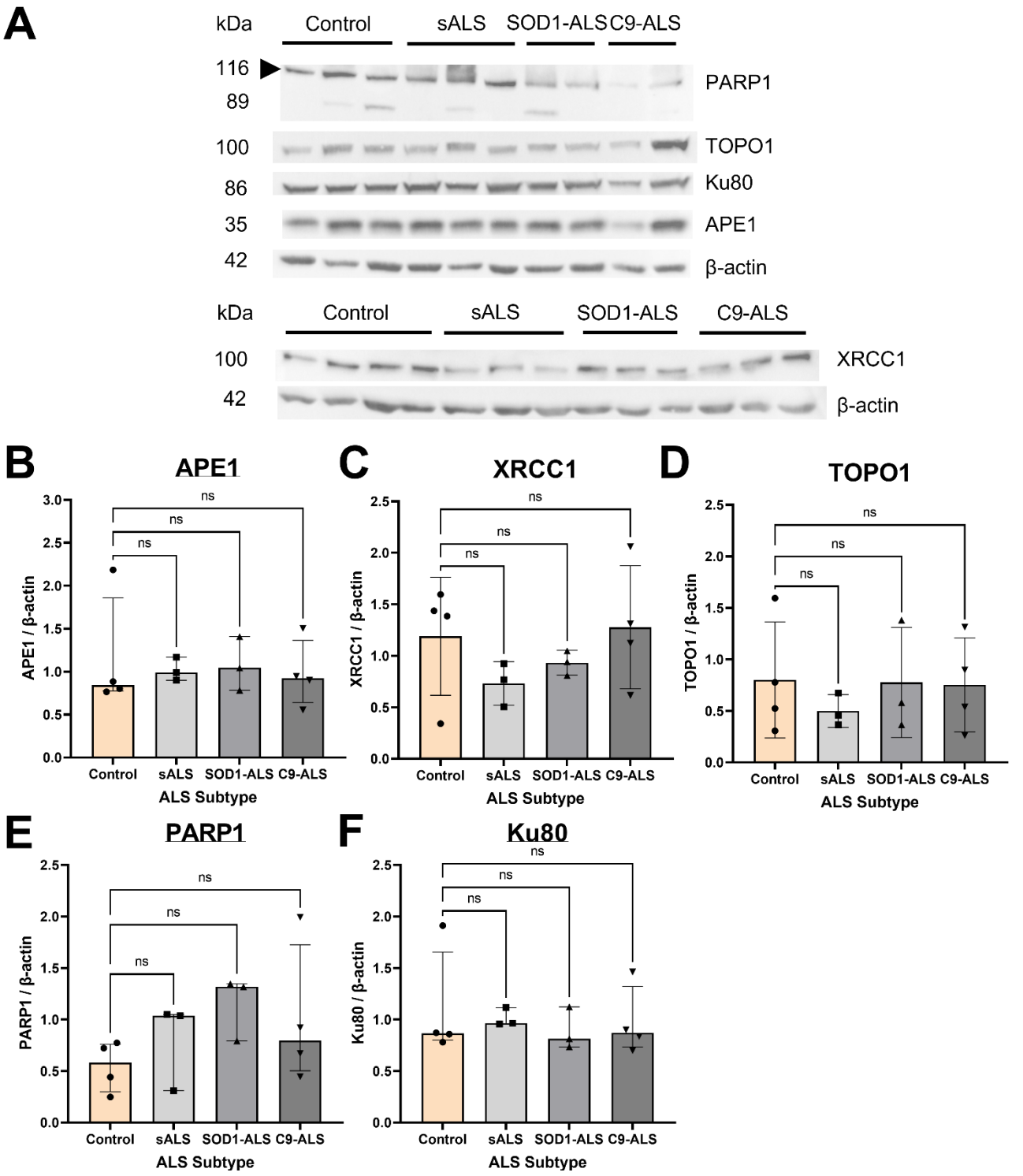

Figure 24. Western blotting of selected DNA repair proteins shows no consistent alteration in ALS astrocytes. A: Example images of Western blot of DNA repair proteins in control (n=4), sALS (n=3), SOD1-ALS (n=3) and C9-ALS (n=4) astrocytes. B: Expression of APE1 in control and ALS astrocytes. Data did not meet assumption for normality, Kruskal-Wallis test (p=0.89). C: Expression of XRCC1 in control and ALS astrocytes. Data met assumption for normality, one-way ANOVA (p=0.45). D: Expression of TOPO1 in control and ALS astrocytes. Data met assumption for normality, one-way ANOVA (p=0.28). E: Expression of PARP1 in control and ALS astrocytes. Data did not meet assumption for normality, Kruskal-Wallis test (p=0.22). F: Expression of Ku80 in control and ALS astrocytes. Data did not meet assumption for normality, Kruskal-Wallis test (p=0.70). Means and standard deviations

shown for one-way ANOVA analysis, median and interquartile range shown for Kruskal-Wallis test analysis.

3.4 Discussion

ALS astrocytes have long been known to be toxic to motor neurons (Ferraiuolo et al., 2011b; Haidet-Phillips et al., 2011; Kia et al., 2018; Madill et al., 2017; Marchetto et al., 2008), but the mechanisms of toxicity remain unclear. DNA damage has been implicated as a possible mechanism involved in cell autonomous motor neuron degeneration (reviewed in Kok et al., 2021) however, its impact in astrocytes is unclear. Hence, I decided to investigate endogenous levels of cellular stressors that can induce DNA damage, DNA damage burden, and DNA repair capabilities in astrocytes derived from ALS patients with different disease backgrounds.

Overall, my data shows that DNA damage repair is not a common mechanism of cellular dysfunction, as most of the astrocyte lines included in this study did not display significant differences in DNA damage, DNA repair or levels of DNA repair proteins. Interestingly, however, DNA damage response dynamics after CPT insult highlighted the presence of 3 groups irrespective of genotype. One group, comprising of SOD1-ALS 102, C9-ALS 183 and C9-ALS 201, showed severe deficits in DNA damage repair where there was little to no decrease in γH2AX foci following CPT withdrawal. A second group, comprising of SOD1-ALS 100, C9-ALS 52 and sALS 12 showed some DNA damage repair but γH2AX levels remained higher that controls. Finally, the third group, comprising of SOD1-ALS ND, C9-ALS 78, sALS 009 and sALS 17, showed DNA repair very similar to controls.

When looking at overall levels of dysfunction in these cells (Table 23), I see a similar grouping. C9-ALS 183, C9-ALS 201, SOD1-ALS 100 and SOD1-ALS 102 astrocytes show dysfunction in multiple categories, C9-ALS 52 and sALS 12 show a milder level of dysfunction, and a final grouping of sALS 009, sALS 17, SOD1-ALS ND and C9-ALS 78 have the mildest dysfunction. It remains to be determined what the cause of the dysfunction might be and whether there are any common links between the severely dysfunctional cell lines.

Reactive oxygen species (ROS) are a biproduct of respiration that are known to induce damage to proteins, RNA and DNA (Turrens, 2003). In my study, I observed an increase in ROS in sALS astrocyte lines 009 and 17, and not in sALS line 12. Based on these results we might have expected to see an increase in DNA damage in 009 and 17 and not in 12, however the opposite was the case. sALS line 12 showed the highest levels of DNA damage (γH2AX, 53BP1) of the sALS lines, although these

levels were mild compared to the more damaged SOD1-ALS and C9-ALS lines, while 009 and 17 had DNA damage levels comparable to controls. sALS 12 was also the only sALS line to show impaired DNA repair capacity. Had I been able to successfully optimise an assay for detection of oxidative DNA damage, it would have been of interest to see if there were signs of oxidative DNA damage in sALS lines 009 or 17. Unfortunately, the widely used antibody for oxidative RNA/DNA damage did not work successfully in my hands, and the staining observed appeared non-specific. Additionally, it proved difficult to optimise the oxidative DNA damage comet assay, with the recombinant OGG1 protein acting unreliably.

The heterogeneity between the sALS lines could indicate there are different underlying mechanisms in sALS 12 than sALS 009 and sALS 17. One explanation may be that sALS 12 has an uncharacterised genetic ALS mutation beyond SOD1, C9ORF72, FUS and TARDBP for which these lines have been screened. An alternative explanation could be that there are potentially subtypes of sALS with different underlying causes that ultimately lead to the same outcome of motor neuron degeneration. Considering that some have speculated that clinical trial failure in ALS may be due to patient heterogeneity (Goyal et al., 2020), it would be of interest to look into this further by expanding the number of sALS lines examined to see how consistent the increase in ROS is and whether ROS levels can be used to categorise sALS patients. ROS are primarily produced by the mitochondria (Turrens, 2003), and a number of genes involved in mitochondrial function have been found to be dysregulated in sALS motor neurons (Alves et al., 2015). Thus, we might expect that the increase in ROS in sALS 009 and sALS 17 could arise due to mitochondrial dysfunction in these lines.

I observed high levels of DNA damage (γH2AX, 53BP1) in SOD1-ALS lines 100 and 102, but only observed a mild increase in 53BP1 foci for SOD1-ALS line ND. As SOD1 is involved in the clearance of ROS (Rosen et al., 1993), we would have expected that the SOD1-ALS astrocytes would show increased ROS and this might be the cause of the DNA damage, however this was not the case. SOD1-ALS lines 100 and 102 had levels of ROS comparable to controls, suggesting DNA damage might be arising from another mechanism. It would be of interest to confirm this finding, using another method of assessing oxidative stress or oxidative damage. Notably, for the CellROX experiment I only used two SOD1-ALS lines, both of which had the A4V mutation, so if we expanded to lines with different mutations we may get different results. A previous study has shown that cells expressing the $SOD1^{A4V}$ protein show reduced SOD1 activity (Borchelt et al., 1994), and we

therefore would expect an accumulation of ROS in SOD1^{A4V} cells. It may be that the SOD1-ALS astrocytes are able to compensate for this reduction in activity somehow.

Formation of R-loops in the genome have been shown to induce DNA damage (Skourti-Stathaki and Proudfoot, 2014) and transcriptional changes (Aguilera and García-Muse, 2012). As ROS are known to induce R-loops (Teng et al., 2018), and R-loops have been found to be increased in C9-ALS motor neurons (Walker et al., 2017), I decided to characterise the levels of R-loops in all the ALS astrocytes. I observed a specific increase in R-loops in two C9-ALS astrocyte lines, 183 and 201, both of which have increased DNA damage, suggesting that an increase in R-loops may be responsible for the observed damage. This C9-ALS astrocyte specific increase in R-loops is likely to arise from the C9ORF72 repeat expansion itself that is prone to R-loop formation (Reddy et al., 2014), or from endogenously expressed DPRs that have been shown previously to promote R-loop formation (Walker et al., 2017).

However, my S9.6 staining was notably sensitive to RNAse A treatment and the observed increase in S9.6 foci was also accompanied by an increase in nucleolin foci, suggesting I may not have been observing R-loops specifically. It has previously been reported that the S9.6 antibody also binds double-stranded RNA, so it is possible that the majority of the signal observed is RNA rather than RNA:DNA hybrids (Smolka et al., 2021). To determine whether R-loops in C9-ALS astrocytes could be potentially causing harmful transcriptional changes, I examined the number of computationally predicted RLFS in the differentially expressed genes between C9-ALS and control astrocytes. R-loops have been known to hinder transcription, thus an increase in R-loops in genes that are downregulated in C9-ALS and sALS compared to controls could indicate that R-loops may be the cause of that downregulation. Unfortunately, I was unable to determine whether this was the case. There are limited numbers of techniques available to assess numbers of R-loops. R-loops can be detected by dot blot (Ramirez et al., 2021), however this is again reliant on the S9.6 antibody and dot blots are more for qualitative rather than quantitative assessment. Other methods typically rely on immunoprecipitation of the DNA:RNA hybrids and then targeted qPCR or sequencing (Sanz and Chédin, 2019), which would provide additional information on which genes the R-loops may be affecting.

Overall, I did not see a consistent increase in DNA damage within any of the genetic subgroups, but I did see elevations in DNA damage in specific cell lines. sALS line 12, SOD1-ALS line 100 and C9-ALS line 183 showed a relatively mild increase in γH2AX, while SOD1-ALS 102 and C9-ALS 201 showed a

more severe increase. For 53BP1, I saw either a mild or severe increase in foci for all the SOD1-ALS and C9-ALS astrocyte lines, but only a mild increase in one sALS line (sALS 12). Previous work suggested that γH2AX was not increased in C9ORF72-ALS patient iPSC-derived astrocytes (Lopez-Gonzalez et al., 2016) or in primary astrocytes from embryonic SOD1-ALS mice (Penndorf et al., 2017). Notably, Lopez-Gonzalez *et al* (2016) did not provide quantification for their findings and Penndorf *et al.* did not observe any DNA damage in their SOD1-ALS mice, despite the many findings of increased levels of DNA damage in SOD1-ALS mice and other models (reviewed in Kok et al., 2021). My results would be the first to indicate that ALS astrocytes from SOD1-ALS and C9-ALS patients may also be vulnerable to the DNA damage insult that affects motor neurons.

As to what might influence differences in severity of DNA damage within genetic subgroups, there could be several possible explanations. Gene specific differences may play an effect, as the two SOD1-ALS lines which had the highest level of DNA damage had the same mutation (A4V) while the third line had a different mutation (D90A). SOD1 has been implicated as playing a role in DNA repair (reviewed in Kok et al., 2021), and the different mutations may affect this role in more or less severe ways. It should be noted however, that the two SOD1-ALS lines with the highest DNA damage were derived from two related patients and therefore there may be another shared genetic cause for the increased DNA damage. It would be of interest to look at astrocytes carrying other SOD1 mutations to see whether increased DNA damage is associated with specific mutations. In C9-ALS, DNA damage could be related to a C9-ALS-specific pathology, such as levels of RNA foci or dipeptide repeat proteins, or alternatively could be related to R-loops as I discussed earlier.

An alternative explanation could be that gender is a contributing factor to DNA damage in ALS astrocytes as three of the four ALS lines with the highest level of DNA damage (SOD1-ALS 100, 102; C9-ALS 201) were female lines. Another female ALS line (sALS 009) did not exhibit increased levels of γH2AX or 53BP1 but was observed to have slightly elevated levels of DNA damage measured using the comet assay. Notably, the two female control lines used in experiments (CS14 and AG) were not observed to have elevated levels of DNA damage compared to the male control lines, indicating this is likely not a gender-specific increase in DNA damage. Supporting this suggestion, previous studies have shown that there are no gender differences in DNA repair in human subjects (Garm et al., 2013; Soares et al., 2014). Gender could however be a contributing factor in the disease context. It was previously shown that female ALS patients show increased expression of inflammatory pathway genes compared to males patients (Santiago et al., 2021), and inflammation

leads to increased production of ROS and reactive nitrogen species, both of which can induce DNA damage (Kay et al., 2019). Thus, it seems likely that if gender is a contributing factor to DNA damage in astrocytes, it is mediated through inflammation. Notably, DNA damage can also promote inflammation, leading to a positive feedback loop (Kay et al., 2019), that may exacerbate the existing effects.

Another possible explanation for cell line-specific DNA damage could be related to timing of patient biopsy. C9-ALS 183 and C9-ALS 201 consistently had high levels of DNA damage, whereas C9-ALS 78 was comparable to controls for several assays. C9-ALS 183 and 201 had shorter onset to death following biopsy compared to C9-ALS 78. Additionally, C9-ALS 201 exhibited consistently more DNA damage than 183 and had a shorter onset to death than 183. It may be that in later stages of disease, ALS astrocytes accumulate more DNA damage and other dysfunctions. Notably, it has previously been suggested that DNA damage in ALS patients increases with age, but is not directly related to disease progression (Bogdanov et al., 2000; Murata et al., 2008). This suggestion should however be taken cautiously, considering the limited sample number and information available. We do not have information on onset to death for the SOD1-ALS lines and for the sALS lines there is not a clear relationship between onset to death and DNA damage. sALS 009 has the shortest onset to death of the sALS lines, in fact onset to death was shorter even than C9-ALS 183, and yet 009 did not exhibit increased DNA damage. It would be of interest to investigate further with more samples whether there is a relationship between DNA damage and onset to death in ALS.

A common feature of lines exhibiting increased endogenous levels of DNA damage was that they also showed impairment in DNA repair kinetics. It is unclear whether DNA repair impairment is the cause of the increased DNA damage or whether the increased DNA damage leads to an impairment in repair. When I looked at expression levels of DNA repair factors, I did not see any consistent patterns of increases within genetic subgroups or across lines that had increased DNA damage. PARP1 showed the most consistent change, with increased PARP1 expression in some of the lines that showed increased DNA damage: sALS 12, SOD1-ALS 100, SOD1-ALS 102 and C9-ALS 201, but PARP1 was also increased in a line that didn't show increased DNA damage: sALS 17. Interestingly, expression of PARP1 has previously been shown to be increased in sALS astrocytes compared to controls (Kim et al., 2003). Notably, Kim *et al*. only observed a significant increase in PARP1 expression in the insoluble fraction of their cell lysates, whereas we interrogated the soluble proteins (albeit generated from a more stringent lysis protocol). PARP1 is a DNA damage sensor as

well as playing a role in recruiting DNA repair factors to facilitate multiple repair pathways, including: BER, NER, single-strand break repair (SSBR), canonical NHEJ, alternative NHEJ, HR, and mismatch-repair (reviewed by Pascal, 2018). The increase in PARP1 observed in some of the lines could be an attempt from the cells to activate DNA repair.

APE1 expression was also elevated in some lines with higher baseline DNA damage: SOD1-ALS 102, C9-ALS 183 and C9-ALS 201, but again was elevated in some lines without baseline DNA damage: SOD1-ALS ND. Notably, APE1 is known to colocalise to the nucleolus and interacts with nucleophosmin (Poletto et al., 2014). SOD1-ALS 102, C9-ALS 183 and C9-ALS 201 showed increased numbers of nucleoli per unit of nuclear area, which may be related to the increased expression of APE1. APE1 is mostly known to be involved in BER, the primary pathway for repairing oxidative DNA damage, as well as repairing alkylated and deaminated bases. APE1 has also been suggested to play a role in double-strand break repair, by facilitating HR and counteracting NHEJ (Ströbel et al., 2017). Separately from DNA repair, APE1 also functions in redox signalling by recruiting transcription factors to DNA when it is in a reduced state, these transcription factors include p53, NFκB, STAT3 and AP-1. The elevation of APE1 in the SOD1-ALS and C9-ALS astrocyte lines could be an indication of unsuccessful attempts at DNA repair through either BER or HR.

Changes in APE1 and PARP1 were the most consistent within the cell lines with higher DNA damage, but there were some other DNA repair factors elevated in fewer lines. Levels of Ku80, a DNA double-strand break detector involved in NHEJ (Davis and Chen, 2013), were increased in C9-ALS 183. Similarly levels of XRCC1, which is involved in SSBR (Brem and Hall, 2005), were increased in C9-ALS 183. Interestingly, levels of XRCC1 were generally decreased in sALS and SOD1-ALS astrocytes, suggestive of a possible impairment in SSBR in these astrocytes. Finally levels of TOPO1, which is a protein involved in relaxation of DNA but can induce abortive single-strand breaks, were increased in C9-ALS 183 and SOD1-ALS 100. Increased TOPO1 could be a potential cause of DNA damage in these lines. It would be of interest to validate this by seeing if TOPO1:DNA cleavage complexes (TOP1cc) are increased in these lines.

Table 23. Summary of astrocyte results by cell line. All data shown as fold change compared to average of controls.

ALS Subtype	Cell Line	Sex	Age	Onset to Death (months)	ROS	R-loops	Nucleoli Number	Nucleoli Size	Comet Tail Moment	γH2AX	53BP1	APE1*	XRCC1*	TOPO1*	PARP1	Ku80*	Survival 24hr After CPT	γH2AX Kinetics	53BP1 Kinetics	Dysfunction Score
C9-ALS	183	Male	50	27	0.87	1.57	1.68	0.61	1.58	4.34	1.87	1.78	1.46	2.02	1.69	1.69	0.90	Abnormal	Abnormal	24
C9-ALS	201	Female	66	19.4	0.89	1.55	1.69	0.52	2.87	17.46	9.56	1.12	0.44	1.38	3.65	0.97	1.27	Abnormal	Abnormal	22
SOD1-ALS (A4V)	100	Female	63	NA	1.14	0.97	0.70	1.53	1.42	4.83	5.34	0.93	0.57	2.12	2.46	0.85	0.84	Abnormal	Abnormal	17
SOD1-ALS (A4V)	102	Female	40	NA	1.02	1.28	1.25	0.59	1.44	10.95	10.10	1.67	0.74	0.89	2.41	1.30	1.07	Abnormal	Abnormal	17
sALS	12	Male	29	72	0.78	1.18	1.07	0.85	0.67	2.51	1.98	1.17	0.65	1.04	1.90	1.11	0.51	Abnormal	Normal	11
C9-ALS	52	Male	49	NA	NA	NA	NA	NA	NA	1.55	1.88	1.07	0.80	0.40	0.81	1.04	0.89	Abnormal	Abnormal	10
sALS	17	Male	47	90	1.77	1.03	1.18	0.73	1.38	1.07	1.17	1.39	0.36	0.70	1.92	1.29	1.02	Normal	Normal	8
SOD1-ALS (D90A)	ND	Male	56	Collected at death	NA	NA	NA	NA	NA	1.55	1.64	1.24	0.67	0.56	1.45	0.94	1.32	Normal	Normal	8
sALS	009	Female	61	21	1.40	0.94	0.75	1.27	2.09	0.99	1.29	1.07	0.54	0.56	0.57	1.12	0.79	Normal	Normal	6
C9-ALS	78	Male	66	31.7	0.88	1.05	1.13	0.85	1.03	1.50	1.85	0.66	0.93	0.82	1.23	0.81	0.85	Normal	Normal	5

*fold change compared to median of controls, to take into account heterogeneity between control lines. All other data compared to mean of controls. For calculation of dysfunction score, see legend below

Dysfunction Category	Fold Change Cut-off	Repair Kinetics Classification	Dysfunction Score
Very severe dysfunction (high)	>5.00		3
Severe dysfunction (high)	1.50-5.00	Abnormal	2
Mild dysfunction (high)	1.30-1.49		1
Similar to control	0.70-1.29	Normal	0
Mild dysfunction (low)	0.50-0.69		1
Severe dysfunction (low)	<0.50		2
Data not available			0

3.5 Conclusion

Similar to what has been observed in ALS motor neurons, we have observed an increase in DNA damage in selected SOD1-ALS and C9-ALS astrocyte lines, but not in sALS astrocytes. Within these groups there was considerable heterogeneity. Cell lines with higher levels of baseline DNA damage were more likely to have changes in expression of DNA repair factors, defective DNA repair kinetics following CPT treatment and an increase in nucleoli. Notably, increased DNA damage was not associated with an increase in ROS, indicating oxidative stress may not be the cause. We cannot discount the possibility that DNA damage or DNA repair deficiencies may be a feature in astrocytes from ALS subtypes we did not examine here. FUS (Mastrocola et al., 2013), NEK1 (Chen et al., 2008, 2011; Spies et al., 2016) and TDP-43 (Hill et al., 2016; Mitra et al., 2019) all play important roles in DDR signalling and DNA repair and thus it is possible that astrocytes from patients with mutations in the genes encoding these proteins may exhibit increases in DNA damage. Future work could focus on identifying the causes of DNA damage in ALS astrocytes and determining whether other ALS subtypes may be similarly affected.

Chapter 4: ALS Astrocyte-Induced DNA Damage

4.1 Introduction

4.1.1 Astrocyte Toxicity in ALS

It has been well established that astrocytes derived from ALS patients, whether sporadic or familial, are toxic to motor neurons (Haidet-Phillips et al., 2011; Kia et al., 2018; Marchetto et al., 2008; Meyer et al., 2014). ALS astrocyte toxicity is thought to be at least in part mediated through secreted factors as application of ALS astrocyte conditioned medium (Kia et al., 2018; Madill et al., 2017; Nagai et al., 2007) or ALS astrocyte exosomes (Varcianna et al., 2019) is sufficient to induce motor neuron death. Furthermore, inhibition of SNARE-dependent exocytosis in astrocytes delayed disease progression in a mouse model of SOD1-ALS (Kawamata et al., 2014). The identity of the toxic secreted factors and the mechanism by which they induce toxicity are currently unknown. Various pathways have been suggested by which ALS astrocytes may induce motor neuron death including: autophagy disruption, oxidative stress, metabolic changes, receptor and ion channel expression changes, inflammation, and secretory changes (Allen et al., 2019; Arredondo et al., 2022; Birger et al., 2019; Ferraiuolo et al., 2011b; Haidet-Phillips et al., 2011; Madill et al., 2017; Song et al., 2016; Varcianna et al., 2019).

Notably, most evidence suggests that astrocytes contribute to disease progression in ALS but not disease onset (Yamanaka et al., 2008b). This could suggest that ALS astrocytes may worsen existing motor neuron pathologies. I have already discussed the evidence that DNA damage is increased in motor neurons from ALS patients (3.1.1) and there is some evidence that DNA damage may be a mechanism involved in ALS astrocyte toxicity (reviewed in Kok et al., 2021). A previous study showed that C9-ALS astrocytes could induce p62 accumulation and a reduction in autophagic flux in motor neurons (Madill et al., 2017). P62 has previously been shown to play a role in DNA damage signalling through its inhibition of the E3 ubiquitin ligase, RNF168 (Wang et al., 2016). This is particularly noteworthy as an increase in p62 accumulation was suggested to be a mechanism by which DNA damage is increased in C9-ALS patient-derived motor neurons (Walker et al., 2017). This study also suggested DNA damage could be increased in motor neurons due to an increase in R-loops (Walker et al., 2017). C9-ALS astrocyte conditioned medium has also been shown to induce an increase in ROS and oxidative stress in motor neurons (Birger et al., 2019), which could lead to oxidative DNA damage. Notably, a study looking at DNA damage induced by C9-ALS DPRs suggested an increase in ROS was responsible (Lopez-Gonzalez et al., 2016).

Before the start of this PhD, Miss Malin Andersson, an MSc student in the Ferraiuolo lab, treated healthy mouse motor neurons with conditioned medium derived from C9-ALS astrocytes and observed an increase in γH2AX foci (Figure 25), indicating an increase in DNA damage. It was thus hypothesised that ALS astrocytes may induce motor neuron death through DNA damage.

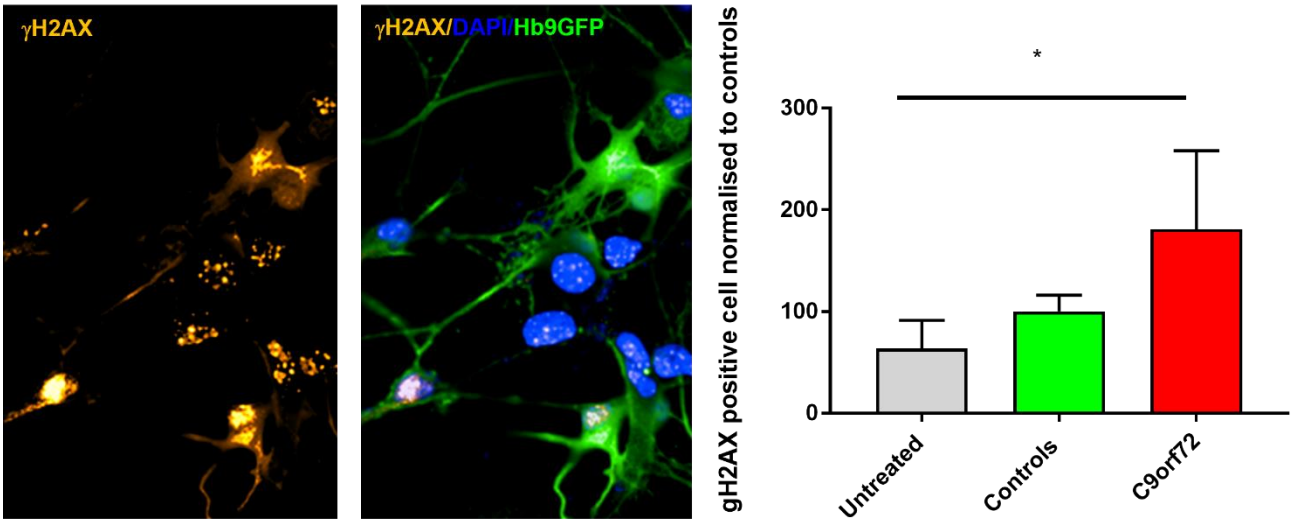

Figure 25. C9-ALS astrocyte conditioned medium induces DNA damage in healthy mouse motor neurons (data and images from Miss Malin Andersson). Hb9-GFP^{+} healthy motor neurons positive for DNA damage repair marker γH2AX after treatment with astrocyte medium only. Untreated (n=2), controls (n=3), C9-ALS (n=3). Compiled data of γH2AX positive motor neurons for the 3 conditions. * indicates $p < 0.05$ using one-way ANOVA test. Each N contains 3-5 biological replicates. Means and standard deviations shown.

4.1.2 Aims and Objectives

The aim of this chapter was to determine whether ALS astrocytes can induce DNA damage or DNA damage-associated cell stressors in motor neurons, whether ALS astrocytes can induce changes in DNA repair and whether any of these features differ according to ALS subtype. To carry out these aims, I treated healthy control iPSC-derived motor neurons with conditioned medium derived from control, sALS, SOD1-ALS and C9-ALS iNPC-derived iAstrocytes and I assessed a number of parameters. To assess DNA damage, Dr Cleide Souza ran immunofluorescence staining and I ran Western blots on the treated motor neurons for γH2AX, a well-established marker of DNA damage (Turinetto and Giachino, 2015). I aimed to validate these datasets by running the comet assay on the treated motor neurons to look more directly at DNA strand breaks. Following on from this work, I looked at whether DNA repair factor protein and transcript expression was altered in motor neurons treated with ALS astrocyte conditioned medium. I used C9-ALS motor neurons as a positive control, as high levels of endogenous DNA damage have been previously reported in C9-ALS motor neurons (Farg et al., 2017; Lopez-Gonzalez et al., 2016; Walker et al., 2017). Because DNA damage

repair is thought to be impaired in C9-ALS motor neurons, I also used C9-ALS GABAergic neurons, as a population of neurons that displays DNA damage, but does not seem to display DDR defects (unpublished data El-Khamisy and Ferraiuolo labs). Finally, I looked at levels of cell stressors characterised in the previous chapter (3.2.1, 3.2.3, 3.2.4): ROS, R-loops and nucleoli, in case any of these stressors was found to be increased in motor neurons treated with ALS astrocyte conditioned medium.

4.2 ALS Astrocytes Induce DNA Damage

4.2.1 γH2AX

To determine whether ALS astrocytes could induce DNA damage in motor neurons I treated healthy iPSC-derived motor neurons with control (n=3), sALS (n=3), SOD1-ALS (n=3) or C9-ALS (n=4) astrocyte conditioned medium for 24 hours and looked at expression of γH2AX (Figure 26), a well-established marker of DNA damage (Turinetto and Giachino, 2015). Dr Cleide Souza of the Ferraiuolo and El-Khamisy lab groups stained the treated motor neurons for γH2AX (Figure 26A-B) and found a significant difference in γH2AX positive cells across the treatment groups (Kruskal-Wallis test, $p<0.0001$). γH2AX positive cells were found to be significantly increased in motor neurons treated with sALS ($p=0.03$) or C9-ALS ($p=0.007$) but not SOD1-ALS ($p>0.99$) astrocyte conditioned medium for 24 hours compared to healthy control astrocyte conditioned medium. I attempted to validate this using Western blotting for γH2AX (Figure 26C-E) but I observed no significant change in γH2AX levels across the treatment groups (one-way ANOVA $p=0.49$). Notably there was a high degree of variability across repeats (Figure 26E). Considering that only a proportion of motor neurons displayed activation of γH2AX, it seems likely that Western blotting is not as sensitive as γH2AX immunofluorescence staining.

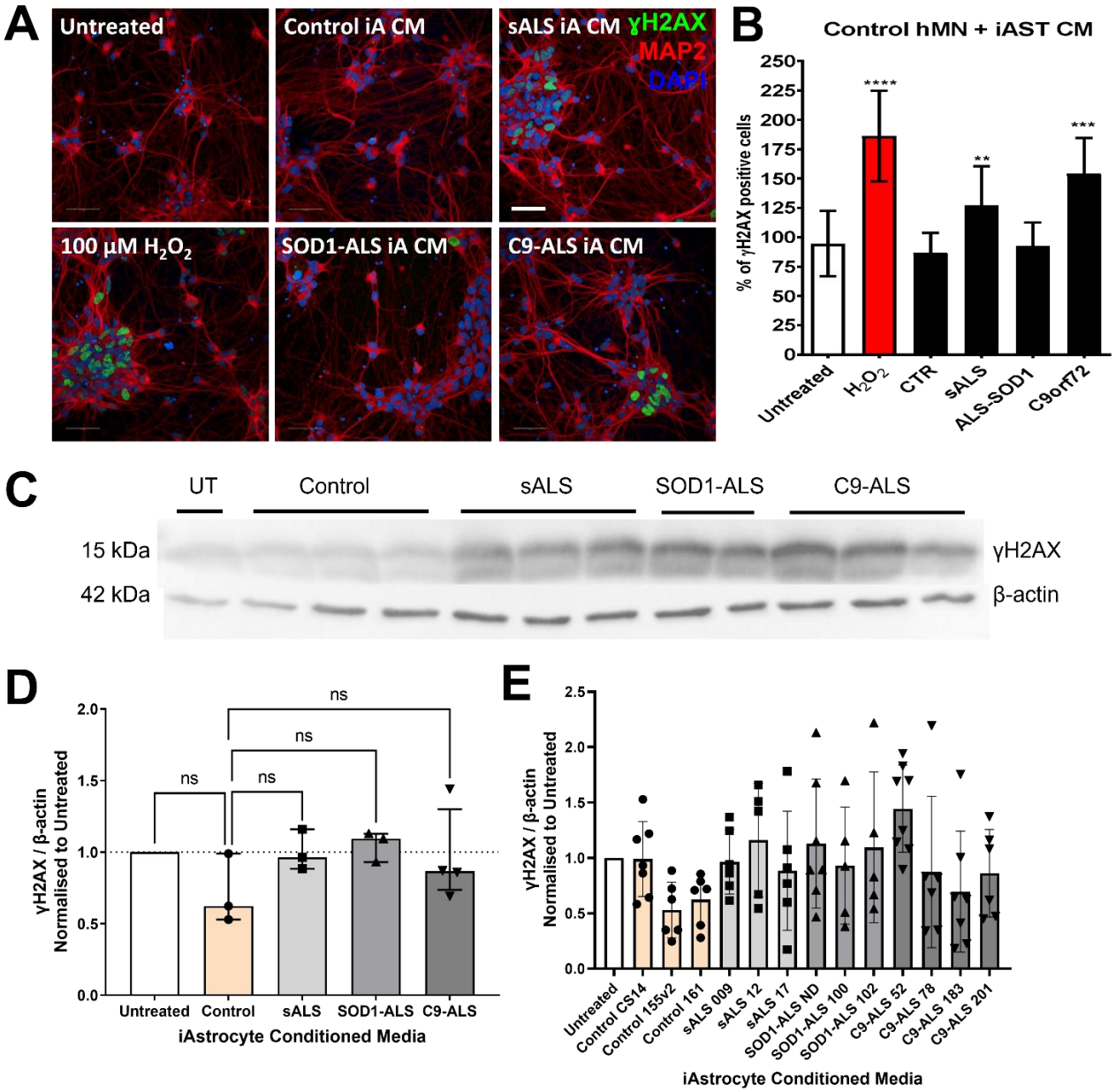

Figure 26. ALS astrocyte conditioned medium induces an increase in γH2AX foci but not protein expression within 24 hours. A-B: Data and images from Dr Cleide Souza. γH2AX staining and foci quantification in motor neurons treated with control (n=3), sALS (n=3), SOD1-ALS (n=3) or C9-ALS (n=4) astrocyte conditioned medium for 24 hours. Data did not meet assumption for normality, Kruskal-Wallis test ($p<0.0001$), Dunn's multiple comparisons test (sALS vs control $p=0.03$; SOD1 vs control $p>0.99$; C9 vs control $p=0.007$). Means and standard deviations shown. C-E: Western blotting for γH2AX in motor neurons treated with control (n=3), sALS (n=3), SOD1-ALS (n=3) or C9-ALS (n=4) astrocyte conditioned medium for 24 hours. D: Quantification grouped by ALS subtype, each datapoint represents the mean result of one astrocyte cell line conditioned medium treatment. Data met assumption for normality, one-way ANOVA ($p=0.49$). Means and standard deviations shown. E: Quantification showing result of each repeat per cell line, each datapoint represents one repeat, means and standard deviations shown.

Notably, I was able to detect an increase in γH2AX levels in motor neurons and GABAergic neurons derived from C9-ALS patients compared to healthy controls (Figure 27). These, in fact, display about double the amount of γH2AX foci via immunostaining compared to their healthy counterpart treated with astrocyte conditioned medium (unpublished data from Dr Souza). For C9-ALS lines 29 and 52 we were able to purchase the isogenic controls, which are the same cell lines but with the C9ORF72 repeat expansion removed, and we observed that γH2AX levels were also increased in the C9-ALS lines compared to their isogenic control counterparts. For motor neurons (Figure 27A), I observed a significant difference across the groups (one-way ANOVA p=0.035) and post-hoc comparison tests confirmed that γH2AX was significantly increased in C9-ALS motor neurons compared to healthy control motor neurons (p=0.039) and trended to significance when compared to isogenic control motor neurons (p=0.082). For GABAergic neurons (Figure 27B), I similarly observed a significant difference across the groups (one-way ANOVA p=0.0020) and post-hoc comparison tests confirmed that γH2AX was significantly increased in C9-ALS GABAergic neurons compared to healthy control GABAergic neurons (p=0.0031) and isogenic control GABAergic neurons (p=0.0037).

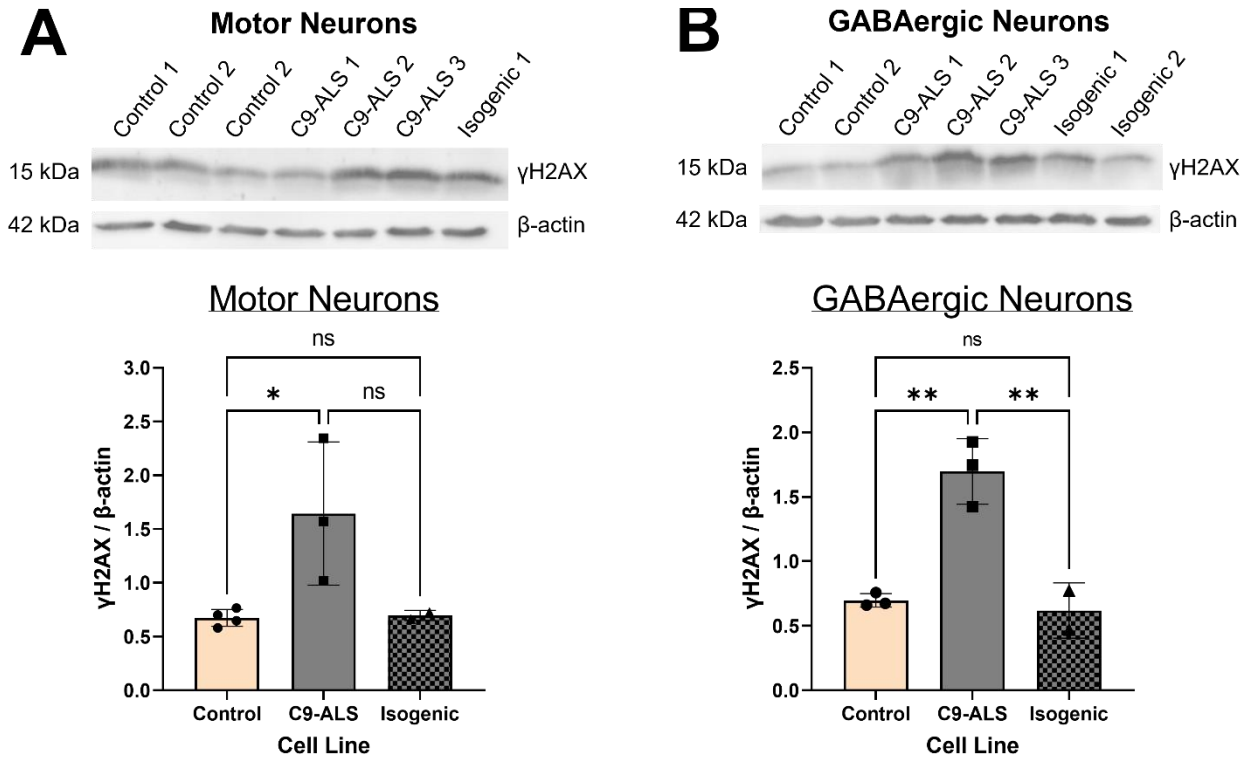

Figure 27. γH2AX levels are increased in C9-ALS motor neurons and GABAergic neurons. A: Western blotting for γH2AX in control (n=4), C9-ALS (n=3) and isogenic control (n=2) motor neurons. Data met assumption for normality, one-way ANOVA (p=0.035), Tukey's multiple comparison tests (control vs C9-ALS p=0.039, control vs isogenic p=0.99, C9-ALS vs isogenic p=0.082). Means and standard

deviations shown, each datapoint represents one cell line. B: Western blotting for γH2AX in control (n=3), C9-ALS (n=3) and isogenic control (n=2) GABAergic neurons. Data met assumption for normality, one-way ANOVA (p=0.0020), Tukey's multiple comparison tests (control vs C9-ALS p= 0.0031, control vs isogenic p=0.90, C9-ALS vs isogenic p=0.0037). Means and standard deviations shown, each datapoint represents one cell line.

4.2.2 DNA Strand Breaks

Having determined that ALS astrocytes induce an increase in γH2AX foci in motor neurons within 24 hours, I wanted to look at DNA damage more directly. To do this I ran the alkaline comet assay, which assays for DNA strand breaks, in motor neurons treated with control (n=3), sALS (n=3), SOD1-ALS (n=3) or C9-ALS (n=4) astrocyte conditioned medium for 24 hours (Figure 28). I observed no change in mean comet tail moment across the groups (Figure 28A, one-way ANOVA p=0.50), suggesting DNA strand breaks are not increased in healthy motor neurons treated with ALS astrocyte conditioned medium. When I separated the data for the individual cell lines, I observed there was considerable variation between repeats (Figure 28B). To determine whether there were any more subtle changes in comet tail moment across the treatment groups, I plotted the comet tail moment for all the cells scored (Figure 28C), this suggested there might be some subtle changes. To look more closely at subtle changes in comet tail moment, I plotted a graph to show the percentage of cells for each condition with different severities of comet tail moment (Figure 28D), ranging from no comet (0 to 1), small comet (1 to 5), medium comet (5-10) and large comet (>10). I did not observe any consistent patterns within the sALS, SOD1-ALS or C9-ALS groups that differed from the controls, indicating this technique may not be sensitive enough to detect the levels of DNA damage we observe by γH2AX staining.

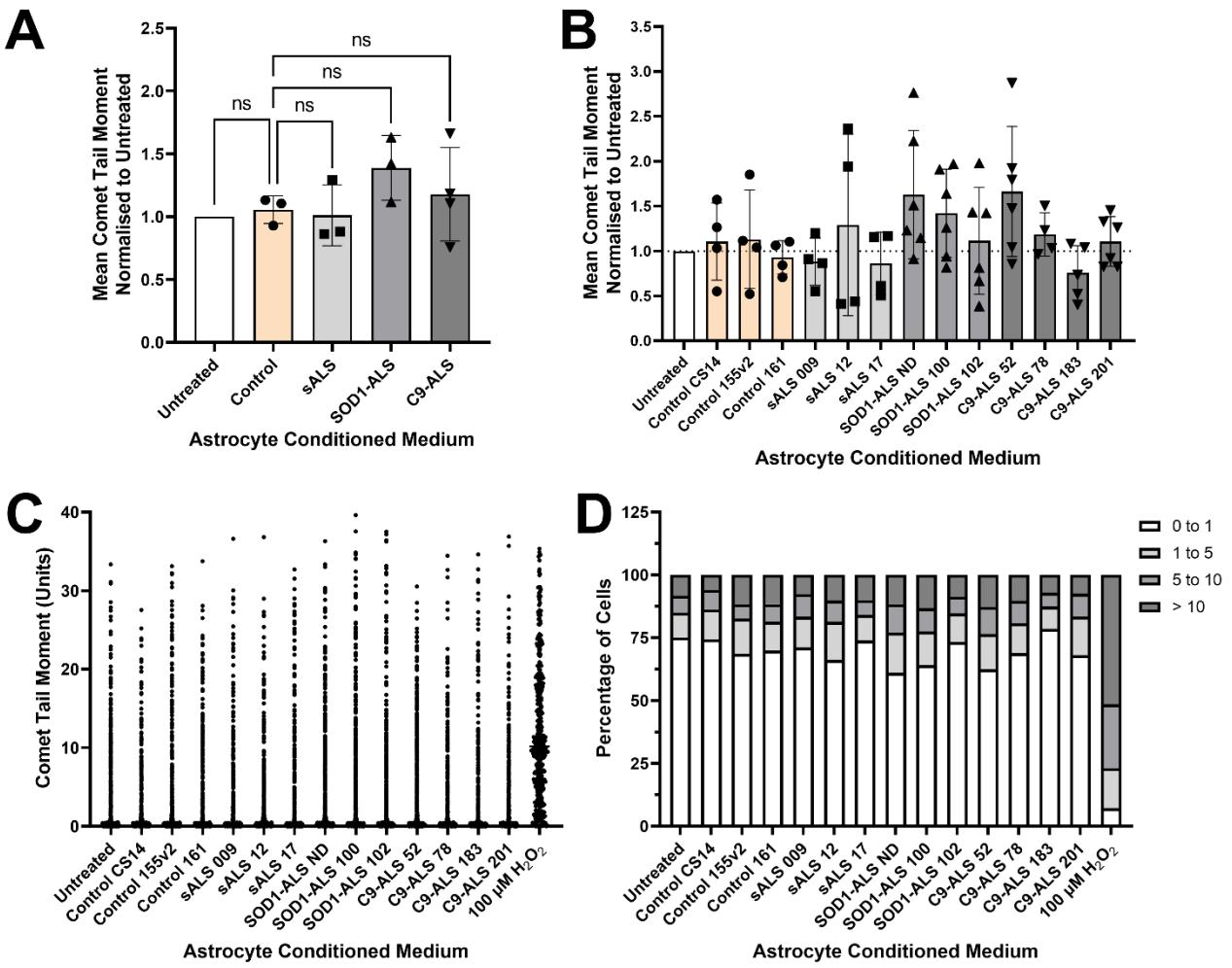

Figure 28. DNA strand breaks are not increased in motor neurons treated with ALS astrocyte conditioned medium. A: Mean comet tail moment data for motor neurons treated with control (n=3), sALS (n-3), SOD1-ALS (n=3) or C9-ALS (n=4) astrocyte conditioned medium. Data met assumption for normality, one-way ANOVA (p=0.50). Means and standard deviations shown, each datapoint represents the mean result of one astrocyte cell line conditioned medium treatment. B: Mean comet tail moment shown for each repeat for each cell line of astrocyte conditioned medium treatment. Means and standard deviations shown, each datapoint represents the mean result for one repeat. C: Scatterplot showing comet tail moment for every cell scored for all repeats and all cell lines, each datapoint represents one cell. D: Graph showing percentage of cells with comet tail moment of 0-1, 1-5, 5-10 and >10, for each cell line.

4.2.3 DNA Repair Proteins

Since immunostaining clearly showed an increase in γH2AX in motor neurons treated with sALS and C9-ALS astrocyte conditioned medium, my next step was to assess whether DNA repair was being activated. To identify what type of DNA damage response was elicited in the motor neurons, I ran Western blotting for DNA single and double-strand break repair factors (TOPO1, Ku80, APE1, PARP1, XRCC1) in motor neurons treated with control or ALS astrocyte conditioned medium for 24 hours (Figure 29). The results were generally quite variable, particularly for XRCC1 and PARP1 where the quality of the Western blot was highly dependent on protein quantity in the lysates. Levels of TOPO1,

XRCC1 and PARP1, but not Ku80 or APE1, were observed to be reduced in motor neurons treated with control or ALS astrocyte conditioned medium compared to the untreated motor neurons, indicating astrocytes may reduce levels of specific DNA repair factors in motor neurons.

Levels of TOPO1 and Ku80 (Figure 29B&C) were not significantly different (TOPO1 one-way AVOVA p=0.16; Ku80 one-way ANOVA p=0.068) in motor neurons treated with control or ALS astrocyte conditioned medium. There was a slight increase in APE1 (Figure 29D) and full length PARP1 (Figure 29F) levels in motor neurons treated with sALS astrocyte conditioned medium compared to control astrocyte conditioned medium, however no significant differences were detected across the groups (APE1 one-way ANOVA p=0.065, full length PARP1 one-way ANOVA p=0.31). There was a significant difference in XRCC1 (Figure 29E) levels across the groups (one-way ANOVA, p=0.021) and it was observed that XRCC1 levels did appear to be reduced in motor neurons treated with SOD1-ALS or C9-ALS astrocyte conditioned medium compared to control astrocyte conditioned medium, however this was only significant for C9-ALS (Dunnett's multiple comparisons test: control vs untreated p=0.59, control vs sALS p=0.59, control vs SOD1-ALS p=0.20, control vs C9-ALS p=0.025).

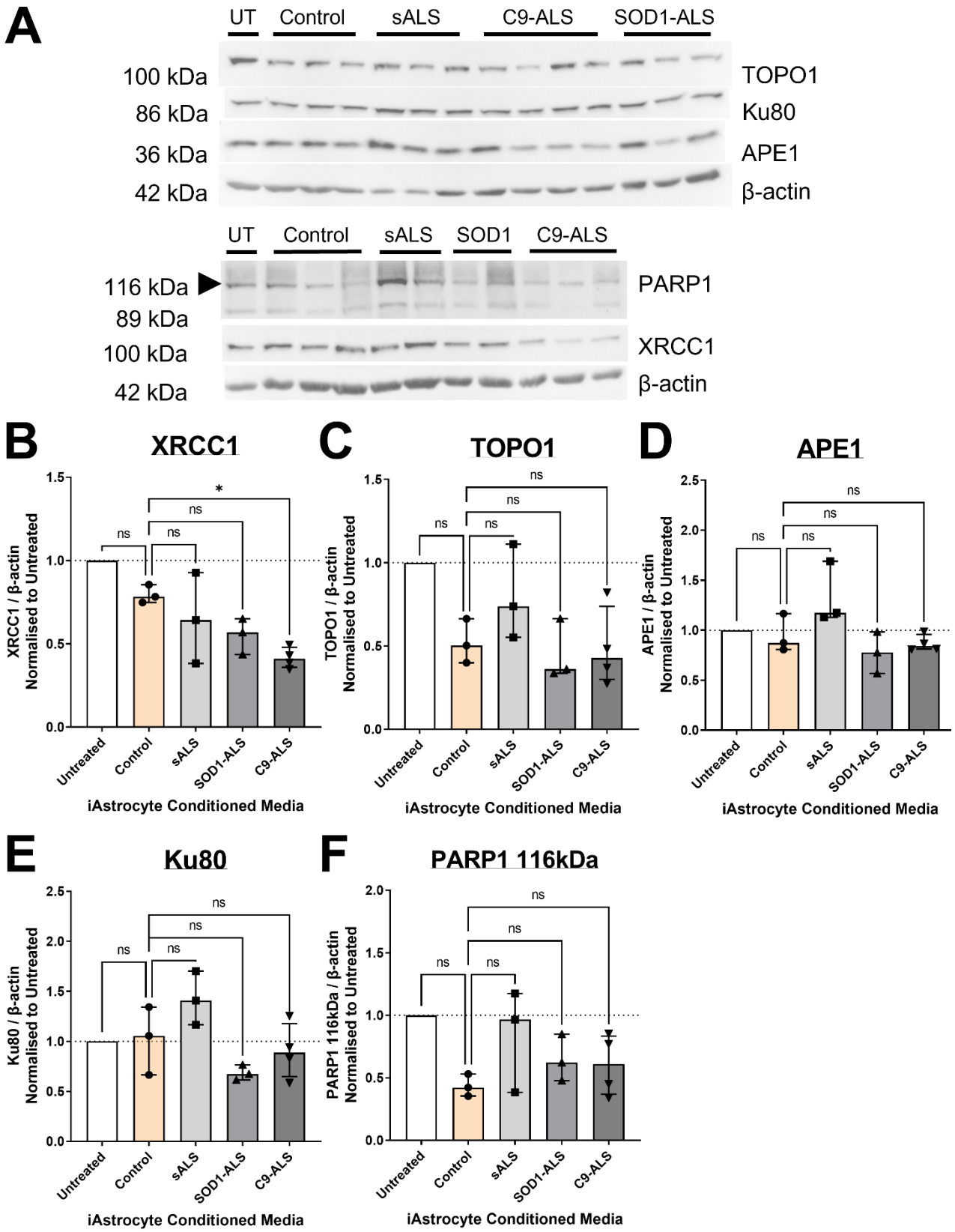

Figure 29. Selected DNA repair factors are not significantly altered in motor neurons treated with ALS astrocyte conditioned medium for 24 hours. A: Representative images of Western blots for TOPO1, Ku80, APE1, PARP1 and XRCC1 in motor neurons treated with control (n=3), sporadic ALS (n=3), SOD1-ALS (n=3) or C9-ALS (n=4) astrocyte conditioned medium for 24 hours. B-G: Quantification of Western blots, means and standard deviations shown, each datapoint represents

the mean result of one astrocyte cell line conditioned medium treatment. All data met assumption of normality. B: Quantification of XRCC1, one-way ANOVA (p=0.021), Dunnett's multiple comparisons test (control vs untreated p=0.59, control vs sALS p=0.59, control vs SOD1-ALS p=0.20, control vs C9-ALS p=0.025). C: Quantification of TOPO1, one-way ANOVA (p=0.16). D: Quantification of APE1, one-way ANOVA (p=0.065). E: Quantification of Ku80, one-way ANOVA (p=0.068).

Considering C9-ALS motor neurons and GABAergic neurons displayed robust and consistent levels of γH2AX activation when measured by Western blotting (Figure 27), these were the best positive controls to determine whether our inability to detect differences in DNA repair protein expression in motor neurons treated with astrocyte conditioned medium was due to Western blotting sensitivity or other disease mechanisms. I ran the same Westerns on iPSC-derived motor neurons from healthy controls, C9-ALS patients and isogenic controls (Figure 30). With the exception of XRCC1, we observed no change in expression for any of the DNA repair proteins. For XRCC1 we observed a significant difference across the groups (one-way ANOVA p=0.034) and post-hoc tests indicated there was a significant increase in XRCC1 expression in C9-ALS motor neurons compared to healthy control (p=0.039) motor neurons and trended towards significance when compared to isogenic control (p=0.082) motor neurons. For TOPO1 (one-way ANOVA p=0.55), Ku80 (one-way ANOVA p=0.90), APE1 (one-way ANOVA p=0.16) and full length PARP1 (one-way ANOVA p=0.56) there were no significant differences across the groups.

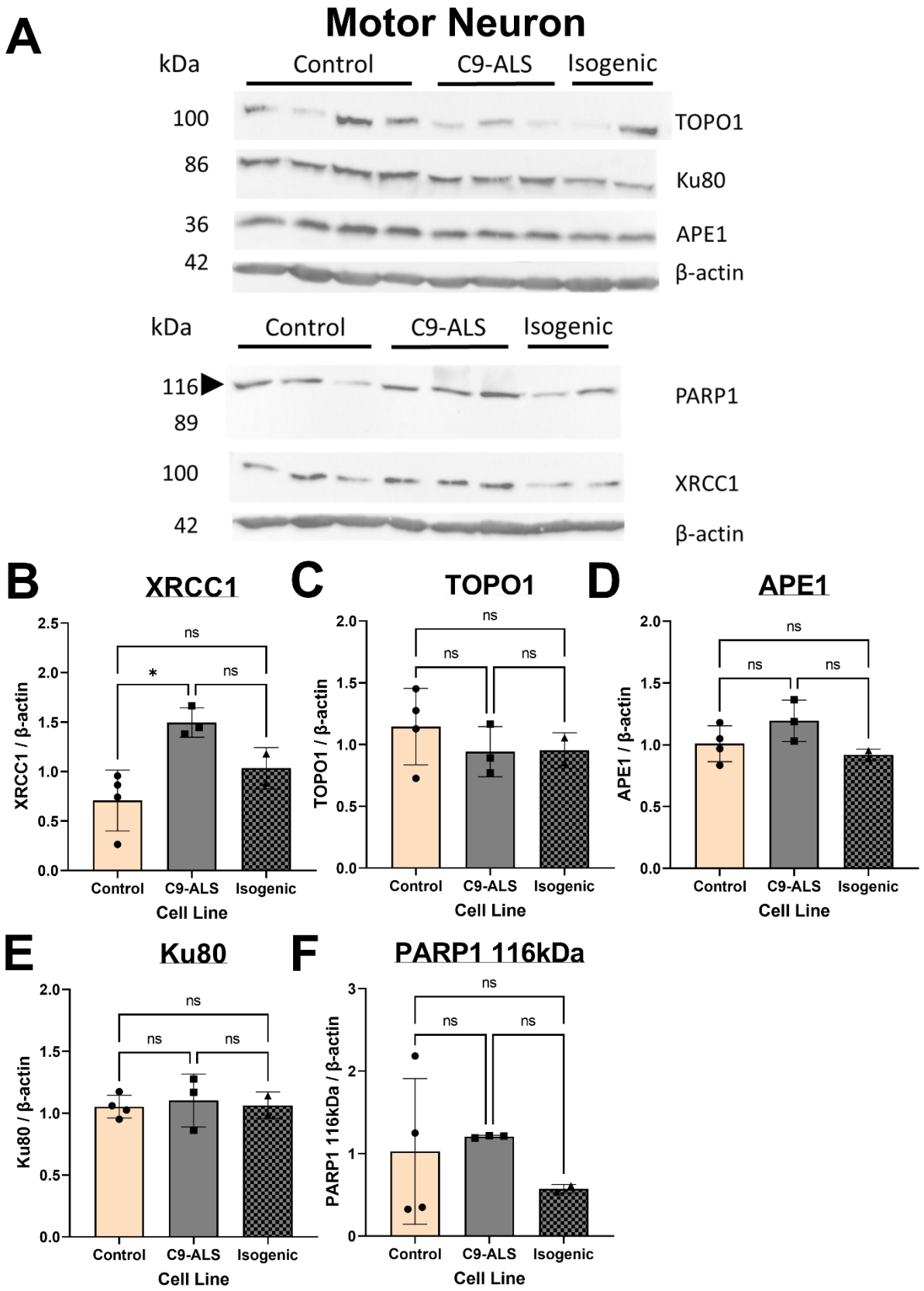

Figure 30. Selected DNA repair factors are not significantly altered in C9-ALS motor neurons. A-F: Western blotting images and quantification for protein levels of XRCC1, TOPO1, APE1, Ku80 and full length 115kDa PARP1 (it was not possible to reliably detect cleaved PARP1) in control (n=4), C9-ALS (n=3) and isogenic control (n=2) iPSC-derived motor neurons. Means and standard deviations shown,

each datapoint represents one cell line. All data met assumption of normality. B: XRCC1 one-way ANOVA (p=0.034), Tukey's multiple comparisons tests (control vs C9-ALS p=0.039, control vs isogenic p=0.99, C9-ALS vs isogenic p=0.082). C: TOPO1 one-way ANOVA p=0.55. D: APE1 one-way ANOVA p=0.16. E: Ku80 one-way ANOVA p=0.90. F: PARP1 116kDa one-way ANOVA p=0.56.

As the lack of DNA repair factor expression change in C9-ALS motor neurons could indicate a pathological failure in DDR (which the El-Khamisy and Ferraiuolo lab are further investigating), I decided to assess the expression of DDR proteins in GABAergic neurons (Figure 31), which we found to be more resistant to DNA damage (unpublished data). Consistent with the level of γH2AX detected at baseline, I found that expression of almost all the assessed DNA repair factors was increased in C9-ALS GABAergic neurons, although this was not always significant.

Similarly to the motor neurons, XRCC1 expression was significantly different across the groups (one-way ANOVA p=0.018) and post-hoc tests showed XRCC1 was significantly increased in C9-ALS GABAergic neurons compared to healthy control (p=0.029) and isogenic control (p=0.029) GABAergic neurons. There was a significant change in APE1 expression across the groups (one-way ANOVA, p=0.0078) and APE1 expression was significantly increased in C9-ALS GABAergic neurons compared to healthy controls (0.013) and isogenic controls (p=0.016). There was also a significant change in full length PARP1 (one-way ANOVA p=0.040) across the groups. Full length PARP1 was significantly increased in C9-ALS GABAergic neurons compared to healthy controls (p=0.046) and trended for significance when comparing to isogenic controls (p=0.089). For both TOPO1 (one-way ANOVA p=0.037) and Ku80 (one-way ANOVA p=0.053), there was a significant or near-significant difference across the groups, however post-hoc tests failed to identify any significant differences. For TOPO1 there were trends toward significance when comparing C9-ALS GABAergic neurons to healthy controls (p=0.063) or isogenic controls (p=0.063), and for Ku80 there were no significant differences when comparing C9-ALS GABAergic neurons to healthy controls (p=0.19) or isogenic controls (p=0.064).

In summary, these data support the findings that C9-ALS motor neurons accumulate DNA damage, but do not display upregulation of DDR factors, while GABAergic neurons also accumulate DNA damage but are capable of upregulating DDR factors. Similarly, healthy motor neurons treated with ALS astrocyte conditioned medium display a significant increase in γH2AX immunostaining, but do not display an increase in DDR proteins via Western blotting. However, it is not clear whether this is caused by a similar impairment in DDR or by the lack of assay sensitivity, as C9-ALS motor neurons and GABAergic neurons both displayed higher levels of DNA damage.

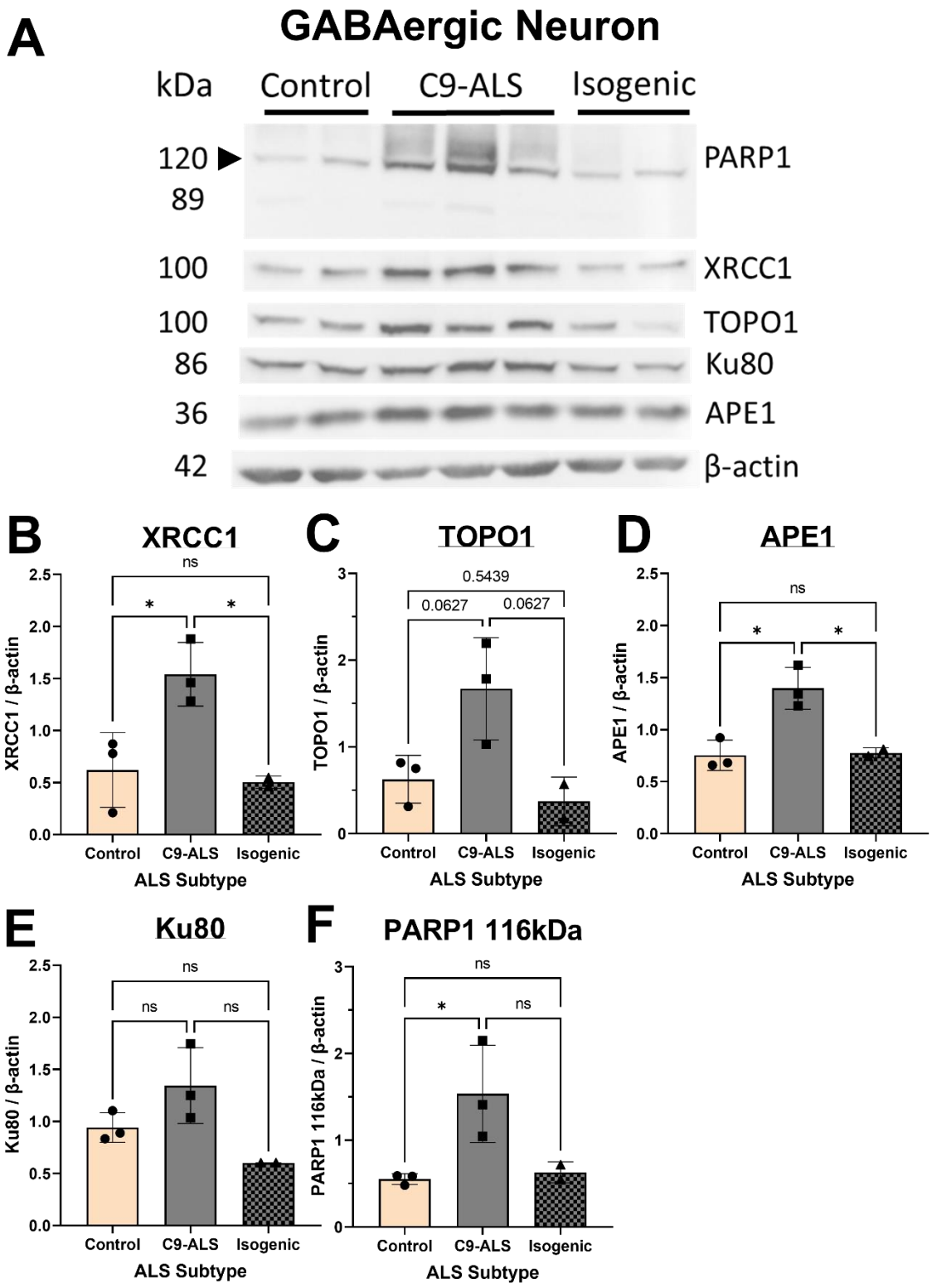

Figure 31. Selected DNA repair factors are upregulated in C9-ALS GABAergic neurons. A-G: Western blotting images and quantification for protein levels of XRCC1, TOPO1, APE1, Ku80 and PARP1 (full-length 116kDa and cleaved 89kDa proteins) in control (n=3), C9-ALS (n=3) and isogenic control (n=2) iPSC-derived GABAergic neurons. Means and standard deviations shown. All data met assumption of normality. B: XRCC1 one-way ANOVA p=0.018 (Tukey's: control vs C9-ALS p=0.029, control vs isogenic p=0.91, C9-ALS vs isogenic p=0.029). C: TOPO1 one-way ANOVA p=0.037 (Tukey's: control vs C9-ALS p=0.063, control vs isogenic p=0.54, C9-ALS vs isogenic p=0.063). D: APE1 one-way ANOVA p=0.0078

(Tukey's: control vs C9-ALS p=0.013, control vs isogenic p=0.88, C9-ALS vs isogenic p=0.016). E: Ku80 one-way ANOVA p=0.053 (Tukey's: control vs C9-ALS p=0.19, control vs isogenic p=0.19, C9-ALS vs isogenic p=0.064). F: PARP1 116kDa one-way ANOVA p=0.04 (Tukey's: control vs C9-ALS p=0.046, control vs isogenic p=0.97, C9-ALS vs isogenic p=0.089).

4.2.4 DNA Repair Transcripts

To validate the Western blotting results for DNA repair factors in motor neurons treated with astrocyte conditioned medium, I decided to look at changes in mRNA transcripts for the same DNA repair factors. Dr Cleide Souza had previously extracted mRNA from motor neurons treated with control (n=3), sALS (n=3) and C9-ALS (n=4) astrocyte conditioned medium for 24 hours and used the Nanostring platform to count the number of mRNA transcripts for 198 different DNA repair factors. Due to limited space on each Nanostring cartridge, we were unable to run the SOD1-ALS astrocyte conditioned medium treated samples at this stage. Also due to time constraints, the experiment has been run in duplicate, with work on the third repeat still ongoing.

Using the raw data generated from this analysis, I was able to look at changes in mRNA transcript count (Figure 32) across the conditions for the DNA repair factors I had examined by Western blotting (XRCC1, TOPO1, APE1, XRCC5 – Ku80, PARP1). I observed no significant difference in normalised mRNA transcript count across the treatment groups for XRCC1 (one-way ANOVA p=0.75), TOPO1 (one-way ANOVA p=0.78), APE1 (one-way ANOVA p=0.19), XRCC5-Ku80 (one-way ANOVA p=0.11) or PARP1 (one-way ANOVA p=0.32). These results are similar to what I observed by Western blotting, with the exception of XRCC1 which was significantly altered in the Western blotting results. Notably we did not observe an increase with CPT treatment for all the factors examined, and this is likely because CPT is specifically a topoisomerase I inhibitor and is unlikely to activate all DNA repair pathways (Liu et al., 2000). Alternatively, we used a lower concentration of CPT to treat the motor neurons to avoid inducing cell death as the motor neurons were very sensitive to higher levels of CPT treatment, and this concentration may have been too low to induce a meaningful increase in DNA repair factor expression.

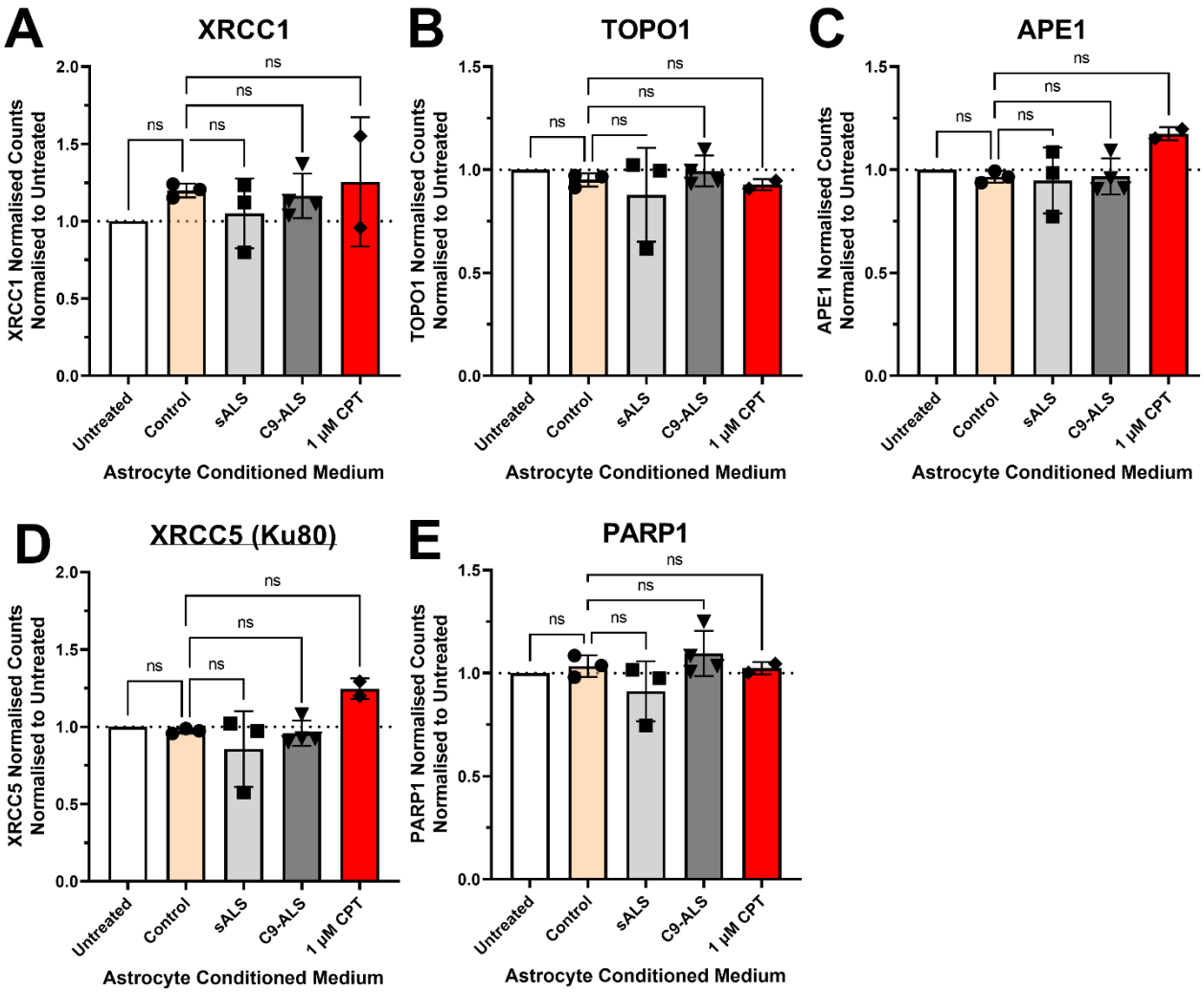

Figure 32. Nanostring analysis of mRNA transcripts in motor neurons treated with control or ALS astrocyte conditioned medium shows no change in selected DNA repair factor expression. Nanostring analysis for DNA repair factors was run on mRNA isolated from motor neurons treated with control (n=3), sALS (n=3) or C9-ALS (n=4) astrocyte conditioned medium for 24 hours. Data represents mean result of two repeats per condition. Means and standard deviations shown, each datapoint represents the mean result of one astrocyte cell line conditioned medium treatment. A: Normalised counts of XRCC1 mRNA transcripts in motor neurons treated with control or ALS astrocyte conditioned medium, one-way ANOVA (p=0.75). B: Normalised counts of TOPO1 mRNA transcripts in motor neurons treated with control or ALS astrocyte conditioned medium, one-way ANOVA (p=0.78). C: Normalised counts of APE1 mRNA transcripts in motor neurons treated with control or ALS astrocyte conditioned medium, one-way ANOVA (p=0.19). D: Normalised counts of XRCC5 (encodes Ku80 protein) mRNA transcripts in motor neurons treated with control or ALS astrocyte conditioned medium, one-way ANOVA (p=0.11). E: Normalised counts of PARP1 mRNA transcripts in motor neurons treated with control or ALS astrocyte conditioned medium, one-way ANOVA (p=0.32).

4.2.5 Astrocyte-Induced Cell Stressors

To determine what stressor(s) may have induced the increase in γH2AX foci in healthy motor neurons treated with astrocyte conditioned medium, I investigated various cell stressors and their

markers. A previous study looking at cell autonomous DNA damage in C9-ALS motor neurons suggested that DNA damage occurred due to an increase in ROS (Lopez-Gonzalez et al., 2016). To determine whether ALS astrocytes were inducing DNA damage in motor neurons through ROS, I stained live motor neurons treated with control or ALS iAstrocyte conditioned media for 24 hours with CellROX reagent (Figure 33) as I had done previously for control and ALS astrocytes (3.2.1). I observed no significant change in CellROX intensity per μm^2 (one-way ANOVA, p=0.43) or in CellROX intensity per cell (Kruskal-Wallis, p=0.97) across our treatment groups, indicating ALS astrocytes were likely not inducing an increase in ROS within 24 hours of treatment and thus that ROS were likely not the cause of astrocyte-induced DNA damage.

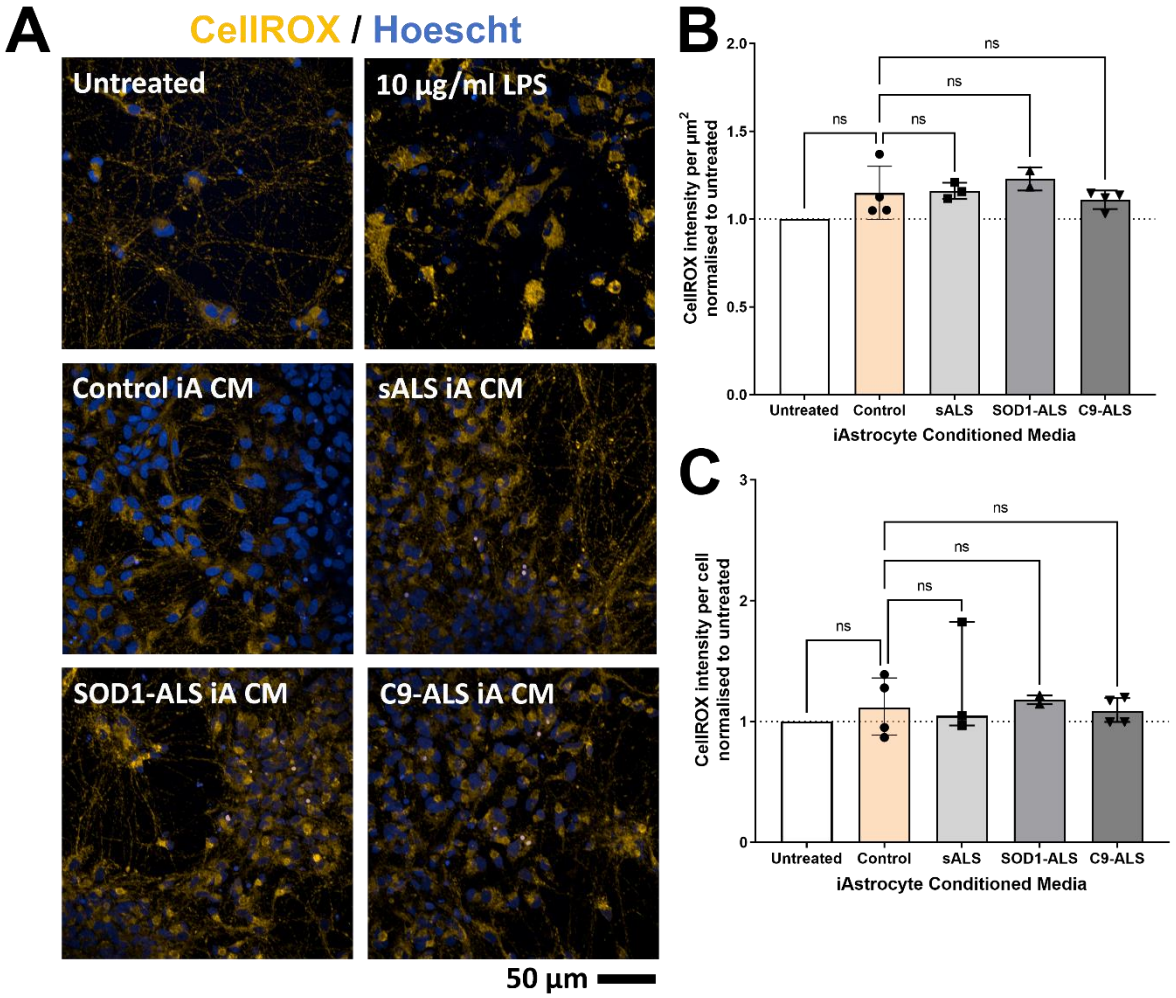

Figure 33. Reactive oxygen species are not increased in motor neurons treated with astrocyte conditioned medium. A: Example images of CellROX staining for ROS in motor neurons treated with control (n=4), sALS (n=3), SOD1-ALS (n=2) or C9-ALS (n=4) astrocyte conditioned medium for 24 hours, or LPS as a positive control. LPS used as a positive control as it has previously been shown to induce increased ROS in microglia (Wang et al., 2004). B: Quantification of CellROX intensity per μm^2 in motor neurons treated with astrocyte conditioned medium for 24 hours. Data met assumption of normality, one-way ANOVA (p=0.43), means and standard deviations shown. C: Quantification of

CellROX intensity per cell in motor neurons treated with astrocyte conditioned medium for 24 hours. Data did not meet assumption of normality, Kruskal-Wallis test (p=0.97), median and interquartile range shown. Each datapoint represents the mean result of one astrocyte cell line conditioned medium treatment.

Another paper looking at cell autonomous DNA damage in C9-ALS motor neurons suggested that DNA damage occurred due to an increase in R-loops (Walker et al., 2017). To determine whether ALS astrocytes induce DNA damage through an increase in R-loops, I stained motor neurons treated with control and ALS astrocyte conditioned medium for R-loops using the S9.6 antibody (Figure 34) as I had previously done for the control and ALS astrocytes (3.2.3). I observed no significant change in S9.6 foci per cell (Kruskal-Wallis, p=0.48), S9.6 foci size (one-way ANOVA, p=0.21), or S9.6 nuclear intensity per μm^2 (one-way ANOVA, p=0.30), showing that R-loops are not increased by ALS astrocyte conditioned medium and thus R-loops are likely not the cause of ALS astrocyte-induced DNA damage. Notably I observed the same staining patterns for the treated motor neurons as I observed in the control and ALS astrocytes (3.2.3), indicating the staining may not be specific to R-loops.

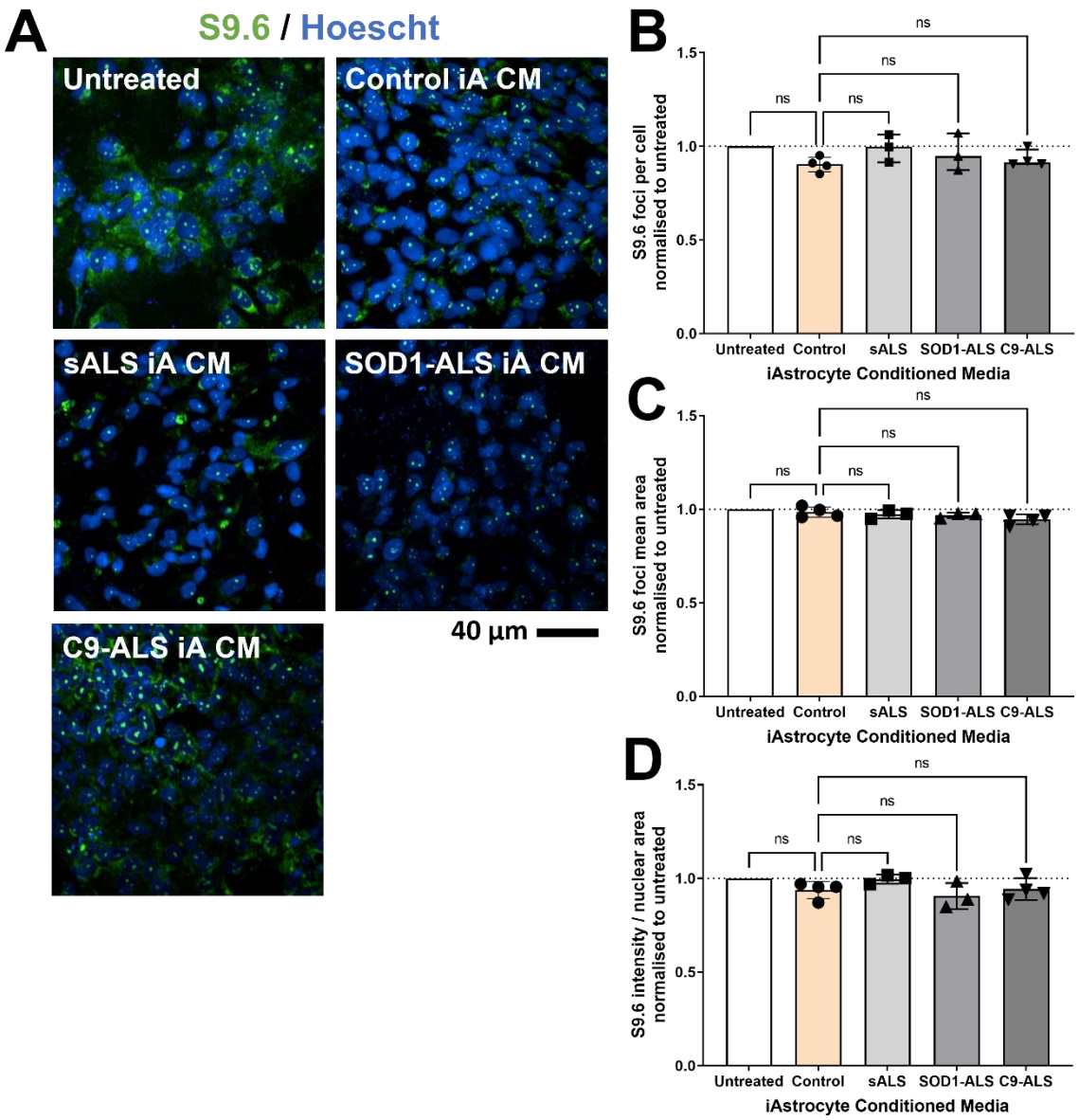

Figure 34. R-loops are not increased in motor neurons treated with astrocyte conditioned medium. A: Example images of R-loop staining with S9.6 antibody in motor neurons treated with control (n=4), sALS (n=3), SOD1-ALS (n=3) or C9-ALS (n=4) astrocyte conditioned medium. B: Quantification of S9.6 foci per cell. Data did not meet assumption of normality, Kruskal-Wallis test (p=0.48), median and interquartile ranges shown. C: Quantification of mean S9.6 foci area. Data met assumption of normality, one-way ANOVA (p=0.21), means and standard deviations shown. D: Quantification of S9.6 intensity divided by nuclear area. Data met assumption of normality, one-way ANOVA (p=0.30), means and standard deviations shown. Each datapoint represents the mean result of one astrocyte cell line conditioned medium treatment.

Following on from looking at R-loops, I also decided to look at nucleoli as nucleoli are known to be involved in DNA damage signalling and repair (Boisvert et al., 2007), so I stained motor neurons treated with control and ALS astrocyte conditioned medium for 24 hours for nucleolin (Figure 35). I observed no significant change in nucleoli per cell (one-way ANOVA, p=0.54), nucleoli size (one-way ANOVA, p=0.46), or nucleolin intensity per μm^2 (one-way ANOVA, p=0.68), showing that nucleoli

number and size are not altered by ALS astrocyte conditioned medium and thus nucleoli are likely not involved in ALS astrocyte-induced DNA damage.

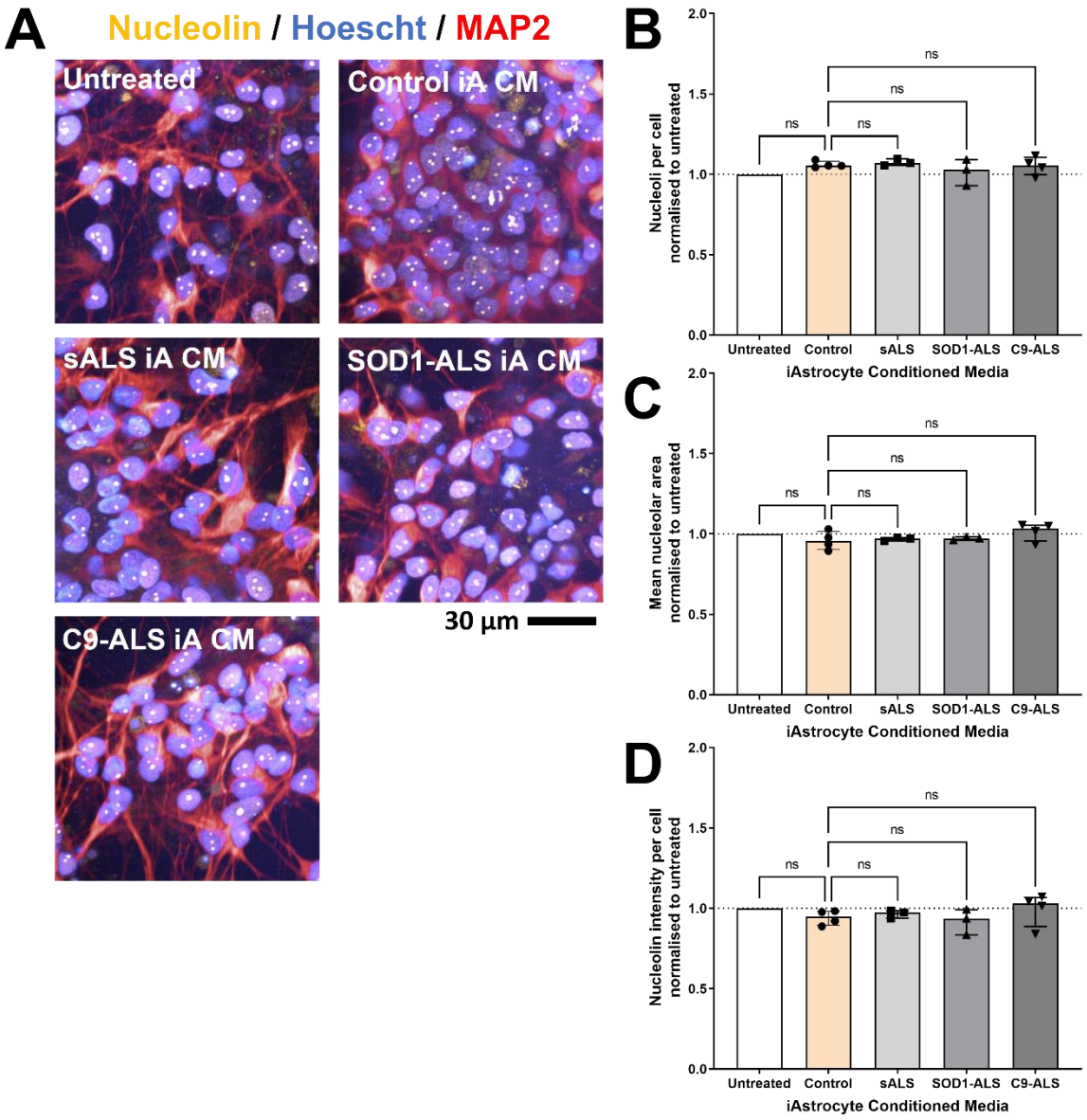

Figure 35. Nucleoli number or morphology are not changed in motor neurons treated with astrocyte conditioned medium. A: Example images of nucleolin staining in motor neurons treated with control (n=4), sALS (n=3), SOD1-ALS (n=3) or C9-ALS (n=4) astrocyte conditioned medium. B: Quantification of nucleoli per cell. Data met assumption of normality, one-way ANOVA (p=0.54), means and standard deviations shown. C: Quantification of mean nucleoli area. Data met assumption of normality, one-way ANOVA (p=0.46), means and standard deviations shown. D: Quantification of nucleolin intensity divided by nuclear area. Data met assumption of normality, one-way ANOVA (p=0.68), means and standard deviations shown. Each datapoint represents the mean result of one astrocyte cell line conditioned medium treatment.

4.3 Discussion

In this study, we set out to expand upon the preliminary data that showed that C9-ALS astrocyte could induce DNA damage in mouse motor neurons. We found that both sALS and C9-ALS astrocyte conditioned medium could induce γH2AX foci formation in motor neurons within 24 hours, but SOD1-ALS astrocyte conditioned medium did not. I was unable to see the same results by measuring γH2AX levels using Western blotting, nor was I able to validate DNA damage directly with the alkaline comet assay. However, detection of increased γH2AX foci in motor neurons treated with sALS or C9-ALS astrocyte conditioned medium for 24 hours was repeatable in subsequent repair kinetic experiments conducted by Dr Cleide Souza.

Assay sensitivity may play a role in the differing results. It is likely that staining and high throughput imaging of γH2AX foci is more sensitive than Western blotting as foci are easily detected and could be quantified in thousands of individual cells, whereas Western blotting provides a more crude overview. Notably, I was also unable to detect changes in γH2AX levels in C9-ALS astrocytes by Western blotting despite clear γH2AX foci staining data (3.3.2). On the other hand, I was able to detect increased γH2AX in C9-ALS motor neurons and GABAergic neurons by Western blotting. However, endogenous γH2AX foci in motor neurons are approximately 100% higher than controls, while ALS astrocyte conditioned medium only induces an approximately 65% increase in γH2AX foci. Thus, Western blotting may not be sensitive enough to detect the smaller changes in γH2AX foci we observe following conditioned medium treatment.

γH2AX measurement has been reported to be 100 times more sensitive at detecting DNA damage compared to the comet assay (Kuo and Yang, 2008), which may explain the negative comet assay results. An alternative explanation could be that the DNA damage induced by the astrocytes is not DNA strand breaks. H2AX has been reported to be phosphorylated under oxidative stress condition, after treatment with alkylation agents, and after induction of interstrand or intrastrand crosslinks (Katsube et al., 2014; Revet et al., 2011). However, these conditions can also be a source of DNA strand breaks so it is unclear if H2AX can be phosphorylated independent of DNA strand breaks.

To attempt to elucidate the type of DNA damage, we looked at expression of different DNA repair factors with Western blotting and by Nanostring analysis, however we observed very little change. The result was unexpected as we predicted that expression of some repair factors would be increased in treated motor neurons to try to facilitate DNA repair. In additional experiments conducted by Dr Cleide Souza (data not shown), it was observed that motor neurons treated with

ALS astrocyte conditioned medium for 24 hours did not exhibit increased pATM or 53BP1 foci, suggestive of an impairment in the early DNA damage response, so the lack of clear increase in DNA repair factor expression is consistent with that data.

A surprising finding was that TOPO1, XRCC1 and PARP1 protein expression were reduced to different extents in motor neurons treated with control astrocyte conditioned medium compared to untreated motor neurons. Transcript expression was not changed for these factors, indicating any changes in expression are not at the transcription level. XRCC1, TOPO1 and PARP1 are involved in the induction and repair of TOPO1-induced single-strand breaks, suggesting healthy astrocytes negatively regulate this pathway. TOPO1 functions during DNA replication and transcription by nicking DNA to relax supercoiling, however this process can be interrupted and result in a single-strand break and a TOPO1:DNA cleavage complex (TOP1cc). PARP1 recognises TOP1cc and recruits TDP1 and XRCC1 to the site to resolve the TOP1cc and DNA single strand break respectively (Chowdhuri and Das, 2021). It is unclear why astrocytes might negatively regulate expression of TOPO1, XRCC1 and PARP1, however reduction in XRCC1 and PARP1 could sensitise motor neurons to DNA damage. PARP1 deficiency and XRCC1 deficiency have individually been shown to sensitise cells to DNA damage induced by alkylation agents (Brem and Hall, 2005; Shibata et al., 2004), while XRCC1 deficiency has also been shown to sensitise cells to DNA damage induced by oxidising agents and ionising radiation (Brem and Hall, 2005). Indeed, XRCC1 inactivation in neurons in mice has been shown to lead to persistent accumulation of DNA strand breaks and neurodegeneration (Lee et al., 2009).

XRCC1 has also been shown to regulate PARP1 activity during BER and vice versa. In cells with PARP1 knocked out, XRCC1 foci fail to form following hydrogen peroxide treatment, suggesting PARP1 recruits XRCC1 to DNA after oxidative DNA damage (El-Khamisy et al., 2003). Similarly, XRCC1 appears to regulate PARP1 activity as cells carrying an XRCC1 mutation causing a premature stop codon show an increase in ADP-ribosylation, indicating increased PARP1 activity (Hoch et al., 2016). Furthermore, in XRCC1 deficient cells treated with an alkylating agent, PARP1 causes an accumulation of DNA single-strand breaks by blocking access to BER repair factors and additionally suppresses global transcription (Adamowicz et al., 2021; Demin et al., 2021). Notably inhibition or knockdown of PARP1 improved both phenotypes in XRCC1 deficient cells (Adamowicz et al., 2021; Demin et al., 2021) and improved motor function and reduced neuron loss in a mouse model where XRCC1 was knocked out in the brain (Hoch et al., 2016).

In my results, control astrocytes induced a reduction in PARP1 levels as well as a reduction in XRCC1, thus control astrocytes may suppress aberrant PARP1 activity in motor neurons by inducing a reduction in PARP1 protein levels. Interestingly, XRCC1 levels were further reduced in motor neurons treated with SOD1-ALS or C9-ALS astrocyte conditioned medium compared to control astrocyte conditioned medium treatment, while PARP1 levels remained relatively similar to untreated motor neurons. This could indicate PARP1 activity is not suppressed in these XRCC1 deficient cells and thus that aberrant PARP1 activity may play a role in ALS astrocyte-induced DNA damage. It would be of interest to see whether catalytically inhibiting PARP1 in motor neurons protects them from astrocyte-induced DNA damage. If not, the reduction in XRCC1 in ALS astrocyte conditioned medium treated motor neurons could also sensitise the cells to DNA damage, which could potentially be corrected by XRCC1 overexpression.

Interestingly, in contrast to the astrocyte conditioned medium results, XRCC1 levels were significantly increased in both C9-ALS motor neurons and GABAergic neurons. To our knowledge this is the first time XRCC1 levels have been investigated in ALS. These findings were somewhat unexpected considering our finding that C9-ALS astrocytes induce a reduction in XRCC1 in motor neurons. It might be possible that the astrocyte activity is a compensatory mechanism. A previous study reported that three XRCC1 polymorphisms were present at increased frequency in sALS patients compared to controls (Coppedè et al., 2010). Another study failed to replicate this finding, however they had a smaller sample size (Fang et al., 2012). XRCC1 dysfunction may play a wider role in ALS that has not yet been investigated. It would be of interest to see whether correcting XRCC1 expression in ALS motor neurons or motor neurons treated with ALS astrocyte conditioned medium, has any effect on cell survival or DNA damage.

With the exception of XRCC1, the remaining DNA repair factors we investigated (APE1, TOPO1, Ku80, PARP1) were unchanged in C9-ALS motor neurons compared to controls. My results differ from previous findings. APE1 levels were reported to be increased in the spinal cord and motor cortex of a mixed population of ALS patients in one study (Shaikh and Martin, 2002), but were found to be decreased in the frontal cortex of sporadic ALS patients and in SOD1-ALS mouse spinal cord motor neurons (Kisby et al., 1997; Nagano et al., 2002). Similarly, PARP1 has been reported to be reduced in sALS patient spinal cord motor neurons (Kim et al., 2003), while cleaved PARP1 levels were increased in the spinal cord of C9-ALS patients (Farg et al., 2017). Ku80 levels have been shown to be increased in C9-ALS motor neurons and were suggested to contribute to neuron death

(Lopez-Gonzalez et al., 2019). TOPO1 has not yet been investigated in ALS, however cells expressing the C9ORF72 repeat expansion exhibit higher levels of TOP1ccs (Walker et al., 2017), suggestive of defective repair. Our results seem to indicate C9-ALS motor neurons exhibit a deficiency in DNA repair, however these results might benefit from additional validation by qPCR to see if transcript levels show the same results.

In contrast to our findings in C9-ALS motor neurons, almost all the DNA repair factors assessed were found to be increased in C9-ALS GABAergic neurons compared to the healthy controls and isogenic controls. Notably, we observed increased γH2AX levels in both C9-ALS motor neurons and C9-ALS GABAergic neurons, so it is somewhat surprisingly that only C9-ALS GABAergic neurons show increased DNA repair factor expression. Interestingly, while we were expecting that γH2AX would be increased in C9-ALS motor neurons, as this is consistent with previously published findings (Farg et al., 2017; Higelin et al., 2018; Walker et al., 2017), it was somewhat surprising that DNA damage was increased in C9-ALS GABAergic neurons as this has not been previously reported. GABAergic neurons have been suggested to be dysfunctional in ALS (reviewed in Turner and Kiernan, 2012) and it may be that DNA damage is also a mechanism by which GABAergic neurons are affected in C9-ALS. Unpublished data from the Ferraiuolo and El-Khamisy lab groups has shown that C9-ALS GABAergic neurons are more efficient at DNA repair than C9-ALS motor neurons, and it may be that the selective increase in DNA repair factor expression in C9-ALS GABAergic neurons facilitates the observed DNA repair.

Previous studies investigating cell autonomous changes in DNA damage in C9-ALS motor neurons have suggested R-loops (Walker et al., 2017) or ROS (Lopez-Gonzalez et al., 2016) may be the cause of DNA damage. We looked at these parameters, along with nucleoli size and morphology, in the motor neurons treated with control and ALS astrocyte conditioned medium, to determine whether these factors could be the cause of astrocyte-induced DNA damage, however we saw no change in R-loops, ROS or nucleoli number or morphology. Notably for oxidative stress, previous published findings showed that C9-ALS astrocytes could induce an increase in ROS in motor neurons treated with conditioned medium (Birger et al., 2019), although they looked at oxidative stress after 8 days of conditioned medium treatment while we looked after 24 hours of treatment. It is therefore likely that astrocyte-induced DNA damage occurs by a different mechanism than cell autonomous increases in DNA damage in ALS.

4.4 Conclusion

In this chapter we have shown that sALS and C9-ALS astrocyte-derived conditioned medium can induce an increase in γH2AX foci in motor neurons within 24 hours of treatment. Healthy astrocytes induce a reduction in protein levels of TOPO1, XRCC1 and PARP1 in motor neurons, although the reason for this remains unclear. C9-ALS astrocytes can induce a further reduction in XRCC1, but other repair factors appear relatively unchanged following ALS astrocyte conditioned medium treatment. Due to the role of XRCC1 in PARP1 regulation, it is possible that aberrant PARP1 activity may lead to astrocyte-induced DNA damage, however this requires further investigation. The lack of change in DNA repair proteins replicates the lack of alteration in C9-ALS motor neurons, with the exception of XRCC1, which is elevated in C9-ALS motor neurons. I also looked at whether ALS astrocytes induce cellular stressors in motor neurons, but I did not observe any change in levels of ROS, R-loops, or nucleoli number or morphology. These data suggest astrocytes do not induce DNA damage through the same mechanisms as cell autonomous DNA damage in ALS.

Chapter 5: Mechanisms of ALS Astrocyte-Induced DNA Damage

5.1 Introduction

5.1.1 DPRs and DNA Damage

While there are no clear candidates for the cause of sALS astrocyte-induced DNA damage, for C9-ALS there have been a number of studies suggesting dipeptide repeat proteins (DPRs) generated from RAN translation of the C9ORF72 repeat expansion may cause cell autonomous increases in motor neuron DNA damage (Lopez-Gonzalez et al., 2016; Nihei et al., 2020; Walker et al., 2017) and DNA repair impairment (Andrade et al., 2020).

RAN translation of the C9ORF72 repeat expansion leads to the production of five different DPR species – polyGA, polyGP, polyGR, polyPR and polyPA (Ash et al., 2013; Zu et al., 2013). The DPRs are not present in equal abundance, with apparent preferential translation of the sense DPRs (GA, GR) over the anti-sense DPRs (PA, PR) (Mackenzie et al., 2015). GP is produced from both the sense and anti-sense RNA repeat expansions (RRE) (Mackenzie et al., 2015) and it remains unclear whether there are differences between the GP produced from sense RRE and the GP produced from anti-sense RRE. The overall abundance of the different DPRs, based on staining analysis from post-mortem tissue has suggested the order follows GA > GP > GR > PA = PR (Mackenzie et al., 2015).

Several studies have attempted to elucidate the properties of the individual DPR species by transfecting or transducing them into cell models. These approaches have been helpful at understanding their differences and how they may contribute to disease. The arginine-rich DPRs (GR and PR) are considered to be the most toxic (Lee et al., 2016; Mizielinska et al., 2014; Wen et al., 2014), with GA also reported to be neurotoxic (Lee et al., 2017), while GP and PA appear to be non-toxic (Lee et al., 2016; Mizielinska et al., 2014; Wen et al., 2014). Strikingly, GA (Nihei et al., 2020; Walker et al., 2017), GR and PR (Farg et al., 2017; Lopez-Gonzalez et al., 2016) have been reported to induce DNA damage when transfected or transduced into cell models, suggesting a possible mechanism by which they induce cell death.

DPRs are not exclusively expressed in motor neurons. In fact, a number of studies have shown high levels of DPR expression in the cortex, hippocampus and cerebellum (Ash et al., 2013; Mackenzie et al., 2015; Schludi et al., 2015). DPRs have also been observed to be present in non-neuronal cells including skeletal muscle cells (Cykowski et al., 2019), and even Sertoli cells in the testes (Ash et al.,

2013). DPRs are, however, not present in all cell types and their absence has been observed in the heart, kidney and spleen (Ash et al., 2013). Importantly, polyGP DPRs have also been observed in astrocytes derived from C9-ALS patients (Zhao et al., 2020), indicating DPRs are present in astrocytes, although there remains to be direct evidence of toxic DPR species present endogenously in C9-ALS astrocytes.

It has previously been demonstrated that NSC34 cells expressing GFP-tagged DPRs can transmit DPRs to non-expressing cells, including astrocytes, through exosome dependent and independent pathways (Westergard et al., 2016). Notably, the Ferraiuolo lab has previously shown that exosomes isolated from C9-ALS patient-derived astrocyte conditioned medium can induce cell death in motor neurons (Varcianna et al., 2019). It is therefore possible that C9-ALS astrocytes could secrete DPRs into the conditioned medium, packaged within exosomes or not, and this could be a mechanism by which C9-ALS astrocytes induce DNA damage and cell death.

5.1.2 P62 and DNA Damage

The p62 protein was first linked with ALS when it was identified as being present in the ubiquitin-positive inclusions present in neurons and glia of FTD and ALS/FTD patients (Arai et al., 2003). Later, mutations in the gene encoding p62, SQSTM1, were found to be linked with a small percentage of familial ALS cases (Fecto et al., 2011; Rubino et al., 2012).

P62 is primarily known for its role as an adaptor in selective autophagy, the cellular process by which proteins and organelles are transported to lysosomes for degradation. Proteins which are targeted for degradation are ubiquitinated and recognised by p62, which binds to ubiquitin through its C-terminal Ub-associated domain (UBA). P62 is then targeted to the site of autophagosome formation on the endoplasmic reticulum, where it binds to LC3 through its LC3-interacting region (LIR) motifs (Komatsu et al., 2012). LC3 is synthesised as proLC3 and cleaved to form LC3-I, which can be conjugated to phosphatidylethanolamine (PE) in the membranes of autophagosomes to form LC3-II. LC3-II on the inner membrane of the autophagosome, along with any bound proteins including p62 and its attached cargo, is degraded following autophagosome-lysosome fusion, whereas LC3-II on the outer membrane is delipidated to become LC3-I (reviewed in Tanida, 2011).

P62 also plays a role in the KEAP1–NRF2 oxidative stress response pathway. Under normal conditions KEAP1 binds NRF2, facilitating the ubiquitination and degradation of NRF2. During oxidative stress, ROS oxidise KEAP1, which allows NRF2 to dissociate and translocate to the nucleus

to activate transcription. In the non-canonical NRF2 activation pathway, p62 can bind to KEAP1 through its KEAP1 interacting region (KIR) motifs, which also allows NRF2 to translocate to the nucleus (Katsuragi et al., 2016).

In addition to playing a role in autophagy and the oxidative stress response, p62 has also been linked with DNA damage signalling. P62 has been found to interact with and inhibit the E3 ligase, RNF168 (Wang et al., 2016). Following DNA damage, RNF168 ubiquitinates histone H2A, which facilitates the recruitment of proteins like BRCA1, RAP80, Rad51 and 53BP1 to sites of DNA damage (van Attikum and Gasser, 2009). Thus, overexpression of p62 leads to a reduction in DNA damage-induced histone H2A ubiquitination (Wang et al., 2016). Importantly, knockdown of p62 in MRC5 cells transfected with DPRs partially rescued DNA damage, indicating p62 may be involved in DPR-induced DNA damage in C9-ALS (Walker et al., 2017). It has previously been shown that astrocyte conditioned medium derived from C9-ALS and sALS patients can induce p62 foci in motor neurons (Madill et al., 2017) and thus p62 may play a role in ALS astrocyte-induced DNA damage.

5.1.3 Aims and Objectives

The aim of this chapter was to determine whether DPRs and/or p62 could be a mechanism by which ALS astrocytes induce DNA damage in motor neurons. While DPRs would be a C9-ALS specific mechanism, p62 might prove a more common downstream mechanism by which both C9-ALS and sALS astrocytes could induce DNA damage.

To carry out these aims, I first characterised DPR expression in the C9-ALS astrocytes compared to the controls by immunocytochemistry. I then attempted to detect DPRs in C9-ALS astrocyte conditioned medium and exosomes through a few different methods including dot blotting and the MSD ELISA. Dr Cleide Souza aimed to replicate previous findings that ALS astrocyte conditioned medium induces p62 foci formation in motor neurons and determine at what time point following treatment this accumulation could be observed in our model. I went on to attempt to validate this by Western blotting, as well as examining changes in expression of proteins associated with p62 function in autophagy and oxidative stress response (KEAP1, LC3B). Following on from this work I attempted to determine whether ALS astrocyte-induced p62 accumulation was mediated through astrocyte-secreted p62. To test this, I attempted to immunodeplete p62 from ALS astrocyte conditioned medium and to knockdown p62 in ALS astrocytes to see whether this would rescue ALS astrocyte-induced DNA damage, cell death and p62 accumulation.

5.2 Detection of DPRs in C9-ALS Astrocytes and Conditioned Medium

5.2.1 DPRs in C9-ALS Astrocytes

Before looking at whether DPRs are present in C9-ALS astrocyte conditioned medium, I wanted to verify that C9-ALS astrocytes do in fact express DPRs. DPRs have generally been difficult to detect and quantify, however several studies have successfully shown DPRs using immunohistochemistry or immunocytochemistry (MacKenzie et al., 2013; Mann et al., 2013). I began by using the antibodies we had available, that had previously been validated in Western blotting, to stain HEK293T cells transfected with the sense and anti-sense RNA repeat expansion (Figure 36), which were kindly provided by Dr Lydia Castelli of the Hautbergue group at SITraN. As polyGP and polyGA are considered the most abundant DPR species, followed by polyGR and then polyPA/PR, I expected that the staining would likely be successful for the more abundant species. Indeed, in the transfected cells I observed diffuse nuclear staining for polyGP, nuclear and cytoplasmic foci for polyGA and nuclear and cytoplasmic foci for polyGR. PolyPA staining appeared to be unsuccessful and we did not have a validated antibody to test for polyPR, hence these have not been taken forward.

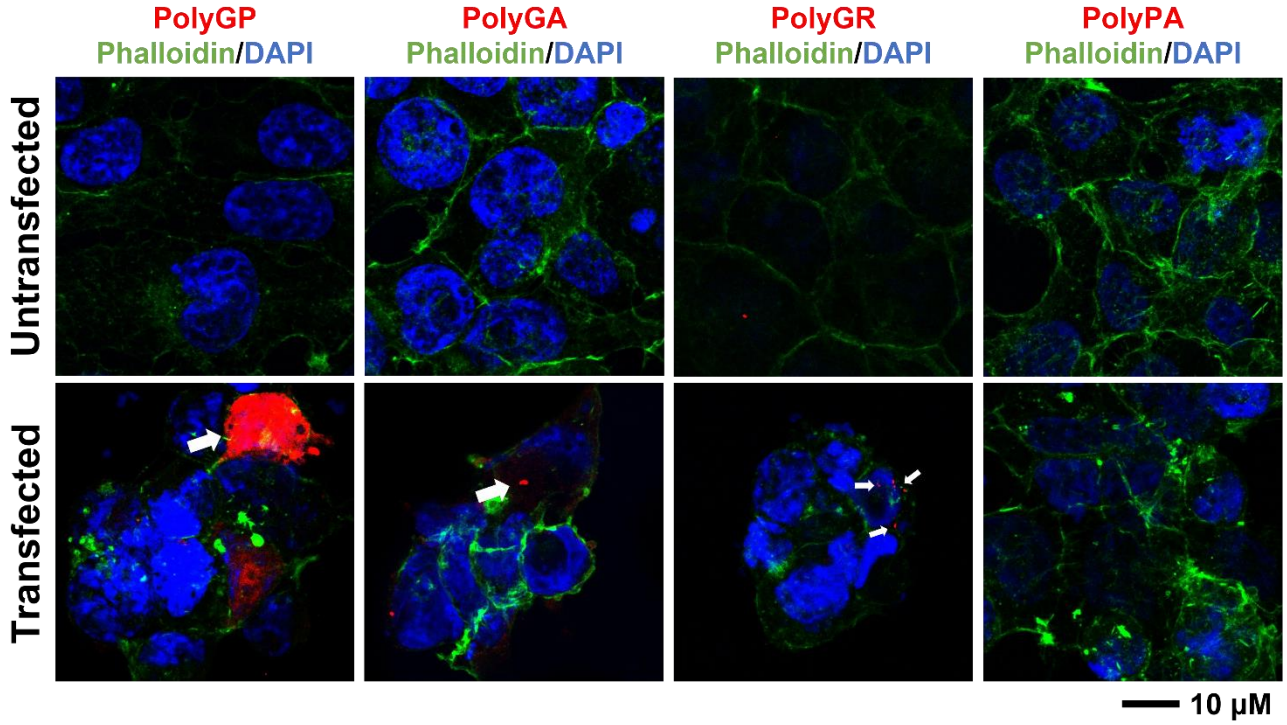

Figure 36. DPR staining in HEK293T cells transfected with the sense and anti-sense RNA repeat expansion. Phalloidin is a cytoplasmic stain. Scale bar represents 10 µm and applies to all images.

Following on from successful detection of DPRs in transfected HEK293T cells, I then went on to stain control and C9-ALS astrocytes for the different DPRs. I started with polyGP (Figure 37) as that

gave us the strongest signal in transfected HEK293T cells. Initial staining was imaged on the high throughput Opera Phenix microscope (Figure 37A). The results appeared promising as we observed specific signal that was only present in the C9-ALS astrocytes and not in the control astrocytes. Notably, however, the staining pattern did appear different to what we observed in the HEK293T cells. Instead of diffuse cytoplasmic staining, I observed the presence of multiple discrete cytoplasmic foci, the majority of which were perinuclear. Cells that contained polyGP positive foci were rare and the number of cells was quite variable between cell lines. Among the C9-ALS lines we observed the abundance of polyGP positive cells across cell lines decreased as follows: C9-ALS 201 > C9-ALS 52 > C9-ALS 183 > C9-ALS 78. Unfortunately I struggled to replicate this with further repeats, where there was either too much background to be able to discriminate between true foci and background foci, or when background was eliminated I struggled to detect foci at all (Figure 37B), with the exception of C9-ALS 201 which had previously been identified as having the most polyGP positive cells. Previous studies have reported that some DPRs co-localise with p62 foci (Mann et al., 2013), so I co-stained for p62 but did not observe colocalization with polyGP foci (Figure 37C).

At the same time as looking at polyGP, I also looked at polyGA (Figure 38) which is thought to be the most abundantly expressed DPR (Mori et al., 2013a). Initial staining and imaging on the Opera Phenix again showed positive signal for polyGA that was specific to C9-ALS astrocytes and was not present in control astrocytes (Figure 38A). The observed signal was very similar to the polyGP signal, with distinct cytoplasmic foci observed in a select few cells per cell line, however the foci did not appear to be as perinuclear. The relative abundance of polyGA foci was similar to polyGP: C9-ALS 201 > C9-ALS 52 > C9-ALS 78, however I failed to observe foci in one C9-ALS line – C9-ALS 183. I repeated the staining and imaged on the Leica confocal and I was able to observe polyGA foci specifically in C9-ALS lines and also some nucleolar polyGA signal (Figure 38B). In a later repeat I did also observe polyGA foci in C9-ALS 183 which were considerably smaller than the foci in 52 and 201, which may account for why they could not be observed in the initial round of polyGA staining imaged on the Opera Phenix. Like with the polyGP staining, I did not observe any colocalization of polyGA foci with p62 foci (Figure 38C).

In addition to looking at polyGP and polyGA, I also briefly looked at staining for polyGR (Figure 39) on the Leica confocal. PolyGR foci were rarer than polyGA or polyGP foci and I only observed a few positive cells where the staining appeared convincing.

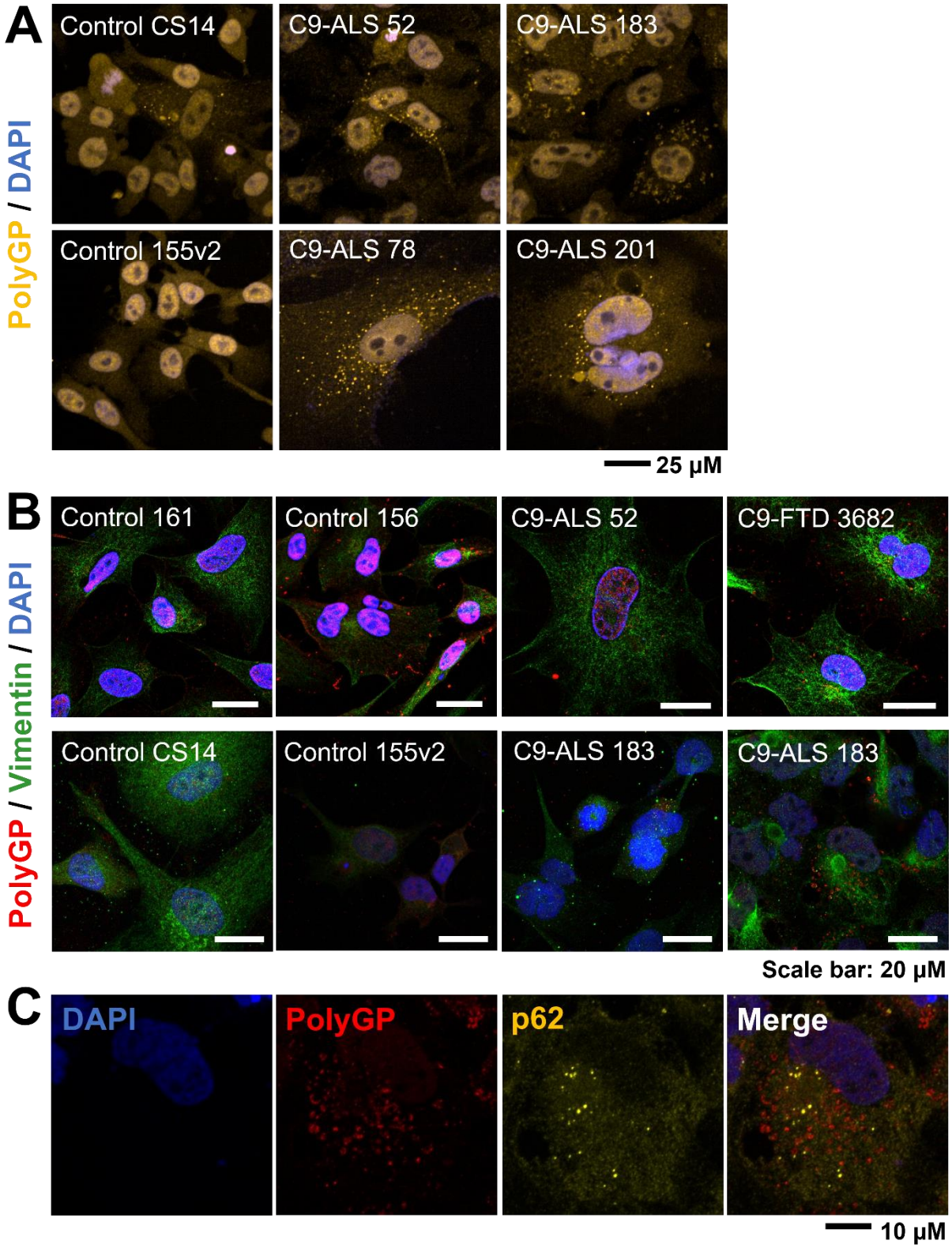

Figure 37. PolyGP immunocytochemistry shows cytoplasmic foci in C9-ALS astrocytes but could not easily be repeated. A: Initial polyGP staining and imaging using the Opera Phenix showed foci positive for polyGP selectively in C9-ALS astrocytes. B: Repeats of the staining imaged on a confocal microscope failed to show clear positive signal that was specific to the C9-ALS astrocytes. C: Confocal imaging of C9-ALS 201 astrocytes does not show colocalization of polyGP and p62 foci.

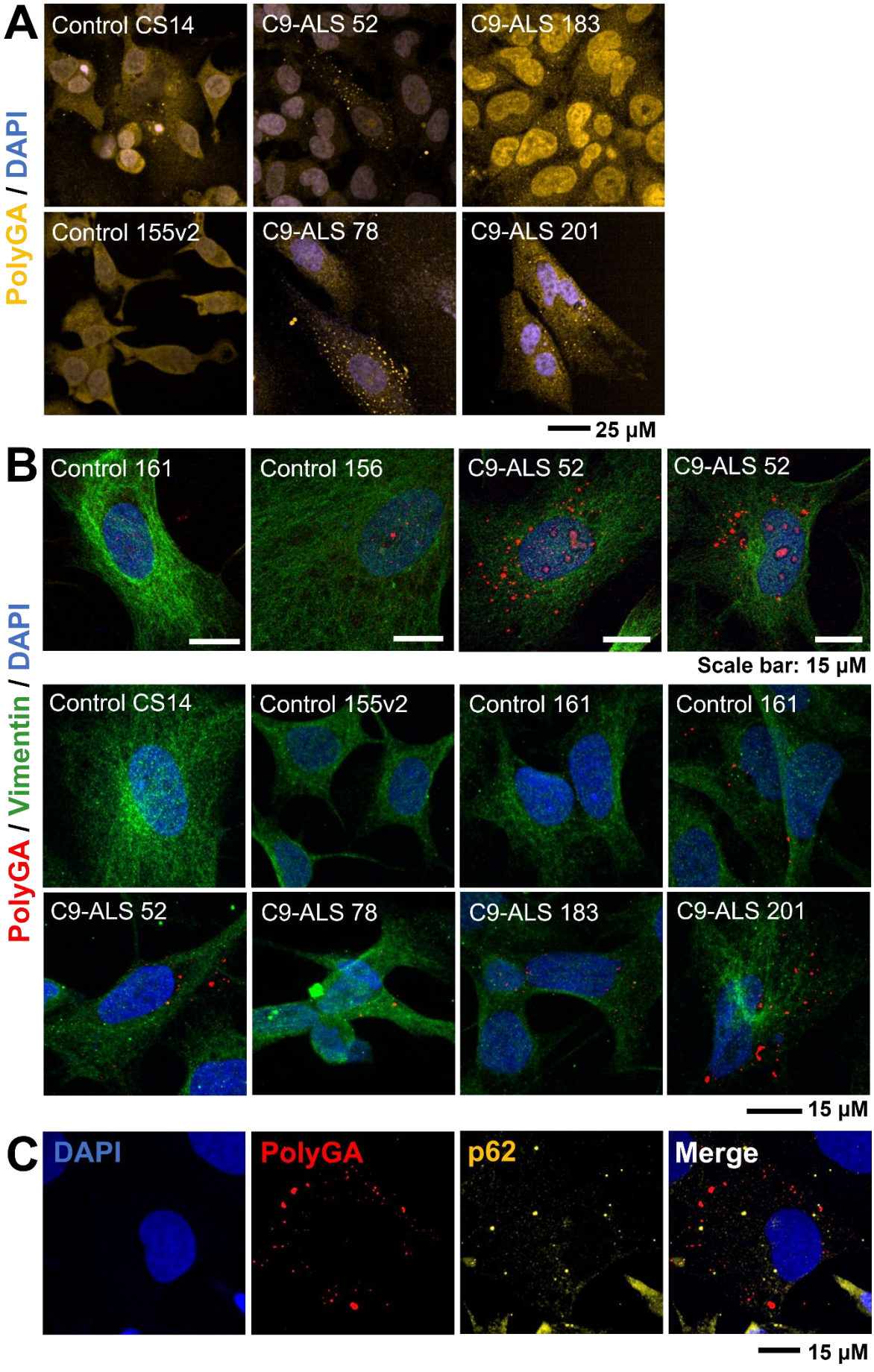
A
PolyGA / DAPI
Control CS14
C9-ALS 52
C9-ALS 183
Control 155v2
C9-ALS 78
C9-ALS 201
25 µM
B
PolyGA / Vimentin / DAPI
Control 161
Control 156
C9-ALS 52
C9-ALS 52
Scale bar: 15 µM
Control CS14
Control 155v2
Control 161
Control 161
C9-ALS 52
C9-ALS 78
C9-ALS 183
C9-ALS 201
15 µM
C
DAPI
PolyGA
p62
Merge
15 µM

Figure 38. PolyGA immunocytochemistry shows small cytoplasmic foci and occasional nucleolar signal in C9-ALS astrocytes. A: Initial polyGA staining and imaging using the Opera Phenix showed foci positive for polyGA selectively in C9-ALS astrocytes. B: Repeats of the staining imaged on the confocal continued to show polyGA foci selectively in C9-ALS astrocytes, although I did observe some background signal in control 161 astrocytes. C: PolyGA foci imaged using the confocal do not appear to colocalise with p62 foci.

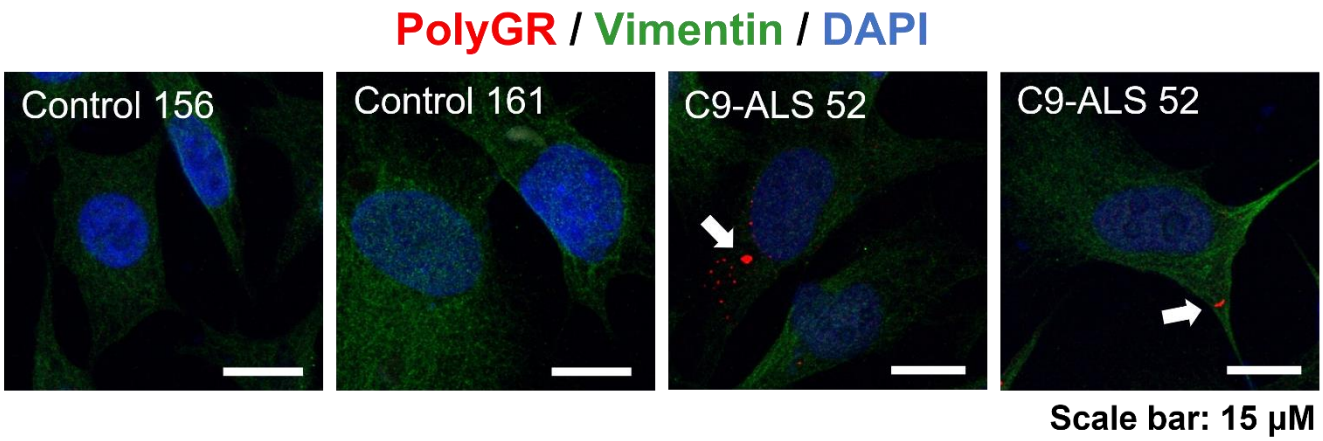

Figure 39. PolyGR immunocytochemistry identifies a few polyGR positive C9-ALS astrocytes. Initial polyGR staining and imaging using a Leica confocal microscope shows some specific signal in C9-ALS astrocytes specifically.

5.2.2 Detecting DPRs in C9-ALS Astrocyte Exosomes

After determining that C9-ALS express DPRs, I sought to investigate whether C9-ALS astrocytes could secrete DPRs into the conditioned medium. As DPRs were previously shown to be present in conditioned medium exosomes (Westergard et al., 2016) and as exosome isolation would likely help to concentrate the DPR presence in the conditioned medium, I collected exosomes from control and C9-ALS astrocyte conditioned medium using a method previously used and validated in the lab (Varcianna et al., 2019). I first attempted to detect DPRs using dot blots as this was the method previously used to detect GFP-tagged DPRs in conditioned medium (Westergard et al., 2016). Unfortunately, I found the antibodies were binding non-specifically to components of the medium and there was a general lack of sensitivity and specificity in the assay, even when trying to probe for DPRs in transfected HEK293T cell lysates (data not shown).

Following on from the failure to detect DPRs in C9-ALS astrocyte conditioned medium exosomes using dot blotting, I then decided to try using the DPR MSD ELISA (Simone et al., 2018) that was established by Professor Adrian Isaacs's research group at UCL and which had recently been set up at SITraN. MSD ELISAs were run by Dr Adrian Higginbottom and/or Dr Ergita Balli at the University of Sheffield. To establish whether the MSD ELISA worked and could detect signal in cells expressing endogenous levels of DPRs, rather than an overexpression model, we ran the MSD ELISA in control

and C9-ALS iPSC-derived motor neurons and GABAergic neurons. The assay had been initially optimised for polyGP, so I began by looking at polyGP levels in the different neuron subtypes (Figure 40). I observed higher levels of signal in the C9-ALS motor neurons and GABAergic neurons compared to the controls, however due to the variability in polyGP levels between the C9-ALS cell lines the results were usually not significant. For the motor neurons, a significant difference was observed across the groups (Kruskal-Wallis test, $p=0.03$), however post-hoc Dunn's multiple comparison tests could not confirm which groups were significantly different (control vs C9-ALS $p=0.17$, control vs isogenic $p>0.99$, C9-ALS vs isogenic $p=0.08$). For GABAergic neurons, there was only a trend towards significance (Kruskal-Wallis test, $p=0.06$). For significance to be reached, we would likely need to run more cell lines.

Following successful results for polyGP I then decided to look at DPRs that would be more relevant for the induction of DNA damage and cell death so I tested whether the MSD ELISA could detect polyGA (Figure 41) and polyGR (Figure 42) in the C9-ALS motor neurons and GABAergic neurons. While I did not have time to complete this work in triplicate, I did observe that for polyGA there was a clear increase in signal in the C9-ALS lines that could differentiate them from the healthy controls and isogenic controls (Figure 41). For polyGR (Figure 42) the results were not as clear and it was harder to distinguish the C9-ALS lines from the controls, likely because polyGR is known to be expressed in lower amounts than polyGP or polyGA (Mackenzie et al., 2015).

In parallel to our work on the motor neurons and GABAergic neurons, fellow Ferraiuolo lab member Allan Shaw ran the MSD ELISA for polyGP and polyGA on control and C9-ALS astrocyte cell lysates and determined that the MSD ELISA could robustly detect DPRs in C9-ALS astrocytes (data not shown). Notably, from the motor neuron and GABAergic neuron data, I observed that the C9-ALS line 52 had considerably more polyGP and polyGA than the other lines. Furthermore, it was observed that the corresponding astrocyte line for 52 also showed high levels of polyGP, indicating this is a feature of the patient cell line regardless of the reprogramming methodology.

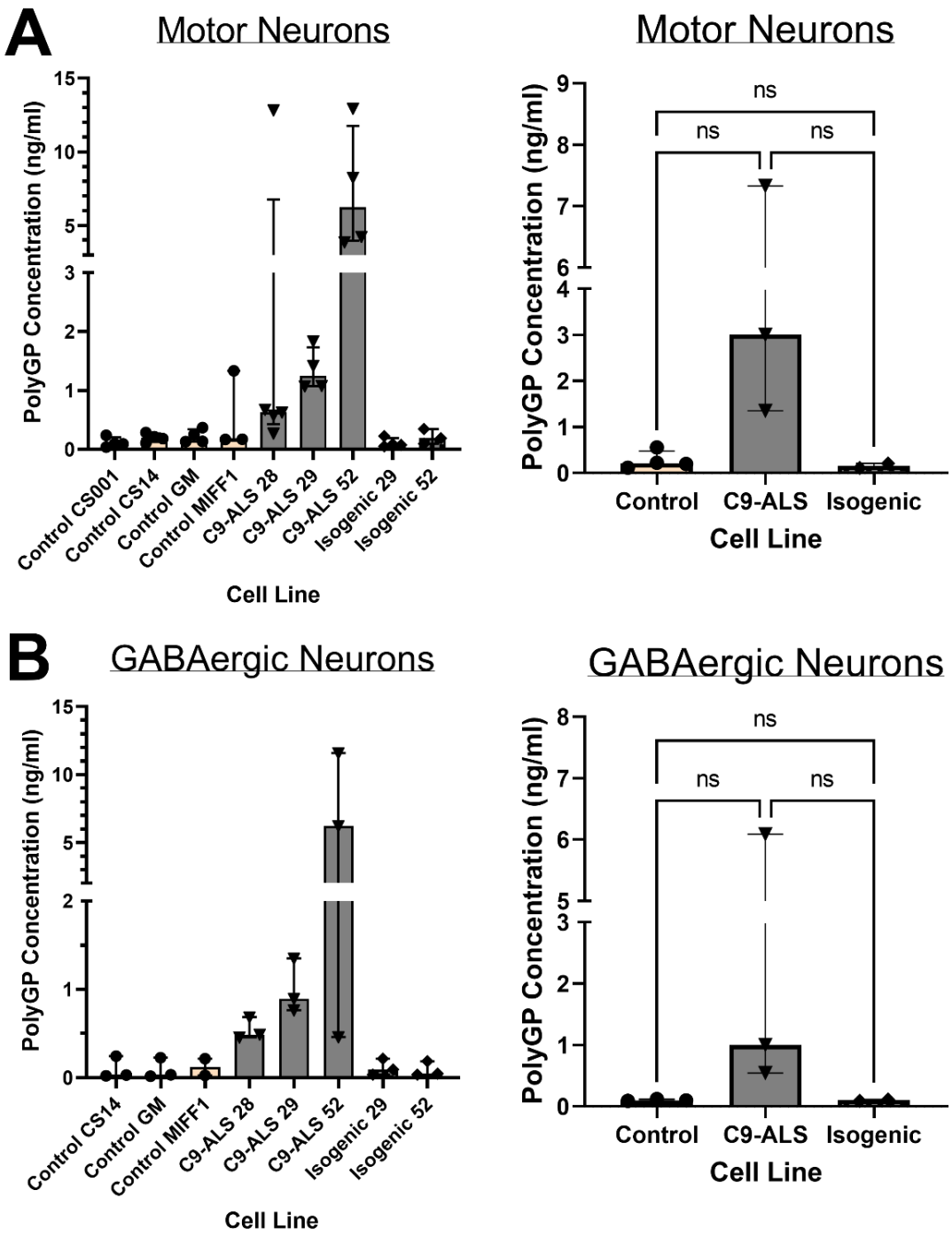

Figure 40. MSD ELISA for PolyGP shows a clear but non-significant increase in polyGP levels in C9-ALS motor neurons and GABAergic neurons. Left panel shows data for the individual cell lines, median and interquartile ranges shown, each datapoint represents one repeat. Right panel shows the grouped data, median and interquartile ranges shown, each datapoint represents one cell line. A: Interpolated polyGP concentration in control (n=4), C9-ALS (n=3) and isogenic control (n=2) motor neurons. Data did not meet assumption for normality, Kruskal-Wallis test (p=0.03), Dunn's multiple comparisons tests (control vs C9-ALS p=0.17, control vs isogenic p>0.99, C9-ALS vs isogenic p=0.08). B: Interpolated polyGP concentration in control (n=3), C9-ALS (n=3) and isogenic control (n=2) GABAergic neurons. Data did not meet assumption for normality, Kruskal-Wallis test (p=0.06).

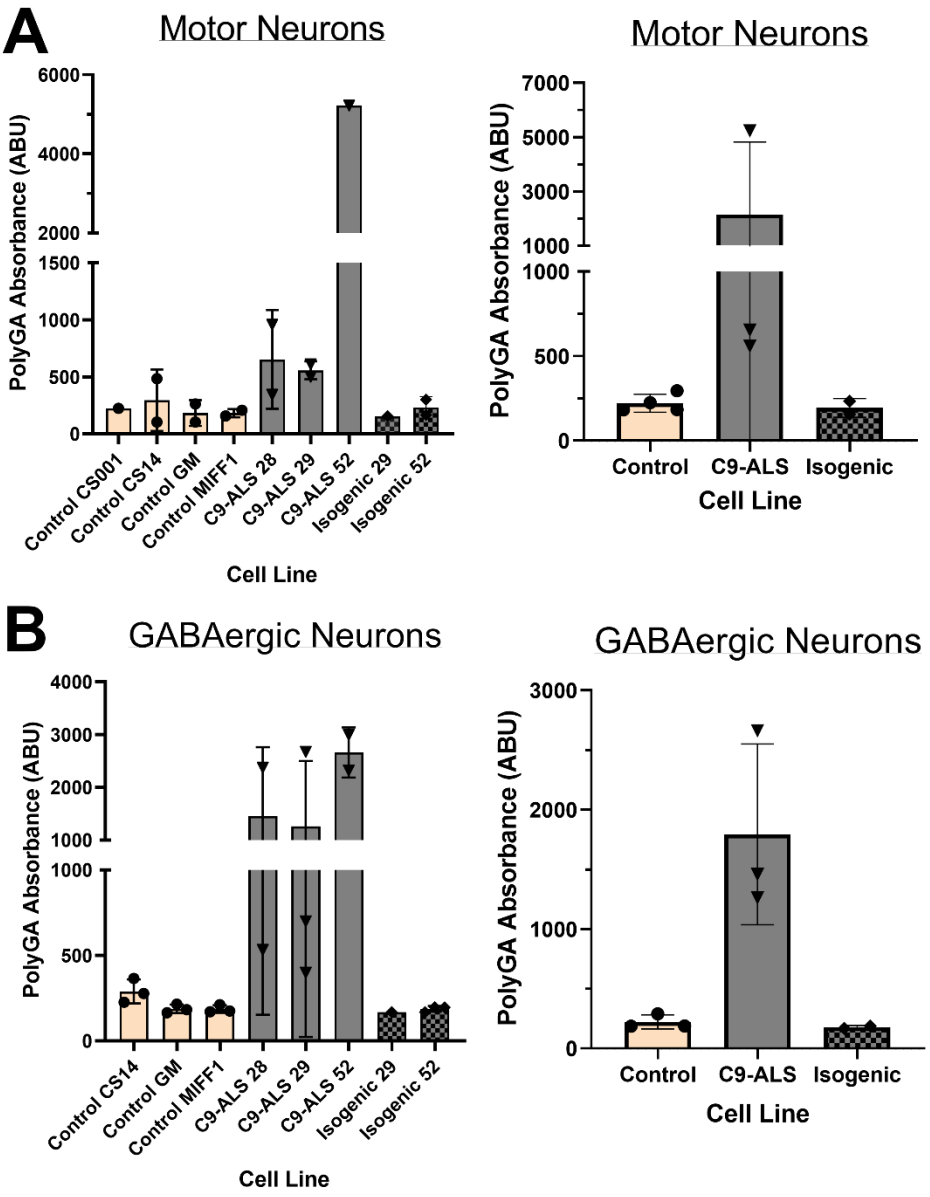

Figure 41. MSD ELISA for polyGA shows a clear increase in polyGA levels in C9-ALS motor neurons and GABAergic neurons. Left panel shows repeat data for the individual cell lines, mean and standard deviations shown, each datapoint represents one repeat. Right panel shows the grouped data, means and standard deviations shown, each datapoint represents one cell line. A: PolyGA detection absorbance values in control (n=4), C9-ALS (n=3) and isogenic control (n=2) motor neurons. B: PolyGA detection absorbance values in control (n=3), C9-ALS (n=3) and isogenic control (n=2) GABAergic neurons. Data for polyGA could not be interpolated due to many of the C9-ALS values exceeding the upper boundaries of the polyGA standard curve. No statistics run due to missing datapoints.

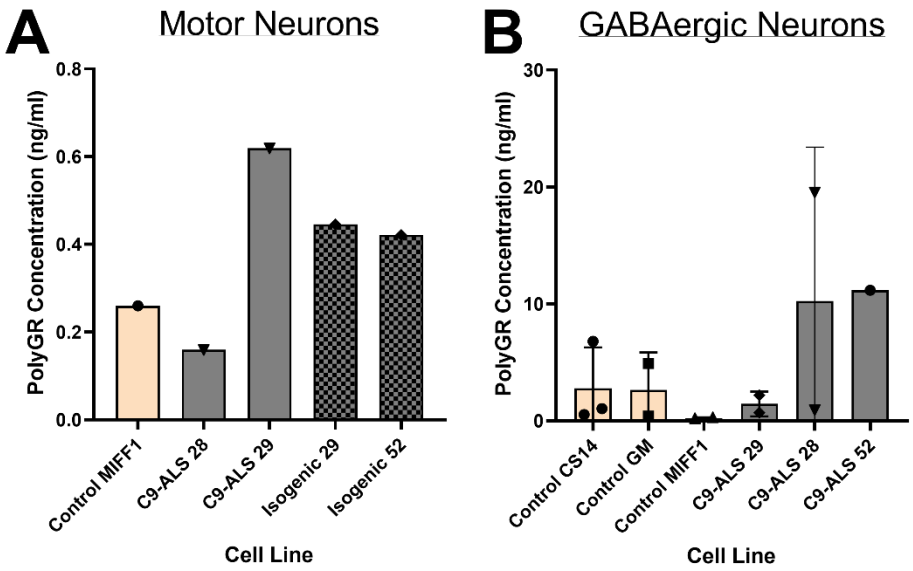

Figure 42. MSD ELISA for polyGR does not reliably show an increase in polyGR levels in C9-ALS motor neurons and GABAergic neurons. A: Interpolated polyGR concentration in control (n=1), C9-ALS (n=2) and isogenic control (n=2) motor neurons. Data represents the mean of one repeat per cell line. B: Interpolated polyGR concentration in control (n=3), C9-ALS (n=3) GABAergic neurons. Means and standard deviations shown, each datapoint represents one repeat. No statistics run due to missing datapoints.

Following on from these successful findings that the MSD ELISA could detect DPRs in both neuron and astrocyte cell lysates derived from C9-ALS patients, I then assessed whether the MSD ELISA could detect secreted DPRs. As I had determined that the MSD ELISA could successfully detect polyGP and polyGA in C9-ALS motor neurons and GABAergic neurons, I focused on these two DPR species. One part of the MSD ELISA protocol involves diluting samples 1:1 in EC buffer, however as I was concerned that diluting the exosomes could suppress low levels of signal, I tested the exosomes undiluted and diluted with the EC buffer as normal.

I first ran unconcentrated control and C9-ALS astrocyte conditioned medium and I observed no difference in signal across our cell lines for polyGP (Figure 43A). Determining that low concentration of proteins may affect the results, I collected the exosomes from the control and C9-ALS astrocyte conditioned medium and ran the ELISA again. Surprisingly, I observed very high levels of signal across both our control and C9-ALS astrocyte conditioned medium exosomes for polyGP (Figure 43B) and polyGA (data not shown), and the same results were observed following a second repeat, indicating the antibody was binding non-specifically. Due to the previous issues observed with antibodies binding components of the medium, I tested a few different media types but surprisingly I did not observe high background for polyGP (Figure 43C) or polyGA (data not shown) in any of the

media types we tested. Theorising that the antibody might be binding a component of the media but only after the medium was ultracentrifuged, I collected exosomes using a medium which lacked knockout serum replacement and ran the MSD ELISA again. This time I observed no high levels of background (Figure 43D), supporting our theory that the antibody had been binding a medium component concentrated after ultracentrifugation. I also observed a small increase in signal in the undiluted C9-ALS astrocyte conditioned medium exosomes (Figure 43D) compared to the controls.

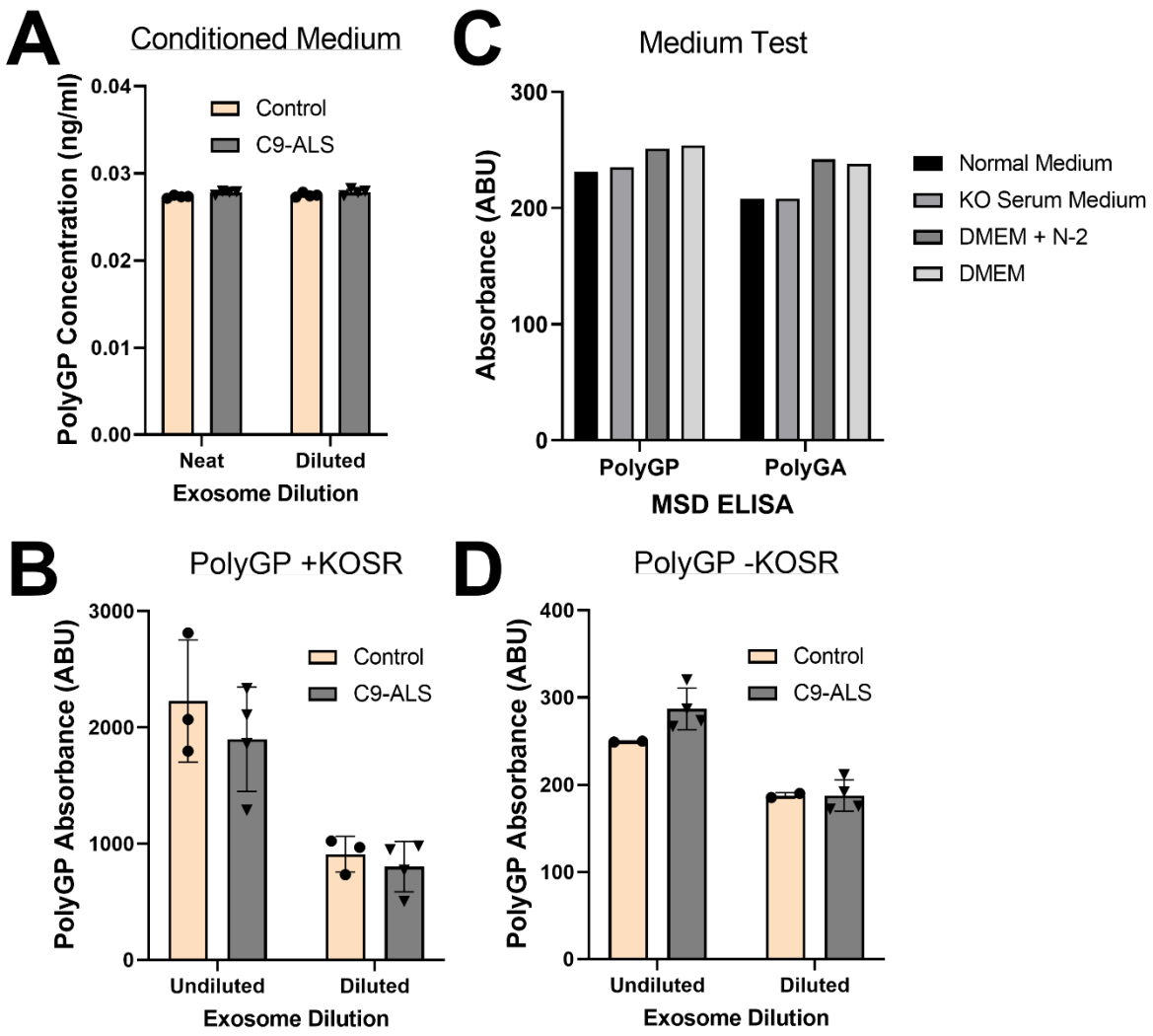

Figure 43. Optimisation of MSD ELISA for conditioned medium exosomes. A: PolyGP could not be detected in C9-ALS astrocyte unconcentrated conditioned medium samples. Means and standard deviations shown, each data point represents one cell line. B: Control and C9-ALS astrocyte exosomes collected using old conditioning protocol (medium containing knockout serum replacement) showed high levels of signal for polyGP, indicating non-specific binding of the antibody. C: Media tests showed that medium not subjected to ultracentrifugation showed low levels of polyGP signal. D: Control and C9-ALS astrocyte exosomes collected using new conditioning protocol (medium without knockout serum replacement) showed low levels of signal and in the undiluted condition the C9-ALS astrocyte exosomes showed higher signal than the controls. KOSR= knockout serum replacement.

Based on these results, I ran the MSD ELISA in triplicate for both GP and GA, using undiluted samples (Figure 44). I observed that polyGP and polyGA signal was mildly increased in the C9-ALS astrocyte exosomes compared to the healthy control astrocyte exosomes, indicating that C9-ALS astrocytes may secrete DPRs into the conditioned medium through exosomes.

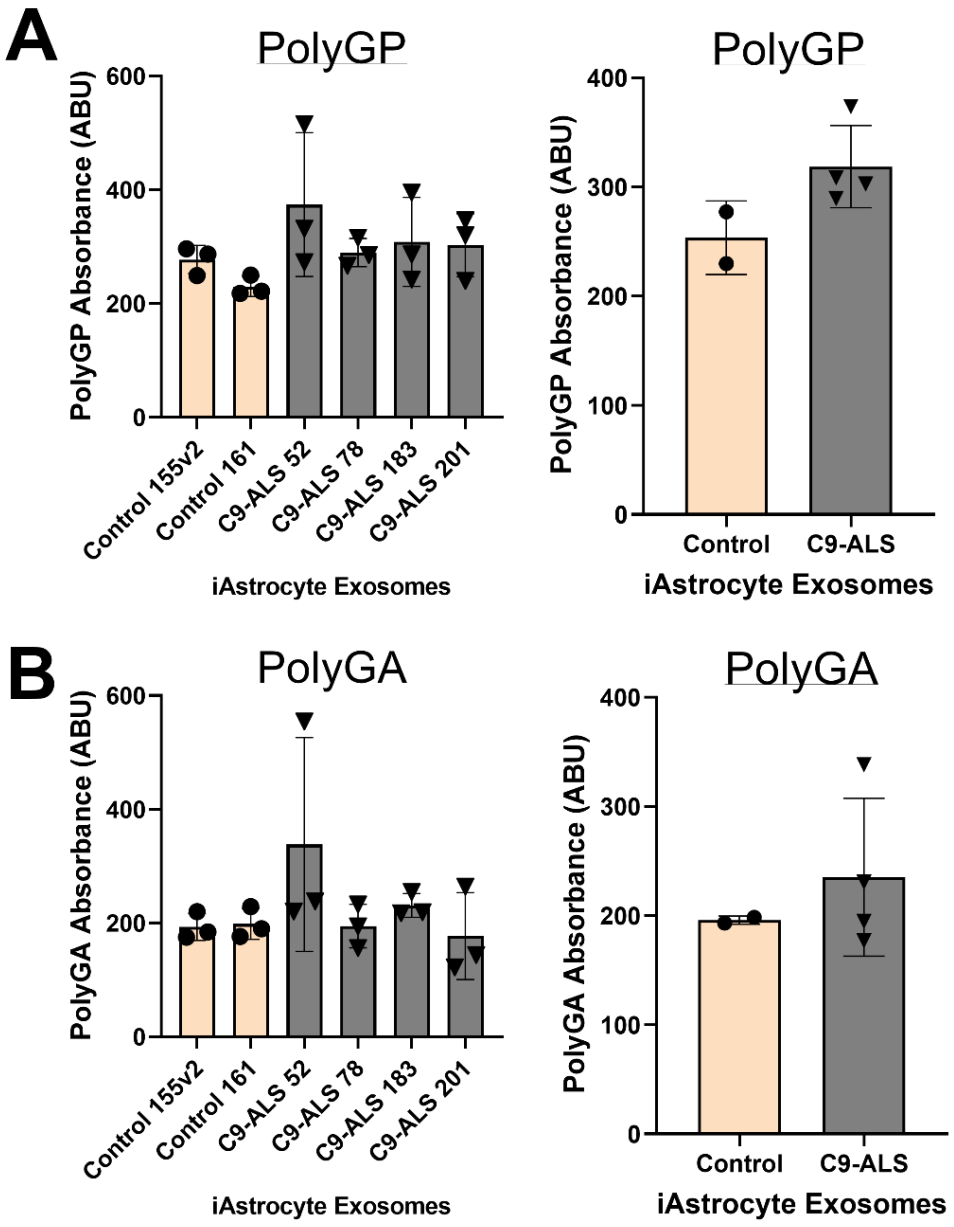

Figure 44. PolyGP and polyGA levels are slightly elevated in C9-ALS astrocyte exosomes. Due to standard curve issues, all data is presented as raw absorbance rather than interpolated. Left panel shows repeat data for the individual cell lines, mean and standard deviations shown, each datapoint represents one repeat. Right panel shows the grouped data, means and standard deviations shown, each datapoint represents one cell line. A: PolyGP detection absorbance values in exosomes from healthy control astrocytes (n=2) or C9-ALS patient-derived astrocytes (n=4). B: PolyGA detection absorbance values in exosomes from healthy control astrocytes (n=2) or C9-ALS patient-derived astrocytes (n=4).

5.2.3 Effect of Secreted DPRs on Motor Neurons

To determine whether secreted DPRs could be sufficient to induce DNA damage in motor neurons, I decided to test whether conditioned medium derived from HEK293T cells transfected with the sense and antisense DPRs could induce an increase in γH2AX foci in motor neurons. Transfected HEK293T cells were kindly provided by Dr Lydia Castelli of the Hautbergue lab group, and following transfection medium was allowed to condition for 48 hours. To increase the chance of observing an effect, I treated the motor neurons with 100% conditioned medium instead of diluting the conditioned medium with fresh motor neuron medium. To determine whether any potential induced DNA damage was the result of protein or RNA action, I treated some of the conditioned medium with proteinase k or RNAse A to deplete proteins and RNA respectively. Motor neurons were treated for 24 hours then fixed and stained for γH2AX (Figure 45).

In one early repeat, the results were very promising as I observed an increase in γH2AX foci in motor neurons treated with transfected HEK293T cell conditioned medium compared to untransfected HEK293T cell conditioned medium (Figure 45B). Notably, the increase in γH2AX foci was lost when the transfected conditioned medium was treated with proteinase k but was not lost when the conditioned medium was treated with RNAse A, indicating DNA damage was being induced by proteins in the conditioned medium. I was, however, unable to replicate this data consistently (Figure 45C), and overall, I observed no significant difference across the treatment groups (one-way ANOVA $p=0.45$). The reason for the inability to replicate the data may have been due to variability in the transfection efficiency of the HEK293T cells between repeats. I attempted to validate transfection by dot blot (Figure 45D), probing for the V5 tag due to previous issues attempting to blot for DPRs. I did observe specific signal for V5 in the transfected cells, but the signal was very faint, thus indicating that the expression of the transfected DPRs was very low in certain experiments. It was also reported by the Hautbergue group, who were using the same cells at the same time, that in some of the repeats the transfected cells had very low levels of DPRs, as detected by Western blotting. Due to the intrinsic variability of the system and the time limitations, I was not able to continue with these experiments and I will be seeking alternative ways to assess the role of secreted DPRs as a means to induce DNA damage in motor neurons.

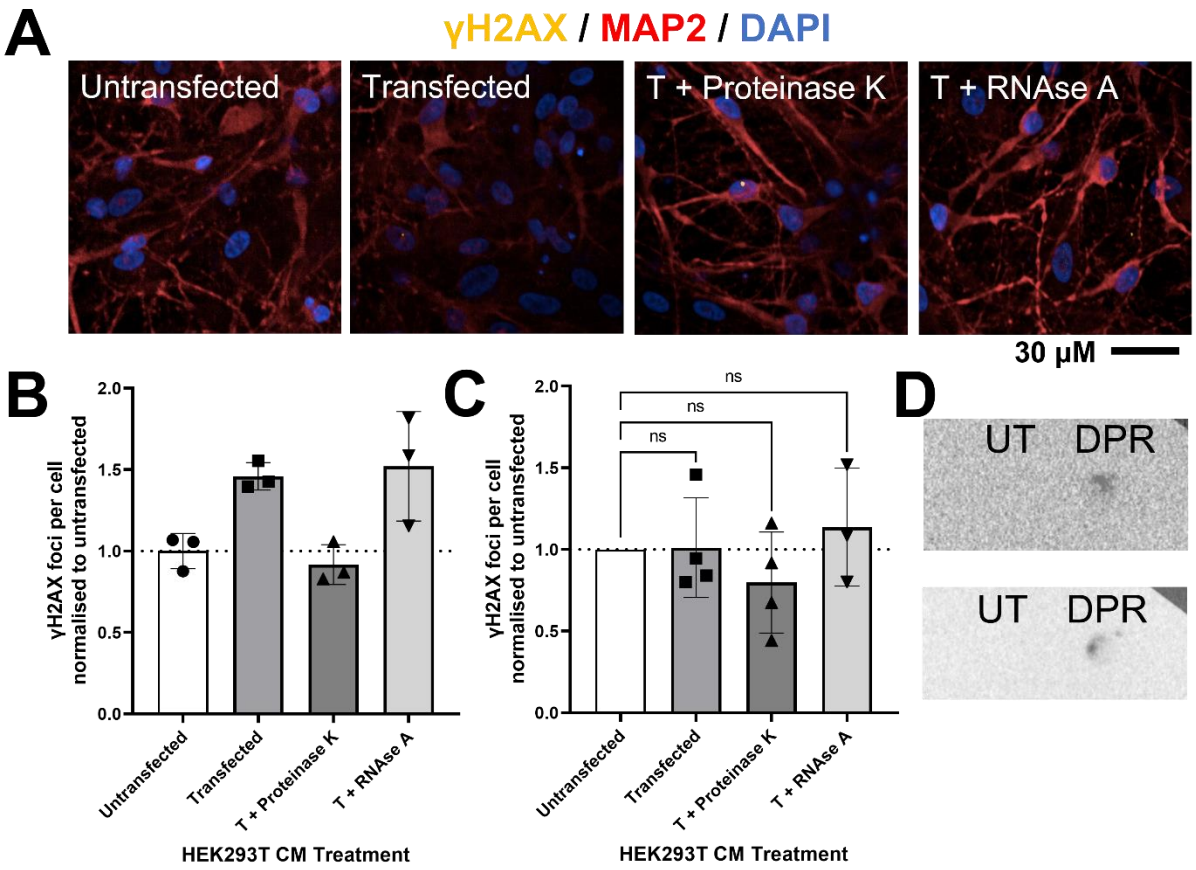

Figure 45. Conditioned medium derived from DPR transfected HEK293T cells does not induce γH2AX foci formation in motor neurons. A: Representative images of γH2AX staining in motor neurons treated with DPR-transfected HEK293T cell conditioned medium, representative of overall data shown in C rather than representative of B. B: Quantification of γH2AX foci in motor neurons treated with transfected HEK293T cell conditioned medium in early promising repeat. Means and standard deviations shown, each datapoint represents one technical replicate (mean result for one well of a 96 well plate). C: Quantification of γH2AX foci in motor neurons treated with transfected HEK293T cell conditioned medium across three to four biological repeats. Data met assumption for normality, one-way ANOVA (p=0.45). Means and standard deviations shown, each datapoint represents one repeat. D: Transfection validation dot blot for V5 tag in cell lysates of untransfected (UT) and DPR transfected (DPR) HEK293T cell lysates.

5.3 P62 as a Mechanism of Astrocyte-Induced DNA Damage

5.3.1 ALS astrocytes induce p62 foci formation in motor neurons

DPR expression has been shown to induce p62 accumulation, and p62 accumulation has been linked with DNA repair impairment (Walker et al., 2017). To determine whether p62 could be involved in ALS astrocyte-induced DNA damage, Dr Cleide Souza treated motor neurons with astrocyte conditioned medium for 24 or 72 hours and stained for p62 (Figure 46). The number of p62 foci were not significantly different (one-way ANOVA, p=0.08) across the treatment conditions after 24 hours (Figure 46B), but were found to be significantly different (one-way ANOVA, p<0.0001) after 72 hours of treatment (Figure 46C). A significant increase in p62 foci was found in

motor neurons treated with sALS (p=0.0003), SOD1-ALS (0.019), and C9-ALS (p<0.0001) astrocyte conditioned medium compared to control astrocyte conditioned medium, indicating ALS astrocyte conditioned medium can induce p62 accumulation in motor neurons within 72 hours of treatment.

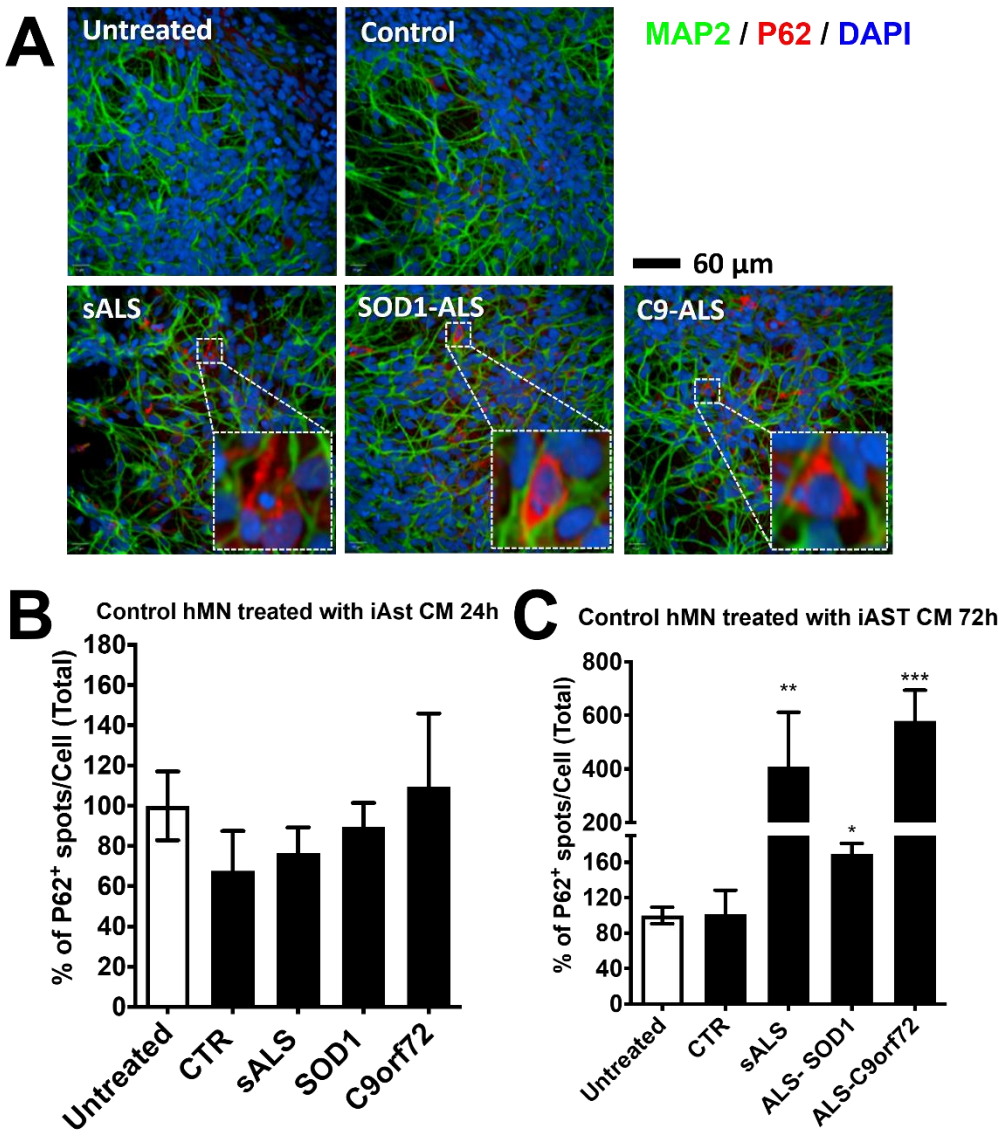

Figure 46. P62 foci are increased in motor neurons treated with ALS astrocyte conditioned medium for 72 hours but not 24 hours (data and images from Dr Cleide Souza). A: Example images of p62 staining in motor neurons treated with control or ALS astrocyte conditioned medium for 72 hours. B: Quantification of p62 foci per cell in motor neurons treated with control (n=3), sALS (n=3), SOD1-ALS (n=3) or C9-ALS (n=4) astrocyte conditioned medium for 24 hours. Data met assumption for normality, one-way ANOVA (p=0.08). Means and standard deviations shown. C: Quantification of p62 foci per cell in motor neurons treated with control (n=3), sALS (n=3), SOD1-ALS (n=3) or C9-ALS (n=4) astrocyte conditioned medium for 72 hours. Data met assumption for normality, one-way ANOVA (p<0.0001), Dunnett's post-hoc test (sALS vs control p=0.0003, SOD1-ALS vs control p=0.019, C9-ALS vs control p<0.0001). Means and standard deviations shown.

To validate the increase in p62, I ran Western blotting for p62 on motor neurons treated with conditioned medium for 24 or 72 hours (Figure 47). I observed no significant change in the overall

levels of p62 in motor neurons treated with control or ALS astrocyte after 24 hours (one-way ANOVA, p=0.63) or after 72 hours (one-way ANOVA, p=0.27).

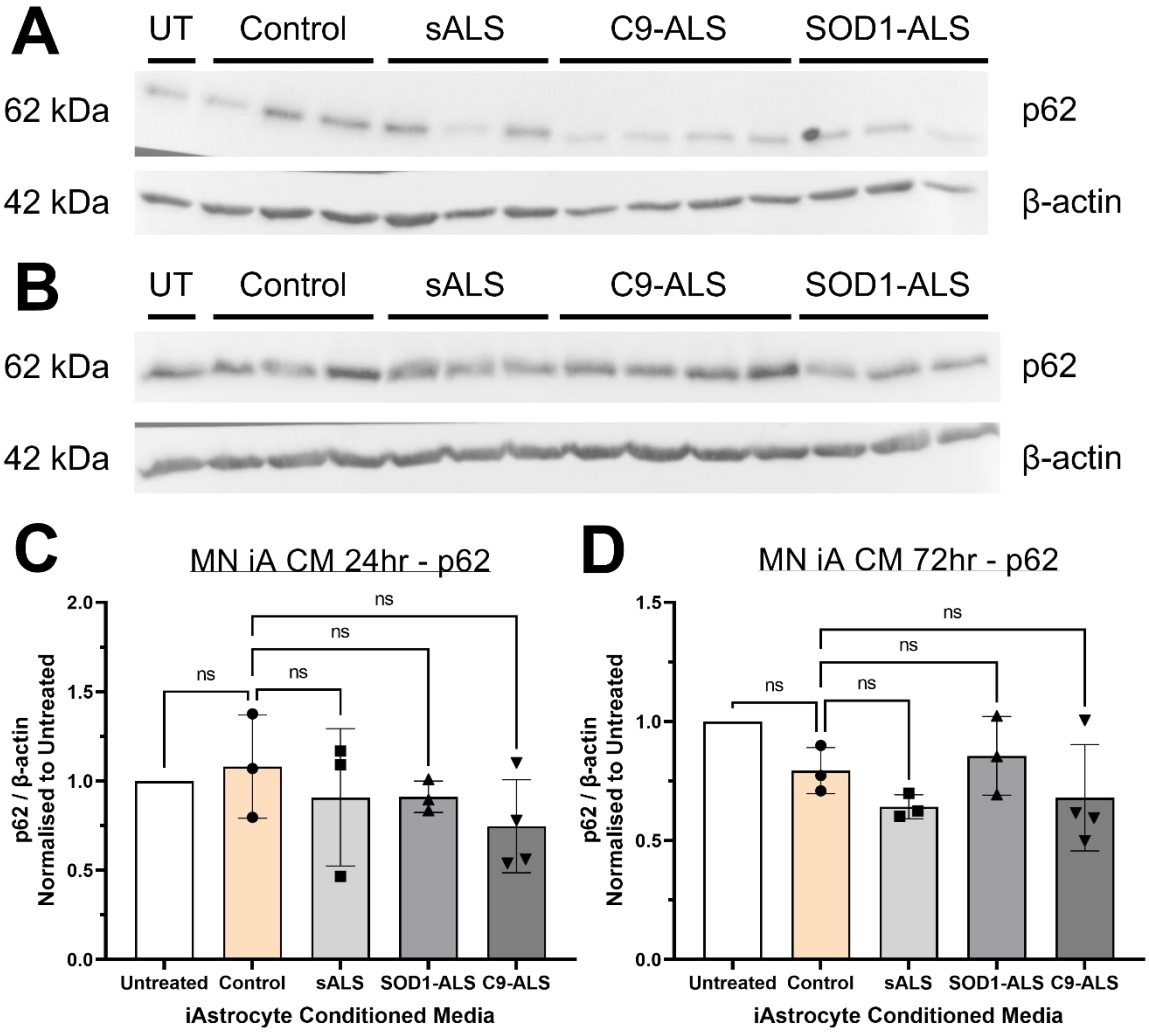

Figure 47. P62 protein levels are not changed in motor neurons treated with ALS astrocyte conditioned medium for 24 or 72 hours. A&C: Western blot and quantification of p62 in motor neurons treated with control (n=3), sALS (n=3), SOD1-ALS (n=3) or C9-ALS (n=4) astrocyte conditioned medium for 24 hours. Data met assumption for normality, one-way ANOVA (p=0.63), means and standard deviations shown. B&D: Western blot and quantification of p62 in motor neurons treated with control (n=3), sALS (n=3), SOD1-ALS (n=3) or C9-ALS (n=4) astrocyte conditioned medium for 72 hours. Data met assumption for normality, one-way ANOVA (p=0.27), means and standard deviations shown.

In addition to probing for p62, I also decided to look at proteins with functions related to p62 (KEAP1, LC3-I and LC3-II) in motor neurons treated with conditioned medium for 72 hours. Note that due to time and limited protein amounts, I was only able to run two repeats of the KEAP1 and LC3 Western blots, so results should be interpreted cautiously. Unfortunately, I was unable to

reliably detect the LC3-II expression band (Figure 48), thus the quantification data has not been presented.

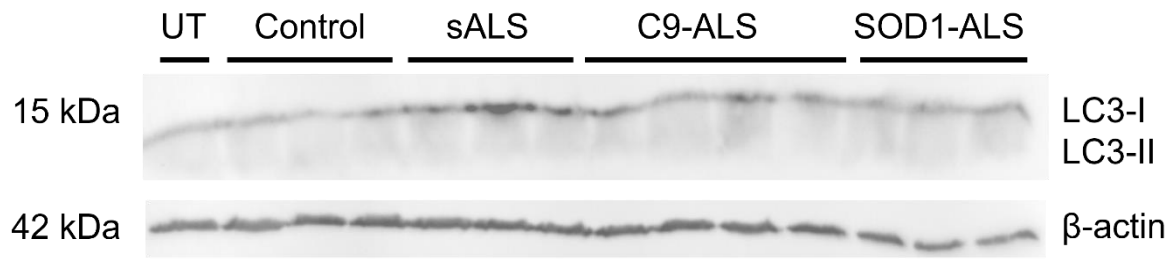

Figure 48. Western blot of LC3-I and LC3-II in motor neurons treated with control or ALS astrocyte conditioned medium for 72 hours. LC3-II expression could not be reliably detected and unfortunately there was not sufficient protein to repeat the experiments.

Western blotting for KEAP1 was more successful (Figure 49), and I observed that KEAP1 expression was reduced in motor neurons treated with control or ALS astrocyte conditioned medium compared to untreated motor neurons. Indeed, there was a significant change in KEAP1 expression across the treatment groups (one-way ANOVA, p=0.001), and post-hoc tests indicated that compared to motor neurons treated with control astrocyte conditioned medium, there was a significant change in untreated motor neurons and in motor neurons treated with SOD1-ALS astrocyte conditioned medium (Dunnett's multiple comparisons' test, control vs untreated p=0.007, control vs sALS p=0.96, control vs SOD1-ALS p=0.015, control vs C9-ALS p=0.60). Note, however, that the SOD1-ALS result seems to be significant due to only one of the two repeats, whereas the control results were consistently reduced compared to untreated in both repeats.

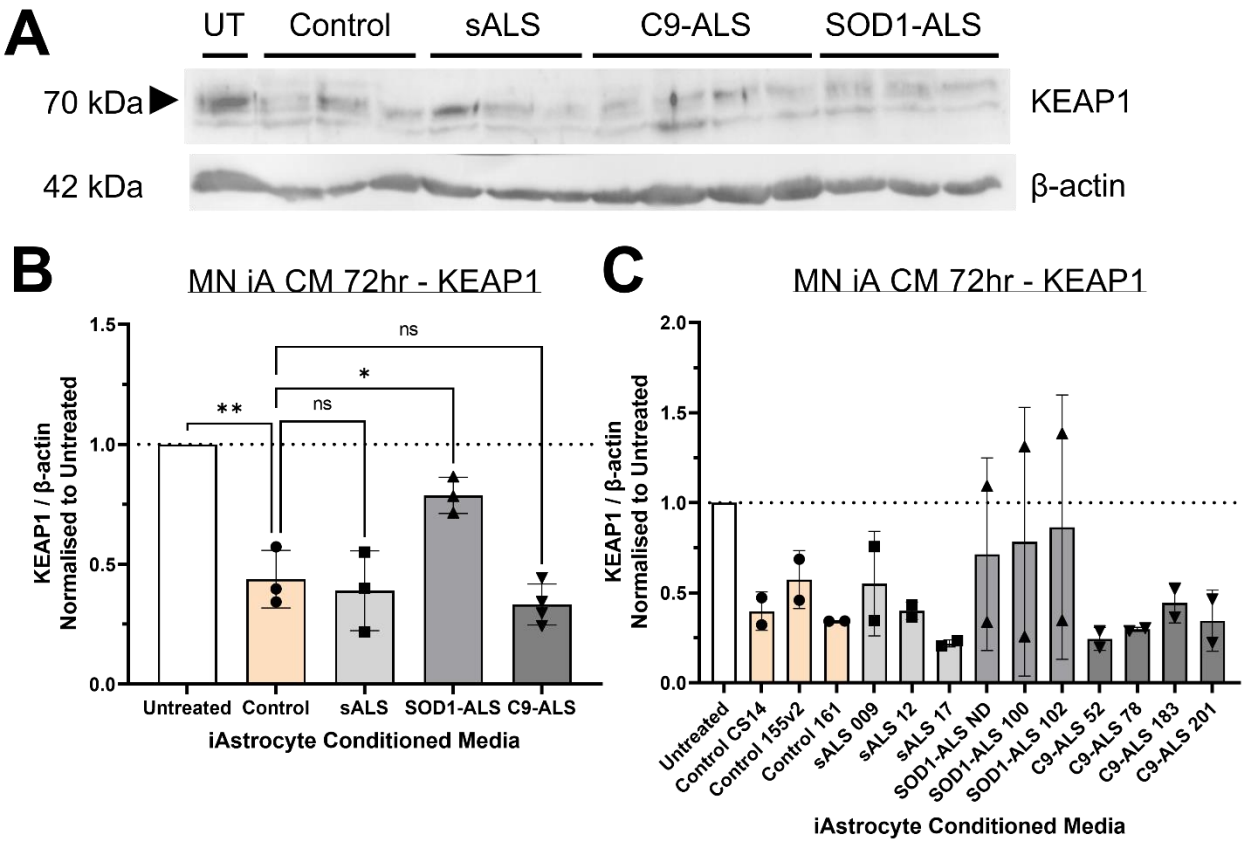

Figure 49. KEAP1 levels are reduced in motor neurons treated with control or ALS astrocyte conditioned medium for 72 hours. A-B: Western blot and quantification of motor neurons treated with control (n=3), sALS (n=3), SOD1-ALS (n=3) or C9-ALS (n=4) astrocyte conditioned medium for 72 hours. Data met assumption for normality, one-way ANOVA (p=0.0010), Dunnett's multiple comparisons test (control vs untreated p=0.0070, control vs sALS p=0.96, control vs SOD1-ALS p=0.015, control vs C9-ALS p=0.60). Means and standard deviations shown, each datapoint represents one cell line. C: KEAP1 data separated by cell line. Means and standard deviations shown, each datapoint represents one repeat. Note that only two biological repeats were run per treatment.

5.3.2 P62 in ALS astrocyte conditioned medium

Previous lab members have reported the presence of p62 in ALS astrocyte conditioned medium exosomes, thus it is possible that the increase in p62 in motor neurons treated with ALS astrocyte conditioned medium could be due to p62 transmission by ALS astrocytes. To determine whether this was the case, I sought to immunodeplete p62 from ALS astrocyte conditioned medium using immunoprecipitation (IP) and determine whether the immunodepletion could rescue DNA damage and p62 accumulation in motor neurons (Figure 51A).

Prior to optimising immunodepletion, I considered that if astrocytes transmit p62, there is a possibility p62 would be packaged into exosomes like many other transmitted proteins. Packaging of p62 could impede immunodepletion attempts, so lysis would be needed to allow the antibodies access to the p62 proteins. Adding lysis buffer to conditioned medium and then applying that

medium to cells could have toxic effects, so I decided to test different lysis conditions to assess their effects on cell toxicity (Figure 50). I tested IP lysis buffer, hypotonic lysis buffer and sonication on astrocyte conditioned medium. I then used the lysed conditioned medium to treat healthy astrocytes in a 1:1 ratio with plain astrocyte medium (the same method used for treating motor neurons with astrocyte conditioned medium) for 48 hours. Treated astrocytes were fixed and stained for Hoescht and CD44 (Figure 50A) and I quantified the total number of cells for each condition (Figure 50B). It was clear that astrocyte conditioned medium containing the standard IP lysis buffer was toxic to cells as almost no cells remained following the treatment. Hypotonic lysis buffer had little effect on cell number, but the cells did appear to have swelled, likely from osmosis. Conditioned medium that was sonicated had little effect on the cells and appeared to be the best candidate.

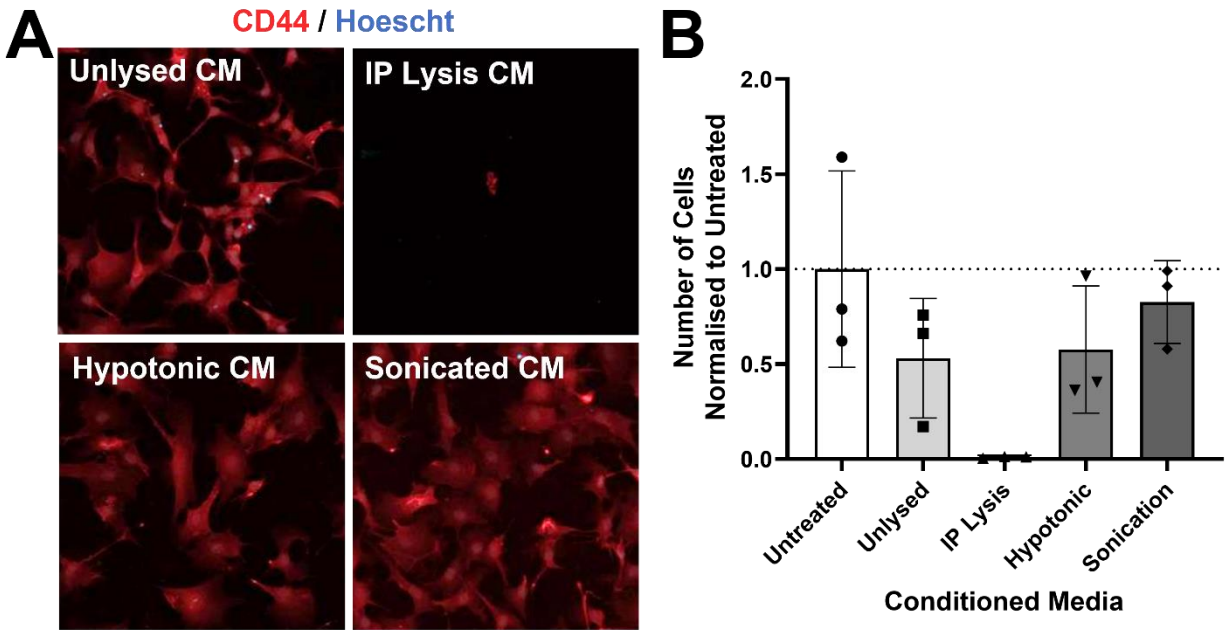

Figure 50. Testing immunodepletion lysis conditions indicates that sonicated conditioned medium is the least toxic to cells. A: Example images of astrocytes treated with astrocyte conditioned medium lysed with IP lysis buffer, hypotonic lysis buffer or sonication for 48 hours. B: Quantification of cell number following treatment with lysed astrocyte conditioned medium.

Next, I worked to optimise p62 IP in astrocyte cell lysates (Figure 51B-D). The first attempts at p62 IP using glycine buffer elution with gentle (Figure 51B) or harsh (Figure 51C) agitation were unsuccessful at detecting p62 from cell lysates, but I did observe successful depletion of p62 from the IP supernatant as there was a clear band for p62 in the no antibody control, which was absent from the other IP supernatant samples. This was not due to an absence of protein as I observed clear bands for all the IP supernatant samples for the loading control. I repeated the p62 IP, this

time with SDS buffer elution which allowed successful detection of p62 in the IP eluate (Figure 51D). I ran some C9-ALS astrocyte conditioned medium samples alongside the cell lysates while running the IP optimisation and notably I was unable to detect p62 under any of the conditions, including the no antibody control (Figure 51E). However, I was able to detect other proteins in the ALS astrocyte conditioned medium, including TDP-43 and LC3B (Figure 51F), so the inability to detect p62 is not due to an inability to detect protein in conditioned medium samples.

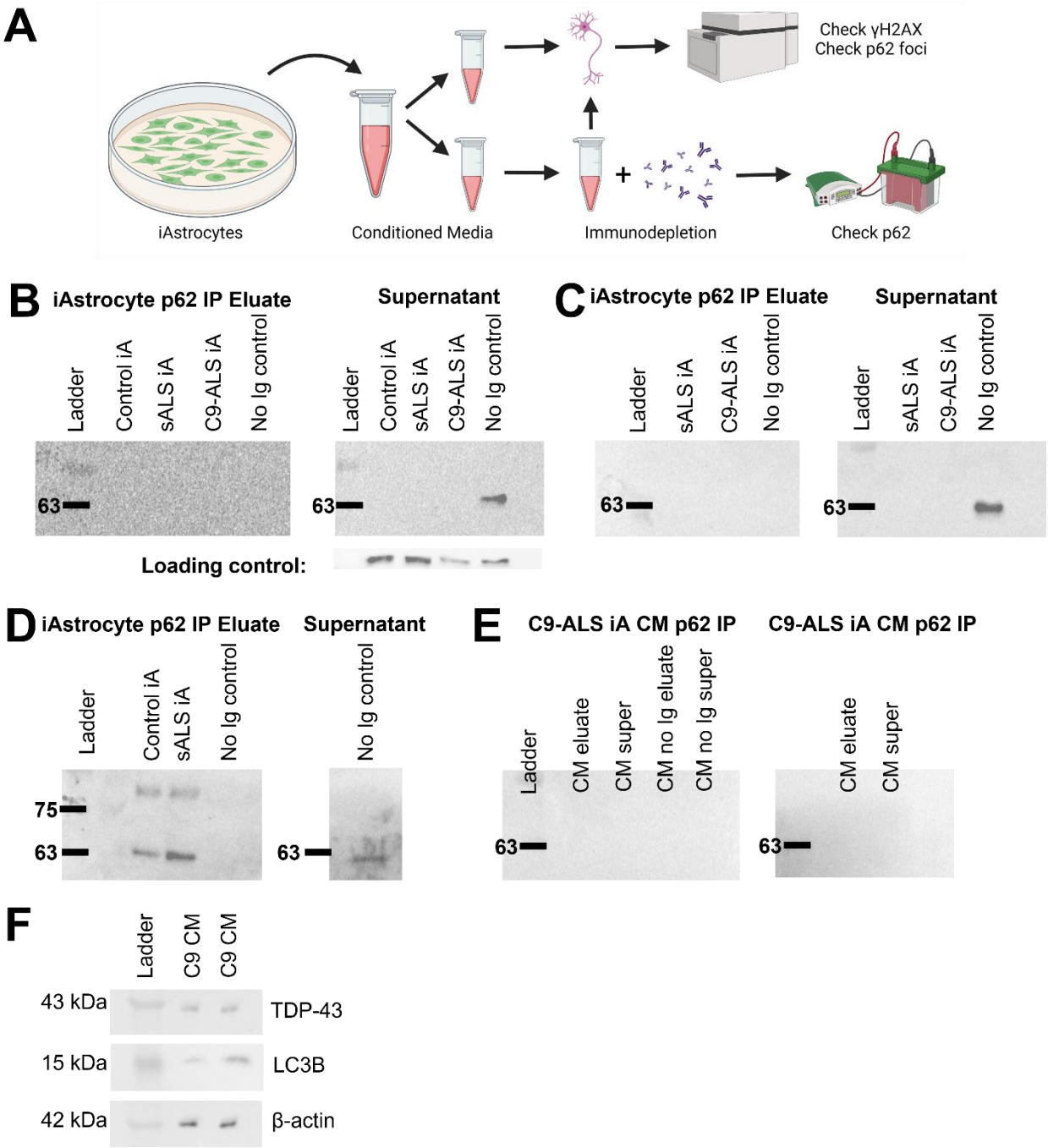

Figure 51. P62 immunoprecipitation was optimised in cell lysates but failed to show p62 expression in astrocyte conditioned medium. A: Schematic showing aim of experiment (created using

Biorender.com). B-C: P62 immunoprecipitation on astrocyte cell lysates using glycine buffer elution with gentle (B) or harsh (C) agitation. Loading control shown in B is Ku80, which we had previously established was always present in samples at high levels, and was used due issues with the membrane preventing detection of β-actin. D: p62 immunoprecipitation on astrocyte cell lysates using SDS buffer elution. E: p62 was not detected in C9-ALS conditioned media even in the no Ig control (left), nor was p62 detected following IP and SDS buffer elution (right). F: It was possible to detect other proteins, including TDP-43, LC3B and beta actin in C9-ALS astrocyte conditioned media.

5.3.3 P62 knockdown in ALS astrocytes

In addition to testing p62 immunodepletion, I also decided to test whether knockdown of p62 in ALS astrocytes could rescue DNA damage and p62 accumulation in motor neurons treated with astrocyte conditioned medium (Figure 52A). I began by testing a low range of MOI for the control AAV2-GFP-U6-scrmb-shRNA (Figure 52B). GFP expression was noticeably increased 72 hours post-transduction in the cells transduced with the highest MOI of virus. There was a large difference in number of GFP positive cells between the highest (800,000) and next highest (50,000) MOI, so I ran another optimisation using a higher range of MOI (Figure 52C). I saw a notable increase in number of GFP positive cells when using the higher range, although due to a technical issue I was unable to look at the cells 72 hours post-transduction. Five days after transduction, I fixed the cells and stained for Hoescht to quantify the percentage of GFP positive cells (Figure 52C). The most successful transduction conditions ranged from 250,000 MOI to 1,000,000 MOI. I also quantified the total cell number (Figure 52C) and observed that there was unfortunately considerable toxicity with the higher MOIs, with approximately 40% of cells being lost following transduction with 1,000,000 MOI of virus.

I settled on a compromise MOI of 500,000 for the following experiments, with expected transduction efficiency of approximately 50%. Using this MOI, I transduced one sALS and one C9-ALS astrocyte line with control AAV2-GFP-U6-scrmb-shRNA or AAV2-GFP-U6-h-SQSTM1-shRNA. I collected conditioned media from the cells 72 hours and 96 hours post-transduction for motor neuron treatment. At 96 hours post-transduction, I also collected the astrocyte cell pellets for Western blotting validation (Figure 52F-H). While quantifying protein concentration using the Bradford assay, I noted that the protein concentration of the SQSTM1-shRNA transduced cells was lower than the scrmb-shRNA transduced cells, indicating there may be an additional cell toxicity conferred from p62 knockdown (Table 24). I observed a p62 knockdown of approximately 30-40% in the transduced astrocytes (Figure 52F-G), with the higher knockdown in the sALS lines. The transduced cells also expressed GFP at varying amounts (Figure 52F&H), indicating the transduction

was successful. However, transduction efficiency was likely too low to show any meaningful effect on motor neuron p62 accumulation or DNA damage rescue. Conditioned medium derived from sALS and C9-ALS astrocyte lines with p62 knockdown was used to treat healthy motor neurons for 24 hours, however due to poor motor neuron quality I have not presented this data.

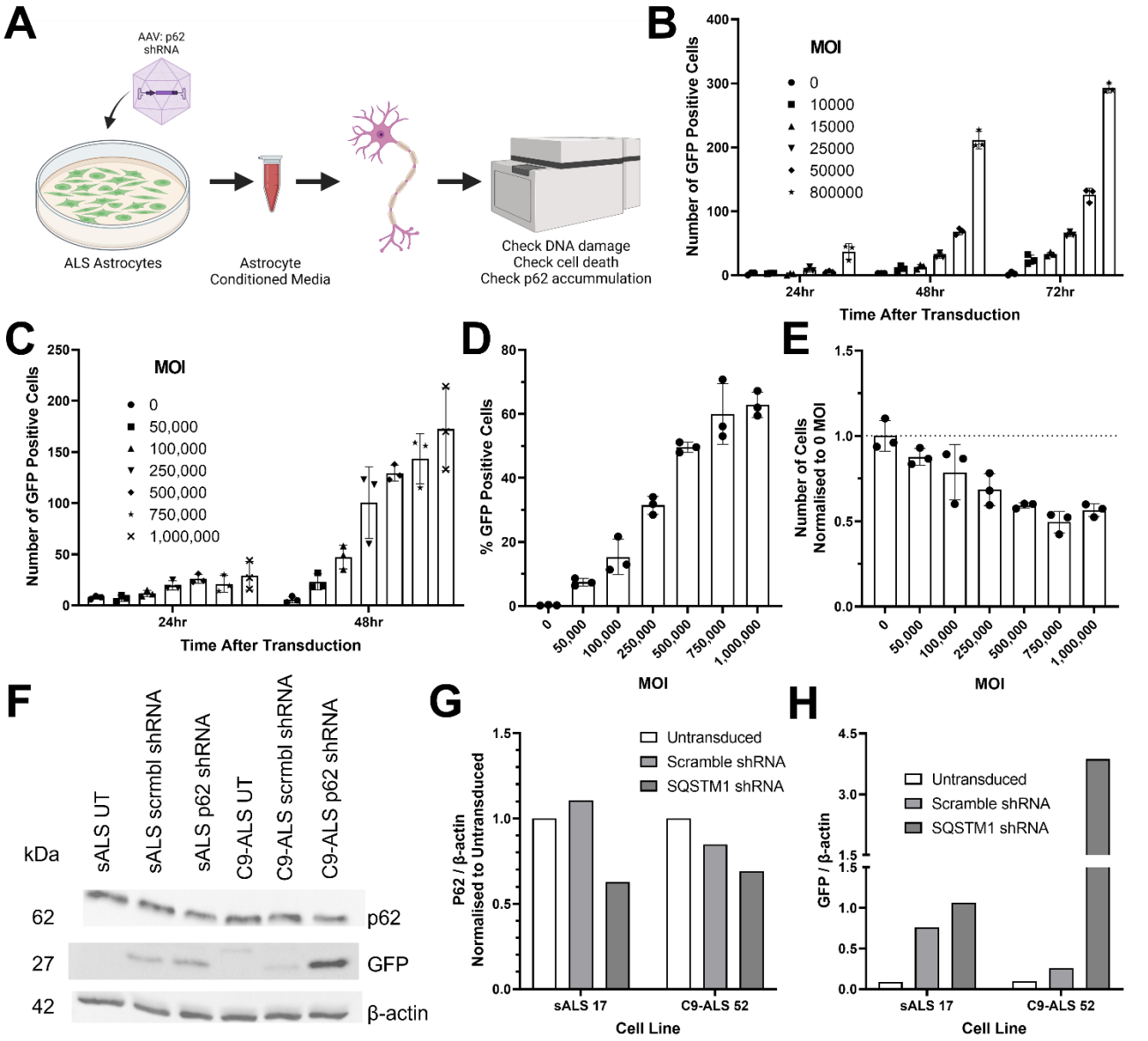

Figure 52. Optimisation and validation of p62 knockdown in astrocytes showed low efficiency and high toxicity. A: Schematic showing aim of experiment (created using Biorender.com). B-E: Transduction optimisation with AAV2 scrambled shRNA. B: Testing of low range of MOI (10,000-800,000) on astrocytes and quantification of GFP positive cells over time. C: Testing of higher range of MOI (50,000-1,000,000) on astrocytes and quantification of GFP positive cells over time. Technical issues prevented collection of data at 72 hours. D: Quantification of percentage of GFP positive cells following fixation 5 days post-transduction. E: Quantification of total cell number following fixation 5 days post-transduction. F-H: Validation of p62 knockdown in astrocytes transduced with 500,000 MOI AAV2 p62 shRNA by Western blotting. F: Western blot showing expression of p62 and GFP in astrocytes transduced with scrambled shRNA or p62 shRNA. G: Quantification of p62 expression in

transduced astrocytes, normalised to untransduced. H: Quantification of GFP expression in transduced astrocytes.

Table 24. Protein concentration of transduced cell lysates for Western blotting indicates toxicity from virus and SQSTM1 knockdown.

Cell Line	Transduction	Protein Concentration (µg/µl)
sALS 17	Untransduced	2.84
sALS 17	scrmb-shRNA	1.59
sALS 17	SQSTM1-shRNA	1.09
C9-ALS 52	Untransduced	4.29
C9-ALS 52	scrmb-shRNA	2.07
C9-ALS 52	SQSTM1-shRNA	1.62

5.4 Discussion

In this chapter, I investigated whether DPRs and p62 accumulation could be mechanisms by which ALS astrocytes induce DNA damage and DNA repair impairment. I was able to detect polyGP and polyGA in our C9-ALS astrocytes and I saw evidence that these DPRs were secreted into the conditioned medium. While the presence of these two DPRs in conditioned medium exosomes suggests it is likely the other DPRs (GR, PR, PA) are also present and secreted, it is possible their expression will be below the detection threshold of current methods to assay endogenous levels of DPRs. At present, there is no evidence for polyGP or polyPA exerting toxicity or causing DNA damage. In fact, polyPA expression has been shown to ameliorate polyGA toxicity (Lee et al., 2017), suggesting an interplay between DPRs that remains poorly understood. PolyGA, polyGR and polyPR have all been shown to induce cell death (Mizielinska et al., 2014) and DNA damage (Lopez-Gonzalez et al., 2016; Walker et al., 2017), however it has been proposed that the mechanisms likely differ between the species, with particular divergence between polyGA and poly GR/PR.

PolyGR/PR- induced DNA damage has been linked to their interactions with nucleoli and nucleolar proteins. A proportion of polyGR and polyPR inclusions co-localise with nucleoli in C9-ALS patient post-mortem tissue and in DPR-expressing cells (Kwon et al., 2014; Lee et al., 2016; White et al., 2019), and overexpression of the nucleolar protein, nucleophosmin, has been shown to reduce polyGR and polyPR-mediated toxicity (Farg et al., 2017). Nucleophosmin has been suggested to play several roles in DNA repair. Depletion of nucleophosmin reduces efficiency of NHEJ and SSA (Andrade et al., 2020), and nucleophosmin has been shown to bind APE1 (Vascotto et al., 2009), indicating a possible role for nucleophosmin in BER. Indeed, there is increased binding of nucleophosmin and APE1 in C9-ALS patients (Farg et al., 2017), though that may be consequence of

increased DNA damage. BER efficiency in cells expressing polyGR or polyPR has not been assessed, but polyGR expression is associated with reduced efficiency of NHEJ, while polyPR seems to have a broader effect and reduces efficiency of SSA and canonical and alternative NHEJ (Andrade et al., 2020). I notably did not observe any alteration in nucleolar number or morphology in motor neurons after 24 hours of conditioned medium treatment (4.2.5), however it remains possible that nucleolar proteins may play a role in ALS astrocyte-induced DNA damage and/or repair impairment. It would be of interest to see whether manipulating expression of nucleophosmin has any effect on DNA damage or toxicity in motor neurons treated with ALS astrocyte conditioned medium.

Another way DPRs could induce alteration in NHEJ is through Ku80. PolyGR has been shown to lead to increased expression of Ku80 (Lopez-Gonzalez et al., 2019), a DNA damage sensor involved in NHEJ (Chang et al., 2017), and partial knockdown of Ku80 suppressed polyGR toxicity (Lopez-Gonzalez et al., 2019), implicating potential overactivation of NHEJ playing a role in polyGR-mediated DNA damage. As we did not observe a change in Ku80 expression in motor neurons treated with C9-ALS astrocyte conditioned medium (4.2.3, 4.2.4), it seems unlikely this is the mechanism by which C9-ALS astrocytes induce DNA damage.

Notably, polyGR and polyPR expression in cells is associated with an increase in pATM foci (Farg et al., 2017; Nihei et al., 2020). Unpublished data from Dr Cleide Souza has shown that motor neurons treated with ALS astrocyte conditioned medium, despite showing an increase in DNA damage, do not show a corresponding increase in pATM. This could suggest C9-ALS astrocyte-induced DNA damage is not mediated through polyGR or polyPR secretion. Interestingly, cell autonomous polyGA-induced DNA damage is also not associated with an increase in pATM (Nihei et al., 2020; Walker et al., 2017). This is likely because polyGA has been shown to aggregate with and sequester ATM in the cytoplasm, preventing its recruitment to sites of DNA damage (Nihei et al., 2020). As Dr Cleide Souza observed that ALS astrocyte-induced DNA damage was also not associated with an increase in pATM, it may be that secreted polyGA is responsible for ALS astrocyte-induced DNA repair impairment. Surprisingly, polyGA expression is not associated with reduced efficiency of homologous recombination (HR), but it is associated with reduced efficiency of NHEJ and single-strand annealing (SSA) (Andrade et al., 2020). It would be of interest to see if these pathways are affected in motor neurons treated with ALS astrocyte conditioned medium.

Another mechanism by which polyGA may induce DNA damage or repair impairment is through depletion of heterogeneous ribonucleoprotein A3 (hnRNP A3). hnRNP A3 is a nuclear protein

thought to be involved in the maintenance of telomere repeats (Tanaka et al., 2007). HnRNP A3 is present in p62-positive inclusions in the hippocampus of C9-ALS patients and binds RNA containing GGGGCC repeats (Mori et al., 2013b). PolyGA has been shown to colocalise with and induce mislocalisation of hnRNP A3, from the nucleus to the cytoplasm (Nihei et al., 2020), resulting in hnRNP A3 nuclear depletion. hnRNP A3 is thought to play a role in DNA repair, and depletion of hnRNP A3 leads to increased DNA double strand breaks (Comegna et al., 2014), thus C9-ALS astrocytes may induce DNA damage through polyGA-mediated hnRNP A3 depletion. It would be of interest to stain motor neurons treated with control or ALS astrocyte conditioned medium for hnRNP A3 to see if this protein is mislocalised and aggregated in these cells. Interestingly, nuclear loss of hnRNP A3 has also been observed in cells expressing ALS-linked mutant FUS^{R522G}, and hnRNP A3 co-localises with cytoplasmic FUS aggregates in these cells (An et al., 2022). Thus, hnRNP A3 nuclear depletion may play a role in cell autonomous, and possibly astrocyte-induced, DNA damage in multiple ALS backgrounds.

A mechanism of polyGA-induced DNA damage that could also link other ALS subtypes is p62 accumulation. PolyGA aggregates and forms nuclear and cytoplasmic inclusions in cells, which are often co-localised with p62. In addition to colocalising with p62, polyGA expression has been shown to lead to increased p62 expression (May et al., 2014). P62 aggregation is not unique to C9-ALS and is also observed in sALS and other fALS subtypes (Gal et al., 2007; King et al., 2015; Mizuno et al., 2006). Additionally, mutations in SQSTM1, the gene encoding p62, have been attributed to a subset of fALS and sALS cases (Fecto et al., 2011). Notably, we were able to observe that ALS astrocytes induce p62 aggregation in motor neurons, although we only observed this effect 72 hours after conditioned medium treatment, compared to DNA damage which was observed after 24 hours of treatment (4.2). I did not observe an increase in p62 expression by Western blotting, suggesting p62 expression itself is not increased but instead existing p62 protein is aggregating into foci. On the other hand, it may be that Western blotting is not sensitive enough to detect changes in p62 protein expression at this timepoint after treatment.

With regards to C9-ALS, it would be interesting to assess whether DPR-transfected HEK293T cell conditioned medium can also induce an increase in p62 foci, as this could indicate whether secreted DPRs are a cause of C9-ALS astrocyte conditioned medium-induced p62 accumulation. I did attempt to look at this at the same time as looking at whether DPR-transfected HEK293T cell

conditioned medium could induce DNA damage, however due to the variability in transfection efficiency, I did not present this data.

Interestingly, SOD1-ALS astrocyte conditioned medium also induced an increase in p62 foci formation, though to a lesser extent than sALS or C9-ALS astrocytes, indicating a possible mechanistic delay in SOD1-ALS astrocytes. Perhaps, SOD1-ALS astrocytes can also induce DNA damage in motor neurons, but at a later timepoint than sALS or C9-ALS astrocytes. Indeed, Dr Cleide Souza showed that there was a significant increase in γH2AX foci in motor neurons treated with sALS, SOD1-ALS or C9-ALS astrocyte conditioned medium after 72 hours of treatment. However, as Dr Cleide Souza reported that caspase-3 expression is also significantly increased in motor neurons treated with ALS astrocyte conditioned medium after 72 hours of treatment, and apoptosis involves DNA cleavage and H2AX phosphorylation (Rogakou et al., 2000), it is difficult to ascertain whether the observed increase in γH2AX foci in motor neurons treated with SOD1-ALS astrocyte conditioned medium is due to astrocyte-induced DNA damage or is a consequence of apoptosis.

An interesting finding, with the caveat that these results have only been obtained from two repeats, was that both control and ALS astrocyte conditioned medium induced a reduction in KEAP1 protein expression in motor neurons within 72 hours of treatment. KEAP1 negatively regulates the NRF2 pathway through KEAP1-mediated proteasome-dependent degradation of NRF2. Maintenance of low levels of NRF2 prevents its translocation to the nucleus and consequent NRF2-dependent transcription of oxidative stress response genes (Baird and Yamamoto, 2020). KEAP1 knockout has been shown to lead to constitutive activation of NRF2 and its target genes (Wakabayashi et al., 2003), thus astrocyte-mediated reduction of KEAP1 may lead to increased NRF2 pathway activation in motor neurons. Notably, p62 can bind to KEAP1 and facilitates its degradation by autophagy, allowing NRF2 to translocate to the nucleus and activate its target genes (Katsuragi et al., 2016). Thus, it is somewhat unexpected that control astrocyte conditioned medium can induce a reduction in KEAP1 despite p62 expression not being changed in motor neurons treated with control astrocyte conditioned medium. It would be of interest to determine whether KEAP1 mRNA expression is altered in motor neurons treated with control or ALS astrocyte conditioned medium, to help determine whether transcription or degradation of KEAP1 is altered in these cells.

Regrettably, we were unable to determine whether p62 immunodepletion from ALS astrocyte conditioned medium or p62 knockdown in ALS astrocytes could rescue ALS astrocyte-induced DNA damage or toxicity. The AAV2 virus I used did not transduce astrocytes efficiently and became toxic at high MOI. The ensuing compromise between transduction efficiency and toxicity resulted in insufficient p62 knockdown in the astrocytes. To continue with this work, I would likely need to use another type of virus that can transduce astrocytes more efficiently, such as lentivirus or adenovirus, that have been reported to work well in the iAstrocyte cell model (unpublished data from Ferraiuolo lab). AAV2 virus transduction efficiency was greater when used on the iPSC-derived motor neurons, and ongoing work by Dr Cleide Souza aims to knockdown p62 in the motor neurons to see whether that rescues ALS astrocyte-induced DNA damage and toxicity.

Some preliminary data of mass spectrometry of control and C9-ALS astrocyte conditioned medium and exosome samples suggested that p62 may not be secreted by ALS astrocytes, in contrast to previous findings in the lab that p62 could be detected in astrocyte exosomes, thus immunodepletion may serve no purpose. I was, however, able to determine which lysis conditions would work best for an immunodepleted conditioned medium treatment experiment. This will be useful for future experiments, as it may be of interest to try immunodepleting other proteins from the conditioned medium to assess the effect on DNA damage and toxicity. Depletion of individual or multiple DPRs, for example, could be interesting to determine which DPR species may contribute to C9-ALS astrocyte-induced DNA damage and toxicity.

5.5 Conclusion

In this chapter I have identified that C9-ALS astrocytes likely secrete DPRs, which may be the cause of C9-ALS astrocyte-induced DNA damage. There are several mechanisms by which DPRs might induce DNA damage, including hnRNP A3 depletion and sequestration of ATM. These pathways may not be restricted to only C9-ALS and all merit further investigation. The cause of sALS astrocyte-induced DNA damage is currently unclear, however p62 aggregation was a common effect observed from both sALS and C9-ALS astrocyte conditioned medium treatment. It remains to be determined what might be causing p62 aggregation, and whether p62 aggregation is upstream or downstream of DNA damage.

Chapter 6: Discussion

It has been well established that DNA damage is a cell autonomous feature of motor neurons derived from ALS patients, with and without genetic mutations (Bogdanov et al., 2000; Ferrante et al., 1997; Fitzmaurice et al., 1996; Kok et al., 2021; Lopez-Gonzalez et al., 2016; Walker et al., 2017), however the effect of DNA damage in glial cells has remained poorly investigated. In this thesis, I sought to determine whether astrocytes in ALS are vulnerable to the same insult motor neurons experience that leads to increased DNA damage and whether ALS astrocytes could contribute to increased motor neuron DNA damage.

In Chapter 1, I showed evidence for the first time that DNA damage may be elevated in ALS astrocytes. Notably, the increase in DNA damage I observed was specific to certain cell lines and was not restricted to any genetic subgroup. Oxidative stress was not associated with increased DNA damage, although as I only used one measure of oxidative stress due to limitations of existing methods, it would be of interest to validate this further using another method. I was able to associate increased DNA damage in the C9-ALS astrocyte population to an increase in R-loops and/or nucleoli. As doubts were raised about the specificity of R-loop staining, this work could do with further validation, for example by using DRIP-seq to identify whether R-loops are increased in C9-ALS and which genes they may be affecting (Sanz and Chédin, 2019). Additionally, it remains to be determined what may be causing DNA damage in SOD1-ALS astrocyte cell lines.

As DNA damage did not appear to be linked specifically to gene mutations, we looked at other features of the patient lines that might be common between lines with increased DNA damage. Due to the limitations in information available, small sample size and lack of isogenic controls, it is difficult to draw final conclusions. We did, however, observe that female ALS astrocytes lines were more likely to display increased DNA damage, which I suggest could be related to upregulation in inflammatory pathways that has been observed in female ALS patients (Santiago et al., 2021), and in female ALS patient astrocyte cell lines (unpublished data from other Ferraiuolo lab team members). Alternatively, I observed within the C9-ALS subgroup that there appeared to be a link between shorter onset to death following biopsy and increased DNA damage, suggesting the inability to repair DNA damage, leading to its accumulation, in astrocytes might be related to late phases of disease progression. This suggestion has previously been examined in motor neurons, with conflicting results (Bogdanov et al., 2000; Murata et al., 2008). Both possible contributors merit further investigation.

Interestingly, we observed little correlation between astrocyte DNA damage and astrocyte-induced DNA damage in motor neurons. Within the C9-ALS astrocyte group, we did observe that astrocyte lines with higher levels of DNA damage (C9-ALS 183 and C9-ALS 201) induced higher levels of DNA damage in motor neurons. However, sALS astrocytes, which exhibited very little DNA damage, were found to induce DNA damage in motor neurons, while SOD1-ALS astrocytes, which exhibited higher levels of DNA damage, did not induce DNA damage in motor neurons. Thus, if astrocyte DNA damage relates to astrocyte-induced DNA damage, it appears to be specific to C9-ALS. A reasonable hypothesis would be that the factors contributing to endogenous DNA damage in astrocytes and their ability to induce DNA damage in neurons are driven by different factors and pathways. Indeed, accumulation of DNA damage seems to be related to abnormal DNA repair dynamics, while DNA damage induction via conditioned medium is related to secreted factors.

Similarly, in terms of mechanisms of astrocyte toxicity, it appears that astrocyte-induced DNA damage is specific to sALS and C9-ALS, with SOD1-ALS astrocyte-induced toxicity likely mediated through a different mechanism. Interestingly, sALS, SOD1-ALS and C9-ALS astrocytes all induced p62 accumulation in motor neurons, although SOD1-ALS astrocytes induced p62 accumulation to a lesser extent. It may be that there are similar downstream mechanisms of toxicity involved, or that SOD1-ALS astrocytes exhibit a mechanistic delay compared to sALS and C9-ALS. It would be of interest to re-examine certain parameters, such as γH2AX staining in SOD1-ALS astrocyte conditioned medium treated neurons at different timepoints, for example after 48 hours of treatment, to determine whether SOD1-ALS astrocytes induce DNA at a later timepoint than sALS and C9-ALS astrocytes.

Our findings from ALS astrocytes raise further questions as to whether other glial cell types may be similarly affected. There is evidence of widespread glial dysfunction in ALS. Oligodendrocytes have been shown to degenerate in a SOD1-ALS mouse model, with impaired oligodendrocyte replacement and re-myelination (Kang et al., 2013). Microglia are also altered, with increased microglia reactivity observed in ALS neuroimaging studies and in post-mortem motor cortex and spinal cord (Brettschneider et al., 2012; Turner et al., 2004). If inflammation is linked with increased DNA damage in female lines, then we might expect that microglia, which are also involved in mediating inflammation in the CNS (Jeong et al., 2013), are similarly affected. Indeed, monocyte-derived microglia-like cells generated from sALS patients have been shown to exhibit increased DNA damage (Quek et al., 2022).

Like astrocytes, ALS oligodendrocytes and microglia induce motor neuron death through cell-to-cell contact and through secreted factors (Ferraiuolo et al., 2016; Frakes et al., 2014). Unpublished data from Dr Cleide Souza in the Ferraiuolo lab group has shown that, contrary to ALS astrocytes, ALS oligodendrocytes do not induce an increase in DNA damage in motor neurons, even if they are able to induce motor neuron death. It remains to be determined, however, whether microglia can induce DNA damage in motor neurons. Microglia toxicity to neurons has been linked to microglial NF-κB activation (Frakes et al., 2014), and inflammation is known to lead to DNA damage (Kay et al., 2019), thus it is possible that ALS microglia also induce DNA damage in motor neurons.

In addition to ALS astrocytes inducing DNA damage, we observed that ALS astrocytes also appear to induce an impairment in the DNA damage response and/or DNA repair. DNA repair factor expression was not increased in motor neurons treated with ALS astrocyte conditioned medium, despite the increase in DNA damage. Notably, in our work C9-ALS motor neurons show a similar DNA repair impairment to the astrocyte conditioned medium treated motor neurons, while C9-ALS GABAergic neurons show an expected increase in DNA repair factor expression. It seems likely that motor neurons are less capable of repairing DNA damage. Interestingly, DNA repair impairment is not restricted to motor neurons as I also observed impaired DNA repair in certain ALS astrocyte cell lines. However, like with DNA damage, we observed little correlation between astrocyte DNA repair impairment and astrocyte-induced DNA repair impairment.

We specifically linked astrocyte-induced DNA repair impairment with a reduction in XRCC1 levels, which were increased in C9-ALS motor neurons. XRCC1 is involved in BER and single-strand break repair (SSBR), both of which can be activated by oxidative DNA damage and alkylation DNA damage (Abbotts and Wilson, 2017; Brem and Hall, 2005). We were not able to link astrocyte-induced DNA damage with an increase in ROS, but it remains to be determined whether reactive nitrogen species or alkylation DNA damage may play a role. XRCC1 has also been shown to regulate PARP1 activity, and in XRCC1-depleted cells PARP1 causes an accumulation of DNA damage (Adamowicz et al., 2021; Demin et al., 2021; Hoch et al., 2016). Notably, while the control astrocytes induced a reduction in both XRCC1 and PARP1, which would prevent aberrant PARP1 activity, C9-ALS astrocytes only induced a reduction in XRCC1 and not in PARP1, meaning PARP1 activity may be unregulated in motor neurons treated with C9-ALS astrocyte conditioned medium. Thus, aberrant PARP1 activity may play a role in ALS astrocyte-induced DNA damage. Interestingly, I observed similar patterns of reduced XRCC1 expression combined with increased PARP1 expression in certain

ALS astrocyte cell lines (Table 23), indicating aberrant PARP1 activity may not be solely an effect the astrocytes exert on motor neurons but could also be occurring in the astrocytes themselves. It would be of interest to determine whether catalytic inhibition of PARP1 is capable of rescuing ALS astrocyte-induced DNA damage and/or toxicity.

Through identifying evidence that C9-ALS astrocytes may secrete DPRs, we should also continue to work on other DNA repair pathways identified from studies of DPR-induced DNA damage. PolyGA may provide a possible mechanism by which C9-ALS astrocyte fail to induce pATM foci formation as polyGA is known to sequester ATM, along with other DNA repair proteins, including hnRNP A3 and HR23B (Nihei et al., 2020; Zhang et al., 2016). PolyGR and polyPR, on the other hand, may interfere with nucleolar function and the role of nucleophosmin in DNA repair (Andrade et al., 2020; Farg et al., 2017). Notably, I did not observe any change in nucleoli number or morphology in motor neurons treated with ALS astrocyte conditioned medium, however as I only looked at nucleoli 24 hours after treatment, it is possible that nucleolar dysfunction may occur later, similarly to p62 accumulation.

PolyGA expression induces p62 accumulation and impairment in ATM-mediated DNA repair (Schludi et al., 2015; Walker et al., 2017), similar to what we observed in motor neurons treated with sALS or C9-ALS astrocyte conditioned medium. P62 depletion reduced DNA damage and restored pATM foci formation in polyGA-expressing cells (Walker et al., 2017), indicating p62 may be a cause of both DNA damage and DNA damage signalling impairment. Thus, while the initiation of p62 aggregation in ALS astrocyte-conditioned medium may be different between sALS and C9-ALS, it is possible p62 aggregation is a common mechanism between these ALS subtypes that may lead to astrocyte-induced DNA damage and repair impairment. Notably, SOD1-ALS astrocyte conditioned medium also induced p62 accumulation, although to a lesser extent, potentially suggesting p62 aggregation may play a role in SOD1-ALS astrocyte-induced toxicity. Further work leading on from the results of this thesis should determine whether p62 aggregation is a cause or consequence of ALS astrocyte-induced DNA damage and repair impairment, as this could help determine whether p62 is a possible therapeutic target in ALS.

6.1 Limitations

With regards to limitations of this work, it is worth noting that in Chapter 1, there were questions raised regarding the validity of some of the staining results. OdG and S9.6 staining, for oxidative DNA damage and R-loops respectively, were found to co-stain with nucleoli, did not increase with

positive control treatments and were removed entirely by RNAse treatment, indicating the staining may have been non-specific. On the other hand, staining for DNA damage markers γH2AX and 53BP1 was validated with positive control treatment and co-localised together, as would be expected. The DNA damage data is therefore likely to be more valid that data R-loops or oxidative DNA damage shown in this thesis.

Another limitation is with regards to the heterogeneity I observed in my results, both between repeats of the same cell line/condition and between different cell lines. It is likely that heterogeneity between cell lines, for example different levels of DNA damage in different C9-ALS astrocyte lines, is due to inherent variability between patients, even if they have the same genetic alteration that leads to disease. It would be of interest to look at the clinical data for these patients to see whether there are any correlations between disease features, such as time between diagnosis and death, and DNA damage. As for heterogeneity between repeats, there are a number of possible sources. The condition and quality of the cells can be a factor. For experiments where motor neurons were treated with conditioned medium, the baseline motor neuron quality could affect the results. In some batches of motor neurons, I observed an elevation in baseline levels of DNA damage, which consequently meant the change in DNA damage following conditioned medium treatment was less than might be expected. There was also variability in intensity between staining plates, and to take this into account I had to normalise to a condition that was consistent on every plate, for example to a specific control cell line for the astrocyte experiments. If that specific control line behaved abnormally for one experiment, that could alter the entire dataset. To reduce variability in future, I will consider normalising to a range of conditions kept consistent on each plate – for example normalising to the average of multiple controls on each plate.

Another limitation of this work is the reliance on cell models of disease and the inherent issues with interclonal variability and genomic instability. Genetic changes in iPSCs can have three possible origins: existing genetic alterations in the somatic cells that are reprogrammed, alterations that arise as a result of the reprogramming process and alterations that arise during prolonged cell culture (Yoshihara et al., 2016). Indeed, it has been reported that iPSC clone cell lines derived from the same donor can exhibit different genetic mutations (including copy number variation) and alterations in DNA methylation (Kilpinen et al., 2017; Mills et al., 2013; Sgodda and Cantz, 2013). It has been suggested that most mutations occur during or immediately after the reprogramming process, with additional mutations occurring over prolonged cell culture periods (Gore et al., 2011;

Ji et al., 2012). It is possible that we are biased to select clones that grow well, which then may have genetic or phenotypic differences that alter the results to no longer be representative of the donor. However, it should also be considered that while these differences exist, generally transcriptomic analysis shows clones from the same donor will cluster close to each other and will differ significantly to clones from a different donor (Shutova et al., 2016; Vitale et al., 2012), indicating individual variability is a stronger contributor to differences than interclonal variability. Thus different clones should still be representative of their donor. Notably, this will likely not impact the work I did involving iNPCs as iNPC reprogramming does not involve clonal selection (Meyer et al., 2014) and other lab members have shown the iNPCs do not exhibit chromosomal abnormalities.

Chapter 7: Appendix

7.1 OG/OdG Staining Optimisation

Immunocytochemistry for the OG/OdG antibody was optimised (Figure 53), testing conditions suggested by the manufacturer and a published protocol (Debelec-Butuner et al., 2016). Ultimately, I settled on fixing with methanol, using 5% donkey serum block and 1:3000 antibody concentration.

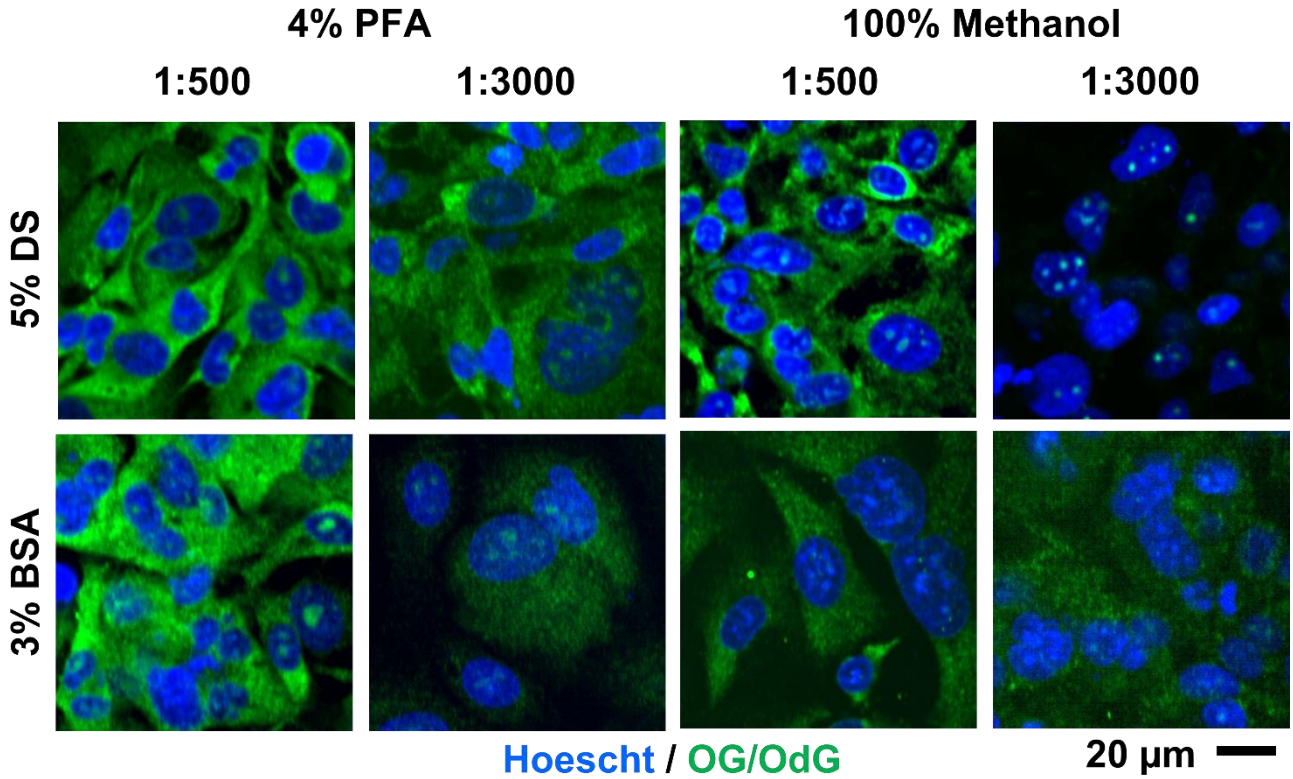

Figure 53. OG/OdG antibody staining optimisation. A: Optimisation of OG and OdG staining, comparing staining results from different fixatives (4% PFA vs 100% methanol), different blocking agents (5% donkey serum vs 3% bovine serum albumin), and different antibody concentrations (1:500 vs 1:3000).

7.2 Astrocyte DNA Repair Factor Expression by Cell Line

I observed considerable variation in protein levels of different DNA repair factors across both control and ALS astrocyte cell lines (Figure 54).

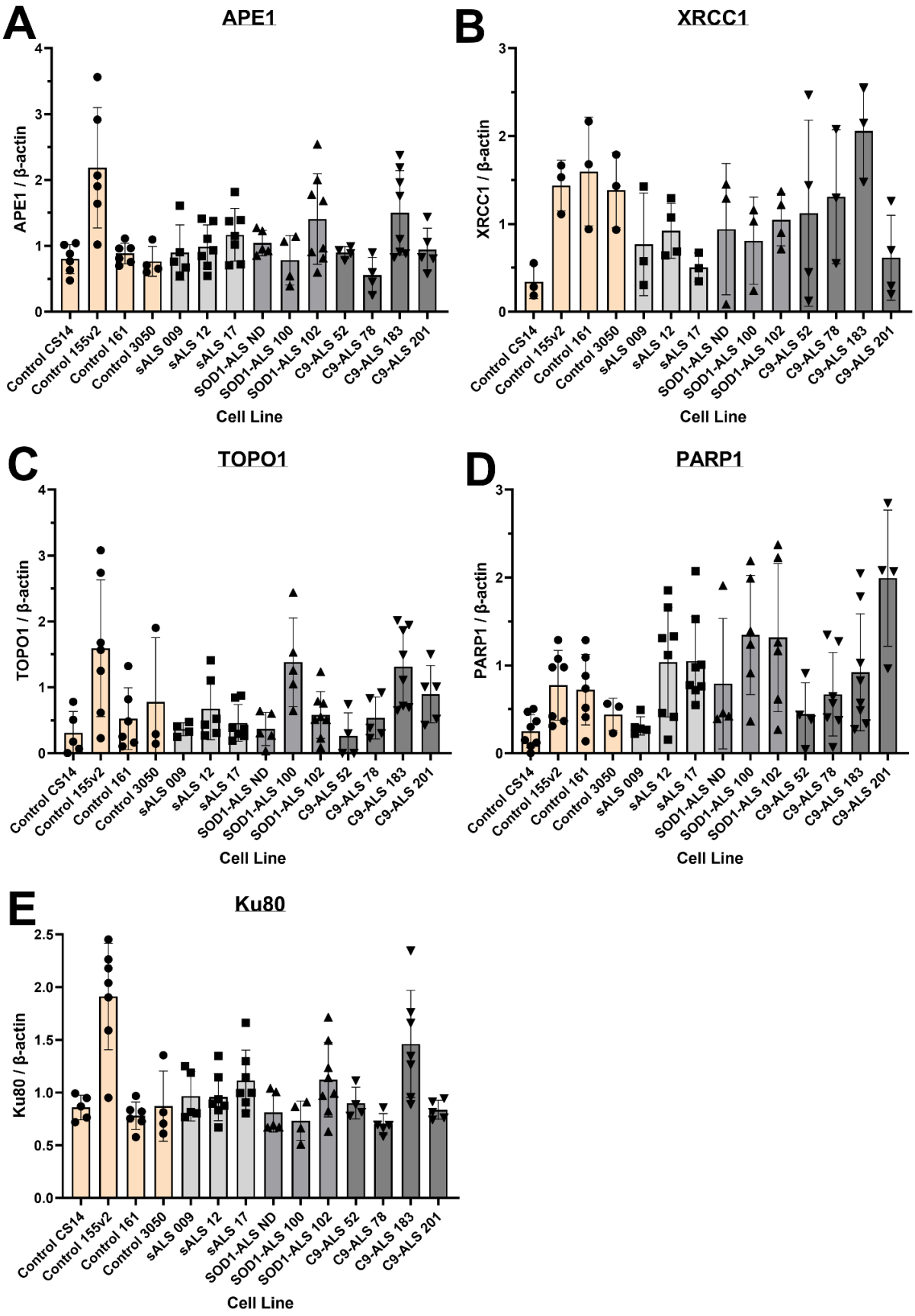

Figure 54. Western blot results for DNA repair factor expression in control and ALS astrocytes separated by cell line. Means and standard deviations shown, each datapoint represents one repeat.

7.3 γH2AX astrocyte DNA repair kinetics post-hoc statistical analysis

For control and ALS astrocytes treated with CPT and allowed to recover, I ran post-hoc Dunnett's multiple comparisons test on γH2AX foci per cell for unnormalized data (Table 25), normalised to untreated (Table 26) and normalised to timepoint 0hr (Table 27).

Table 25. Dunnett's multiple comparison test for unnormalized γH2AX foci per cell data.

Dunnett's multiple comparisons test	Mean Diff.	95.00% CI of diff.	Below threshold?	Summary	Adjusted P Value
Row 1 (untreated)					
Control vs. sALS	-0.2125	-0.8201 to 0.3950	No	ns	0.3953
Control vs. SOD1-ALS	-1.887	-9.125 to 5.351	No	ns	0.4508
Control vs. C9-ALS	-1.641	-6.327 to 3.045	No	ns	0.4396
Row 2 (time 0hr)					
Control vs. sALS	-0.1871	-4.872 to 4.497	No	ns	0.9982
Control vs. SOD1-ALS	-3.162	-11.76 to 5.441	No	ns	0.4298
Control vs. C9-ALS	-0.9589	-7.126 to 5.209	No	ns	0.9215
Row 3 (time 1hr)					
Control vs. sALS	-1.742	-8.262 to 4.777	No	ns	0.6122
Control vs. SOD1-ALS	-4.242	-14.05 to 5.564	No	ns	0.2819
Control vs. C9-ALS	-2.858	-9.168 to 3.452	No	ns	0.3640
Row 4 (time 3hr)					
Control vs. sALS	-1.246	-5.729 to 3.237	No	ns	0.6369
Control vs. SOD1-ALS	-4.354	-18.56 to 9.849	No	ns	0.4146
Control vs. C9-ALS	-2.874	-8.795 to 3.046	No	ns	0.3168
Row 5 (time 6hr)					
Control vs. sALS	-1.396	-7.168 to 4.375	No	ns	0.7375
Control vs. SOD1-ALS	-5.959	-25.82 to 13.90	No	ns	0.4309
Control vs. C9-ALS	-3.938	-9.866 to 1.991	No	ns	0.1772
Row 6 (time 24hr)					
Control vs. sALS	-1.777	-7.221 to 3.666	No	ns	0.4393
Control vs. SOD1-ALS	-5.705	-25.07 to 13.66	No	ns	0.4013
Control vs. C9-ALS	-6.332	-19.97 to 7.302	No	ns	0.2886

Table 26. Dunnett's multiple comparison test for γH2AX foci per cell data normalised to untreated.

Dunnett's multiple comparisons test	Mean Diff.	95.00% CI of diff.	Below threshold?	Summary	Adjusted P Value
Row 1 (untreated)					
Control vs. sALS	0.000				
Control vs. SOD1-ALS	0.000				
Control vs. C9-ALS	0.000				
Row 2 (time 0hr)					
Control vs. sALS	9.504	-6.524 to 25.53	No	ns	0.2026
Control vs. SOD1-ALS	18.64	-0.1191 to 37.39	No	ns	0.0509
Control vs. C9-ALS	20.96	10.17 to 31.74	Yes	**	0.0023
Row 3 (time 1 hr)					
Control vs. sALS	1.654	-26.27 to 29.57	No	ns	0.9674
Control vs. SOD1-ALS	10.71	-7.398 to 28.81	No	ns	0.1360
Control vs. C9-ALS	11.24	-0.4429 to 22.92	No	ns	0.0555
Row 4 (time 3hr)					
Control vs. sALS	2.888	-12.62 to 18.40	No	ns	0.6791
Control vs. SOD1-ALS	10.34	-4.062 to 24.73	No	ns	0.0989

Control vs. C9-ALS	10.41	-0.1672 to 21.00	No	ns	0.0523
Row 5 (time 6hr)					
Control vs. sALS	3.442	-5.295 to 12.18	No	ns	0.4503
Control vs. SOD1-ALS	8.695	-5.255 to 22.64	No	ns	0.1578
Control vs. C9-ALS	8.862	-1.070 to 18.79	No	ns	0.0734
Row 6 (time 24hr)					
Control vs. sALS	0.5109	-6.771 to 7.793	No	ns	0.9827
Control vs. SOD1-ALS	4.267	-0.2186 to 8.752	No	ns	0.0590
Control vs. C9-ALS	2.945	-3.900 to 9.790	No	ns	0.4070

Table 27. Dunnett's multiple comparison test for γH2AX foci per cell data normalised to timepoint 0hr.

Dunnett's multiple comparisons test	Mean Diff.	95.00% CI of diff.	Below threshold?	Summary	Adjusted P Value
Row 1 (untreated)					
Control vs. sALS	-0.01546	-0.09307 to 0.06216	No	ns	0.6360
Control vs. SOD1-ALS	-0.1394	-0.7311 to 0.4524	No	ns	0.5040
Control vs. C9-ALS	-0.1413	-0.4609 to 0.1784	No	ns	0.3073
Row 2 (time 0hr)					
Control vs. sALS	0.000				
Control vs. SOD1-ALS	0.000				
Control vs. C9-ALS	0.000				
Row 3 (time 1 hr)					
Control vs. sALS	-0.1086	-0.3236 to 0.1064	No	ns	0.3085
Control vs. SOD1-ALS	-0.1792	-0.4139 to 0.05562	No	ns	0.1202
Control vs. C9-ALS	-0.2414	-0.5187 to 0.03582	No	ns	0.0821
Row 4 (time 3hr)					
Control vs. sALS	-0.07526	-0.3041 to 0.1536	No	ns	0.5550
Control vs. SOD1-ALS	-0.1425	-0.6749 to 0.3899	No	ns	0.6061
Control vs. C9-ALS	-0.2010	-0.5145 to 0.1125	No	ns	0.2010
Row 5 (time 6hr)					
Control vs. sALS	-0.06453	-0.3925 to 0.2635	No	ns	0.8534
Control vs. SOD1-ALS	-0.2306	-1.151 to 0.6895	No	ns	0.5835
Control vs. C9-ALS	-0.2985	-0.6856 to 0.08853	No	ns	0.1193
Row 6 (time 24hr)					
Control vs. sALS	-0.1274	-0.6875 to 0.4328	No	ns	0.5630
Control vs. SOD1-ALS	-0.3356	-1.833 to 1.162	No	ns	0.5366
Control vs. C9-ALS	-0.5856	-2.037 to 0.8658	No	ns	0.3581

7.4 53BP1 astrocyte DNA repair kinetics post-hoc statistical analysis

For control and ALS astrocytes treated with CPT and allowed to recover, I ran post-hoc Dunnett's multiple comparisons test on 53BP1 foci per cell for unnormalized data (Table 28), normalised to untreated (Table 29) and normalised to timepoint 0hr (Table 30).

Table 28. Dunnett's multiple comparison test for unnormalized 53BP1 foci per cell data.

Dunnett's multiple comparisons test	Mean Diff.	95.00% CI of diff.	Below threshold?	Summary	Adjusted P Value
Row 1 (untreated)					
Control vs. sALS	-0.2611	-0.9521 to 0.4299	No	ns	0.3127
Control vs. SOD1-ALS	-2.110	-9.202 to 4.981	No	ns	0.3828

Control vs. C9-ALS	-1.147	-4.441 to 2.146	No	ns	0.4428
Row 2 (time 0hr)					
Control vs. sALS	-1.563	-3.644 to 0.5168	No	ns	0.1257
Control vs. SOD1-ALS	-3.605	-8.146 to 0.9363	No	ns	0.0902
Control vs. C9-ALS	-0.1767	-2.291 to 1.938	No	ns	0.9876
Row 3 (time 1 hr)					
Control vs. sALS	-1.357	-4.264 to 1.550	No	ns	0.3762
Control vs. SOD1-ALS	-3.375	-9.713 to 2.962	No	ns	0.2157
Control vs. C9-ALS	-0.8021	-3.448 to 1.843	No	ns	0.6861
Row 4 (time 3hr)					
Control vs. sALS	-0.8847	-3.083 to 1.313	No	ns	0.4688
Control vs. SOD1-ALS	-3.973	-17.69 to 9.747	No	ns	0.4359
Control vs. C9-ALS	-0.9477	-4.672 to 2.777	No	ns	0.7460
Row 5 (time 6hr)					
Control vs. sALS	-0.8396	-3.900 to 2.221	No	ns	0.6936
Control vs. SOD1-ALS	-4.285	-20.86 to 12.29	No	ns	0.5109
Control vs. C9-ALS	-1.123	-4.727 to 2.480	No	ns	0.6742
Row 6 (time 24hr)					
Control vs. sALS	-1.256	-3.052 to 0.5403	No	ns	0.1504
Control vs. SOD1-ALS	-3.784	-16.51 to 8.947	No	ns	0.4050
Control vs. C9-ALS	-1.583	-4.292 to 1.127	No	ns	0.2305

Table 29. Dunnett's multiple comparison test for 53BP1 foci per cell data normalised to untreated.

Dunnett's multiple comparisons test	Mean Diff.	95.00% CI of diff.	Below threshold?	Summary	Adjusted P Value
Row 1 (untreated)					
Control vs. sALS	0.000				
Control vs. SOD1-ALS	0.000				
Control vs. C9-ALS	0.000				
Row 2 (time 0hr)					
Control vs. sALS	6.224	-7.721 to 20.17	No	ns	0.3871
Control vs. SOD1-ALS	11.37	-6.846 to 29.59	No	ns	0.1763
Control vs. C9-ALS	12.61	2.313 to 22.90	Yes	*	0.0240
Row 3 (time 1 hr)					
Control vs. sALS	4.258	-9.498 to 18.01	No	ns	0.5942
Control vs. SOD1-ALS	10.53	-2.277 to 23.34	No	ns	0.0911
Control vs. C9-ALS	9.817	0.7697 to 18.86	Yes	*	0.0364
Row 4 (time 3hr)					
Control vs. sALS	2.899	-6.020 to 11.82	No	ns	0.5474
Control vs. SOD1-ALS	7.258	-0.5306 to 15.05	No	ns	0.0624
Control vs. C9-ALS	6.919	1.276 to 12.56	Yes	*	0.0217
Row 5 (time 6hr)					
Control vs. sALS	3.820	-5.853 to 13.49	No	ns	0.4901
Control vs. SOD1-ALS	7.892	-1.646 to 17.43	No	ns	0.0940
Control vs. C9-ALS	7.419	-1.422 to 16.26	No	ns	0.0883
Row 6 (time 24hr)					
Control vs. sALS	0.8933	-4.730 to 6.516	No	ns	0.9087
Control vs. SOD1-ALS	4.279	-0.6519 to 9.211	No	ns	0.0808
Control vs. C9-ALS	3.301	-1.556 to 8.158	No	ns	0.1785

Table 30. Dunnett's multiple comparison test for 53BP1 foci per cell data normalised to timepoint 0hr.

Dunnett's multiple comparisons test	Mean Diff.	95.00% CI of diff.	Below threshold?	Summary	Adjusted P Value
Row 1 (untreated)					
Control vs. sALS	-0.02422	-0.1127 to 0.06431	No	ns	0.4937
Control vs. SOD1-ALS	-0.2309	-1.218 to 0.7562	No	ns	0.5076
Control vs. C9-ALS	-0.1797	-0.6349 to 0.2756	No	ns	0.3697
Row 2 (time 0hr)					
Control vs. sALS	0.000				
Control vs. SOD1-ALS	0.000				
Control vs. C9-ALS	0.000				
Row 3 (time 1 hr)					
Control vs. sALS	-0.05567	-0.1921 to 0.08078	No	ns	0.4678
Control vs. SOD1-ALS	-0.07452	-0.6231 to 0.4741	No	ns	0.8368
Control vs. C9-ALS	-0.2248	-0.8255 to 0.3759	No	ns	0.4245
Row 4 (time 3hr)					
Control vs. sALS	-0.04713	-0.3796 to 0.2853	No	ns	0.8600
Control vs. SOD1-ALS	-0.2174	-1.510 to 1.075	No	ns	0.6948
Control vs. C9-ALS	-0.2547	-0.9162 to 0.4069	No	ns	0.4004
Row 5 (time 6hr)					
Control vs. sALS	-0.02257	-0.3273 to 0.2821	No	ns	0.9893
Control vs. SOD1-ALS	-0.2363	-1.690 to 1.217	No	ns	0.7576
Control vs. C9-ALS	-0.2766	-0.8416 to 0.2884	No	ns	0.3278
Row 6 (time 24hr)					
Control vs. sALS	-0.05157	-0.1915 to 0.08839	No	ns	0.5221
Control vs. SOD1-ALS	-0.2714	-1.550 to 1.007	No	ns	0.5838
Control vs. C9-ALS	-0.3284	-0.9638 to 0.3070	No	ns	0.2472

7.5 Cell number following CPT treatment post-hoc statistical analysis

For control and ALS astrocytes treated with CPT and allowed to recover, I ran post-hoc Dunnett's multiple comparisons test on number of cells normalised to untreated (Table 31).

Table 31. Dunnett's multiple comparison test results for cell number normalised to untreated.

Dunnett's multiple comparisons test	Mean Diff.	95.00% CI of diff.	Below threshold?	Summary	Adjusted P Value
Row 1 (untreated)					
Control vs. sALS	0.000				
Control vs. SOD1-ALS	0.000				
Control vs. C9-ALS	0.000				
Row 2 (time 0hr)					
Control vs. sALS	-0.02722	-0.1824 to 0.1280	No	ns	0.8670
Control vs. SOD1-ALS	-0.07665	-0.6078 to 0.4545	No	ns	0.8395
Control vs. C9-ALS	-0.1210	-0.3245 to 0.08260	No	ns	0.2447
Row 3 (time 1 hr)					
Control vs. sALS	0.04431	-0.1257 to 0.2143	No	ns	0.7424
Control vs. SOD1-ALS	-0.05003	-0.6708 to 0.5707	No	ns	0.9557
Control vs. C9-ALS	-0.07713	-0.3372 to 0.1830	No	ns	0.6692
Row 4 (time 3hr)					
Control vs. sALS	0.1454	-0.1904 to 0.4813	No	ns	0.3322
Control vs. SOD1-ALS	-0.07932	-0.5463 to 0.3877	No	ns	0.7932
Control vs. C9-ALS	-0.03254	-0.4798 to 0.4147	No	ns	0.9849

Row 5 (time 6hr)					
Control vs. sALS	0.2116	-0.2297 to 0.6530	No	ns	0.2433
Control vs. SOD1-ALS	-0.009027	-0.7159 to 0.6978	No	ns	0.9997
Control vs. C9-ALS	-0.01632	-0.4949 to 0.4623	No	ns	0.9982
Row 6 (time 24hr)					
Control vs. sALS	0.1807	-0.4952 to 0.8566	No	ns	0.4674
Control vs. SOD1-ALS	-0.06175	-0.7068 to 0.5833	No	ns	0.9073
Control vs. C9-ALS	0.01904	-0.2986 to 0.3367	No	ns	0.9903

References

Abbotts, R., and Wilson, D.M. (2017). Coordination of DNA single strand break repair. Free Radic. Biol. Med. *107*, 228–244.

Adamowicz, M., Hailstone, R., Demin, A.A., Komulainen, E., Hanzlikova, H., Brazina, J., Gautam, A., Wells, S.E., and Caldecott, K.W. (2021). XRCC1 protects transcription from toxic PARP1 activity during DNA base excision repair. Nat. Cell Biol. *23*, 1287–1298.

Aguilera, A., and García-Muse, T. (2012). R Loops: From transcription byproducts to threats to genome stability. Mol. Cell *46*, 115–124.

Aguirre, N., Flint Beal, M., Matson, W.R., and Bogdanov, M.B. (2005). Increased oxidative damage to DNA in an animal model of amyotrophic lateral sclerosis. Free Radic. Res. *39*, 383–388.

Allen, S.P., Hall, B., Castelli, L.M., Francis, L., Woof, R., Siskos, A.P., Kouloura, E., Gray, E., Thompson, A.G., Talbot, K., et al. (2019). Astrocyte adenosine deaminase loss increases motor neuron toxicity in amyotrophic lateral sclerosis. Brain *142*, 586–605.

Almad, A.A., Taga, A., Joseph, J., Gross, S.K., Welsh, C., Patankar, A., Richard, J.P., Rust, K., Pokharel, A., Plott, C., et al. (2022). Cx43 hemichannels contribute to astrocyte-mediated toxicity in sporadic and familial ALS. Proc. Natl. Acad. Sci. U. S. A. *119*, e2107391119.

Alonso, A., Logroscino, G., Jick, S.S., and Hernán, M.A. (2009). Incidence and lifetime risk of motor neuron disease in the United Kingdom: a population-based study. Eur. J. Neurol. *16*, 745–751.

Alves, C.J., Dariolli, R., Jorge, F.M. de H., Monteiro, M.R., Maximino, J.R., Martins, R.S., Strauss, B.E., Krieger, J.E., Callegaro, D., and Chadi, G. (2015). Gene expression profiling for human iPS-derived motor neurons from sporadic ALS patients reveals a strong association between mitochondrial functions and neurodegeneration. Front. Cell. Neurosci. *9*.

Amin, N., and Pearce, B. (1997). Glutamate toxicity in neuron-enriched and neuron–astrocyte co-cultures: effect of the glutamate uptake inhibitor l-trans-pyrrolidine-2,4-dicarboxylate. Neurochem. Int. *30*, 271–276.

An, H., Litscher, G., Watanabe, N., Wei, W., Hashimoto, T., Iwatsubo, T., Buchman, V.L., and Shelkovnikova, T.A. (2022). ALS-linked cytoplasmic FUS assemblies are compositionally different from physiological stress granules and sequester hnRNPA3, a novel modifier of FUS toxicity. Neurobiol. Dis. *162*, 105585.

Andrade, N.S., Ramic, M., Esanov, R., Liu, W., Rybin, M.J., Gaidosh, G., Abdallah, A., Del'olio, S., Huff, T.C., Chee, N.T., et al. (2020). Dipeptide repeat proteins inhibit homology-directed DNA double strand break repair in C9ORF72 ALS/FTD. Mol. Neurodegener. *15*, 1–18.

Arai, T., Nonaka, T., Hasegawa, M., Akiyama, H., Yoshida, M., Hashizume, Y., Tsuchiya, K., Oda, T., and Ikeda, K. (2003). Neuronal and glial inclusions in frontotemporal dementia with or without motor neuron disease are immunopositive for p62. Neurosci. Lett. *342*, 41–44.

Arai, T., Hasegawa, M., Akiyama, H., Ikeda, K., Nonaka, T., Mori, H., Mann, D., Tsuchiya, K., Yoshida, M., Hashizume, Y., et al. (2006). TDP-43 is a component of ubiquitin-positive tau-negative inclusions in frontotemporal lobar degeneration and amyotrophic lateral sclerosis. Biochem. Biophys. Res. Commun. *351*, 602–611.

Arredondo, C., Cefaliello, C., Dyrda, A., Jury, N., Martinez, P., Díaz, I., Amaro, A., Tran, H., Morales, D., Pertusa, M., et al. (2022). Excessive release of inorganic polyphosphate by ALS/FTD astrocytes causes non-cell-autonomous toxicity to motoneurons. Neuron *110*, 1656–1670.

Ash, P.E.A., Bieniek, K.F., Gendron, T.F., Caulfield, T., Lin, W.-L., DeJesus-Hernandez, M., van Blitterswijk, M.M., Jansen-West, K., Paul, J.W., Rademakers, R., et al. (2013). Unconventional translation of C9ORF72 GGGGCC expansion generates insoluble polypeptides specific to c9FTD/ALS. Neuron *77*, 639–646.

van Attikum, H., and Gasser, S.M. (2009). Crosstalk between histone modifications during the DNA damage response. Trends Cell Biol. *19*, 207–217.

Baird, L., and Yamamoto, M. (2020). The molecular mechanisms regulating the KEAP1-NRF2 pathway. Mol. Cell. Biol. *40*, e00099-20.

Barbosa, L.F., Cerqueira, F.M., Macedo, A.F.A., Garcia, C.C.M., Angeli, J.P.F., Schumacher, R.I., Sogayar, M.C., Augusto, O., Carrì, M.T., Di Mascio, P., et al. (2010). Increased SOD1 association with chromatin, DNA damage, p53 activation, and apoptosis in a cellular model of SOD1-linked ALS. Biochim. Biophys. Acta - Mol. Basis Dis. *1802*, 462–471.

Basso, M., Pozzi, S., Tortarolo, M., Fiordaliso, F., Bisighini, C., Pasetto, L., Spaltro, G., Lidonnici, D., Gensano, F., Battaglia, E., et al. (2013). Mutant copper-zinc superoxide dismutase (SOD1) induces protein secretion pathway alterations and exosome release in astrocytes: Implications for disease spreading and motor neuron pathology in amyotrophic lateral sclerosis. J. Biol. Chem. *288*, 15699–15711.

Batiuk, M.Y., Martirosyan, A., Wahis, J., de Vin, F., Marneffe, C., Kusserow, C., Koeppen, J., Viana, J.F., Oliveira, J.F., Voet, T., et al. (2020). Identification of region-specific astrocyte subtypes at single cell resolution. Nat. Commun. *11*.

De Benedetti, S., Lucchini, G., Del Bò, C., Deon, V., Marocchi, A., Penco, S., Lunetta, C., Gianazza, E., Bonomi, F., and Iametti, S. (2017). Blood trace metals in a sporadic amyotrophic lateral sclerosis geographical cluster. BioMetals *30*, 355–365.

Bezzi, P., Gundersen, V., Galbete, J.L., Seifert, G., Steinhäuser, C., Pilati, E., and Volterra, A. (2004). Astrocytes contain a vesicular compartment that is competent for regulated exocytosis of glutamate. Nat. Neurosci. *7*, 613–620.

Birger, A., Ben-Dor, I., Ottolenghi, M., Turetsky, T., Gil, Y., Sweetat, S., Perez, L., Belzer, V., Casden, N., Steiner, D., et al. (2019). Human iPSC-derived astrocytes from ALS patients with mutated C9ORF72 show increased oxidative stress and neurotoxicity. EBioMedicine *50*, 274–289.

Blanco-Suarez, E., Liu, T.F., Kopelevich, A., and Allen, N.J. (2018). Astrocyte-secreted chordin-like 1 drives synapse maturation and limits plasticity by increasing synaptic GluA2 AMPA receptors. Neuron *100*, 1116–1132.

Blasco, H., Garcon, G., Patin, F., Veyrat-Durebex, C., Boyer, J., Devos, D., Vourc'h, P., Andres, C.R., and Corcia, P. (2017). Panel of oxidative stress and inflammatory biomarkers in ALS: a pilot study. Can. J. Neurol. Sci. / J. Can. Des Sci. Neurol. *44*, 90–95.

Bogdanov, M., Brown, R.H., Matson, W., Smart, R., Hayden, D., O'Donnell, H., Flint Beal, M., and Cudkowicz, M. (2000). Increased oxidative damage to DNA in ALS patients. Free Radic. Biol. Med. *29*, 652–658.

Boillée, S., Yamanaka, K., Lobsiger, C.S., Copeland, N.G., Jenkins, N.A., Kassiotis, G., Kollias, G., and Cleveland, D.W. (2006). Onset and progression in inherited ALS determined by motor neurons and microglia. Science (80-.). *312*, 1389–1392.

Boisvert, F.-M., van Koningsbruggen, S., Navascués, J., and Lamond, A.I. (2007). The multifunctional nucleolus. Nat. Rev. Mol. Cell Biol. *8*, 574–585.

Borchelt, D.R., Lee, M.K., Slunt, H.S., Guarnieri, M., Xu, Z.S., Wong, P.C., Brown, R.H., Price, D.L., Sisodia, S.S., and Cleveland, D.W. (1994). Superoxide dismutase 1 with mutations linked to familial amyotrophic lateral sclerosis possesses significant activity. Proc. Natl. Acad. Sci. U. S. A. *91*, 8292–8296.

Bortner, C.D., Oldenburg, N.B.E., and Cidlowski, J.A. (1995). The role of DNA fragmentation in apoptosis. Trends Cell Biol. *5*, 21–26.

Bosco, D.A., Morfini, G., Karabacak, N.M., Song, Y., Gros-Louis, F., Pasinelli, P., Goolsby, H., Fontaine, B.A., Lemay, N., McKenna-Yasek, D., et al. (2010). Wild-type and mutant SOD1 share an aberrant conformation and a common pathogenic pathway in ALS. Nat. Neurosci. *13*, 1396–1403.

Bouzier-Sore, A.K., Merle, M., Magistretti, P.J., and Pellerin, L. (2002). Feeding active neurons: (re)emergence of a nursing role for astrocytes. J. Physiol. *96*, 273–282.

Brem, R., and Hall, J. (2005). XRCC1 is required for DNA single-strand break repair in human cells. Nucleic Acids Res. *33*, 2512–2520.

Brettschneider, J., Toledo, J.B., van Deerlin, V.M., Elman, L., McCluskey, L., Lee, V.M.Y., and Trojanowski, J.Q. (2012). Microglial activation correlates with disease progression and upper motor neuron clinical symptoms in amyotrophic lateral sclerosis. PLoS One *7*, e39216.

Bröer, S., and Brookes, N. (2001). Transfer of glutamine between astrocytes and neurons. J. Neurochem. *77*, 705–719.

Bylicky, M.A., Mueller, G.P., and Day, R.M. (2019). Radiation resistance of normal human astrocytes: The role of non-homologous end joining DNA repair activity. J. Radiat. Res. *60*, 37–50.

Byrne, S., Walsh, C., Lynch, C., Bede, P., Elamin, M., Kenna, K., McLaughlin, R., and Hardiman, O. (2011). Rate of familial amyotrophic lateral sclerosis: a systematic review and meta-analysis. J. Neurol. Neurosurg. Psychiatry *82*, 623–627.

Cadet, J., and Davies, K.J.A. (2017). Oxidative DNA damage & repair: An introduction. Free Radic. Biol. Med. *107*, 2–12.

Chang, H.H.Y., Pannunzio, N.R., Adachi, N., and Lieber, M.R. (2017). Non-homologous DNA end joining and alternative pathways to double-strand break repair. Nat. Rev. Mol. Cell Biol. *18*, 495–506.

Chang, Y.J., Jeng, U.S., Chiang, Y.L., Hwang, I.S., and Chen, Y.R. (2016). The glycine-alanine dipeptide repeat from C9orf72 hexanucleotide expansions forms toxic amyloids possessing cell-to-cell transmission properties. J. Biol. Chem. *291*, 4903–4911.

Chapman, J.R., Sossick, A.J., Boulton, S.J., and Jackson, S.P. (2012). BRCA1-associated exclusion of 53BP1 from DNA: damage sites underlies temporal control of DNA repair. J. Cell Sci. *125*, 3529–3534.

Chen, Y., Chen, P.-L., Chen, C.-F., Jiang, X., and Riley, D.J. (2008). Never-in-mitosis related Kinase 1 functions in DNA damage response and checkpoint control. Cell Cycle *7*, 3194–3201.

Chen, Y., Chen, C.-F., Riley, D.J., and Chen, P.-L. (2011). Nek1 kinase functions in DNA damage response and checkpoint control through a pathway independent of ATM and ATR. Cell Cycle *10*, 655–663.

Chowdhuri, S.P., and Das, B.B. (2021). Top1-PARP1 association and beyond: from DNA topology to break repair. NAR Cancer *3*, zcab003.

Chung, W.S., Clarke, L.E., Wang, G.X., Stafford, B.K., Sher, A., Chakraborty, C., Joung, J., Foo, L.C., Thompson, A., Chen, C., et al. (2013). Astrocytes mediate synapse elimination through MEGF10 and MERTK pathways. Nature *504*, 394–400.

Clement, A.M., Nguyen, M.D., Roberts, E.A., Garcia, M.L., Boillée, S., Rule, M., McMahon, A.P., Doucette, W., Siwek, D., Ferrante, R.J., et al. (2003). Wild-type nonneuronal cells extend survival of SOD1 mutant motor neurons in ALS mice. Science (80-.). *302*, 113–117.

Collins, A.R. (2004). The comet assay for DNA damage and repair: principles, applications, and limitations. Mol. Biotechnol. *26*, 249–261.

Collins, A.R. (2014). Measuring oxidative damage to DNA and its repair with the comet assay. Biochim. Biophys. Acta - Gen. Subj. *1840*, 794–800.

Comegna, M., Succoio, M., Napolitano, M., Vitale, M., D'Ambrosio, C., Scaloni, A., Passaro, F., Zambrano, N., Cimino, F., and Faraonio, R. (2014). Identification of miR-494 direct targets involved in senescence of human diploid fibroblasts. FASEB J. *28*, 3720–3733.

Coppedè, F., Migheli, F., Lo Gerfo, A., Fabbrizi, M.R., Carlesi, C., Mancuso, M., Corti, S., Mezzina, N., Del Bo, R., Comi, G.P., et al. (2010). Association study between XRCC1 gene polymorphisms and sporadic amyotrophic lateral sclerosis. Amyotroph. Lateral Scler. *11*, 122–124.

Cornel, A.M., Mimpen, I.L., and Nierkens, S. (2020). MHC class I downregulation in cancer: underlying mechanisms and potential targets for cancer immunotherapy. Cancers (Basel). *12*, 1760.

Cronin, M., Anderson, P.N., Cook, J.E., Green, C.R., and Becker, D.L. (2008). Blocking connexin43 expression reduces inflammation and improves functional recovery after spinal cord injury. Mol. Cell. Neurosci. *39*, 152–160.

Cykowski, M.D., Dickson, D.W., Powell, S.Z., Arumanayagam, A.S., Rivera, A.L., and Appel, S.H. (2019). Dipeptide repeat (DPR) pathology in the skeletal muscle of ALS patients with C9ORF72 repeat expansion. Acta Neuropathol. *138*, 667–670.

Van Damme, P., Robberecht, W., and Van Den Bosch, L. (2017). Modelling amyotrophic lateral sclerosis: progress and possibilities. Dis. Model. Mech. *10*, 537–549.

Davis, A.J., and Chen, D.J. (2013). DNA double strand break repair via non-homologous end-joining. Transl. Cancer Res. *2*, 130–143.

Debelec-Butuner, B., Bostancı, A., Heiserich, L., Eberle, C., Ozcan, F., Aslan, M., Roggenbuck, D., and Korkmaz, K.S. (2016). Automated cell-based quantitation of 8-OHdG damage. In Stem Cell Heterogeneity: Methods and Protocols, K. Turksen, ed. (New York, NY: Springer New York), pp. 299–308.

DeJesus-Hernandez, M., Mackenzie, I.R., Boeve, B.F., Boxer, A.L., Baker, M., Rutherford, N.J., Nicholson, A.M., Finch, N.A., Flynn, H., Adamson, J., et al. (2011). Expanded GGGGCC hexanucleotide repeat in noncoding region of C9ORF72 causes chromosome 9p-linked FTD and ALS. Neuron *72*, 245–256.

Dekker, A.M., Seelen, M., van Doormaal, P.T.C., van Rheenen, W., Bothof, R.J.P., van Riessen, T., Brands, W.J., van der Kooi, A.J., de Visser, M., Voermans, N.C., et al. (2016). Large-scale screening in sporadic amyotrophic lateral sclerosis identifies genetic modifiers in C9orf72 repeat carriers. Neurobiol. Aging *39*, 220.e9-220.e15.

Demin, A.A., Hirota, K., Tsuda, M., Adamowicz, M., Hailstone, R., Brazina, J., Gittens, W., Kalasova, I., Shao, Z., Zha, S., et al. (2021). XRCC1 prevents toxic PARP1 trapping during DNA base excision repair. Mol. Cell *81*, 3018–3030.

Deng, H.-X., Zhai, H., Bigio, E.H., Yan, J., Fecto, F., Ajroud, K., Mishra, M., Ajroud-Driss, S., Heller, S., Sufit, R., et al. (2010). FUS-immunoreactive inclusions are a common feature in sporadic and non-SOD1 familial amyotrophic lateral sclerosis. Ann. Neurol. *67*, 739–748.

Desmarais, J.A., Unger, C., Damjanov, I., Meuth, M., and Andrews, P. (2016). Apoptosis and failure of checkpoint kinase 1 activation in human induced pluripotent stem cells under replication stress. Stem Cell Res. Ther. *7*.

Dimos, J.T., Rodolfa, K.T., Niakan, K.K., Weisenthal, L.M., Mitsumoto, H., Chung, W., Croft, G.F., Saphier, G., Leibel, R., Goland, R., et al. (2008). Induced pluripotent stem cells generated from patients with ALS can be differentiated into motor neurons. Science (80-.). *321*, 1218–1221.

Dols-Icardo, O., Garcia-Redondo, A., Rojas-Garcia, R., Sanchez-Valle, R., Noguera, A., Gomez-Tortosa, E., Pastor, P., Hernandez, I., Esteban-Perez, J., Suarez-Calvet, M., et al. (2014). Characterization of the repeat expansion size in C9orf72 in amyotrophic lateral sclerosis and frontotemporal dementia. Hum. Mol. Genet. *23*, 749–754.

Du, Z.-W., Chen, H., Liu, H., Lu, J., Qian, K., Huang, C.-L., Zhong, X., Fan, F., and Zhang, S.-C. (2015). Generation and expansion of highly pure motor neuron progenitors from human pluripotent stem cells. Nat. Commun. *6*.

El-Khamisy, S.F., Masutani, M., Suzuki, H., and Caldecott, K.W. (2003). A requirement for PARP-1 for the assembly or stability of XRCC1 nuclear foci at sites of oxidative DNA damage. Nucleic Acids Res. *31*, 5526–5533.

El-Khamisy, S.F., Katyal, S., Patel, P., Ju, L., McKinnon, P.J., and Caldecott, K.W. (2009). Synergistic decrease of DNA single-strand break repair rates in mouse neural cells lacking both Tdp1 and aprataxin. DNA Repair (Amst). *8*, 760–766.

Enterzari-Taher, M., Eisen, A., Stewart, H., and Nakajima, M. (1997). Abnormalities of cortical inhibitory neurons in amyotrophic lateral sclerosis. Muscle Nerve *20*, 65–71.

Fang, F., Umbach, D.M., Xu, Z., Ye, W., Sandler, D.P., Taylor, J.A., and Kamel, F. (2012). No association between DNA repair gene XRCC1 and amyotrophic lateral sclerosis. Neurobiol. Aging *33*, 1015.e25-1015.e26.

Fang, L., Teuchert, M., Huber-Abel, F., Schattauer, D., Hendrich, C., Dorst, J., Zettlmeissel, H., Wlaschek, M., Scharffetter-Kochanek, K., Kapfer, T., et al. (2010). MMP-2 and MMP-9 are elevated in spinal cord and skin in a mouse model of ALS. J. Neurol. Sci. *294*, 51–56.

Farg, M.A., Konopka, A., Soo, K.Y., Ito, D., and Atkin, J.D. (2017). The DNA damage response (DDR) is induced by the C9orf72 repeat expansion in amyotrophic lateral sclerosis. Hum. Mol. Genet. *26*, 2882–2896.

Fecto, F., Yan, J., Vemula, S.P., Liu, E., Yang, Y., Chen, W., Zheng, J.G., Shi, Y., Siddique, N., Arrat, H., et al. (2011). SQSTM1 mutations in familial and sporadic amyotrophic lateral sclerosis. Arch. Neurol. *68*, 1440–1446.

Ferraiuolo, L., Kirby, J., Grierson, A.J., Sendtner, M., and Shaw, P.J. (2011a). Molecular pathways of motor neuron injury in amyotrophic lateral sclerosis. Nat. Rev. Neurol. *7*, 616–630.

Ferraiuolo, L., Higginbottom, A., Heath, P.R., Barber, S., Greenald, D., Kirby, J., and Shaw, P.J. (2011b). Dysregulation of astrocyte–motoneuron cross-talk in mutant superoxide dismutase 1-related amyotrophic lateral sclerosis. Brain *134*, 2627–2641.

Ferraiuolo, L., Meyer, K., Sherwood, T.W., Vick, J., Likhite, S., Frakes, A., Miranda, C.J., Braun, L., Heath, P.R., Pineda, R., et al. (2016). Oligodendrocytes contribute to motor neuron death in ALS via SOD1-dependent mechanism. Proc. Natl. Acad. Sci. U. S. A. *113*, E6496–E6505.

Ferrante, R.J., Browne, S.E., Shinobu, L.A., Bowling, A.C., Baik, M.J., MacGarvey, U., Kowall, N.W., Brown, R.H., and Beal, M.F. (1997). Evidence of increased oxidative damage in both sporadic and familial amyotrophic lateral sclerosis. J. Neurochem. *69*, 2064–2074.

Fitzmaurice, P.S., Shaw, I.C., Kleiner, H.E., Miller, R.T., Monks, T.J., Lau, S.S., Mitchell, J.D., and Lynch, P.G. (1996). Evidence for DNA damage in amyotrophic lateral sclerosis. Muscle Nerve *19*, 797–798.

Forsberg, K., Graffmo, K., Pakkenberg, B., Weber, M., Nielsen, M., Marklund, S., Brännström, T., and Andersen, P.M. (2019). Misfolded SOD1 inclusions in patients with mutations in C9orf72 and other ALS/FTD-associated genes. J. Neurol. Neurosurg. Psychiatry *90*, 861–869.

Frakes, A.E., Ferraiuolo, L., Haidet-Phillips, A.M., Schmelzer, L., Braun, L., Miranda, C.J., Ladner, K.J., Bevan, A.K., Foust, K.D., Godbout, J.P., et al. (2014). Microglia induce motor neuron death via the classical NF-κB pathway in amyotrophic lateral sclerosis. Neuron *81*, 1009–1023.

Freibaum, B.D., and Taylor, J.P. (2017). The role of dipeptide repeats in C9ORF72-related ALS-FTD. Front. Mol. Neurosci. *10*.

Gadient, R.A., Cron, K.C., and Otten, U. (1990). Interleukin-1 β and tumor necrosis factor-α synergistically stimulate nerve growth factor (NGF) release from cultured rat astrocytes. Neurosci. Lett. *117*, 335–340.

Gage, F.H. (2002). Neurogenesis in the adult brain. J. Neurosci. *22*, 612–613.

Gal, J., Ström, A.L., Kilty, R., Zhang, F., and Zhu, H. (2007). P62 accumulates and enhances aggregate formation in model systems of familial amyotrophic lateral sclerosis. J. Biol. Chem. *282*, 11068–11077.

Gallo, V., Bueno-De-Mesquita, H.B., Vermeulen, R., Andersen, P.M., Kyrozis, A., Linseisen, J., Kaaks, R., Allen, N.E., Roddam, A.W., Boshuizen, H.C., et al. (2009). Smoking and risk for amyotrophic lateral sclerosis: analysis of the EPIC cohort. Ann. Neurol. *65*, 378–385.

Garm, C., Moreno-Villanueva, M., Bürkle, A., Petersen, I., Bohr, V.A., Christensen, K., and Stevnsner,

T. (2013). Age and gender effects on DNA strand break repair in peripheral blood mononuclear cells. Aging Cell *12*, 58–66.

Gatto, N., Dos Santos Souza, C., Shaw, A.C., Bell, S.M., Myszczynska, M.A., Powers, S., Meyer, K., Castelli, L.M., Karyka, E., Mortiboys, H., et al. (2020). Directly converted astrocytes retain the ageing features of the donor fibroblasts and elucidate the astrocytic contribution to human CNS health and disease. Aging Cell *20*, e13281.

Ghasemi, M., and Brown, R.H. (2017). Genetics of amyotrophic lateral sclerosis. Cold Spring Harb. Perspect. Med. *8*, a024125.

Giglia-Mari, G., Zotter, A., and Vermeulen, W. (2011). DNA damage response. Cold Spring Harb. Perspect. Biol. *3*, a000745.

Di Giorgio, F.P., Boulting, G.L., Bobrowicz, S., and Eggan, K.C. (2008). Human embryonic stem cell-derived motor neurons are sensitive to the toxic effect of glial cells carrying an ALS-causing mutation. Cell Stem Cell *3*, 637–648.

Gnügge, R., and Symington, L.S. (2021). DNA end resection during homologous recombination. Curr. Opin. Genet. Dev. *71*, 99–105.

Goetz, C.G. (2000). Amyotrophic lateral sclerosis: early contributions of Jean-Martin Charcot. Muscle Nerve *23*, 336–343.

Goldstein, M., Derheimer, F.A., Tait-Mulder, J., and Kastan, M.B. (2013). Nucleolin mediates nucleosome disruption critical for DNA double-strand break repair. Proc. Natl. Acad. Sci. U. S. A. *110*, 16874–16879.

Gomes, C., Sequeira, C., Barbosa, M., Cunha, C., Vaz, A.R., and Brites, D. (2020). Astrocyte regional diversity in ALS includes distinct aberrant phenotypes with common and causal pathological processes. Exp. Cell Res. *395*, 112209.

Gorbunova, V., Seluanov, A., Mao, Z., and Hine, C. (2007). Changes in DNA repair during aging. Nucleic Acids Res. *35*, 7466–7474.

Gore, A., Li, Z., Fung, H.L., Young, J.E., Agarwal, S., Antosiewicz-Bourget, J., Canto, I., Giorgetti, A., Israel, M.A., Kiskinis, E., et al. (2011). Somatic coding mutations in human induced pluripotent stem cells. Nature *471*, 63–67.

Goyal, N.A., Berry, J.D., Windebank, A., Staff, N.P., Maragakis, N.J., van den Berg, L.H., Genge, A., Miller, R., Baloh, R.H., Kern, R., et al. (2020). Addressing heterogeneity in amyotrophic lateral sclerosis CLINICAL TRIALS. Muscle Nerve *62*, 156–166.

Grad, L.I., Yerbury, J.J., Turner, B.J., Guest, W.C., Pokrishevsky, E., O'Neill, M.A., Yanai, A., Silverman, J.M., Zeineddine, R., Corcoran, L., et al. (2014). Intercellular propagated misfolding of wild-type Cu/Zn superoxide dismutase occurs via exosome-dependent and -independent mechanisms. Proc. Natl. Acad. Sci. U. S. A. *111*, 3620–3625.

Guttenplan, K.A., Weigel, M.K., Prakash, P., Wijewardhane, P.R., Hasel, P., Rufen-Blanchette, U., Münch, A.E., Blum, J.A., Fine, J., Neal, M.C., et al. (2021). Neurotoxic reactive astrocytes induce cell death via saturated lipids. Nature *599*, 102–107.

Haeusler, A.R., Donnelly, C.J., Periz, G., Simko, E.A.J., Shaw, P.G., Kim, M.-S., Maragakis, N.J.,

Troncoso, J.C., Pandey, A., Sattler, R., et al. (2014). C9orf72 nucleotide repeat structures initiate molecular cascades of disease. Nature *507*, 195–200.

Haidet-Phillips, A.M., Hester, M.E., Miranda, C.J., Meyer, K., Braun, L., Frakes, A., Song, S., Likhite, S., Murtha, M.J., Foust, K.D., et al. (2011). Astrocytes from familial and sporadic ALS patients are toxic to motor neurons. Nat. Biotechnol. *29*, 824–828.

Han, J., and Huang, J. (2019). DNA double-strand break repair pathway choice: the fork in the road. Genome Instab. Dis. *1*, 10–19.

Harlan, B.A., Pehar, M., Killoy, K.M., and Vargas, M.R. (2019). Enhanced SIRT6 activity abrogates the neurotoxic phenotype of astrocytes expressing ALS-linked mutant SOD1. FASEB J. *33*, 7084–7091.

Hassanian, S.M., Avan, A., and Ardeshirylajimi, A. (2017). Inorganic polyphosphate: a key modulator of inflammation. J. Thromb. Haemost. *15*, 213–218.

Heithoff, B.P., George, K.K., Phares, A.N., Zuidhoek, I.A., Munoz-Ballester, C., and Robel, S. (2021). Astrocytes are necessary for blood–brain barrier maintenance in the adult mouse brain. Glia *69*, 436–472.

Higelin, J., Demestre, M., Putz, S., Delling, J.P., Jacob, C., Lutz, A.-K., Bausinger, J., Huber, A.-K., Klingenstein, M., Barbi, G., et al. (2016). FUS mislocalization and vulnerability to DNA damage in ALS patients derived hiPSCs and aging motoneurons. Front. Cell. Neurosci. *10*, 290.

Higelin, J., Catanese, A., Semelink-Sedlacek, L.L., Oeztuerk, S., Lutz, A.-K., Bausinger, J., Barbi, G., Speit, G., Andersen, P.M., Ludolph, A.C., et al. (2018). NEK1 loss-of-function mutation induces DNA damage accumulation in ALS patient-derived motoneurons. Stem Cell Res. *30*, 150–162.

Hill, S.J., Mordes, D.A., Cameron, L.A., Neuberg, D.S., Landini, S., Eggan, K., and Livingston, D.M. (2016). Two familial ALS proteins function in prevention/repair of transcription-associated DNA damage. Proc. Natl. Acad. Sci. U. S. A. *113*, E7701–E7709.

Hoch, N.C., Hanzlikova, H., Rulten, S.L., Tétreault, M., Komulainen, E., Ju, L., Hornyak, P., Zeng, Z., Gittens, W., Rey, S.A., et al. (2016). XRCC1 mutation is associated with PARP1 hyperactivation and cerebellar ataxia. Nature *541*, 87–91.

Hochstim, C., Deneen, B., Lukaszewicz, A., Zhou, Q., and Anderson, D.J. (2008). Identification of positionally distinct astrocyte subtypes whose identities are specified by a homeodomain code. Cell *133*, 510–522.

Hollensworth, S.B., Shen, C.C., Sim, J.E., Spitz, D.R., Wilson, G.L., and Ledoux, S.P. (2000). Glial cell type-specific responses to menadione-induced oxidative stress. Free Radic. Biol. Med. *28*, 1161–1174.

Hwang, J., Jin, J., Jeon, S., Moon, S.H., Park, M.Y., Yum, D.Y., Kim, J.H., Kang, J.E., Park, M.H., Kim, E.J., et al. (2020). SOD1 suppresses pro-inflammatory immune responses by protecting against oxidative stress in colitis. Redox Biol. *37*, 101760.

Igoudjil, A., Magrane´, J., Fischer, L.R., Kim, H.J., Hervias, I., Dumont, M., Cortez, C., Glass, J.D., Starkov, A.A., and Manfredi, G. (2011). In vivo pathogenic role of mutant SOD1 localized in the mitochondrial intermembrane space. J. Neurosci. *31*, 15826–15837.

Iguchi, Y., Eid, L., Parent, M., Soucy, G., Bareil, C., Riku, Y., Kawai, K., Takagi, S., Yoshida, M.,

Katsuno, M., et al. (2016). Exosome secretion is a key pathway for clearance of pathological TDP-43. Brain *139*, 3187–3201.

Ihara, Y., Nobukuni, K., Takata, H., and Hayabara, T. (2005). Oxidative stress and metal content in blood and cerebrospinal fluid of amyotrophic lateral sclerosis patients with and without a Cu, Zn-superoxide dismutase mutation. Neurol. Res. *27*, 105–108.

Ingre, C., Roos, P.M., Piehl, F., Kamel, F., and Fang, F. (2015). Risk factors for amyotrophic lateral sclerosis. Clin. Epidemiol. *7*, 181–193.

Jackson, S.P., and Bartek, J. (2009). The DNA-damage response in human biology and disease. Nature *461*, 1071–1078.

Janzer, R.C., and Raff, M.C. (1987). Astrocytes induce blood–brain barrier properties in endothelial cells. Nature *325*, 253–257.

Jasin, M., and Rothstein, R. (2013). Repair of strand breaks by homologous recombination. Cold Spring Harb. Perspect. Biol. *5*, a012740.

Jenjaroenpun, P., Wongsurawat, T., Sutheeworapong, S., and Kuznetsov, V.A. (2017). R-loopDB: a database for R-loop forming sequences (RLFS) and R-loops. Nucleic Acids Res. *45*, D119–D127.

Jeong, H.-K., Ji, K., Min, K., and Joe, E.-H. (2013). Brain inflammation and microglia: facts and misconceptions. Exp. Neurobiol. *22*, 59–67.

Ji, J., Ng, S., Sharma, V., Neculai, D., Hussein, S., Sam, M., Trinh, Q., Church, G.M., McPherson, J.D., Nagy, A., et al. (2012). Elevated coding mutation rate during the reprogramming of human somatic cells into induced pluripotent stem cells. Stem Cells *30*, 435–440.

Jovičić, A., and Gitler, A.D. (2017). Distinct repertoires of microRNAs present in mouse astrocytes compared to astrocyte-secreted exosomes. PLoS One *12*, e0171418.

Jovičič, A., Mertens, J., Boeynaems, S., Bogaert, E., Chai, N., Yamada, S.B., Paul, J.W., Sun, S., Herdy, J.R., Bieri, G., et al. (2015). Modifiers of C9orf72 dipeptide repeat toxicity connect nucleocytoplasmic transport defects to FTD/ALS. Nat. Neurosci. *18*, 1226–1229.

Kang, S.H., Li, Y., Fukaya, M., Lorenzini, I., Cleveland, D.W., Ostrow, L.W., Rothstein, J.D., and Bergles, D.E. (2013). Degeneration and impaired regeneration of gray matter oligodendrocytes in amyotrophic lateral sclerosis. Nat. Neurosci. *16*, 571–579.

Karyka, E., Ramirez, N.B., Webster, C.P., Marchi, P.M., Graves, E.J., Godena, V.K., Marrone, L., Bhargava, A., Ray, S., Ning, K., et al. (2022). SMN-deficient cells exhibit increased ribosomal DNA damage. Life Sci. Alliance *5*.

Katsube, T., Mori, M., Tsuji, H., Shiomi, T., Wang, B., Liu, Q., Nenoi, M., and Onoda, M. (2014). Most hydrogen peroxide-induced histone H2AX phosphorylation is mediated by ATR and is not dependent on DNA double-strand breaks. J. Biochem. *156*, 85–95.

Katsuragi, Y., Ichimura, Y., and Komatsu, M. (2016). Regulation of the Keap1–Nrf2 pathway by p62/SQSTM1. Curr. Opin. Toxicol. *1*, 54–61.

Katyal, S., El-Khamisy, S.F., Russell, H.R., Li, Y., Ju, L., Caldecott, K.W., and McKinnon, P.J. (2007). TDP1 facilitates chromosomal single-strand break repair in neurons and is neuroprotective in vivo. EMBO J. *26*, 4720–4731.

Kawamata, H., Ng, S.K., Diaz, N., Burstein, S., Morel, L., Osgood, A., Sider, B., Higashimori, H., Haydon, P.G., Manfredi, G., et al. (2014). Abnormal intracellular calcium signaling and SNARE-dependent exocytosis contributes to SOD1G93A astrocyte-mediated toxicity in amyotrophic lateral sclerosis. J. Neurosci. *34*, 2331–2348.

Kay, J., Thadhani, E., Samson, L., and Engelward, B. (2019). Inflammation-induced DNA damage, mutations and cancer. DNA Repair (Amst). *83*, 102673.

Kazak, L., Reyes, A., and Holt, I.J. (2012). Minimizing the damage: repair pathways keep mitochondrial DNA intact. Nat. Rev. Mol. Cell Biol. *13*, 659–671.

Khosravi, B., LaClair, K.D., Riemenschneider, H., Zhou, Q., Frottin, F., Mareljic, N., Czuppa, M., Farny, D., Hartmann, H., Michaelsen, M., et al. (2020). Cell-to-cell transmission of C9orf72 poly-(Gly-Ala) triggers key features of ALS/FTD. EMBO J. *39*, e102811.

Kia, A., McAvoy, K., Krishnamurthy, K., Trotti, D., and Pasinelli, P. (2018). Astrocytes expressing ALS-linked mutant FUS induce motor neuron death through release of tumor necrosis factor-alpha. Glia *66*, 1016–1033.

Kilpinen, H., Goncalves, A., Leha, A., Afzal, V., Alasoo, K., Ashford, S., Bala, S., Bensaddek, D., Casale, F.P., Culley, O.J., et al. (2017). Common genetic variation drives molecular heterogeneity in human iPSCs. Nature *546*, 370–375.

Kim, S.H., Henkel, J.S., Beers, D.R., Sengun, I.S., Simpson, E.P., Goodman, J.C., Engelhardt, J.I., Siklós, L., and Appel, S.H. (2003). PARP expression is increased in astrocytes but decreased in motor neurons in the spinal cord of sporadic ALS patients. J. Neuropathol. Exp. Neurol. *62*, 88–103.

King, A., Troakes, C., Smith, B., Nolan, M., Curran, O., Vance, C., Shaw, C.E., and Al-Sarraj, S. (2015). ALS-FUS pathology revisited: singleton FUS mutations and an unusual case with both a FUS and TARDBP mutation. Acta Neuropathol. Commun. *3*.

Kisby, G.E., Milne, J., and Sweatt, C. (1997). Evidence of reduced DNA repair in amyotrophic lateral sclerosis brain tissue. Neuroreport *8*, 1337–1340.

Kobayashi, J., Fujimoto, H., Sato, J., Hayashi, I., Burma, S., Matsuura, S., Chen, D.J., and Komatsu, K. (2012). Nucleolin participates in DNA double-strand break-induced damage response through MDC1-dependent pathway. PLoS One *7*, e49245.

Kok, J.R., Palminha, N.M., Dos Santos Souza, C., El-Khamisy, S.F., and Ferraiuolo, L. (2021). DNA damage as a mechanism of neurodegeneration in ALS and a contributor to astrocyte toxicity. Cell. Mol. Life Sci. *78*, 5707–5729.

Komatsu, M., Kageyama, S., and Ichimura, Y. (2012). p62/SQSTM1/A170: Physiology and pathology. Pharmacol. Res. *66*, 457–462.

Kostrominova, T.Y. (2010). Advanced age-related denervation and fiber-type grouping in skeletal muscle of SOD1 knockout mice. Free Radic. Biol. Med. *49*, 1582–1593.

Krejci, L., Altmannova, V., Spirek, M., and Zhao, X. (2012). Homologous recombination and its regulation. Nucleic Acids Res. *40*, 5795–5818.

Kuno, R., Yoshida, Y., Nitta, A., Nabeshima, T., Wang, J., Sonobe, Y., Kawanokuchi, J., Takeuchi, H., Mizuno, T., and Suzumura, A. (2006). The role of TNF-alpha and its receptors in the production of

NGF and GDNF by astrocytes. Brain Res. *1116*, 12–18.

Kunst, C.B., Mezey, E., Brownstein, M.J., and Patterson, D. (1997). Mutations in SOD1 associated with amyotrophic lateral sclerosis cause novel protein interactions. Nat. Genet. *15*, 91–94.

Kuo, L.J., and Yang, L.-X. (2008). Gamma-H2AX - a novel biomarker for DNA double-strand breaks. In Vivo *22*, 305–309.

Kwon, I., Xiang, S., Kato, M., Wu, L., Theodoropoulos, P., Wang, T., Kim, J., Yun, J., Xie, Y., and McKnight, S.L. (2014). Poly-dipeptides encoded by the C9orf72 repeats bind nucleoli, impede RNA biogenesis, and kill cells. Science (80-.). *345*, 1139–1145.

Lanjakornsiripan, D., Pior, B.J., Kawaguchi, D., Furutachi, S., Tahara, T., Katsuyama, Y., Suzuki, Y., Fukazawa, Y., and Gotoh, Y. (2018). Layer-specific morphological and molecular differences in neocortical astrocytes and their dependence on neuronal layers. Nat. Commun. *9*, 1–15.

Lapasset, L., Milhavet, O., Prieur, A., Besnard, E., Babled, A., Ät-Hamou, N., Leschik, J., Pellestor, F., Ramirez, J.M., De Vos, J., et al. (2011). Rejuvenating senescent and centenarian human cells by reprogramming through the pluripotent state. Genes Dev. *25*, 2248–2253.

Lawyer, T., and Netsky, M.G. (1953). Amyotrophic lateral sclerosis: a clinicoanatomic study of fifty-three cases. A.M.A. Arch. Neurol. Psychiatry *69*, 171–192.

LeDoux, S.P., Williams, B.A., Hollensworth, B.S., Shen, C., Thomale, J., Rajewsky, M.F., Brent, T.P., and Wilson, G.L. (1996). Glial cell-specific differences in repair of O6-methylguanine. Cancer Res. *56*, 5615–5619.

Lee, K.H., Zhang, P., Kim, H.J., Mitrea, D.M., Sarkar, M., Freibaum, B.D., Cika, J., Coughlin, M., Messing, J., Molliex, A., et al. (2016). C9orf72 dipeptide repeats impair the assembly, dynamics, and function of membrane-less organelles. Cell *167*, 774–788.

Lee, Y., Katyal, S., Li, Y., El-Khamisy, S.F., Russell, H.R., Caldecott, K.W., and McKinnon, P.J. (2009). The genesis of cerebellar interneurons and the prevention of neural DNA damage require XRCC1. Nat. Neurosci. *12*, 973–980.

Lee, Y.B., Baskaran, P., Gomez-Deza, J., Chen, H.J., Nishimura, A.L., Smith, B.N., Troakes, C., Adachi, Y., Stepto, A., Petrucelli, L., et al. (2017). C9orf72 poly GA RAN-translated protein plays a key role in amyotrophic lateral sclerosis via aggregation and toxicity. Hum. Mol. Genet. *26*, 4765–4777.

Li, T., Niu, J., Yu, G., Ezan, P., Yi, C., Wang, X., Koulakoff, A., Gao, X., Chen, X., Sáez, J.C., et al. (2020). Connexin 43 deletion in astrocytes promotes CNS remyelination by modulating local inflammation. Glia *68*, 1201–1212.

Liddelow, S.A., and Barres, B.A. (2017). Reactive astrocytes: production, function, and therapeutic potential. Immunity *46*, 957–967.

Lieber, M.R. (2010). The mechanism of double-strand DNA break repair by the nonhomologous DNA end-joining pathway. Annu. Rev. Biochem. *79*, 181–211.

Liesi, P., and Silver, J. (1988). Is astrocyte laminin involved in axon guidance in the mammalian CNS? Dev. Biol. *130*, 774–785.

Lin, L., Yuan, J., Sander, B., and Golas, M.M. (2015). In vitro differentiation of human neural progenitor cells into striatal GABAergic neurons. Stem Cells Transl. Med. *4*, 775–788.

Lin, Y., McMahon, A., Driscoll, G., Bullock, S., Zhao, J., and Yan, S. (2021). Function and molecular mechanisms of APE2 in genome and epigenome integrity. Mutat. Res. Mutat. Res. *787*, 108347.

Lirussi, L., Antoniali, G., Vascotto, C., D'Ambrosio, C., Poletto, M., Romanello, M., Marasco, D., Leone, M., Quadrifoglio, F., Bhakat, K.K., et al. (2012). Nucleolar accumulation of APE1 depends on charged lysine residues that undergo acetylation upon genotoxic stress and modulate its BER activity in cells. Mol. Biol. Cell *23*, 4079–4096.

Liu, L.F., Desai, S.D., Li, T.K., Mao, Y., Sun, M., and Sim, S.P. (2000). Mechanism of action of camptothecin. Ann. N. Y. Acad. Sci. *922*, 1–10.

Lopez-Gonzalez, R., Lu, Y., Gendron, T.F., Karydas, A., Tran, H., Yang, D., Petrucelli, L., Miller, B.L., Almeida, S., and Gao, F.-B. (2016). Poly(GR) in C9ORF72-related ALS/FTD compromises mitochondrial function and increases oxidative stress and DNA damage in iPSC-derived motor neurons. Neuron *92*, 383–391.

Lopez-Gonzalez, R., Yang, D., Pribadi, M., Kim, T.S., Krishnan, G., Choi, S.Y., Lee, S., Coppola, G., and Gao, F.B. (2019). Partial inhibition of the overactivated Ku80-dependent DNA repair pathway rescues neurodegeneration in C9ORF72-ALS/FTD. Proc. Natl. Acad. Sci. U. S. A. *116*, 9628–9633.

Mackenzie, I.R.A., Bigio, E.H., Ince, P.G., Geser, F., Neumann, M., Cairns, N.J., Kwong, L.K., Forman, M.S., Ravits, J., Stewart, H., et al. (2007). Pathological TDP-43 distinguishes sporadic amyotrophic lateral sclerosis from amyotrophic lateral sclerosis with SOD1 mutations. Ann. Neurol. *61*, 427–434.

Mackenzie, I.R.A., Frick, P., and Neumann, M. (2014). The neuropathology associated with repeat expansions in the C9ORF72 gene. Acta Neuropathol. *127*, 347–357.

Mackenzie, I.R.A., Frick, P., Grässer, F.A., Gendron, T.F., Petrucelli, L., Cashman, N.R., Edbauer, D., Kremmer, E., Prudlo, J., Troost, D., et al. (2015). Quantitative analysis and clinico-pathological correlations of different dipeptide repeat protein pathologies in C9ORF72 mutation carriers. Acta Neuropathol. *130*, 845–861.

MacKenzie, I.R., Arzberger, T., Kremmer, E., Troost, D., Lorenzl, S., Mori, K., Weng, S.M., Haass, C., Kretzschmar, H.A., Edbauer, D., et al. (2013). Dipeptide repeat protein pathology in C9ORF72 mutation cases: clinico-pathological correlations. Acta Neuropathol. *126*, 859–879.

Madill, M., McDonagh, K., Ma, J., Vajda, A., McLoughlin, P., O'Brien, T., Hardiman, O., and Shen, S. (2017). Amyotrophic lateral sclerosis patient iPSC-derived astrocytes impair autophagy via non-cell autonomous mechanisms. Mol. Brain *10*.

Mahmoud, S., Gharagozloo, M., Simard, C., and Gris, D. (2019). Astrocytes maintain glutamate homeostasis in the CNS by controlling the balance between glutamate uptake and release. Cells *8*, 184.

Majounie, E., Renton, A.E., Mok, K., Dopper, E.G.P., Waite, A., Rollinson, S., Chiò, A., Restagno, G., Nicolaou, N., Simon-Sanchez, J., et al. (2012). Frequency of the C9orf72 hexanucleotide repeat expansion in patients with amyotrophic lateral sclerosis and frontotemporal dementia: a cross-sectional study. Lancet Neurol. *11*, 323–330.

Mancuso, R., Oliván, S., Mancera, P., Pastén-Zamorano, A., Manzano, R., Casas, C., Osta, R., and Navarro, X. (2012). Effect of genetic background on onset and disease progression in the SOD1-G93A model of amyotrophic lateral sclerosis. Amyotroph. Lateral Scler. *13*, 302–310.

Mann, D.M., Rollinson, S., Robinson, A., Bennion Callister, J., Thompson, J.C., Snowden, J.S., Gendron, T., Petrucelli, L., Masuda-Suzukake, M., Hasegawa, M., et al. (2013). Dipeptide repeat proteins are present in the p62 positive inclusions in patients with frontotemporal lobar degeneration and motor neurone disease associated with expansions in C9ORF72. Acta Neuropathol. Commun. *1*, 1–13.

Marchetto, M.C.N., Muotri, A.R., Mu, Y., Smith, A.M., Cezar, G.G., and Gage, F.H. (2008). Non-cell-autonomous effect of human SOD1G37R astrocytes on motor neurons derived from human embryonic stem cells. Cell Stem Cell *3*, 649–657.

Marchi, P.M., Marrone, L., Brasseur, L., Coens, A., Webster, C.P., Bousset, L., Destro, M., Smith, E.F., Walther, C.G., Alfred, V., et al. (2022). C9ORF72-derived poly-GA DPRs undergo endocytic uptake in iAstrocytes and spread to motor neurons. Life Sci. Alliance *5*, e202101276.

Marina, N., Christie, I.N., Korsak, A., Doronin, M., Brazhe, A., Hosford, P.S., Wells, J.A., Sheikhbahaei, S., Humoud, I., Paton, J.F.R., et al. (2020). Astrocytes monitor cerebral perfusion and control systemic circulation to maintain brain blood flow. Nat. Commun. *11*, 1–9.

Mastrocola, A.S., Kim, S.H., Trinh, A.T., Rodenkirch, L.A., and Tibbetts, R.S. (2013). The RNA-binding protein fused in sarcoma (FUS) functions downstream of poly(ADP-ribose) polymerase (PARP) in response to DNA damage. J. Biol. Chem. *288*, 24731–24741.

Mattout, A., Biran, A., and Meshorer, E. (2011). Global epigenetic changes during somatic cell reprogramming to iPS cells. J. Mol. Cell Biol. *3*, 341–350.

May, S., Hornburg, D., Schludi, M.H., Arzberger, T., Rentzsch, K., Schwenk, B.M., Grässer, F.A., Mori, K., Kremmer, E., Banzhaf-Strathmann, J., et al. (2014). C9orf72 FTLD/ALS-associated Gly-Ala dipeptide repeat proteins cause neuronal toxicity and Unc119 sequestration. Acta Neuropathol. *128*, 485–503.

Metea, M.R., Kofuji, P., and Newman, E.A. (2007). Neurovascular coupling is not mediated by potassium siphoning from glial cells. J. Neurosci. *27*, 2468–2471.

Meyer, K., Ferraiuolo, L., Miranda, C.J., Likhite, S., McElroy, S., Renusch, S., Ditsworth, D., Lagier-Tourenne, C., Smith, R.A., Ravits, J., et al. (2014). Direct conversion of patient fibroblasts demonstrates non-cell autonomous toxicity of astrocytes to motor neurons in familial and sporadic ALS. Proc. Natl. Acad. Sci. U. S. A. *111*, 829–832.

Miller, R.G., Mitchell, J.D., and Moore, D.H. (2012). Riluzole for amyotrophic lateral sclerosis (ALS)/motor neuron disease (MND). Cochrane Database Syst. Rev.

Mills, J.A., Wang, K., Paluru, P., Ying, L., Lu, L., Galvão, A.M., Xu, D., Yao, Y., Sullivan, S.K., Sullivan, L.M., et al. (2013). Clonal genetic and hematopoietic heterogeneity among human-induced pluripotent stem cell lines. Blood *122*, 2047–2051.

Mirza-Aghazadeh-Attari, M., Mohammadzadeh, A., Yousefi, B., Mihanfar, A., Karimian, A., and Majidinia, M. (2019). 53BP1: A key player of DNA damage response with critical functions in cancer. DNA Repair (Amst). *73*, 110–119.

Mitra, J., Guerrero, E.N., Hegde, P.M., Liachko, N.F., Wang, H., Vasquez, V., Gao, J., Pandey, A., Taylor, J.P., Kraemer, B.C., et al. (2019). Motor neuron disease-associated loss of nuclear TDP-43 is linked to DNA double-strand break repair defects. Proc. Natl. Acad. Sci. U. S. A. *116*, 4696–4705.

Mitsumoto, H., Santella, R.M., Liu, X., Bogdanov, M., Zipprich, J., Wu, H.-C., Mahata, J., Kilty, M., Bednarz, K., Bell, D., et al. (2008). Oxidative stress biomarkers in sporadic ALS. Amyotroph. Lateral Scler. *9*, 177–183.

Mizielinska, S., Grönke, S., Niccoli, T., Ridler, C.E., Clayton, E.L., Devoy, A., Moens, T., Norona, F.E., Woollacott, I.O.C., Pietrzyk, J., et al. (2014). C9orf72 repeat expansions cause neurodegeneration in Drosophila through arginine-rich proteins. Science (80-.). *345*, 1192–1194.

Mizielinska, S., Ridler, C.E., Balendra, R., Thoeng, A., Woodling, N.S., Grässer, F.A., Plagnol, V., Lashley, T., Partridge, L., and Isaacs, A.M. (2017). Bidirectional nucleolar dysfunction in C9orf72 frontotemporal lobar degeneration. Acta Neuropathol. Commun. *5*.

Mizuno, Y., Amari, M., Takatama, M., Aizawa, H., Mihara, B., and Okamoto, K. (2006). Immunoreactivities of p62, an ubiqutin-binding protein, in the spinal anterior horn cells of patients with amyotrophic lateral sclerosis. J. Neurol. Sci. *249*, 13–18.

Moore, H.M., Bai, B., Boisvert, F.M., Latonen, L., Rantanen, V., Simpson, J.C., Pepperkok, R., Lamond, A.I., and Laiho, M. (2011). Quantitative proteomics and dynamic imaging of the nucleolus reveal distinct responses to UV and ionizing radiation. Mol. Cell. Proteomics *10*.

Mori, K., Weng, S.-M., Arzberger, T., May, S., Rentzsch, K., Kremmer, E., Schmid, B., Kretzschmar, H.A., Cruts, M., Van Broeckhoven, C., et al. (2013a). The C9orf72 GGGGCC repeat is translated into aggregating dipeptide-repeat proteins in FTLD/ALS. Science (80-.). *339*, 1335–1338.

Mori, K., Lammich, S., Mackenzie, I.R.A., Forné, I., Zilow, S., Kretzschmar, H., Edbauer, D., Janssens, J., Kleinberger, G., Cruts, M., et al. (2013b). HnRNP A3 binds to GGGGCC repeats and is a constituent of p62-positive/TDP43-negative inclusions in the hippocampus of patients with C9orf72 mutations. Acta Neuropathol. *125*, 413–423.

Muller, F.L., Song, W., Liu, Y., Chaudhuri, A., Pieke-Dahl, S., Strong, R., Huang, T.-T., Epstein, C.J., Roberts, L.J., Csete, M., et al. (2006). Absence of CuZn superoxide dismutase leads to elevated oxidative stress and acceleration of age-dependent skeletal muscle atrophy. Free Radic. Biol. Med. *40*, 1993–2004.

Murata, T., Ohtsuka, C., and Terayama, Y. (2008). Increased mitochondrial oxidative damage and oxidative DNA damage contributes to the neurodegenerative process in sporadic amyotrophic lateral sclerosis. Free Radic. Res. *42*, 221–225.

Murayama, S., Inoue, K., Kawakami, H., Bouldin, T.W., and Suzuki, K. (1991). A unique pattern of astrocytosis in the primary motor area in amyotrophic lateral sclerosis. Acta Neuropathol. *82*, 456–461.

Nagai, M., Re, D.B., Nagata, T., Chalazonitis, A., Jessell, T.M., Wichterle, H., and Przedborski, S. (2007). Astrocytes expressing ALS-linked mutated SOD1 release factors selectively toxic to motor neurons. Nat. Neurosci. *10*, 615–622.

Nagano, I., Murakami, T., Manabe, Y., and Abe, K. (2002). Early decrease of survival factors and DNA repair enzyme in spinal motor neurons of presymptomatic transgenic mice that express a mutant SOD1 gene. In Life Sciences, (Pergamon), pp. 541–548.

Naumann, M., Pal, A., Goswami, A., Lojewski, X., Japtok, J., Vehlow, A., Naujock, M., Günther, R., Jin, M., Stanslowsky, N., et al. (2018). Impaired DNA damage response signaling by FUS-NLS mutations leads to neurodegeneration and FUS aggregate formation. Nat. Commun. *9*, 335.

Neumann, M., Sampathu, D.M., Kwong, L.K., Truax, A.C., Micsenyi, M.C., Chou, T.T., Bruce, J., Schuck, T., Grossman, M., Clark, C.M., et al. (2006). Ubiquitinated TDP-43 in frontotemporal lobar degeneration and amyotrophic lateral sclerosis. Science (80-.). *314*, 130–133.

Nihei, K., McKee, A.C., and Kowall, N.W. (1993). Patterns of neuronal degeneration in the motor cortex of amyotrophic lateral sclerosis patients. Acta Neuropathol. *86*, 55–64.

Nihei, Y., Mori, K., Werner, G., Arzberger, T., Zhou, Q., Khosravi, B., Japtok, J., Hermann, A., Sommacal, A., Weber, M., et al. (2020). Poly-glycine–alanine exacerbates C9orf72 repeat expansion-mediated DNA damage via sequestration of phosphorylated ATM and loss of nuclear hnRNPA3. Acta Neuropathol. *139*, 99–118.

Ogawa, L.M., and Baserga, S.J. (2017). Crosstalk between the nucleolus and the DNA damage response. Mol. Biosyst. *13*, 443–455.

Onn, L., Portillo, M., Ilic, S., Cleitman, G., Stein, D., Kaluski, S., Shirat, I., Slobodnik, Z., Einav, M., Erdel, F., et al. (2020). SIRT6 is a DNA double-strand break sensor. Elife *9*, e51636.

Panier, S., and Boulton, S.J. (2013). Double-strand break repair: 53BP1 comes into focus. Nat. Rev. Mol. Cell Biol. *15*, 7–18.

Paré, B., Lehmann, M., Beaudin, M., Nordström, U., Saikali, S., Julien, J.P., Gilthorpe, J.D., Marklund, S.L., Cashman, N.R., Andersen, P.M., et al. (2018). Misfolded SOD1 pathology in sporadic amyotrophic lateral sclerosis. Sci. Rep. *8*.

Parsons, J.L., and Dianov, G.L. (2013). Co-ordination of base excision repair and genome stability. DNA Repair (Amst). *12*, 326–333.

Pascal, J.M. (2018). The comings and goings of PARP-1 in response to DNA damage. DNA Repair (Amst). *71*, 177–182.

Paulson, O.B., and Newman, E.A. (1987). Does the release of potassium from astrocyte endfeet regulate cerebral blood flow? Science (80-.). *237*, 896–898.

Pekny, M., and Pekna, M. (2014). Astrocyte reactivity and reactive astrogliosis: costs and benefits. Physiol. Rev. *94*, 1077–1098.

Pellerin, L., and Magistretti, P.J. (1994). Glutamate uptake into astrocytes stimulates aerobic glycolysis: a mechanism coupling neuronal activity to glucose utilization. Proc. Natl. Acad. Sci. *91*, 10625–10629.

Penndorf, D., Tadić, V., Witte, O.W., Grosskreutz, J., and Kretz, A. (2017). DNA strand breaks and TDP-43 mislocation are absent in the murine hSOD1G93A model of amyotrophic lateral sclerosis in vivo and in vitro. PLoS One *12*, e0183684.

Phoenix, P., Raymond, M.A., Massé, É., and Drolet, M. (1997). Roles of DNA Topoisomerases in the Regulation of R-loop Formation in Vitro*. J. Biol. Chem. *272*, 1473–1479.

Pickles, S., Semmler, S., Broom, H.R., Destroismaisons, L., Legroux, L., Arbour, N., Meiering, E., Cashman, N.R., and Vande Velde, C. (2016). ALS-linked misfolded SOD1 species have divergent impacts on mitochondria. Acta Neuropathol. Commun. *4*.

Pietrzak, M., Smith, S.C., Geralds, J.T., Hagg, T., Gomes, C., and Hetman, M. (2011). Nucleolar disruption and apoptosis are distinct neuronal responses to etoposide-induced DNA damage. J.

Neurochem. *117*, 1033–1046.

Poletto, M., Lirussi, L., David M. Wilson, 3rd, and Tell, G. (2014). Nucleophosmin modulates stability, activity, and nucleolar accumulation of base excision repair proteins. Mol. Biol. Cell *25*, 1641–1652.

Post, Y., and Clevers, H. (2019). Defining adult stem cell function at its simplest: the ability to replace lost cells through mitosis. Cell Stem Cell *25*, 174–183.

Qiu, H., Lee, S., Shang, Y., Wang, W.-Y., Au, K.F., Kamiya, S., Barmada, S.J., Finkbeiner, S., Lui, H., Carlton, C.E., et al. (2014). ALS-associated mutation FUS-R521C causes DNA damage and RNA splicing defects. J. Clin. Invest. *124*, 981–999.

Quek, H., Cuní-López, C., Stewart, R., Colletti, T., Notaro, A., Nguyen, T.H., Sun, Y., Guo, C.C., Lupton, M.K., Roberts, T.L., et al. (2022). ALS monocyte-derived microglia-like cells reveal cytoplasmic TDP-43 accumulation, DNA damage, and cell-specific impairment of phagocytosis associated with disease progression. J. Neuroinflammation *19*, 1–21.

Ramirez, P., Crouch, R.J., Cheung, V.G., and Grunseich, C. (2021). R-loop analysis by dot-blot. J. Vis. Exp. *167*, e62069.

Ranneh, Y., Ali, F., Akim, A.M., Hamid, H.A., Khazaai, H., and Fadel, A. (2017). Crosstalk between reactive oxygen species and pro-inflammatory markers in developing various chronic diseases: a review. Appl. Biol. Chem. *60*, 327–338.

Ransy, C., Vaz, C., Lombès, A., and Bouillaud, F. (2020). Use of H2O2 to Cause Oxidative Stress, the Catalase Issue. Int. J. Mol. Sci. *21*, 1–14.

Ray Chaudhuri, A., and Nussenzweig, A. (2017). The multifaceted roles of PARP1 in DNA repair and chromatin remodelling. Nat. Rev. Mol. Cell Biol. *18*, 610–621.

Re, D.B., Le Verche, V., Yu, C., Amoroso, M.W., Politi, K.A., Phani, S., Ikiz, B., Hoffmann, L., Koolen, M., Nagata, T., et al. (2014). Necroptosis drives motor neuron death in models of both sporadic and familial ALS. Neuron *81*, 1001–1008.

Reddy, K., Schmidt, M.H.M., Geist, J.M., Thakkar, N.P., Panigrahi, G.B., Wang, Y.-H., and Pearson, C.E. (2014). Processing of double-R-loops in (CAG)·(CTG) and C9orf72 (GGGGCC)·(GGCCCC) repeats causes instability. Nucleic Acids Res. *42*, 10473–10487.

Renton, A.E., Majounie, E., Waite, A., Simón-Sánchez, J., Rollinson, S., Gibbs, J.R., Schymick, J.C., Laaksovirta, H., van Swieten, J.C., Myllykangas, L., et al. (2011). A hexanucleotide repeat expansion in C9ORF72 is the cause of chromosome 9p21-linked ALS-FTD. Neuron *72*, 257–268.

Renton, A.E., Chiò, A., and Traynor, B.J. (2014). State of play in amyotrophic lateral sclerosis genetics. Nat. Neurosci. *17*, 17–23.

Revet, I., Feeney, L., Bruguera, S., Wilson, W., Dong, T.K., Oh, D.H., Dankort, D., and Cleaver, J.E. (2011). Functional relevance of the histone γH2Ax in the response to DNA damaging agents. Proc. Natl. Acad. Sci. U. S. A. *108*, 8663–8667.

Riancho, J., Castanedo-Vázquez, D., Gil-Bea, F., Tapia, O., Arozamena, J., Durán-Vían, C., Sedano, M.J., Berciano, M.T., Lopez de Munain, A., and Lafarga, M. (2020). ALS-derived fibroblasts exhibit reduced proliferation rate, cytoplasmic TDP-43 aggregation and a higher susceptibility to DNA

damage. J. Neurol. 1–9.

Ribon, M., Leone, C., Chiot, A., Berriat, F., Rampanana, M., Cottin, J., Bohl, D., Millecamps, S., Lobsiger, C.S., Heneka, M.T., et al. (2021). Deletion of the inflammatory S100-A9/MRP14 protein does not influence survival in hSOD1G93A ALS mice. Neurobiol. Aging *101*, 181–186.

Richard, J.P., and Maragakis, N.J. (2015). Induced pluripotent stem cells from ALS patients for disease modeling. Brain Res. *1607*, 15–25.

Rogakou, E.P., Nieves-Neira, W., Boon, C., Pommier, Y., and Bonner, W.M. (2000). Initiation of DNA fragmentation during apoptosis induces phosphorylation of H2AX histone at serine 139. J. Biol. Chem. *275*, 9390–9395.

Rosen, D.R., Siddique, T., Patterson, D., Figlewicz, D.A., Sapp, P., Hentati, A., Donaldson, D., Goto, J., O'Regan, J.P., Deng, H.-X., et al. (1993). Mutations in Cu/Zn superoxide dismutase gene are associated with familial amyotrophic lateral sclerosis. Nature *362*, 59–62.

Rosenegger, D.G., Tran, C.H.T., Wamsteeker Cusulin, J.I., and Gordon, G.R. (2015). Tonic local brain blood flow control by astrocytes independent of phasic neurovascular coupling. J. Neurosci. *35*, 13463–13474.

Ross, W., and Hall, P.A. (1995). Ki67: From antibody to molecule to understanding? J. Clin. Pathol. - Clin. Mol. Pathol. *48*, M113–M117.

Rubino, E., Rainero, I., Chiò, A., Rogaeva, E., Galimberti, D., Fenoglio, P., Grinberg, Y., Isaia, G., Calvo, A., Gentile, S., et al. (2012). SQSTM1 mutations in frontotemporal lobar degeneration and amyotrophic lateral sclerosis. Neurology *79*, 1556–1562.

Rux, D.R., and Wellik, D.M. (2017). Hox genes in the adult skeleton: novel functions beyond embryonic development. Dev. Dyn. *246*, 310–317.

Saccon, R.A., Bunton-Stasyshyn, R.K.A., Fisher, E.M.C., and Fratta, P. (2013). Is SOD1 loss of function involved in amyotrophic lateral sclerosis? Brain *136*, 2342–2358.

Santiago, J.A., Quinn, J.P., and Potashkin, J.A. (2021). Network analysis identifies sex-specific gene expression changes in blood of amyotrophic lateral sclerosis patients. Int. J. Mol. Sci. *22*, 7150.

Sanz, L.A., and Chédin, F. (2019). High-resolution, strand-specific R-loop mapping via S9.6-based DNA–RNA immunoprecipitation and high-throughput sequencing. Nat. Protoc. *14*, 1734–1755.

Schiffer, D., Cordera, S., Cavalla, P., and Migheli, A. (1996). Reactive astrogliosis of the spinal cord in amyotrophic lateral sclerosis. J. Neurol. Sci. *139*, 27–33.

Schludi, M.H., May, S., Grässer, F.A., Rentzsch, K., Kremmer, E., Küpper, C., Klopstock, T., Ceballos-Baumann, A., Danek, A., Diehl-Schmid, J., et al. (2015). Distribution of dipeptide repeat proteins in cellular models and C9orf72 mutation cases suggests link to transcriptional silencing. Acta Neuropathol. *130*, 537–555.

Schneider, L., Fumagalli, M., and Di Fagagna, F.D.A. (2012). Terminally differentiated astrocytes lack DNA damage response signaling and are radioresistant but retain DNA repair proficiency. Cell Death Differ. *19*, 582–591.

Schousboe, A., Sarup, A., Bak, L.K., Waagepetersen, H.S., and Larsson, O.M. (2004). Role of astrocytic transport processes in glutamatergic and GABAergic neurotransmission. Neurochem. Int.

45, 521–527.

Scotter, E.L., Chen, H.J., and Shaw, C.E. (2015). TDP-43 proteinopathy and ALS: insights into disease mechanisms and therapeutic targets. Neurotherapeutics *12*, 352–363.

Sellier, C., Campanari, M.-L., Julie Corbier, C., Gaucherot, A., Kolb-Cheynel, I., Oulad-Abdelghani, M., Ruffenach, F., Page, A., Ciura, S., Kabashi, E., et al. (2016). Loss of C9ORF72 impairs autophagy and synergizes with polyQ Ataxin-2 to induce motor neuron dysfunction and cell death. EMBO J. *35*, 1276–1297.

Serio, A., Bilican, B., Barmada, S.J., Ando, D.M., Zhao, C., Siller, R., Burr, K., Haghi, G., Story, D., Nishimura, A.L., et al. (2013). Astrocyte pathology and the absence of non-cell autonomy in an induced pluripotent stem cell model of TDP-43 proteinopathy. Proc. Natl. Acad. Sci. U. S. A. *110*, 4697–4702.

Sgodda, M., and Cantz, T. (2013). Small but significant: inter- and intrapatient variations in iPS cell–based disease modeling. Mol. Ther. *21*, 5–7.

Shaikh, A.Y., and Martin, L.J. (2002). DNA base-excision repair enzyme apurinic/apyrimidinic endonuclease/redox factor-1 is increased and competent in the brain and spinal cord of individuals with amyotrophic lateral sclerosis. NeuroMolecular Med. *2*, 47–60.

Shefner, J.M., Al-Chalabi, A., Baker, M.R., Cui, L.Y., de Carvalho, M., Eisen, A., Grosskreutz, J., Hardiman, O., Henderson, R., Matamala, J.M., et al. (2020). A proposal for new diagnostic criteria for ALS. Clin. Neurophysiol. *131*, 1975–1978.

Shi, Y., Lin, S., Staats, K.A., Li, Y., Chang, W.H., Hung, S.T., Hendricks, E., Linares, G.R., Wang, Y., Son, E.Y., et al. (2018). Haploinsufficiency leads to neurodegeneration in C9ORF72 ALS/FTD human induced motor neurons. Nat. Med. *24*, 313–325.

Shibata, A., Kamada, N., Masumura, K.I., Nohmi, T., Kobayashi, S., Teraoka, H., Nakagama, H., Sugimura, T., Suzuki, H., and Masutani, M. (2004). Parp-1 deficiency causes an increase of deletion mutations and insertions/rearrangements in vivo after treatment with an alkylating agent. Oncogene *24*, 1328–1337.

Shutova, M. V., Surdina, A. V., Ischenko, D.S., Naumov, V.A., Bogomazova, A.N., Vassina, E.M., Alekseev, D.G., Lagarkova, M.A., and Kiselev, S.L. (2016). An integrative analysis of reprogramming in human isogenic system identified a clone selection criterion. Cell Cycle *15*, 986–997.

Simone, R., Balendra, R., Moens, T.G., Preza, E., Wilson, K.M., Heslegrave, A., Woodling, N.S., Niccoli, T., Gilbert-Jaramillo, J., Abdelkarim, S., et al. (2018). G-quadruplex-binding small molecules ameliorate C9orf72 FTD/ALS pathology in vitro and in vivo. EMBO Mol. Med. *10*, 22–31.

Skourti-Stathaki, K., and Proudfoot, N.J. (2014). A double-edged sword: R loops as threats to genome integrity and powerful regulators of gene expression. Genes Dev. *28*, 1384–1396.

Smolka, J.A., Sanz, L.A., Hartono, S.R., and Chédin, F. (2021). Recognition of RNA by the S9.6 antibody creates pervasive artifacts when imaging RNA:DNA hybrids. J. Cell Biol. *220*, e202004079.

Soares, J.P., Cortinhas, A., Bento, T., Leitão, J.C., Collins, A.R., Gaivã, I., and Mota, M.P. (2014). Aging and DNA damage in humans: a meta-analysis study. Aging (Albany NY) *6*, 432–439.

Song, S.W., Miranda, C.J., Braun, L., Meyer, K., Frakes, A.E., Ferraiuolo, L., Likhite, S., Bevan, A.K.,

Foust, K.D., McConnell, M.J., et al. (2016). Major histocompatibility complex class I molecules protect motor neurons from astrocyte-induced toxicity in amyotrophic lateral sclerosis. Nat. Med. *22*, 397–403.

Spies, J., Waizenegger, A., Barton, O., Sürder, M., Wright, W.D., Heyer, W.-D., and Löbrich, M. (2016). Nek1 regulates Rad54 to orchestrate homologous recombination and replication fork stability. Mol. Cell *62*, 903–917.

Ströbel, T., Madlener, S., Tuna, S., Vose, S., Lagerweij, T., Wurdinger, T., Vierlinger, K., Wöhrer, A., Price, B.D., Demple, B., et al. (2017). Ape1 guides DNA repair pathway choice that is associated with drug tolerance in glioblastoma. Sci. Rep. *7*, 1–13.

Swain, U., and Subba Rao, K. (2011). Study of DNA damage via the comet assay and base excision repair activities in rat brain neurons and astrocytes during aging. Mech. Ageing Dev. *132*, 374–381.

Takahashi, K., and Yamanaka, S. (2006). Induction of pluripotent stem cells from mouse embryonic and adult fibroblast cultures by defined factors. Cell *126*, 663–676.

Takahashi, K., Tanabe, K., Ohnuki, M., Narita, M., Ichisaka, T., Tomoda, K., and Yamanaka, S. (2007). Induction of pluripotent stem cells from adult human fibroblasts by defined factors. Cell *131*, 861–872.

Takata, N., and Hirase, H. (2008). Cortical layer 1 and layer 2/3 astrocytes exhibit distinct calcium dynamics in vivo. PLoS One *3*, e2525.

Tan, J., Wang, X., Phoon, L., Yang, H., and Lan, L. (2020). Resolution of ROS-induced G-quadruplexes and R-loops at transcriptionally active sites is dependent on BLM helicase. FEBS Lett. *594*, 1359–1367.

Tanaka, E., Fukuda, H., Nakashima, K., Tsuchiya, N., Seimiya, H., and Nakagama, H. (2007). HnRNP A3 binds to and protects mammalian telomeric repeats in vitro. Biochem. Biophys. Res. Commun. *358*, 608–614.

Tandan, R., and Bradley, W.G. (1985). Amyotrophic lateral sclerosis: Part 1. Clinical features, pathology, and ethical issues in management. Ann. Neurol. *18*, 271–280.

Tang, Y., Liu, M.-L., Zang, T., and Zhang, C.-L. (2017). Direct reprogramming rather than iPSC-based reprogramming maintains aging hallmarks in human motor neurons. Front. Mol. Neurosci. *10*, 359.

Tanida, I. (2011). Autophagy basics. Microbiol. Immunol. *55*, 1–11.

Taylor, J.P., Brown, R.H., and Cleveland, D.W. (2016). Decoding ALS: from genes to mechanism. Nature *539*, 197–206.

Teng, Y., Yadav, T., Duan, M., Tan, J., Xiang, Y., Gao, B., Xu, J., Liang, Z., Liu, Y., Nakajima, S., et al. (2018). ROS-induced R loops trigger a transcription-coupled but BRCA1/2-independent homologous recombination pathway through CSB. Nat. Commun. *9*, 1–12.

Tong, J., Huang, C., Bi, F., Wu, Q., Huang, B., Liu, X., Li, F., Zhou, H., and Xia, X.G. (2013). Expression of ALS-linked TDP-43 mutant in astrocytes causes non-cell-autonomous motor neuron death in rats. EMBO J. *32*, 1917–1926.

Tran, H., Almeida, S., Moore, J., Gendron, T.F., Chalasani, U., Lu, Y., Du, X., Nickerson, J.A., Petrucelli, L., Weng, Z., et al. (2015). Differential toxicity of nuclear RNA foci versus dipeptide repeat

proteins in a Drosophila model of C9ORF72 FTD/ALS. Neuron *87*, 1207–1214.

Tripathi, P., Rodriguez-Muela, N., Klim, J.R., de Boer, A.S., Agrawal, S., Sandoe, J., Lopes, C.S., Ogliari, K.S., Williams, L.A., Shear, M., et al. (2017). Reactive astrocytes promote ALS-like degeneration and intracellular protein aggregation in human motor neurons by disrupting autophagy through TGF-β1. Stem Cell Reports *9*, 667–680.

Turinetto, V., and Giachino, C. (2015). Multiple facets of histone variant H2AX: a DNA double-strand-break marker with several biological functions. Nucleic Acids Res. *43*, 2489–2498.

Turner, M.R., and Kiernan, M.C. (2012). Does interneuronal dysfunction contribute to neurodegeneration in amyotrophic lateral sclerosis? Amyotroph. Lateral Scler. *13*, 245–250.

Turner, M.R., Cagnin, A., Turkheimer, F.E., Miller, C.C.J., Shaw, C.E., Brooks, D.J., Leigh, P.N., and Banati, R.B. (2004). Evidence of widespread cerebral microglial activation in amyotrophic lateral sclerosis: an [11C](R)-PK11195 positron emission tomography study. Neurobiol. Dis. *15*, 601–609.

Turner, M.R., Bowser, R., Bruijn, L., Dupuis, L., Ludolph, A., McGrath, M., Manfredi, G., Maragakis, N., Miller, R.G., Pullman, S.L., et al. (2013). Mechanisms, models and biomarkers in amyotrophic lateral sclerosis. Amyotroph. Lateral Scler. Front. Degener. *14*, 19–32.

Turrens, J.F. (2003). Mitochondrial formation of reactive oxygen species. J. Physiol. *552*, 335–344.

Valavanidis, A., Vlachogianni, T., and Fiotakis, C. (2009). 8-hydroxy-2' -deoxyguanosine (8-OHdG): A critical biomarker of oxidative stress and carcinogenesis. J. Environ. Sci. Heal. Part C *27*, 120–139.

Valori, C.F., Brambilla, L., Martorana, F., and Rossi, D. (2014). The multifaceted role of glial cells in amyotrophic lateral sclerosis. Cell. Mol. Life Sci. *71*, 287–297.

Vance, C., Rogelj, B., Hortobágyi, T., De Vos, K.J., Nishimura, A.L., Sreedharan, J., Hu, X., Smith, B., Ruddy, D., Wright, P., et al. (2009). Mutations in FUS, an RNA processing protein, cause familial amyotrophic lateral sclerosis type 6. Science (80-.). *323*, 1208–1211.

Varcianna, A., Myszczynska, M.A., Castelli, L.M., O'Neill, B., Kim, Y., Talbot, J., Nyberg, S., Nyamali, I., Heath, P.R., Stopford, M.J., et al. (2019). Micro-RNAs secreted through astrocyte-derived extracellular vesicles cause neuronal network degeneration in C9orf72 ALS. EBioMedicine *40*, 626–635.

Vargas, M.R., Johnson, D.A., Sirkis, D.W., Messing, A., and Johnson, J.A. (2008). Nrf2 activation in astrocytes protects against neurodegeneration in mouse models of familial amyotrophic lateral sclerosis. J. Neurosci. *28*, 13574–13581.

Vascotto, C., Fantini, D., Romanello, M., Cesaratto, L., Deganuto, M., Leonardi, A., Radicella, J.P., Kelley, M.R., D'Ambrosio, C., Scaloni, A., et al. (2009). APE1/Ref-1 interacts with NPM1 within nucleoli and plays a role in the rRNA quality control process. Mol. Cell. Biol. *29*, 1834–1854.

Vitale, A.M., Matigian, N.A., Ravishankar, S., Bellette, B., Wood, S.A., Wolvetang, E.J., and Mackay-Sim, A. (2012). Variability in the generation of induced pluripotent stem cells: importance for disease modeling. Stem Cells Transl. Med. *1*, 641–650.

Wakabayashi, N., Itoh, K., Wakabayashi, J., Motohashi, H., Noda, S., Takahashi, S., Imakado, S., Kotsuji, T., Otsuka, F., Roop, D.R., et al. (2003). Keap1-null mutation leads to postnatal lethality due to constitutive Nrf2 activation. Nat. Genet. *35*, 238–245.

Wald-Altman, S., Pichinuk, E., Kakhlon, O., and Weil, M. (2017). A differential autophagy-dependent response to DNA double-strand breaks in bone marrow mesenchymal stem cells from sporadic ALS patients. Dis. Model. Mech. *10*, 645–654.

Walker, C., Herranz-Martin, S., Karyka, E., Liao, C., Lewis, K., Elsayed, W., Lukashchuk, V., Chiang, S.-C., Ray, S., Mulcahy, P.J., et al. (2017). C9orf72 expansion disrupts ATM-mediated chromosomal break repair. Nat. Neurosci. *20*, 1225–1235.

Wang, H., Katagiri, Y., McCann, T.E., Unsworth, E., Goldsmith, P., Yu, Z.X., Tan, F., Santiago, L., Mills, E.M., Wang, Y., et al. (2008). Chondroitin-4-sulfation negatively regulates axonal guidance and growth. J. Cell Sci. *121*, 3083–3091.

Wang, H., Yang, Y., Liu, J., and Qian, L. (2021). Direct cell reprogramming: approaches, mechanisms and progress. Nat. Rev. Mol. Cell Biol. *22*, 410–424.

Wang, T., Qin, L., Liu, B., Liu, Y., Wilson, B., Eling, T.E., Langenbach, R., Taniura, S., and Hong, J.S. (2004). Role of reactive oxygen species in LPS-induced production of prostaglandin E2 in microglia. J. Neurochem. *88*, 939–947.

Wang, Y., Zhang, N., Zhang, L., Li, R., Fu, W., Ma, K., Li, X., Wang, L., Wang, J., Zhang, H., et al. (2016). Autophagy regulates chromatin ubiquitination in DNA damage response through elimination of SQSTM1/p62. Mol. Cell *63*, 34–48.

Warita, H., Hayashi, T., Murakami, T., Manabe, Y., and Abe, K. (2001). Oxidative damage to mitochondrial DNA in spinal motoneurons of transgenic ALS mice. Mol. Brain Res. *89*, 147–152.

Weisskopf, M.G., McCullough, M.L., Calle, E.E., Thun, M.J., Cudkowicz, M., and Ascherio, A. (2004). Prospective study of cigarette smoking and amyotrophic lateral sclerosis. Am. J. Epidemiol. *160*, 26–33.

Wen, X., Tan, W., Westergard, T., Krishnamurthy, K., Markandaiah, S.S., Shi, Y., Lin, S., Shneider, N.A., Monaghan, J., Pandey, U.B., et al. (2014). Antisense proline-arginine RAN dipeptides linked to C9ORF72-ALS/FTD form toxic nuclear aggregates that initiate in vitro and in vivo neuronal death. Neuron *84*, 1213–1225.

Westergard, T., Jensen, B.K., Wen, X., Cai, J., Kropf, E., Iacovitti, L., Pasinelli, P., and Trotti, D. (2016). Cell-to-cell transmission of dipeptide repeat proteins linked to C9orf72-ALS/FTD. Cell Rep. *17*, 645–652.

White, M.R., Mitrea, D.M., Zhang, P., Stanley, C.B., Cassidy, D.E., Nourse, A., Phillips, A.H., Tolbert, M., Taylor, J.P., and Kriwacki, R.W. (2019). C9orf72 poly(PR) dipeptide repeats disturb biomolecular phase separation and disrupt nucleolar function. Mol. Cell *74*, 713–728.

Yamamoto, A., Nakamura, Y., Kobayashi, N., Iwamoto, T., Yoshioka, A., Kuniyasu, H., Kishimoto, T., and Mori, T. (2007). Neurons and astrocytes exhibit lower activities of global genome nucleotide excision repair than do fibroblasts. DNA Repair (Amst). *6*, 649–657.

Yamanaka, K., Boillee, S., Roberts, E.A., Garcia, M.L., McAlonis-Downes, M., Mikse, O.R., Cleveland, D.W., and Goldstein, L.S.B. (2008a). Mutant SOD1 in cell types other than motor neurons and oligodendrocytes accelerates onset of disease in ALS mice. Proc. Natl. Acad. Sci. U. S. A. *105*, 7594–7599.

Yamanaka, K., Chun, S.J., Boillee, S., Fujimori-Tonou, N., Yamashita, H., Gutmann, D.H., Takahashi,

R., Misawa, H., and Cleveland, D.W. (2008b). Astrocytes as determinants of disease progression in inherited amyotrophic lateral sclerosis. Nat. Neurosci. *11*, 251–253.

Yang, D., Abdallah, A., Li, Z., Lu, Y., Almeida, S., and Gao, F.-B. (2015). FTD/ALS-associated poly(GR) protein impairs the Notch pathway and is recruited by poly(GA) into cytoplasmic inclusions. Acta Neuropathol. *130*, 525–535.

Yim, M.B., Kang, J.H., Yim, H.S., Kwak, H.S., Chock, P.B., and Stadtman, E.R. (1996). A gain-of-function of an amyotrophic lateral sclerosis-associated Cu,Zn-superoxide dismutase mutant: An enhancement of free radical formation due to a decrease in Km for hydrogen peroxide. Proc. Natl. Acad. Sci. U. S. A. *93*, 5709–5714.

Yoshihara, M., Hayashizaki, Y., and Murakawa, Y. (2016). Genomic instability of iPSCs: challenges towards their clinical applications. Stem Cell Rev. Reports *13*, 7–16.

Yoshihara, T., Ishigaki, S., Yamamoto, M., Liang, Y., Niwa, J.I., Takeuchi, H., Doyu, M., and Sobue, G. (2002). Differential expression of inflammation- and apoptosis-related genes in spinal cords of a mutant SOD1 transgenic mouse model of familial amyotrophic lateral sclerosis. J. Neurochem. *80*, 158–167.

Yoshino, H., and Kimura, A. (2006). Investigation of the therapeutic effects of edaravone, a free radical scavenger, on amyotrophic lateral sclerosis (Phase II study). Amyotroph. Lateral Scler. *7*, 247–251.

Zaksauskaite, R., Thomas, R.C., Van Eeden, F., and El-Khamisy, S.F. (2021). Tdp1 protects from topoisomerase 1-mediated chromosomal breaks in adult zebrafish but is dispensable during larval development. Sci. Adv. *7*.

Zarei, S., Carr, K., Reiley, L., Diaz, K., Guerra, O., Altamirano, P.F., Pagani, W., Lodin, D., Orozco, G., and Chinea, A. (2015). A comprehensive review of amyotrophic lateral sclerosis. Surg. Neurol. Int. *6*.

Zhang, Y.J., Gendron, T.F., Grima, J.C., Sasaguri, H., Jansen-West, K., Xu, Y.F., Katzman, R.B., Gass, J., Murray, M.E., Shinohara, M., et al. (2016). C9ORF72 poly(GA) aggregates sequester and impair HR23 and nucleocytoplasmic transport proteins. Nat. Neurosci. *19*, 668–677.

Zhao, C., Devlin, A., Chouhan, A.K., Selvaraj, B.T., Stavrou, M., Burr, K., Brivio, V., He, X., Mehta, A.R., Story, D., et al. (2020). Mutant *C9orf72* human iPSC-derived astrocytes cause non-cell autonomous motor neuron pathophysiology. Glia *68*, 1046–1064.

Zhou, Q., Lehmer, C., Michaelsen, M., Mori, K., Alterauge, D., Baumjohann, D., Schludi, M.H., Greiling, J., Farny, D., Flatley, A., et al. (2017). Antibodies inhibit transmission and aggregation of C9orf72 poly-GA dipeptide repeat proteins. EMBO Mol. Med. *9*, 687–702.

Zhou, Q., Mareljic, N., Michaelsen, M., Parhizkar, S., Heindl, S., Nuscher, B., Farny, D., Czuppa, M., Schludi, C., Graf, A., et al. (2020). Active poly-GA vaccination prevents microglia activation and motor deficits in a C9orf72 mouse model. EMBO Mol. Med. *12*, e10919.

Ziemens, D., Oschmann, F., Gerkau, N.J., and Rose, C.R. (2019). Heterogeneity of activity-induced sodium transients between astrocytes of the mouse hippocampus and neocortex: mechanisms and consequences. J. Neurosci. *39*, 2620–2634.

Zou, Z.-Y., Zhou, Z.-R., Che, C.-H., Liu, C.-Y., He, R.-L., and Huang, H.-P. (2017). Genetic epidemiology of amyotrophic lateral sclerosis: a systematic review and meta-analysis. J. Neurol. Neurosurg.

Psychiatry *88*, 540–549.

Zu, T., Liu, Y., Bañez-Coronel, M., Reid, T., Pletnikova, O., Lewis, J., Miller, T.M., Harms, M.B., Falchook, A.E., Subramony, S.H., et al. (2013). RAN proteins and RNA foci from antisense transcripts in C9ORF72 ALS and frontotemporal dementia. Proc. Natl. Acad. Sci. U. S. A. *110*, E4968–E4977.